University of Alberta

A New Generation Neural Prosthesis

By

Richard Williamson ©

A thesis
Submitted to the Faculty of Graduate Studies and Research
In partial fulfillment of the requirements for the degree
of Doctor of Philosophy
in
Medical Sciences – Biomedical Engineering

Edmonton, Alberta
Fall, 1999

National Library of Canada
Acquisitions and Bibliographic Services
395 Wellington Street
Ottawa ON K1A 0N4
Canada

Bibliothèque nationale du Canada
Acquisitions et services bibliographiques
395, rue Wellington
Ottawa ON K1A 0N4
Canada

Your file Votre référence

Our file Notre référence

The author has granted a non-exclusive licence allowing the National Library of Canada to reproduce, loan, distribute or sell copies of this thesis in microform, paper or electronic formats.

L'auteur a accordé une licence non exclusive permettant à la Bibliothèque nationale du Canada de reproduire, prêter, distribuer ou vendre des copies de cette thèse sous la forme de microfiche/film, de reproduction sur papier ou sur format électronique.

The author retains ownership of the copyright in this thesis. Neither the thesis nor substantial extracts from it may be printed or otherwise reproduced without the author's permission.

L'auteur conserve la propriété du droit d'auteur qui protège cette thèse. Ni la thèse ni des extraits substantiels de celle-ci ne doivent être imprimés ou autrement reproduits sans son autorisation.

0-612-46945-X

Canada

University of Alberta

Library Release Form

Name of Author : **Richard Williamson**
Title of Thesis : **A New Generation Neural Prosthesis**
Degree : **Doctor of Philosophy**
Year this Degree Granted : **1999**

Permission is hereby granted to the University of Alberta Library to reproduce single copies of this thesis and to lend or sell such copies for private, scholarly, or scientific purposes only.

The author reserves all other publication and other rights in association with the copyright in the thesis, and except as hereinbefore provided, neither the thesis nor any substantial portion thereof may be printed or otherwise reproduced in any material form whatever without the author's written permission

11246 – 75 Ave
Edmonton, Alberta
T6G 0H3

Aug 10, 99

UNIVERSITY OF ALBERTA

FACULTY OF GRADUATE STUDIES AND RESEARCH

The undersigned certify that they have read, and recommend to the Faculty of Graduate Studies and Research for acceptance, a thesis entitled **A New Generation Neural Prosthesis** submitted by **Richard Williamson** in partial fulfillment of the requirements of for the degree of Doctor of Philosophy in Medical Sciences – Biomedical Engineering.

Brian J. Andrews (Supervisor)

Zoltan Koles

Ken Fyfe

Arthur Prochazka

Hasan Uludag

Aftab Patla (external)

Date : July 7, 99

Abstract

Neural prostheses for locomotion have limited clinical application, in part due to poor control. Two significant limitations are the lack of appropriate feedback sensors and a means of dynamically suppressing spasticity. Results are presented that support the feasibility of a high frequency nerve block and new signal processing techniques that enable existing sensors to be extended to present functional electrical stimulation techniques and to future possibilities incorporating nerve blocking.

The proposed sensor system limited encumbrance by connecting clustered sensors with a serial bus. Knee flexion angle and angular velocity were determined analytically to within 3° and 10°/s respectively in both paraplegic and able bodied trials from accelerometers and rate gyroscopes attached to the shank and thigh. A supervised machine learned rule induction controller detected gait phases to an average transition error of 40 ms in able bodied walking from three accelerometers placed on the shank when combined with a heuristic rule. Supervised machine learning also detected knee and hip angle and angular velocity to within 3° and 18°/s using accelerometers and a magnetic system worn on the belt and shank. Knee buckling was predicted bilaterally to a minimum of 300 ms before knee flexion reached 5° as determined by the strain gauge. The combination of these studies leads to a sensor system located either on the shank and thigh, or on the shank and belt, that can minimally determine knee flexion/extension, knee buckling, and gait events.

Localized nerve blocking was demonstrated through spatially extended non-linear nodal models. Sinusoidal excitation through a monopolar electrode was simulated for frog (FH), rabbit (CRRSS), rat (SE) and human (SRB) models of axons. It was previously thought that sinusoidal currents would only cause repetitive action potential generation in the axons, and a block would be due to Wedenski inhibition. Repetitive action potential generation was observed in the CRRSS model. Repetitive action potential generation and a block contingent upon electrode placement was observed in the FH model. Repetitive action potential generation for frequencies below 15 kHz and a localized block for frequencies above 7 kHz was observed in the SE model. Repetitive action potential generation for frequencies up to 20 kHz and localized blocking for frequencies above 1.2 kHz was observed in the SRB model. A physical trial supported the concept that the block was local to the blocking electrode.

Acknowledgement

I would like to thank my family, John and Kevin, and parents Colleen and George, for their support and advice during these studies. Their calming and reasoned influence help direct my sanguine enthusiasm.

I would like to thank my advisor, Brian, for his direction and insight. I appreciate and recognize the advice and support of Zoly Koles, Richard Snyder, Peter Allen, and Hassan Ululag at the Department of Biomedical Engineering, Jim Raso and Doug Hill at the Glenrose Rehabilitation Hospital, Arthur Prochazka, and Tessa Gordon for arranging the animal studies and Neil Tyreman for performing the surgery, Ken Fyfe for his discussions on analytical solutions to sensor problems, and Ross Davis and Thierry Houdeyer at the Neural Engineering Clinic.

I would also like to thank Corey, Dave, and Donal and the others for never discussing any of the work, other than to turn an interested and supportive ear.

My dissertation was supported by the Natural Science and Engineering Research Council (NSERC), and the University of Alberta's Faculty of Medicine. Additional resources were provided by NEC and Cochlear Pty.

Table of Contents

1 Introduction 1
1.1 Introduction 1
1.1.1 Populations Who Could Use FES in Rehabilitation 5
1.2 Literature Review 7
1.2.1 Functional Electrical Stimulation Methods (FES) 7
1.2.2 Sensors and Control techniques for lower limb FES 8
1.3 Nerve Blocking 17
1.3.1 Anodal Blocking 17
1.3.2 Collision Blocking 18
1.3.3 Blocking through high frequency activation 19
1.3.4 A Possible Localized Action Potential Transmission Block 19
1.4 Thesis Hypothesis and Objectives 23
1.5 Bibliography 30

2 Gait Event Detection for FES Using Accelerometers and Supervised Machine Learning 37
2.1 Introduction 37
2.2 Methods and Materials 40
2.2.1 Subjects and Walkpaths 40
2.2.2 Accelerometers 40
2.2.3 Determination of reference gait phases 41
2.2.4 Rough Sets 42
2.2.5 Adaptive Logic Networks 43
2.2.6 Training the machine learning algorithms 44
2.2.7 Calculation of Detection Accuracy 46
2.2.8 Comparison of hand-crafted and machine-learned stance-swing detectors 47
2.2.9 Multiple Gait Phase Detection 47
2.3 Results 48
2.3.1 Comparison of hand-crafted and machine learned stance-swing detectors 48
2.3.2 Multiple Gait Phase Detection 49
2.3.4 Variability of detection accuracy based on variance of the teacher signal 51
2.3.5 Real Time Operation 51
2.4 Discussion 51
2.5 Conclusions 55
2.6 Bibliography 73

3 Detection of Absolute Knee flexion angle and angular velocity 75
3.1 Introduction 75
3.2 Theory of Operation 78
3.2.1 Determination of Angle and Angular Velocity 78
3.2.2 Auto-Nulling the Rate Gyroscopes and Auto-Resetting the Integrators 78
3.3 Methods and Results 80
3.3.1 The Sensors 80
3.3.2 Data Acquisition and Signal Pre-processing 82
3.3.3 Bench Tests Using an Articulated Plastic Model 83
3.3.4 Sit-Stand-Sit Trials with Able Bodied Subjects 86

3.3.5 Paraplegic Sit to Stand Trial Using FES 87
3.4 Discussion 90
3.5 Conclusion 92
3.6 Bibliography 108

4 A Sensor System for Lower Limb FES Control 110
4.1 Introduction 110
4.2 Methods 113
4.2.1 The Sensors 113
4.2.2 The Clusters, Configurations, and Data Acquisition 114
4.2.3 Gait phase detection 115
4.2.4 Determination of angle and angular velocity: Analytical approach 116
4.2.5 Knee and hip kinematics: "Virtual Sensor" approach 119
4.2.6 Detecting and predicting knee buckling 119
4.3 Results 121
4.3.1 Gait Phase detection 121
4.3.2 Knee Kinematics: Analytical Approach 121
4.3.3 Knee and Hip Kinematics: "Virtual Sensor" Approach 122
4.3.4 Detecting and Predicting Knee Buckling 122
4.4 Discussion 123
4.5 Conclusion 126
4.6 Bibliography 141

5 Electrical Nerve Blocking : A computer simulation 144
5.1 Introduction 144
5.2 Background 145
5.3 Methods 147
5.3.1 Spatially Extended Nodal Kinetic Models 147
5.4 Results 152
5.4.1 Excitation and Blocking Using High Frequency Currents 152
5.4.2 Integrity of Models During High Frequency Excitation and Blocking 154
5.4.3 A Potential Mechanism for Blocking 154
5.5 Discussion 155
5.6 Conclusions 159
5.7 Bibliography 174

6 Electrical Nerve Blocking : Practical Considerations 176
6.1 Introduction 176
6.2 Methods 178
6.2.1 Modeling 178
6.2.2 Parameter Changes 178
6.2.3 Noise on the Input of the System 179
6.2.4 Animal Model 179
6.3 Results 180
6.3.1 Parameter Changes 180
6.3.2 Noise on the Input of the System 181
6.3.3 Experimental Results 181
6.4 Discussion 183

6.5 Conclusion **185**
6.6 Bibliography **193**

7 Discussion **195**
7.1 Introduction **195**
7.2 The Sensor System **195**
7.2.1 Knee Flexion Angle and Angular Velocity 195
7.2.2 Knee Buckle Prediction 197
7.2.3 Gait Phase Prediction 197
7.3 Electrical Nerve Blocking **199**
7.4 A New Neural Prosthesis **200**
7.5 Implications of This Study to FES **204**
7.6 Bibliography **208**

8 Conclusions **210**
8.1 Recommendations for Future Research **210**

List of Tables

Table 2.1 Physical characteristics and average walking speed of each subject.....66
Table 2.2 Gait phases from FSR recordings.....67
Table 2.3 Comparison of accuracy for stance swing determination.....68
Table 2.4 Results of multiple gait phase determination by RBC.....69
Table 2.5 Results of postfiltered RBC determination of stance swing.....70
Table 2.6 Results of postfiltered RBC determination of multiple gait phases.....71
Table 2.7 Real time implementation of RS and ALN.....72
Table 3.1 Tilt calculations by accelerometer and integral of rate gyroscope.....102
Table 3.2 Rate of change of tilt calculated from accelerometers and rate gyroscopes.103
Table 3.3 Comparisons of angle and angular velocity as calculated on a 2-D model...104
Table 3.4 Comparisons of knee flexion angle and angular velocity as calculated on able bodied volunteers.....105
Table 3.5 Comparisons of knee flexion angle and angular velocity as calculated on a paraplegic volunteer.....106
Table 3.6 The effect of FES on the calculation of knee angle and angular velocity.....107
Table 4.1 Five gait phases detected by post filtered Rough Sets rule based controller.137
Table 4.2 Accuracy for the analytic calculation of joint angle.....138
Table 4.3 "Virtual Sensor" calculation of knee and hip angle and angular velocity....139
Table 4.4 Time prior to and knee flexion angle at prediction of knee buckling.....140
Table 5.1 Integrity of models during blocking and excitation due to high frequency currents.....171
Table 6.1 Change in blocking current due to changes in SRB model parameters.....191
Table 6.2 Blocking and stimulation due to sinusoidal currents at different frequencies.....192

List of Figures

Figure 1.1 EMG and Achilles tendon force recordings....28
Figure 1.2 Standing times in paraplegia....29
Figure 2.1 Subject wearing calf strap with three accelerometers....57
Figure 2.2 Gait phases determined from FSR foot pressures....58
Figure 2.3 Accelerometer recording and coincident gait phase....60
Figure 2.4 Filtered accelerometers as tilt meters....61
Figure 2.5 Five gait phases determined by accelerometers and a RBC....62
Figure 2.6 Distribution of errors using postfiltered Rough Sets gait phase detector...64
Figure 2.7 Variance of gait phase duration....65
Figure 3.1 Determination of knee angle from accelerometers and rate gyroscopes...94
Figure 3.2 Sensor clusters....95
Figure 3.3 Mounting of sensor clusters and goniometer on a 2 dimensional model...96
Figure 3.4 Static difference between goniometer and accelerometers....97
Figure 3.5 Angle calculated on 2 dimensional model....98
Figure 3.6 Knee angle calculated on able bodied volunteer....99
Figure 3.7 Paraplegic volunteer wearing sensor clusters....100
Figure 3.8 Knee angle calculated on paraplegic volunteer....101
Figure 4.1 Subject wearing sensor configuration 1....127
Figure 4.2 Subject wearing sensor configuration 2....128
Figure 4.3 Subject wearing sensor configuration 3....129
Figure 4.4 Analytical determination of knee angle....130
Figure 4.5 Forces in the AFO during standing....131
Figure 4.6 Relative length of errors using gait phase detector....132
Figure 4.7 Knee angle calculated on a paraplegic volunteer....133
Figure 4.8 Knee angle and angular velocity from "Virtual Sensors"....134
Figure 4.9 Hip angle and angular velocity from "Virtual Sensors" 135
Figure 4.10 Strain gauge threshold prediction of knee buckling....136
Figure 5.1 Schematic for spatially extending nonlinear nodal kinetic models....163
Figure 5.2 Four effects of high frequency current on the SENN-SRB model....164
Figure 5.3 Diameter – current relationship for CRRSS, FH, SE, and SRB models...165

Figure 5.4 Frequency – current relationship for CRRSS, FH, SE, and SRB models.166
Figure 5.5 Influence of electrode position on high frequency current effects.....167
Figure 5.6 Electrode placement – current relationship for SRB model.....168
Figure 5.7 Single node evaluation of stimulation due to high frequency currents in SRB model.....170
Figure 5.8 Single node evaluation of blocking due to high frequency currents in SRB model.....172
Figure 6.1 Blocking currents required for systematic and random noise levels.....187
Figure 6.2 Relationship of systematic and random noise to minimum blocking current.....188
Figure 6.3 Stimulation and blocking due to application of high frequency currents to rat nerve.....190
Figure 7.1 EMG recording of child with crouched gait due to cerebral palsy.....207

List of Abbreviations

AFO	Ankle foot orthosis
ALN	Adaptive logic network
CRRSS	Chui, Ritchie, Rogert, Stagg, and Sweeney model (of ionic currents in a rabbit node of Ranvier)
FES	Functional electrical stimulation
FH	Frankenhaeuser Huxley model (of ionic currents in a frog node of Ranvier)
FRO	Floor reaction orthosis
FSR	Force Sensing Resistor
GRF	Ground reaction force
pfRS	post-intuitive filtered Rough Set
MEMS	Micromachined electromechanical sensor
RBC	Rule based controller
RBD	Rule based detector
RS	Rough sets
SCI	Spinal cord injury
SE	Schwarz Eikhof model (of ionic currents in a rat and cat node of Ranvier)
SENN	Spatially extended nonlinear nodal model
SRB	Schwarz Reid Bostock model (of ionic currents in human node of Ranvier)

1 Introduction

1.1 Introduction

Medical applications of electrical shocks have been used for millennia, indicated by records of the use of electric fish by Greek and Roman physicians. Further applications followed, based upon the new methods of electrical current generation such as the bimetallic 'battery' of Luigi Galvani's dissection calipers and the electrostatic and electromagnetic machines of Benjamin Franklin and Michael Faraday. These methods of generating electrical currents are now known as Galvanism, Franklinism and Faradism, the latter being most widely used in modern electrotherapy. Electrical currents were also applied for the relief of paralysis. Starting in the 19th century, Duchenne used an induction coil faradic stimulator to assist a paraplegic patient to stand up. In 1961, Liberson described a battery powered transistor stimulator with automatic control via a heel switch to correct for foot drop (Liberson et al., 1961). These early attempts to restore motor function using electrical stimulation laid the foundation of the field of Functional Electrical Stimulation - FES (McNeal, 1977).

Since the 1960's, FES has steadily developed into an international research activity, manifested in a variety of surface and implanted systems (Bhadra and Peckham, 1997, Graupe and Kohn, 1997, Stein et. al. 1992, Pedotti et. al., 1996, Kralj and Bajd, 1989). The field is now represented by the International FES Society and is an important member of societies such as the IEEE Engineering in Medicine and Biology Society (EMBS). Despite this longstanding history and effort, limitations to wide clinical application remain, including significant problems in the control of movement. Some of these issues will be discussed below and addressed in this study.

Advocacy and research into the regeneration of the spinal cord have spawned hope for an eventual cure for paralysis (Giovanini et. al., 1997, Ramon-Cueto et. al, 1998). However, the cure is distant in the future. In the meantime, FES can be used to avoid many of the debilitating sequela of spinal cord injuries (SCI). Additionally, the neural regeneration will most likely only lessen the degree of the lesion, leaving niches for neural prostheses to be used to further optimize functional recovery.

Some limitations to the development of future neural prostheses are represented in the following two clinical cases. The first case taken is a child with muscle weakness and spasticity in the gastrocnemius (Dietz and Berger, 1983). The second case is an example of maximum standing duration of paraplegic individuals (Bajd et. al, 1984).

Case 1: Spastic Hemiplegia in the Cerebral Palsied Child

A common problem in hemiplegic (Hirschberg and Nathanson, 1951, Knutsson and Richards, 1976, Dietz, 1986) and diplegic (Knutsson and Sodeberg, 1995, Perry 1992, Berger, 1986) gait is due to a weak and spastic gastrocnemius. The spasticity observed in this case has been described as a mass extensor synergy (Perry et. al. 1993), an underlying spinal mechanism that is not properly inhibited in this individual. Figure 1.1 (top) displays the EMG recording during a typical case.

For this individual, the gastrocnemius causes ankle plantar flexion during late swing, resulting in foot floor contact prior to heel strike in coordination with the knee and hip extension. This shortens the stride length, denies the individual a proper rocking motion over the ankle, and partially eliminates the forward momentum of the gait. In addition to disrupting the gait, the abnormal loading pattern during early stance can lead to a progressive deformity in the child that could only be partially corrected through surgery. An underlying muscular weakness of the gastrocnemius is also observed.

The present methods for assisting individuals with lower motor impairments such as this are limited. Braces, such as rigid ankle foot orthoses (AFO), localized nerve blocks (Wong, 1998) via phenol, lidocaine, or botulinum toxin, muscle relaxants such as baclofen (Albright, 1996), and tendon lengthening can all be performed to mask the effect of spasticity of the gastrocnemius and soleus muscles. Generally, these techniques either disable the muscle activation, or disable the moments about the joint caused by muscle activation. Considering that ankle plantar flexion has been shown to provide 30% of the propulsion of the leg during normal walking, limitations to these techniques are apparent. If the muscles are unable to generate a moment about the joint or their action is blocked due to a brace, a normal, efficient gait cycle is not achieved. Muscle transfers can be useful in some instances, but are limited by two factors. The inappropriate muscle activity must be able to produce a desired moment about a joint after the surgery, hence be

synergistic with a second muscle group. Additionally, the proximity of the muscle to the transfer point must be considered, i.e. a spastic gastrocnemius could not be attached to a tibialis anterior tendon. The present techniques used to address phasic spasticity do not detect if the contraction of the muscle is due to spasticity, and can not suppress the muscular contraction only for the duration of the spasticity.

Ideally, the neural prosthesis would stimulate the tibial nerve from mid-stance until pre-swing to assist plantar flexion of the ankle, and block the tibial nerve during late swing and loading response to prevent spastic plantar flexion. Further compensation would be provided to other muscle groups as required. The present techniques described above continuously affect the gait pattern, whether or not the muscle is functioning appropriately. Therefore, the number and types of cases of spasticity that can be addressed are limited to ones in which benefits of the brace or absent muscle activity are greater than the limits imposed by its use.

The addition of temporary, localized nerve blocking to a FES system would open the application of an assistive device to a large number of patients. Most problems in gait can be described by muscular weakness, spasticity, or limited range of joint motion. The limited range of motion could be due to long-term disuse, which is corrected through muscle lengthening procedures, or spasticity. FES has already been shown to assist individuals with muscular weakness. The addition of a temporary block would enhance FES systems so they could also assist individuals through the suppression of spasticity.

For the block to be effective in this instance, it must be able to be turned on and off quickly. An absolute minimum switching dynamic of the block for the above child would be given by the duration of stance and swing, approximately 1 second in normal walking. A sensor system would be required to detect the turn on and turn off times of the block. Ideally, the switching dynamics of the block should be in accordance with the temporal discrimination of spasticity. Consideration of the switching dynamics of the block would be required in the development of the discrimination algorithm. This would be simplified if the block could be turned on and off instantly.

Case 2: Prolonged Standing After SCI

In a trial to determine maximum standing duration of a paraplegic individual assisted by FES, eight spinal cord injured patients were maintained in a standing posture. The duration of the standing ranged from a few minutes to two hours. Personal communication indicated that the patients with long duration standing had contractures of the gastrocnemius or soleus muscle. The maximum standing times for individuals without contractures ranged from 5 to 10 minutes.

Long term standing is desired for rehabilitation of spinal cord injured subjects to allow for periodic rest breaks to be taken during ambulation for recovery from upper limb and FES induced fatigue. Posture switching (Krajl et. al., 1986), carousal stimulation (Happak et. al., 1989), and intrafascicular stimulation (Veltink et. al., 1989) have all been shown to increase the amount of time a muscle can be stimulated before fatigue. Each of these techniques only delays the onset of fatigue, typically by a factor of 3 to 5. These techniques might not be applicable for an ambulating individual who desires to take a break during a sustained walk without further fatiguing the muscles.

Braces have been proposed to reduce the duty cycle of FES activation, hence alleviating muscle fatigue. Conventional orthotics are cumbersome, hence do not receive long term usage (Coghlan et. al. 1980). Minimal bracing, such as the hybrid orthosis, (Andrews, and Baxendale, 1986) has been shown to lengthen standing times. However, a controller is then required to compensate for knee buckling.

Brandell (Brandell, 1982) has discussed a 'universal' FES system. This system would be flexible enough to adapt to the specific problems associated with upper motor neuron disabilities, such as stroke, hemiplegia, cerebral palsy, and spinal cord injury. Presently, FES has been shown to overcome limitations of muscular weakness in each of these cases (Hendron, 1980, Stein et. al. 1992, Pedotti et. al., 1996). However, spasticity is a persistent problem in many of these individuals. Ideally, a 'universal' FES system would be able to address problems due to muscular weakness and spasticity.

The inability to suppress spasticity is not the only limitation of present neural prostheses. The sensors that are used for control of the stimulation have not been refined for practical, everyday use. Closed loop control has been discussed as an advancement of

many systems even though the sensors for closed loop control are often unavailable or unsuitable for long term use. Goniometers, used for measuring knee joint angles, are cumbersome and bulky, and are not suitable for use outside a laboratory. Hand switch control, often used to activate stimulation pulses, is only sufficient for slow gait. If multiple events need to be triggered for faster or smoother gait patterns, the complexity and timing involved in using hand switches would be restrictive (Lajoie, et. al, 1999).

The author envisions a neural prosthesis that would overcome these limitations. The controller would use convenient, available, and unobtrusive sensors to provide feedback for a FES system. Muscular stimulation and nerve blocking patterns could then be generated from the controller. This neural prosthesis is developing incrementally. Advancements in controllers for standing (Dolan and Andrews, 1998, Davoodi and Andrews, 1998) and walking (Kobetic and Marsolais, 1994, Franken et. al., 1995) have been described. Implanted FES systems are being developed to provide a better reliability and repeatability of stimulation (Kilgore et. al., 1997, Davis et. al., 1997). Further developments in the area of stimulation included spinal cord stimulation, and sacral root stimulation (Rushton et. al., 1996). These methods hope to provide better repeatability and precise control of stimulated muscles. A 'universal' neural prosthesis could become a reality subsequent to the development of applicable sensor systems for feedback control and a method for blocking of unwanted peripheral nerve activity. The population that could benefit from this type of device ranges from individuals debilitated by a variety of neural muscular disorders such as spinal cord injury, stroke, and cerebral palsy.

1.1.1 Populations Who Could Use FES in Rehabilitation

Spinal cord injury causes a disruption of the upper motor neurons from connecting with the lower motor neurons. This has the effect of disrupting or eliminating the signals from the brain used to control the areas below the injury.

The incidence of spinal cord injury in the United States is approximately 40 per million, and the prevalence is about 183 000 to 203 000. Most of the individuals who suffer spinal cord injury are male (81.9%). The mean age at incidence is 31.5 years. The most common lesions are C5 followed by C4, C6, T12 and L1. Between 1991 and 1998,

the incidence rates for the neurological levels were: complete paraplegia (28.9%), incomplete tetraplegia (28.6%), incomplete paraplegia (21.8%), and complete tetraplegia (18.4%).

Stroke affects about 1% today's population. In 1991, there were 2.9 million stroke survivors in the USA, of whom 20% needed help to ambulate (Framingham study, National Stroke Association). Stroke, or ischemia, is caused by a loss of blood circulation in the brain, damaging the controller of neuromuscular actions. The resultant loss can be muscular, sensory, or a combination of the two. The extent of the damage due to stroke and the effects of the stroke vary on an individual by individual basis. FES can be used in rehabilitation to restore lost motor activity through activation of intact neural pathways.

Spasticity is a problem after stroke and SCI. Kerrigan (Kerrigan et. al., 1991) studied spastic paresis leading to the condition of stiff-legged gait. In the study, each of the patients referred to the clinic with this condition had inappropriate activity in at least one quadriceps muscle during pre-swing or initial swing phase of gait. Inappropriate activity of the hamstrings occurred in 9 of the 23 patients during pre-swing. Treatments for this condition were not discussed.

In cerebral palsy gait, a common problem is the inappropriate synergistic activation of muscles. It is suggested that primitive reflexes lead to this synergistic activation of muscles, and become more apparent in cerebral palsy due to decreased supra-spinal inhibition. These inappropriate synergistic actions interfere with the objectives of certain phases of gait. Perry (Perry et. al. 1993) describes an example of this condition. Spastic gastrocnemius or soleus activity during terminal swing can cause an abrupt end to the swing phase of gait. This prevents the normal ankle position that is necessary for the smooth transition of forward momentum by disabling proper loading of the leg. In turn, the gait pattern is slowed and requires greater physical effort due to poor conservation of momentum.

In each of these neurological impairments, muscle weakness and spasticity can affect the gait pattern. A device that could address both of these conditions would have a larger area of influence than one that only addressed muscle weakness.

The envisioned FES system addresses both muscular weakness and spasticity. Precise timing for nerve blocking, required to control spasticity, would be triggered by a real time sensor system. This requires a nerve blocking technique with sufficiently rapid dynamics, and a precise method of sensing when the nerve should be blocked.

A method for this type of control is not presently available for FES. The artificial sensors that have been used in FES are inadequate for everyday use (Marsolais and Kobetic, 1988, Johnson et. al., 1995, Crago et. al., 1986). A dynamic, electrical nerve block that is safe for mixed nerves and can be asserted and removed quickly does not exist.

The goal of this thesis is to further the development of FES systems that could stimulate, block, or selectively stimulate axons as activated by a controller using feedback derived from appropriate sensor systems.

1.2 Literature Review

1.2.1 Functional Electrical Stimulation Methods (FES)

Many FES systems have been used to assist standing and walking in paraplegic individuals. The typical systems used surface (Kralj and Bajd, 1989), percutaneous (Kobetic and Marsolais, 1994), or implanted (Kilgore et. al., 1997, Davis et. al., 1997, Sharma, 1998) electrodes for stimulation. Further developments in the area of stimulation technique include spinal cord stimulation, and sacral root stimulation (Rushton et. al., 1996).

The time required to don and doff a system can be a deterrent from using the system. This lead to the development of implanted systems. The implanted systems are telemetrically powered by a radio frequency (RF) power source. The efficiency of inductive power transmission ranges from 60-70%. Communication with the implant and an external control unit occurs through amplitude modulation of the RF power. The external control unit transmits each stimulus channel's amplitude and pulse width to the implanted stimulator by amplitude modulation of the RF power source. The implanted stimulator detects and interprets the amplitude modulated RF signal through a microprocessor and controls the stimulus level for each channel. Telemetry is also used to

transmit implanted sensor recordings from the implant to the external controller. Modulation of the implanted receivers' admittance will alter the back EMF of the external control unit's transmitting coil. The external control unit demodulates this back EMF to obtain the implanted sensor recordings. The system of Kilgore et. al. controls 32 channels of stimulation in this manner. The system of Davis et. al. controls 24 channels of stimulation whereas the system of Sharma et. al. controls 16 channels.

1.2.2 Sensors and Control techniques for lower limb FES

The first use of FES for neuromuscular control on a continuing basis was the drop foot stimulator designed by Liberson and colleagues (Liberson et. al. 1961). This was first applied to patients with hemiplegia. A footswitch was used to determine stance and swing phase. During swing, the tibialis anterior is stimulated though the common peroneal nerve at the head of the fibula.

Automatic detection of the stance and swing transition is a common application of sensors within FES. Kostov (Kostov et. al., 1995) used force sensing resistors placed in the insole of a shoe, and Adaptive Logic Networks (ALN) to determine stance and swing in hemiplegia. The ALN required training on a day to day basis, imposing a possible limit on the application of this technique in a clinical setting. Dai (Dai et. al., 1996) and Willemsen (Willemsen et. al., 1990a) have used accelerometers to determine stance and swing phases in hemiplegia. Willemsen mounted the accelerometers on mechanical links attached laterally to the leg. This added encumbrance to the individual, and limited its application. Crutch and foot forces have also been used as inputs to rule based intention detectors (Andrews et. al., 1989, Kirkwood and Andrews, 1989). Symmons et. al. proposed a combination of myoelectric potential, crutch forces, foot contact patterns, and vertical acceleration of the thigh for trigger signals (Symmons et. al., 1986). Both the Symmons' and the Andrews' systems require a large number of interconnected sensors to provide feedback for the controller, and hence would be difficult to work with clinically. The external bracing of Willemsen, complex wiring of Symmons and Andrews, and day to day training required by Kirkwood and Kostov restricted the potential application of their respective devices. Liberson's system has had the most clinical success of this group, due

to the ease of application of his device; future designs of the sensor system should limit the number of sensor sites and interconnecting wires.

Many drop foot systems have appeared commercially, such as the WalkAide™ based on work by Dai et. al, the Odstock drop foot stimulator, and the MicroFes™ system presently distributed from Ljubljana. In the Odstock and MicroFes™ systems, foot switches were used to control a surface stimulation pattern. In the WalkAide™, a tilt sensor determines stance and swing. However, the clinical indications required for use of the device, such as normal and not spastic activity of the gastrocnemius - soleus muscle group, limit the population that can be assisted. Further refinements of the system are required in order to widen the population that could be assisted by these devices.

Descriptions of closed loop FES systems for paraplegic standing and walking often include joint angles as input variables for the controller. Kirkwood et. al. expanded automatic gait event detection from two to four phases (Kirkwood et. al., 1989). They used machine learned rule induction based on knee and hip angles, and foot forces. They defined four gait phases: maximum right knee flexion to maximum right hip flexion, maximum right hip flexion to maximum left knee flexion, maximum left knee flexion to maximum left hip flexion, and maximum left hip flexion to maximum right knee flexion. Their rule-based controller used these same joint angles to determine the gait phase. It was not discussed if attributes such as angular velocity derived from joint angle were used for inputs. By using the angular velocity of the joints, the four gait phases described in this study should be determined accurately without the necessity of rule induction. However, the advances of this study could be considered the discussion of the redundancy of the sensors used to determine the gait phases, and demonstration of machine learning as a tool for detection of multiple gait phases.

Ng and Chizeck (Ng and Chizeck, 1997) used knee, hip, and ankle angle and angular velocity to determine gait phases. These variables, along with their simple derivatives, were inputs for a fuzzy logic based gait phase detection system. Ng and Chizeck detected five gait phases: weight acceptance, mid-stance, terminal stance, early swing and late swing, and compared the performance of the detector with a video taped recording of the paraplegic walking. The stimulation sequence used to generate the

walking patterns was not described beyond noting that a switch was used to trigger the stepping pattern. The overall accuracy of the gait phase identification technique was below 75% on a sample by sample basis. Possible future refinements of the system are described that could lead to better results.

Kobetic and Marsolais (Kobetic and Marsolais, 1994) used the gait phases as defined by Perry (Perry, 1992) to develop electrical stimulation patterns that compensated for the absent motor control in each of these gait phases. They coordinated the stimulation of 38 electrodes to control the gait pattern. Feed-forward control was used within each gait cycle. The feed-forward control routines were based on a timing sequence initiated at heel contact. The gait patterns were evaluated on the degree that each approximated a normal gait pattern. Stepping cadences were approximately 65 steps/min, and speeds of 0.6-0.8 m/s were measured. Muscular fatigue was described as a problem in the implementation of this technique. It was suggested that fuzzy logic could be used to enhance this controller. However, it was not indicated whether fuzzy logic would be used to trigger multiple stimulation patterns, as suggested by the work of Chizeck, or if fuzzy logic would be used to refine the feed-forward control routines, as suggested by the work of Crago et. al. (Crago et. al, 1996).

Abbas et. al. (Abbas et. al. 1991) examined closed loop control of coronal hip angle in individuals. He noted that closed loop control performed better than open loop control for postural positioning and that day to day deviations were reduced using closed loop control.

Closed loop control has been modeled for sit to stand maneuvers in which the endpoint velocities were thought to be potentially damaging. Dolan et. al. (Dolan et. al., 1998) have modeled and performed one human trial using a switching curve to regulate stimulation patterns. Davoodi and Andrews (Davoodi and Andrews, 1998) used genetic algorithms to perform closed loop control of standing and sitting. For both of these controllers, the continuous detection of knee flexion angle and angular velocity is necessary. The method for obtaining these angles was assumed to be from a goniometer.

Wood et. al. (Wood et. al., 1998) performed physical trials of quiet standing using closed loop PID control of the knee flexion angle. Knee angle was detected by a

potentiometer worn in a neoprene knee brace. Using this arrangement, the sensor required calibration prior to trial. This could be distracting for everyday implementation.

Granat et. al. (Granat et. al, 1992) used a one-step ahead controller to accommodate for a habituating knee flexion withdrawal response. Franken et. al. (Franken et. al. 1995) followed this study by describing a cycle to cycle controller. They noted that although the instantaneous control of the angle of the knee is not important. However, the knee flexion angle and hip angle at the endpoint of the swing phase are important, and determined these angles with goniometers. Appropriate hip and knee flexion angle ranges could be maintained by adjusting stimulation parameters using the cycle to cycle controller. These studies highlight a further problem for FES controllers. The force derived from electrical stimulation of a muscle is dependent upon the angle, angular velocity, and fatigue of the muscle as well as the positioning of the electrodes. Open loop or feed-forward control account for angle and angular velocity dependence, but are unable to reconcile deviations due to fatigue and electrode placement. Feedback controllers, which evaluate the performance of the system, could refine feed-forward control routines to achieve a better stimulation paradigm, as noted for the cycle to cycle controller.

In each of the above controller descriptions, a joint angle has been used as feedback for the system. The electrogoniometer has been the sensor used in all of these trials, save Wood et. al. and Kobetic et. al., to determine the angles across the joint. This device has not been proposed for application outside the laboratory, possibly due to its high power consumption. Crago et. al. (Crago et. al., 1986) note that this device could be used for feedback control of the knees and ankles. However, the device required calibration prior to each sit to stand transition due to the slipping of the mountings. This problem makes this device inappropriate for use outside the laboratory. The application of each of the controllers listed above is limited by the application of the goniometer. A new method for detection of joint angles could allow for the further realization of these control techniques.

Goniometers are self contained methods for measuring joint angles. Other methods of determining joint angles, such as photography (Murray, 1967) are not self contained hence unsuitable for feedback control of FES.

An electromagnetic system is a possible alternative method to goniometric determination of joint angles. The initial positioning and orientation of the devices, and interference due to magnetic materials could pose problems for accurate reconstruction of angles. A commercial electromagnetic system was used to characterize the position and orientation of a mechanical ball and socket joint (An et. al, 1988). Other commercial systems, such as the Flock of Birds™ and Motion Star™ are also available. Phase and magnitude information (Lou et. al., 1997) has been described to determine relative position and displacement of a transmitter/receiver pair. Chandler (Chandler, 1973) used synchronous detection of magnetic transmitter and receiver coils to obtain finger and wrist joint angles. The placement of the coils was critical to the accuracy of the device, and the response of the system was nonlinear. Calibration for each individual subject was necessary. In each of these cases, the relative position of the transmitter to the receiver was determined. This is a problem in lower limb FES, as the entire body will move during a gait cycle and a stationary point of the body might not be resolved to use as a reference.

Optical (Kunz and Dubendorfer, 1997), conductive (Johnson et. al., 1981), and discrete goniometers (Roth et. al., 1981) have been described. Alignment of optical goniometers would be difficult, as they are not traditionally used for medical applications. A consistent line of sight between the two ends of the optical goniometer is required by this system. The conductive goniometer proposed was highly nonlinear. Although this signal could be digitally linearized, compensation could not be made for rotations about other axes. The digital goniometer requires that the axis of rotation to be centered about the axis of rotation of the joint, which is difficult and potentially encumbering in the knee.

Many goniometric systems have used an exoskeleton to accurately measure joint motion in three dimensions (Johnston and Schmidt, 1969, Lamoreux, 1971, Chao, 1978, 1980, Mills and Hull, 1991, Perry and Antonelli, 1981). These systems involved a mechanical assembly to strictly measure angles in a number of dimensions. Precision potentiometers have been used to determine joint angles. Petrofsky et. al. (Petrofsky et.

al., 1984) used this type of system for feedback control of walking on a treadmill. A treadmill was used in the experiment to ensure that the patient did not move too far from the electronics required to record the goniometer signals. These goniometers also included rigid mechanical linkages used to isolate rotations to a predetermined axis. The encumbrance of these devices limits their potential application to practical feedback control systems for FES.

Implantable goniometers, based on Hall effect transducers implanted in the bone, have been investigated to reduce the encumbrance to the user. Only qualitative results are available for the application of the device in the hand (Johnson and Peckham, 1994, Strojnik et. al, 1995), and the device is not widely available.

Control of quiet standing is another area that needs to be addressed by a sensor and signal processing system for lower limb FES. Veltink (Veltink and Franken, 1996) used accelerometers to determine simulated knee buckling in able bodied subjects. This technique has not been applied to control for FES, and it is questionable if accelerometers attached to the thigh during paraplegic standing would provide a signal of high enough precision for threshold detection for effective knee buckling control. Mulder et. al. (Mulder et. al., 1992) described a hysteresis loop for control of prolonged FES standing using goniometers. He reported that the duration of standing, until fatigue, could be increased by 2.5 to 12 times and muscular torque decreased.

Andrews (Andrews et. al., 1989) described a feedback controller for prolonged standing incorporating an above knee prosthesis instrumented with a strain gauge. The use of force across an ankle foot brace could predict knee buckling. However, a zero frequency, i.e. DC, sensitive strain gauge was used. The DC level of the strain gauge moved with redistribution of the weight, hence a single threshold of the DC level was insufficient in detection knee buckling.

Based on closed loop tests similar to those reported by Petrofsky, it has been suggested that artificial sensors are not suitable for everyday use (Johnson et. al., 1995). However, feedback control of FES walking and standing is consistently suggested as an improvement for most systems. Kobetic and Marsolais (Kobetic and Marsolais, 1994) use preprogrammed feed-forward control for FES walking in lieu of feedback control as

available sensors are not appropriate, and mention feedback control as a necessary advancement for further application of FES (Kobetic and Marsolais, 1994, Marsolais and Kobetic, 1988, Franken et. al., 1995). Hambrecht (Hambrecht, 1972) noted this early in the development of the FES field, mentioning the necessity for miniaturized sensors and controllers that do not require conscious effort of the patient.

For this reason, the naturally occurring myoelectric and epineural potentials have been considered for use in FES control. Myoelectric potentials are a primary source of joint control in the upper limb. They have used voluntary contractions of intact muscles as a high level state controller (Chandler, 1973, Hildebrant and Meyer-Waarden, 1984, Sexena et. al., 1995, Hart et al., 1998, Scott et. al., 1996, Graupe, 1998) of FES contractions of paralyzed muscles. In these systems, the myoelectric potentials measured from an intact muscle group are used to trigger a feed-forward control routine.

There are problems in attempting to use myoelectric potentials for feedback control of lower limbs. The myoelectric potential of a muscle may provide feedback of the force of the muscle. However, the position, velocity, and fatigue of the muscle, and the position of the electrode with respect to the active motor units affect the relationship between force and the myoelectric potential. This is simplified in FES, as a single level of stimulation should consistently recruit the same motor units and produce repeatable, fatigue dependant M waves. Graupe compensated for fatiguing muscles based on the shape of the M wave (Graupe et. al., 1988). Subsequently, Erfanian et. al. (Erfanian et. al., 1998) produced a model relating the EMG during an isometric contraction to force of the contraction. The model that was produced compensated for fatigue. Models have been developed to compensate for limitations due to length and velocity changes (Shue et. al., 1995) and have been suggested for use in adaptive control of neural prostheses. However, a complete relationship of muscular force as a function of myoelectric potential in dynamically moving muscles has not been reported. Even with an accurate measure of muscle force due to FES, the application to lower limb FES is not direct. Most lower limb FES systems use joint position and not joint forces for feedback variables.

Graupe (Graupe, 1989) produced an event triggered FES system which discriminated four states of walking by analysis of myoelectric potentials from the erector

spinae. The individual would make a postural change to prepare himself/herself for the next step. Individuals were trained to produce repeatable myoelectric potentials of the erector spinae used for control. Feed-forward control was used during each cycle of the gait. Although these myoelectric potential signatures were expected in preparation for the next cycle, training of the individuals was required to achieve a proper discrimination, adding a cognitive burden to the physical demands of walking.

Sensory feedback from epineural potentials is also being investigated, primarily for slip and touch control. Upshaw and Sinkjaer and Haugland and Sinkjaer (Upshaw and Sinkjaer, 1997, Haugland and Sinkjaer, 1995) investigated heel strike and heel lift off detection from epineural potentials. This could enable a completely implantable device for the control of drop foot. The detection accuracy from this method is greater than 90%. Haugland and Hoffer (Haugland and Hoffer, 1994) have examined detection of slip for control of hand function.

Epineural control has been discussed for the detection of joint angles. Models for single Ia afferents, which contain length and velocity information from the muscle, have been well documented (Prochazka and Gorassini, 1998 a, b).

Sinkjaer et al. (Sinkjaer et. al., 1997) investigated whole nerve recordings to determine joint angle. They detected joint angle from a passively moving joint, in which the nerve activity was dominated by muscle spindle activity. The activity of tendon organ afferents was reported as a possible complicating factor of the technique. This also precluded the use of nerve recordings from stimulated muscle.

Yoshida and Horch (Yoshida and Horch, 1996) demonstrated closed loop control of ankle motion in an acute animal study. The range of motion for the ankle was small, and intrafascicular electrodes were used to obtain precise recordings of the epineural potential. It was noted that migration of the intrafascicular electrodes could limit further application of this approach (Sinkjaer et. al., 1997).

The advent of micro-machined electromechanical sensors (MEMS) provides an opportunity for new sensors to be applied to FES. These sensors are miniature and convenient to use, the necessities noted by Hambrecht (Hambrecht, 1972).

Accelerometers and rate gyroscopes, available in the development of MEMS, are low cost, robust and commercial available.

Accelerometers have been widely used in gait analysis. Multiple accelerometer combinations have derived angular acceleration, velocity, and tilt of a leg through integration (Morris 1973, Smidt, 1977). In the field of FES, Willemsen et. al. (Willemsen et. al., 1991, Willemsen et. al, 1990 a,b) proposed a signal processing method using accelerometers to obtain the knee joint angle and angular velocity. The accelerometers were mounted to metallic rods aligned with the shank and the thigh. An assumption was made that these rods would rotate within a single plane. A novel analytical formula that avoided numerical integration determined the angular kinematics. Heyn et. al. (Heyn et. al. 1996) extended this study by using rate gyroscopes to directly measure the angular velocity of the leg segment. Unfortunately, the mounting rods of the sensors could be too encumbering for daily use.

Rate gyroscope signals can be used to estimate joint angle by numerical integration. However, the rate gyroscopes typically display a non-zero offset, referred to as a DC component, when at rest. Drift of this DC component, commonly due to temperature, leads to unbounded error of the integral. Miyazaki (Miyazaki, 1997) and Kataria and Abbas (Kataria and Abbas, 1998) low pass filtered the rate gyroscope output to determine the DC component, and integrated the residual signal to determine angle. Hentry (Hentry and Ewins, 1998) compensated for the drift at the end of each step in a walking trial. Since the angles are not calculated in real time, this technique could not be used for control purposes.

Silicon based MEMS have a potential to be used for FES control. These sensors are now readily available, are small in size, and are low power. These sensors could be incorporated within the bracing or surface electrode systems and do not add encumbrance to the user. The sensors also have the potential to be implanted with a neural prosthesis. This would allow for a completely implantable neural prosthesis.

Modern signal processing techniques, such as machine learning algorithms, hand crafted rule bases, and inductively learned rule bases, have been applied to sensor signals to generate variables that could be used for control of FES. The drawback in these

methods was not in the failing of the signal processing techniques, but in the choice of sensors used. For this reason, the approach was taken to choose sensors that could be conveniently placed on the body, possibly to be implanted or incorporated into present components of the neural prosthesis, and apply the signal processing techniques to generate the control signals commonly used in lower limb FES. Design goals of limited encumbrance, don/doff time and reliability were considered in constructing the sensor system. The sensor system should also be low profile, and use the same sensors for the detection of control states and variables within the state.

1.3 Nerve Blocking

Further refinements for FES control could be achieved if spasticity could be suppressed through nerve blocking. Three techniques that are presently investigated are anodal blocking, collision blocking, and blocking by high frequency activation.

1.3.1 Anodal Blocking

Rijkoff (Rijkoff et. al., 1997, 1998) has investigated blocking by anodal currents, as suggested by Brindley and Craggs (Brindley and Craggs, 1980), to produce a hyperpolarization of the neural membrane. The action potential is unable to propagate through the hyperpolarization, and hence a transmission block of the nerve is produced. Chronic application of this technique could be limited. The waveform that is used is monophasic, and could compromise the integrity of the electrodes (Robblee and Rose 1990). Rijkoff does not discuss this concern in his assessment of the technique. Rijkoff proposed selective activation of small axons by this block. Selective activation was achieved by using large cathodal currents to depolarize all of the axons, and a smaller anodal current to hyperpolarize the large axons. Hence, propagation of the action potential would only occur in the small diameter axons. However, the depolarization of the small, pain sensing axons could be a deterrent if applied to a mixed nerve as would be seen in the control of phasic spasticity.

1.3.2 Collision Blocking

Mortimer et. al. investigated collision blocking through quadratrapezoidal waveforms (Grunewald et. al., 1998, Sweeney and Mortimer, 1986, van den Hornet and Mortimer, 1981 a,b). Unidirectional action potentials were generated by cuff electrodes. The action potentials propagated only in the proximal direction from the stimulating electrode, colliding with action potentials that would be generated by spasticity or other neural muscular stimulation.

By adjusting the current level used, Fang and Mortimer (Fang and Mortimer, 1991) demonstrated that small diameter axons could be activated without activating larger diameter fibers. van den Hornet and Mortimer had previously reported that the quadratrapezoidal pulses could cause bidirectional activation of small diameter fibers. Refinements of this technique have included changes in the shape of the cuff electrode (Sweeney and Mortimer, 1986).

This technique has only been proposed for work on motor nerves. The unipolar activation would elicit action potentials in the Ia and gamma afferents in addition to the motor fibers that the technique is attempting to block. The reflexes associated with the mass activation of the Ia afferents, which lie within the diameter range of the motor fibers, would be activated. Additionally, the block is suggested to cause bi-directional activation of the small diameter fibers within the axon (Fang and Mortimer, 1991, van den Hornet and Mortimer, 1981). Noxious stimulus due to the stimulation of the small diameter, pain sensing axons would prevent this technique from being applied in mixed nerves.

The effects of chronic use of this technique can be hypothesized based upon the work conducted by Agnew and McCreery (Agnew et. al., 1990). They demonstrated that repeated action potential generation in a nerve even at frequencies as low as 50 Hz can cause early axonal death when sustained for 8 hours. Early axonal death was attributed to the continuous mass activation of the nerves. This continuous, mass activation of the nerve is necessary for collision blocking. If collision blocking is applied to suppress spasticity, it could require 8 hours of stimulation a day, at a duty cycle of 50%. This type

of chronic evaluation of collision blocking investigating early axonal death has not been published to date.

1.3.3 Blocking through high frequency activation

Shaker et. al. (Shaker et. al., 1998) used repetitive stimulation at 600 Hz to produce a muscular block based on previous reports of Solomonow (Solomonow, 1984). At this frequency, the motor units of each axon stimulated are unable to produce a muscular contraction. This technique has great susceptibility to the early axonal death, described by Agnew and McCreery. Based on Agnew and McCreery's report, continuous stimulation at 600 Hz for 8 hours a day at a 50% duty cycle, as could be necessary to suppress phasic spasticity, could lead to early axonal death.

The present methods of nerve blocking have not been explored for control of phasic spasticity, and might not be appropriate. Collision blocking and blocking through repetitive stimulation requires high frequency activation of the nerve. The chronic effects of these stimulation patterns have not been explored, but potentially cause early axonal death. Anodal blocking uses monophasic stimulation, which compromises electrode integrity. A safe and effective method for blocking of peripheral nerves is necessary. From the work of Agnew and McCreery, the desired block should not cause activation of the nerve. Additionally, for control of phasic spasticity, the block should be able to be turned on and off quickly. If used in mixed nerves, the block should not cause activation of the smaller diameter fibers.

1.3.4 A Possible Localized Action Potential Transmission Block

Rattay (Rattay, 1990) presented a possibility for a neural block that is exhibited in models of axons. This block was localized to the area of the stimulation, and the electrical currents that caused the block were biphasic. Additionally, the block did not continuously generate action potentials.

Tanner (Tanner, 1962) demonstrated a nerve block produced by 20 kilocycle (kC) [sic] oscillating current of unspecified shape and amplitude, that suppressed the compound action potential recordings in dissected frog nerve. Woo and Campbell (Woo and

Campbell, 1964) followed this study and described a tetanic contraction elicited by 20 kC monophasic pulses applied to dissected cat nerves. They also demonstrated that the 20 kC current could produce a localized transmission block of action potentials in an isolated cat neuron.

Solomonow (Solomonow, 1984) used rectangular monophasic pulses in the range of 600 Hz to 20 kHz. He produced a block of the muscular contraction over the entire range of frequencies. He attributed the muscular block to an endplate depletion mechanism, although did not test this hypothesis. Shaker et. al. (Shaker et. al., 1998) applied Solomonow's blocking technique for the control of micturition. Using a single bipolar electrode, they interspersed 30 Hz stimulation of fiber diameters with 600 Hz stimulation of the large diameter fibers, and produced a block of the contraction of motor units innervated by large diameter axons and contraction of the motor units innervated by small diameter axons. Their results were consistent from trial to trial but did not achieve the 100% blocking effectiveness reported by Solomonow.

Muller (Muller, 1969) placed a monopolar electrode 2 cm from a dissected frog nerve and blocked the conduction of action potentials by using a 5 kHz waveform of an amplitude of two to six times the threshold for stimulation. It was not described if the conduction block was either a conduction block or fatigue block. He referenced a previous hypothesis that middle frequency currents can lower the resting membrane potential of the axon without eliciting a full depolarization. He was unsure how the 5 kHz waveform could cause this depolarization.

Bowman (Bowman, 1985) provided an extensive description of high frequency currents for electrical nerve blocking. Bowman's experimental setup included proximal and distal stimulating electrodes, with a blocking electrode placed in between. In his experiments, he recorded both action potentials of single nerve fibers and muscular force. He described that high frequency electrical currents could cause a block of muscular contraction by two separate mechanisms. The first block of muscular contraction was due to fatigue at the neuromuscular junction, characterized by an inability of a distally placed electrode to cause stimulation of the muscle. The recovery time for the muscle was in the order of 30 seconds. The second block of muscular contraction was due to a local nerve

conduction block. This block allowed a distally placed electrode to generated muscle twitches. He reported that the frequency range for the two blocking methods overlapped. The muscular junction block occurred at lower currents and the localized conduction blocking occurred at higher currents. His results varied from trial to trial and were conducted on 25 cats. His explanation for variation in results was due to technical difficulties of the procedure.

Bowman (Bowman, 1985) also described a block in a human nerve. He used the previously described technique, both a distal and proximal stimulating electrode with a blocking electrode placed in the middle, to distinguish between a localized conduction block and a muscular junction block. In only one of the three individuals tested, a local conduction block was observed. An explanation for the variance of these results from trial to trial was not included.

Bowman (Bowman, 1985) modeled the effect of an increased intracellular Na^+ level within the nerve, and concluded that a localized transmission block could be achieved through a local increase in the Na^+ level within the axon.

The results from tests performed on animals that described a block of muscular contraction due to high frequency electrical stimulation are varied and inconclusive. Most of the groups used monophasic current pulses. Woo and Campbell (Woo and Campbell, 1964) described a tetanic contraction of the muscle. Solomonow (Solomonow, 1984) hypothesized but did not test if the block was muscular in nature. Bowman's circuit included capacitive coupling of the output of a monophasic source. His experiments of cat and human nerve had various results. Woo and Campbell (Woo and Campbell, 1964) and Muller (Muller, 1969) reported that the conduction of action potentials in a single nerve fiber could be blocked, as suggested by Rattay's model. The experimental protocol necessary to distinguish between these two conditions has not been used in each experiment. Hence, each report of a block of muscular contraction due to the high frequency electrical stimulation could be due to either a localized conduction block of the axon, or fatigue at the neuromuscular junction.

Rattay's description of the blocking within a model of the axon provides a different direction. Through the models, the results of the individual animal tests could be validated

for the different protocols. Additionally, the mechanism for the blocking procedure could be proposed. From experiments conducted on models of axons, an experimental protocol could be conducted to specifically reinforce or disprove localized axon conduction blocking in animal tests.

Ionic currents of axons have been modeled by a number of groups. Hodgkin and Huxley (Hodgkin and Huxley, 1952) produced the seminal work in this area with the giant squid axon. Frankenhauser and Huxley (Frankenhauser and Huxley, 1964) described the ionic currents in the myelinated frog axon. Chiu et. al. (Chiu et. al., 1979) described the currents in the rabbit axon and compared their results to the frog. Sweeney (Sweeney et. al., 1987) completed the numerical description of this work. Schwarz and Eikhof (Schwarz and Eikhof, 1987) described the action potentials in the rat and cat axons. In 1995, Schwarz, Reid, and Bostock (Schwarz et. al., 1995) described the ionic currents in human nodes of Ranvier.

These models of the currents at individual nodes can be incorporated into a cable model describing the conduction of the action potential through the axon. McNeal (McNeal, 1976) described a model of the conduction that assumed the myelin sheath was a perfect insulator. Rattay (Rattay, 1990) has adapted this model to include stimulation from external stimulus.

The inclusion of the active nodal kinetics into a model for conduction in an axon has been previously reported. Reilly et. al. (Reilly et. al., 1985) imported ionic currents of the FH equations into the cable model described by McNeal, naming the result a spatially extended nonlinear node model (SENN). Frijns (Frijns et. al., 1994 a,b) has also described a SENN model using both the FH and the SE equations for applications in cochlea. He has matched the characteristics of repetitive firing, conduction velocity, and currents across the membrane as described by the model for cats at both 20 and 37 °C. When incorporating his model with a myelin sheath, the conduction velocity of his model dropped to one half of the expected conduction velocity for an axon of that size. There are other descriptions of cable models of the nerve with active nodes (Stephanova and Bostock, 1995, Halter and Clark, 1991). However, each is limited, as they adjust the ionic

currents described by the published ionic current model, or adjust the parameters of a cable model to produce results that can be measured experimentally.

The animal studies suggest that a conduction block might exist, although it has eluded investigators using only animal trials. However, models of axons can be generated, and have been used previously to describe properties of nerves. Rattay has suggested through models that a localized nerve blocking technique could exist, however, he did not characterize the effects of the block. This suggests a more extensive investigation of nerve blocking first through models be conducted, with the subsequent findings to be confirmed or refuted through previous descriptions in the literature or new physical trials.

The method used to produce an electrical nerve block must exhibit a number of characteristics that could be tested in the models prior to a physical trial. First, it must be safe to use. It should not excite the intact nervous system, whether to initiate pain or reflexes. The currents that are used should have a zero DC component to maintain the integrity of the electrodes. It should also be possible to turn the block on and off in accordance with the resolution of the control and sensing techniques. Present nerve blocking approaches do not resolve these issues, although biphasic stimulation could offer a solution.

1.4 Thesis Hypothesis and Objectives

A feedback controlled neural prosthesis that could control both the stimulation and blocking of axons has not been proposed even though techniques for nerve blocking and feedback control have been described previously. This type of neural prosthesis should be able to address two fundamental problems of upper motor lesions, i.e. muscular weakness and spasticity. This neural prosthesis would combine stimulation or nerve blocking with the sensor system. The switching dynamics for the control in the neural prosthetic would be limited by both limited by time required to turn the block on and off, and the temporal resolution of the gait phases. Similarly, the precision of the control of joint angles is limited by both the level of precision for the selectivity of the axons and corresponding motor units, and the level of resolution of the joint angles.

Most FES systems have not achieved widespread use, possibly due to the complexity of the sensor or stimulator systems and limited effectiveness. The development of implants reduces the cumbersome donning and doffing times of surface electrode systems, hence increasing the effectiveness and decreasing the complexity of the system to the user. Feedback control, commonly mentioned as a requirement to deal with fatigue in FES, has been well documented based on sensor variables.

Two obstacles still preclude the development of a feedback controlled neural prosthesis that includes stimulation and nerve blocking. Feedback controlled FES requires a sensor system. The controllers that are being developed for FES use feedback variables such as joint angle, gait phase, and knee stability. Previous techniques using artificial sensors were limited by the bulk and encumbrance of the sensors and the number of interconnecting wires. The recent production of MEMS in conjunction with signal processing techniques could overcome these limitations.

There are two types of feedback for finite state control of FES. Sensors are used to determine states in which a control routine would be active. The determination of states can be as simple as a handswitch that indicates a desire to start a standing routine, or a gait event detector that would initiate a feed-forward or feedback controller during the gait cycle. Sensors are also used by a feedback controller within a state to maintain a desired trajectory of motion, and by an adaptive feed-forward controller to adjust a stimulation paradigm in response to fatigue.

Based upon these sensors, feedback control of nerve stimulation and blocking could occur. Electrical nerve blocking has not been proposed for the reduction of phasic spasticity, commonly seen in pathological lower limb movement.

Spasticity exists in the individuals with upper motor lesions. Both muscle weakness and undesired muscle actions can restrict individuals from accomplishing motor tasks. Electrical nerve blocking has not been described for suppression of phasic spasticity during gait. However, the literature and available models of ionic currents within the nodes of Ranvier suggest that localized and dynamic transmission block of the nerve could exist. Further investigation in this area is warranted. This could be tested first in computer models and validated in animal trials.

The following hypotheses were formulated based on the literature review.

H1) that modern signal processing techniques used with specifically placed sensors can estimate state variables for neural prosthetic control of locomotion. This was divided into three testable objectives.

1a) Knee flexion angle and angular velocity in sit to stand and stand to sit transitions can be determined in real time to the same accuracy as a Penny and Giles goniometer through signal processing and the new sensor system. This will be tested in sit to stand trials involving able bodied and paraplegic individuals. The manufacturers of the goniometer specify the nonlinearity of the device as 2 degrees, with 3 degrees of error due to cross talk. If the accuracy of the sensor system and signal processing is within the accuracy of the goniometer, the hypothesis will be supported.

1b) The sensor system can detect gait phases in real time. The required precision for the timing of a multiple gait phase predictor has not been documented. However, the technique for determining stance and swing by a commercial system has been described. From this, a required time precision of the gait phase detector is implied. Gait phase detection will be tested in a walking trial of able-bodied volunteers. If the precision of the multiple gait phase detector is similar to that of the reported commercial system, the hypothesis will be supported.

1c) The sensor system can provide a predictive signal of incipient knee buckling when wearing a floor reaction orthosis (FRO). Recordings of the sensor system will be made for multiple knee buckles performed in a trial with a paraplegic volunteer. The hypothesis will be supported if a predictor is able to determine a knee buckle before the knee reaches 175 degrees of extension.

H2) that a safe, localized and dynamic peripheral nerve block can be achieved electrically. This will be examined using four testable objectives.

2a) High frequency electrical stimulation applied to spatially extended nonlinear nodal (SENN) models will produce a localized block of axon transmission. This was examined in 4 SENN models. A localized block will allow for conduction of

action potentials generated on either side of the block but not through the area of the block. If a localized block is displayed in the computer models, the hypothesis will be supported.

2b) The block determined by the spatially extended nodal kinetic model is resistant to changes in the parameters of the model. Altering the nodal kinetics of the SRB model will test the stability of the block. If the alteration of nodal kinetics of the model does not change the block qualitatively, the hypothesis will be supported.

2c) The block determined by the spatially extended nodal models of the axon can be generated if noise is added to the high frequency blocking signal. If the models demonstrate that noise added to blocking signal does not prevent a localized block of the nerve from occurring, the hypothesis is supported.

2d) The localized electrical nerve block determined from the models can be demonstrated in an animal. If the results of hypothesis 2a are displayed, then the models are accurately representing the results from animal trials, and the hypothesis is supported.

The thesis experiments are formatted into the following papers/chapters.

1) **Gait phase detection using artificial sensors:** This paper applies a low profile sensor set to the problem of gait phase detection. Three accelerometers are placed below the knee. From their signals, five gait phases are determined. By constraining the size of the sensors and the location, the design criteria for a sensor system for a neural prosthesis are met.

2) **Determination of knee flexion angle and angular velocity during sit to stand transitions using accelerometers and rate gyroscopes**. This paper will discuss the extraction of the state variables of knee flexion angle and angular velocity from the low profile clusters of accelerometers and rate gyroscopes. Knee flexion angle and angular velocity are variables that are used in the closed loop control methods proposed by other investigators. Knee flexion angle and angular velocity were

estimated by the combination of rate gyroscopes and accelerometers in both an able bodied and a paraplegic subject.

3) **A sensor system for functional electrical stimulation**. A single set of sensors is used to determine joint angle, gait phase, and knee stability. This paper will combine the detection of knee flexion angle and angular velocity for stand to sit and sit to stand transitions, the detection of gait phases, and the prediction of knee instability.
4) **Electrical Nerve Blocking I: Computer Simulations.** This paper describes a potential for electrical nerve blocking on the basis of frequency and fiber diameter in SENN models of the FH, SE, CRRSS, and SRB. The paper discusses the problems with potential use of the block, and the various effects due to high frequency stimulation. A mechanism hypothesizing the cause of the block is proposed.
5) **Electrical Nerve Blocking II: Practical Implications.** This paper looks more in depth into practical issues of a prediction of nerve blocking from computer modeling. Noise is added to the blocking waveform and the effects are noted. Variation of the models' parameters is investigated. A physical trial on a rat is discussed.

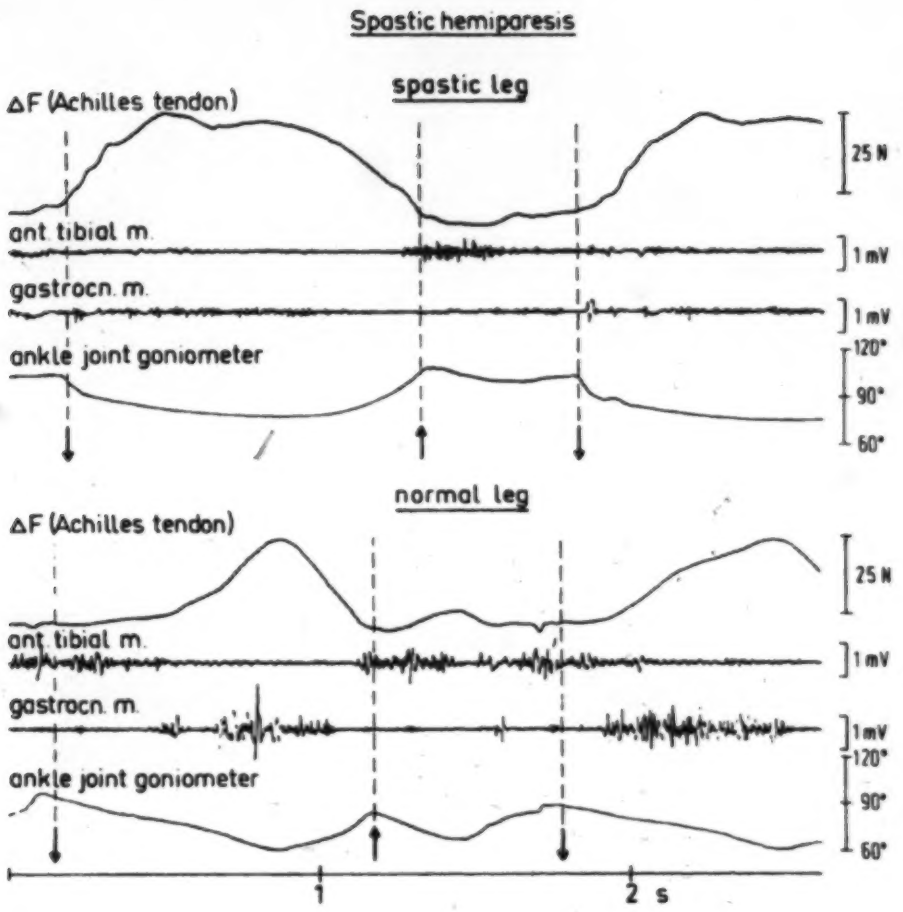

Figure 1.1. EMG and Achilles tendon force recordings during walking for an able bodied individual and one with spastic hemiplegia. The up arrows represent toe off. The down arrows represent heel contract.

(Top) The weak but spastic gastrocnemius EMG recording is shown. The normal burst of activity prior to swing not generated. Additionally, premature onset of the gastrocnemius is seen during swing that continues through early stance, disabling normal heel rocker motion.

(Bottom) A normal EMG recording of the gastrocnemius and Achilles tendon force is shown. A burst of activity in the gastrocnemius occurs prior to swing. The onset of EMG activity in the gastrocnemius is in mid-stance.

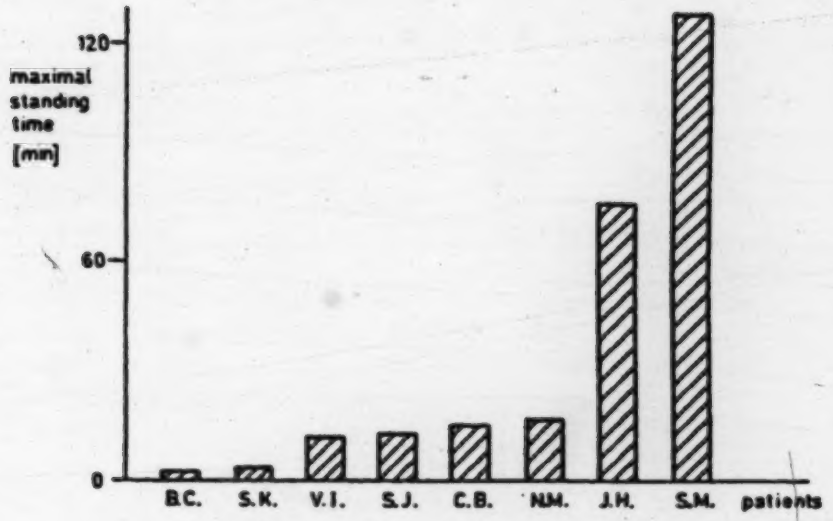

Figure 1.2. Maximum standing duration for paraplegic individuals assisted by FES. The subjects stood assisted by surface FES applied to the quadriceps. The maximum standing duration was determined by duration in which the force from quadriceps stimulation was sufficient to maintain standing. Subjects J.H. and S.M. had contractures of the Achilles tendon. These contractures allowed for prolonged standing by restricting dorsiflexion of the ankle.

1.5 Bibliography

Abbas, J.J., and Chizeck, H.J. (1991), "Feedback control of coronal plan hip angle in paraplegic subjects using functional neuromuscular stimulation", IEEE Trans. BME 38(7) 287-298

Albright, A.L. (1996), "Intrathecal baclofen in cerebral palsy movement disorders", J. Child Neurology 11: (Suppl 1): S29-35

An, K.N., Jacobsen, M.C., Berglund, L.J., Chao, E.Y., (1988) "Application of a magnetic tracking device to kinesiologic studies", J. Biomech. 21(7):613-20

Andrews, B.J, Barnett, R., Phillips, G., Kirkwood, C., Donaldson, N., Rushton, D., and Perkins, T. (1989), "Rule Base control of a hybrid FES orthosis for assisting paraplegic locomotion", Automedica, 11:175-199

Andrews, B.J., and Baxendale, R.H., (1986) "A hybrid orthosis incorporating artificial reflexes for spinal cord damaged patients", J. Physiol. 19P

Andrews, B.J., and Wheeler, G.D. (1995), "Functional and therapeutic benefits of electrical stimulation after spinal cord injury", Curr. Opin. Neurol. 8:461-6

Agnew, W.F., McCreery, D.B., Bullara. L.A., and Yuen, T.G.H. (1990), "Effects of prolonged electrical stimulation of peripheral nerve", Neural Prostheses: Fundamental Studies, Prentice Hall, Englewood Cliffs, NJ 07832

Bajd, T., Kralj, A., Krajnik, J., Turk, R., Benko, H., and Sega., J., (1984) " Standing by FES in paraplegic patients", Proc. 8th Int. Symp. Ext. Contr. Hum. Extr., Dubrovnik

Bhadra, N., and Peckham, P.H., (1997) "Peripheral nerve stimulation for restoration of motor function", J. Clin. Neuro. 14(5):378-93

Bowman, B.R. (1981), "Electrical Block of Peripheral Motor Activity", Ph.D. Thesis, Edvard Kardelh University of Ljubljana

Bracken, M.B., Shepard, M.J., Holford, T.R., Leo-Summers, L., Aldrich E.F., Fazl, M., Fehlings, M., Herr, D.L., Hitchon, P.W., Marshall, L.F., Nockels, R.P., Pascale V., Perot, P.L. Jr., Piepmeier, J., Sonntag, V.K., Wagner, F., Wilberger, J.E., Winn, H.R., and Young, W., (1997) ,"Administration of methylprednisolone for 24 or 48 hours or tirilazad mesylate for 48 hours in the treatment of acute spinal cord injury. Results of the Third National Acute Spinal Cord Injury Randomized Controlled Trial", JAMA 277:(20):1597-604

Brandell, B.R., (1982) "Development of a universal control unit for functional electrical stimulation (FES)," Am. J. Phys. Med. 61(6):279-301

Brindley GS. Craggs MD. (1980) "A technique for anodally blocking large nerve fibres through chronically implanted electrodes" J. Neurology, Neurosurgery & Psychiatry 43(12):1083-90

Chandler, S.A.G., (1973) The control of limb movements by functional electrical stimulation, Ph.D. Thesis, University of Southampton

Chao, E.Y., (1978)"Experimental methods for biomechanical measurement of joint kinematics", CRC. Handbook of Bioengineering in Medicine and Biology, 1:285-411

Chao, E.Y., (1980), "Justification of triaxial goniometer for the measurement of joint rotation", J. Biomech. 13:989-1006

Crago, P.E., Chizeck, H.J., Neuman, M.R., and Hambrecht, F.T., (1986) "Sensors for Use with Functional neuromuscular Stimulation", IEEE Trans. BME 33:(2):256-268

Crago, P.E., Lan, N., Veltink, P.H., Abbas, J.J., and Kantor, C., (1996) "New control strategies for neuroprosthetic systems", J. Rehab. Res. Devel. 33:(2):158-172

Coghlan, J.K., Robinson C.E., Newmarch, B., and Jackson, G., (1980) "Lower extremity bracing in paraplegia – a follow-up study" Paraplegia 18:(1):25-32

Chiu, S.Y., Ritchie, J.M., Rogart, R.B., and Stagg, D., (1979) "A quantitative description of the membrane currents in rabbit myelinated nerve", J. Physiol., 292:146-166

Dai, R., Stein, R.B., Andrews, B.J., James, K.B., and Wieler, M., (1996) "Application of tilt sensors in Functional Electrical Stimulation", IEEE Trans. Rehab Eng. 4:(2):63-72

Davoodi, R., and Andrews, B.J., (1998) "Computer simulation of FES standing up in paraplegia: A self adaptive fuzzy controller with reinforcement learning", IEEE Trans. Rehab. Eng. 6:(2):151-61

Davis, R., Houdayer, T., Andrews, B.J., Emmons S., and Patrick, J., (1997) "Paraplegia: prolonged closed-loop standing with implanted nucleus FES-22 stimulator and Andrews' foot-ankle orthosis." Stereotact. Funct. Neurosurg. 69(1-4 Pt 2):281-7.

Dietz, V., and Berger, W., (1983) "Normal and impaired regulation of muscle stiffness in gait: a new hypothesis about muscle hypertonia", Exp. Neurol. 79:680-7

Dolan, M.J., Andrews, B.J., and Veltink, P.H., (1998) "Switching curve controller for FES assisted standing up and sitting down, " IEEE Trans. Rehab. Eng 6:(2):167-71

Erfanian, A., Chizeck, H.J., and Hashemi, R.M., (1998) "Using evoked EMG as a synthetic force sensor of isometric electrically stimulated muscle" IEEE Trans. BME 45(2):188-202

Fang, Z.P, and Mortimer, J.T., (1991) "Selective activation of small motor axons by quadratrapezoidal current pulses", IEEE Trans. BME 38(2):168-74

Franken, H.M., Veltink, P.H., Baardman, G., Redmeyer, R.A., and Boom, H.B.K., (1995) "Cycle to cycle control of swing phase of paraplegic gait induced by surface electrical stimulation", Med. Biol. Eng. & Comp. 33:440-451

Frankenhauser, B., and Huxley, A.L., (1964) "The action potential in the myelinated nerve fiber of Xenopus Laevis as computed on the basis of voltage clamp data," J. Physiol., 109:302-315

Frijns, J.H., and ten Kate, J.H., (1994a) "A model of myelinated nerve fibers for electrical prosthesis design." Med. Biol. Eng. & Comp. 32(4):391-8

Frijns, J.H., Mooij, J., and ten Kate, J.H., (1994b) "A quantitative approach to modeling mammalian myelinated nerve fibers for electrical prosthesis design" IEEE Trans. BME 41(6):556-66

Graupe, D., and Kohn, K.H., (1997) "Transcutaneous functional neuromuscular stimulation of certain traumatic complete thoracic paraplegics for independent short-distance ambulation" Neurological Research. 19(3):323-33

Graupe, D., Kohn, K.H., and Basseas, S., (1988) "Above- and below-lesion EMG pattern mapping for controlling electrical stimulation of paraplegics to facilitate unbraced walker-assisted walking", J. BME 10(4):305-11

Graupe, D. (1989), "EMG Pattern Analysis for Patient response control of FES in Paraplegics for Walker Supported Walking," IEEE Trans. BME 36(7):711-719

Grunewald, V., Bhadra, N., Creasey, G.H., and Mortimer, J.T., (1998) "Functional conditions of micturition induced by selective sacral anterior root stimulation: experimental results in a canine animal model." World J. Urol. 16(5):329-36

Halter, J., and Clark, J., (1991) "A distributed-parameter model of the myelinated nerve fiber", J. Theor. Biology 148:345-382

Hambrecht, (1972) "Neural control aspects of functional neuromuscular stimulation", FNS Workshop, Bethesday Maryland

Hentry, J.R., and Ewins, D.J., (1998) "Applications of gyroscopic angular velocity sensors in FES systems", Proc. Int. Work. Vienna FES, pg 157-60

Haugland, M.K., and Hoffer, J.A., (1994) "Slip information provided by nerve cuff signals: Application in closed loop control of functional electrical stimulation", IEEE Trans. Rehab. Eng. 2(1):29-36

Haugland, M.K., Sinkjaer, T., (1995) "Cutaneous whole nerve recordings used for correction of footdrop in hemiplegic man" IEEE Trans. Rehab. Eng., 3(4)

Happak, W., Gruber, H., Holle, J., Mayr, W., Schmutterer, C., Windberger, U., Losert, U., and Thoma, H., (1989) "Multichannel indirect muscle stimulation reduces muscle fatigue", Proc. Vienna Int. Work. FES, 163-5

Hendron, C.H., (1980) "Therapeutic effects of FES for the correction of gait abnormalities in children with cerebral palsy", Bull. Prost. Othot. 10-33 115

Heyn, R. E., Mayagoitia, A., Nene, V., and Veltink, P.H., (1996) "The kinematics of the swing phase obtained from accelerometer and gyroscope measurements", Proc. IEEE EMBS, pg 857-8

Hines AE. Birn H. Teglbjaerg PS. Sinkjaer T. (1996) "Fiber type composition of articular branches of the tibial nerve at the knee joint in man" Anatomical Record 246(4):573-8

Hildebrandt, J.J., and Meyer-Waarden, K., (1984) "Development of an EMB-controlled 8 channel system for neuromuscular functional stimulation", Proc. 8th Int. Symp. Ext. Contr. Hum. Ext. Dubrovnick

Hodgkin, A.L., and Huxley, A.F., (1952) "A quantitative description of membrane current and its application to conduction and excitation in nerve," J. Physiol., 117:500-544

Johnson, K.O., Popovic, D., Riso, R.R., Koris, M., Van Doren, C., and Kantor, C., (1995) "Perspectives on the role of afferent signals in control of motor neuroprostheses" Med. Eng. & Phys. 17(7):481-96

Johnson, M.W., Peckham, P.H., (1994) "Implantable transducer for two-degree-of-freedom joint angle sensing" Proc. IEEE EMBS 16:446-7

Johnson, F. Watts., W.G., and Evans, D.F., (1981)"Goniometer for continuous recording of knee angle", Med. Biol. Eng. & Comput. 19:255-256

Johnston, R.C., and Smidt, G.L., (1969), "Measurement of hip joint motion during walking. Evaluation of an electrogoniometric method", J. Bone Joint. Surg. 51A:1083-1094

Kataria, P., and Abbas, J.J., (1998) "Estimating body segment orientation using a lightweight, inexpensive gyroscope" Proc. BMES Conf. P S-133

Kerrigan, D.C., Gronley, J., and Perry, J. (1991), "Stiff legged gait in spastic paresis", American Journal of Physical Medicine and Rehabilitation, 70(6):294-300

Kilgore, K.L., Peckham, P.H., Keith, M.W., Thrope, G.B., Wuolle, K.S., Bryden, A.M., and Hart, R.L., (1997) "An implanted upper-extremity neuroprosthesis. Follow-up of five patients" J Bone Joint Surg Am 79(4):533-41

Kirkwood, C.A., and Andrews, B.J., (1989) "Finite State Control of FES Systems: Application of AI Inductive Learning Techniques," Proc. IEEE EMBS pp 1020-1021

Kirkwood, C.A., Andrews, B.J., and Mowforth, P., (1989) "Automatic detection of gait events: a case study using inductive learning techniques", J. BME, 11(6):511-6

Kobetic, R., and Marsolais, E.B., (1994) "Synthesis of Paraplegic Gait with Multichannel Functional Neuromuscular stimulation", IEEE Trans. Rehab. Eng. 2(2):66-79

Kostov, A., Andrews, B.J., Popovic D., Stein R., and Armstrong, W. (1995), "Machine learning in control of functional electrical stimulation systems for locomotion, IEEE Trans. BME. 42(6):541-551

Kralj, A., and Bajd, T., (1989), Functional electrical stimulation: Standing and walking after spinal cord injury CRC Press, CA.

Krajl, A., Bajd, T., Turk, R., and Benko, H., (1986) "Posture switching for prolonging functional electrical stimulation standing in paraplegic patients" Paraplegia. 24(4):221-30

Kunz, R.E. Dubendorfer, J. (1997), "Novel miniature integrated optical goniometers", Sens. Actua. A: Phys. 60:23-28

Lajoie, Y., Barbeau, H., Hamelin, M, (1999) "Attentional requirements of walking in spinal cord injured patients compared to normal subjects", Spinal Cord, 37:245-50

Lamoreux, L.A., (1971), "Kinematic measurement in the study of human walking", Bull. Pros. Res. 10-15: 3 - 85

Liberson, W.T., Holmquest, H.J., Scot, D., and Dow, M. (1961), "Functional electrotherapy: Stimulation of the peroneal nerve synchronized with the swing phase of the gait of hemiplegic patients," Archives of Physical Medicine and Rehabilitation, 42:101-105

Lou, E., Durdle, N.G., Raso, V.J., and Hill, D.L., (1997) "Measurement of the magnetic field in the near-field region and self inductance in free space due to a multiturn square-loop:, IEE Sci. Meas. Tech. 144(6):252-6

Marsolais, E.B., and Kobetic, R., (1988) "Development of a practical electrical stimulation system for restoring gait in the paralyzed patient" Clin. Ortho. & Rel. Res. (233):64-74

McNeal, D.R., (1976) "Analysis of a model for the excitation of myelinated nerve", IEEE Trans. BME, vol. 23, pp. 329-337

McNeal, D.R. (1977) , "2000 years of electrical stimulation", Functional Electrical Stimulation, eds. Hambrecht, F.T., & Reswick, J.B., Marcel Dekkar, NY

Mills, O.S., Hull, M.L., (1991) "Apparatus to obtain rotational flexibility of the human knee under moment loads in vivo", J. Biomech. 24:351-369

Miyazaki, S (1997) "Long term unconstrained measurement of stride length and walking velocity utilizing a piezoelectric gyroscope", IEEE Trans. BME 44(8): 753-9

Morris, J.R., (1973) "Accelerometry--a technique for the measurement of human body movements" J Biomech. 6(6):729-36

Mulder, A.J., Veltink, P.H., Boom H.B.K., and Zilvold, G., (1992) "Low level finite state control of knee joint in paraplegic standing", J. BME 14:3-6

Muller, A., (1969) "Studies on electroanesthesia with middle frequency current", Proc. 2nd International Symposium on Electrotherapeutic Sleep and Electroanethesia, Grax, Aust., pp. 291-295

Murray, M.P. (1967) "Gait as a total pattern of movement", Am. J. Phys. Med. 46:290-333

Nash, M.S., Jacobs, P.L., Montalvo, B.M., Klose, K.H., Guest, R.S., and Needham-Shropshire, B.M., "Evaluation of a training program for persons with Sci paraplegia using the Parastep®1 Ambulation system: Part 5. Lower extremity blood flow and hyperemic Responses to Occlusion are Augmented by Ambulation Training", Arch. Phys. Medicine and Rehabilitation, 78:808-813,

Ng, S.K., and Chizeck, H.J., (1997) "Fuzzy model identification for classification of gait events in paraplegics", IEEE Trans. Fuzzy Systems, 5(4):536-544

Peckham, P.H., and Creasey, G.H., (1992) "Neural Prostheses: clinical applications of functional electrical stimulation after spinal cord injury", Paraplegia 30(2) 96-101

Pedotti, A., Ferrarin, M., Quintern, J., Riener, R., (1996) Neuroprosthetics, Springer-Verlag, ISBM 3-540-61084-7

Perry, J., (1992) Gait Analysis: Normal and Pathological Function, Thorofare, N.J.: SLACK Inc. 1992

Perry, J., (1993) "Determinants of Muscle function in the spastic lower extremity", Clin. Ortho. Rel. Res. 288:10-26

Perry, J., and Antonelli, D., (1981) "Evaluation of CARS-UBC triaxial goniometer", Bull. Pros. Ortho. 10-35:225-6

Phillips, C. (1991), Functional electrical rehabilitation: technological restoration for restoring after spinal cord injury, Springer-Verlag, New York

Phillips, C.A., (1988) "Sensory feedback control of upper and lower extremity motor prosthesis", CRC Crit. Reviews 16(2)-105-40

Petrofsky, J.S., Phillips, C.A., and Heaton, H.H.,(1984) "Feedback control system for walking in man", Comp. Biol. Med. 14(2):135-49

Prochazka, A., and Gorassini, M., (1998a) "Ensemble firing of muscle afferents recorded during normal locomotion in cats" J. Physiol. 507 (Pt 1):293-304

Prochazka, A., and Gorassini, M., (1998b) "Models of ensemble firing of muscle spindle afferents recorded during normal locomotion in cats" J. Physiol. 507 (Pt 1):277-91

Rattay, F., (1990) Electrical Nerve Stimulation, Wein, Austria, Springer-Verlag,

Reilly, J.P., Freeman, V.T., and Larkin, W.D., (1985) "Sensory effects of transient electrical stimulation--evaluation with a neuroelectric model," IEEE Trans. BME 32(12):1001-11

Rijkhoff, N.J., Wijkstra, H., van Kerrebroeck, P.E., and Debruyne, F.M., (1997) "Selective detrusor activation by electrical sacral nerve root stimulation in spinal cord injury." J. Urol. 157(4):1504-8

Rijkhoff, N.J., Wijkstra, H., van Kerrebroeck, P.E., and Debruyne, F.M., (1998) "Selective detrusor activation by sacral ventral nerve-root stimulation: results of intraoperative testing in humans during implantation of a Finetech-Brindley system" World J. Urol 16(5):337-41

Robblee, L.S., and Rose, T.L (1990), "Electrochemical guidelines for selection of protocols and electrode materials for neural stimulation," 25-66 from Neural prostheses: Fundamental studies, WF Agnew, DB McCreery, eds. Prentice Hall, 1990 , New Jersey, 07632

Roth, P.J., Unsworth, A., Haslock, I. (1981) "Discrete step goniometer for the human elbow", Eng. Med. 10:79-83

Rushton, D.N., Donaldson, N de N., Barr, F.M.D., Harper, V.J., Perkins, T.A., Taylor, P.N., and Tromans, A.M., (1996) "Lumbar anterior root stimulator for lower limb control in paraplegics" in Neuroprosthetics: from basic research to clinical application, M Ferrarin, A Pedotti, J Quintern, R Riener (eds), Springer-Verlag, Munich, 611-22

Schwarz, J.R., and Eikhof, G., (1987) "Na^+ currents and action potentials in rat myelinated nerve fibers at 20 and 37°C," Pflugers Arch., 409:569-577

Shaker, H.S., Tu, L.M., Robin, S., Arabi, K., Hassouna, M., Sawan, M., and Elhilali, M.M., (1998) "Reduction of bladder outlet resistance by selective sacral root stimulation using high-frequency blockade in dogs: An acute study," J. Urology, 160, 901-907

Sharma, M., Marsolais, E.B., Polando, G., Triolo, R.J., Davis, J.A. Jr., Bhadra, N., and Uhlir, J.P., (1998) "Implantation of a 16-channel functional electrical stimulation walking system" Clin. Ortho. & Rel. Res. (347):236-42

Shue, G., Crago, P.E., and Chizeck, H.J., (1995) "Muscle-joint models incorporating activation dynamics, moment-angle, and moment-velocity properties" IEEE Trans. BME 42(2): 212-23

Sinkjaer, T., Riso, R., Mosallaie, F. K, Jensen, W., and Lawrence, S., (1997), "Nerve cuff recordings of muscle afferent activity during passive joint motion in a rabbit", IFESS'97, 219-220

Smidt, G.L., Deusinger, R.H., Arora, J., and Albright, J.P., (1977), "An automated accelerometry system for gait analysis" J. Biomech. 10(5-6):367-75

Stallard, J., Major, R.E., and Patrick, J.H., (1989) "A review of the Fundamental Design Problems of providing ambulation for paraplegic patients", Paraplegia. 27(1):70-5

Stein, R.B., Peckham, P.H., Popovic, D. B., (1992) Neural Prostheses, Oxford University Press, ISBN 0-19-507216-2

Stephanova, D.I., and Bostock, H.,(1995) "A distributed-parameter model of the myelinated human motor nerve fibre: temporal and spatial distributions of action potentials and ionic currents". Biological Cybernetics, 73 275-280

Solomonow, M., (1984) "External control of the neuromuscular system", IEEE Trans. BME, 31:572-763

Sweeney, J.D., Mortimer, J.T., (1986) "An asymmetric two electrode cuff for generation of unidirectionally propagated action potentials", IEEE Trans. BME 33(6):541-9

Symmons, J., McNeal, D., Waters, R., and Perry, J., "Trigger Switches for Implantable Gait Stimulation", RESNA 9th Ann. Conf. 319-321

Sweeney, J.D., Mortimer, J.T., and Durand, D., (1987) "Modeling of mammalian myelinated nerve for functional neuromuscular electrostimulation", Proc. 9th IEEE EMBS, Boston, MA, pp. 1577-1578

Tanner, J., (1962) "Reversible blocking of nerve conduction by alternating current excitation," Nature, 195:712-713

Tuma, R.F., Vasthare, U.S., Arfors, K.E., and Young, W.F., (1997) "Hypertonic saline administration attenuates spinal cord injury", Journal of Trauma 42(5 Suppl): S54-60

van den Honert, C., Mortimer, J.T., (1981a) "A technique for collision block of peripheral nerve: single stimulus analysis", IEEE Trans. BME 28(5):373-8

van den Honert, C., Mortimer, J.T., (1981b) "A technique for collision block of peripheral nerve: frequency dependence" IEEE Trans. BME 28(5):379-82

Veltink, P.H., van Alste, J.A., and Boom, H.B., (1989) "Multielectrode intrafascicular and extraneural stimulation", Med. & Biol. Eng. & Comp. 27(1):19-24

Veltink, P.H., and Franken H.M., (1996) "Detection of knee unlock during stance by accelerometry." IEEE Trans Rehab. Eng. 4(4):395-402

Upshaw B.J., and Sinkjaer T., (1997) "Natural versus artificial sensors applied in peroneal nerve stimulation" Artif. Organs 21(3):227-31

Willemsen, A.T., Bloemhof, F., and Boom, H.B., (1990a) "Automatic Stance Swing Detection from Accelerometer Data for Peroneal Nerve Stimulation," IEEE Trans. BME, 37(12):1201-8

Willemsen, A.T., van Ålste, J.A., and Boom, H.B., (1990b) "Real-time gait assessment utilizing a new way of accelerometry" J. Biomech. 23(8):859-63

Willemsen, A.T., Frigo, C., and Boom, H.B., (1991) "Lower extremity angle measurement with accelerometers--error and sensitivity analysis" IEEE Trans. BME 38(12):1186-93

Wong, V., (1998) "Use of botulinum toxin injection in 17 children with spastic cerebral palsy", Pediatric Neurology 18(2):124-32

Woo, N., and Campbell, B., (1964) "Asynchronous firing and block of peripheral nerve conduction by 20 kc alternating current", Bull. L.A. Neurol. Soc., 29:87-94

Wood, D.E., Harper, V.J., Barr., F.M.D., Taylor, P.N., Phillips, G.F., Ewins, D.J., (1998) "Experience in using knee angles as a part of a closed loop algorithm to control FES assisted paraplegic standing", Proc. Int. Work. FES Vienna 137-140

Yarkony G.M. (editor) (1994) , Spinal Cord Injury : Medical Management and Rehabilitation, Apsen Publishers, Gaithersburg, Maryland 20878

Yoshida, K., and Horch K., (1996) "Closed-loop control of ankle position using muscle afferent feedback with functional neuromuscular stimulation", IEEE BME 43(2):167-76

2 Gait Event Detection for FES Using Accelerometers and Supervised Machine Learning

2.1 Introduction

Walking assisted by functional electrical stimulation has been demonstrated, and commercial systems such as the Parastep™ System, the MicroFes™, and the WalkAide™ are now available. In the latter two systems, the stance and swing phases of gait are determined automatically using an insole pressure sensor and a shank inclinometer respectively. In FES assisted paraplegic locomotion, such as with the Parastep™ system, the patient presses and releases a momentary acting handswitch to directly define the stance and swing phases for each step. Skill in operating the switches is learned over several weeks during gait training sessions. This system relies on the flexion reflex, elicited by electrically stimulating a sensory nerve such as the common peroneal (Kralj and Bajd, 1989). This reflex is highly variable in its amplitude and temporal characteristics (Granat et. al, 1993). The patient can learn how to accommodate for these delays in the build up of the flexion response by pressing the handswitch earlier. The patient also learns how to coordinate the press and release handswitch control actions with the upper body mediated postural adjustments. However, the resulting FES assisted paraplegic gait remains slow and energy consuming.

A high degree of concentration and dexterous precision is required to operate the control handswitches. This may be limiting, particularly, with increased walking speeds that have been achieved with incomplete spinal injuries or paraplegics performing FES aided swing-through gait (Heller et. al, 1996). Various handcrafted stance swing detectors for FES control have been proposed. These include detection of heel off (Liberson et. al, 1961), shank inclinations (Dai et. al, 1996), foot contact using switches or accelerometers (Willemsen et. al, 1990), EMG signatures from preserved muscles (Chandler, 1973, Graupe, 1989), EEG signals directly from the motor cortex (Craggs, 1974) and sural nerve ENG signals from foot pressure afferents (Upshaw and Sinkjaer, 1997). These methods depend critically upon human expertise in understanding of how a particular sensor output can be uniquely related to the gait event and the ability to articulate the

specific rules for detection of that gait event. This places restrictions on the type and number of sensors used, their anatomical location and alignment. The combination or fusion of data from several sensors may in theory improve the detector's accuracy, but the increased complexity may entail manual tuning to the individual, a process unsuited to clinical practice. Further refinement of FES walking has been demonstrated by Marsolais and colleagues. His walking technique required that the gait cycle be subdivided beyond stance and swing to obtain a more natural looking and faster gait (Kobetic and Marsolais, 1994).

Andrews et al. (Andrews et. al, 1989) presented a hand crafted rule based intention-to-step detector used to predict stance-swing transitions. The intention detector was formulated from direct observations of manually controlled FES gait. Flexion withdrawal stimulation was applied whenever two voluntary actions occurred within a preset time window: the anticipatory postural adjustments of a shift of body weight to the stance side, and the advancement and loading of the opposite crutch as sensed by shoe insole and crutch handgrip pressure sensors. This method required a human expert to select and position the sensors, and precisely articulate the detection rules. Adjustments to rule parameters were required for each patient. In the patients exhibiting slower reflex flexion, it was difficult to reliably detect an earlier event corresponding with manual switch pressing, resulting in a slower gait. In these patients, a compensating anticipatory switch was necessary for increased walking speed.

Kirkwood and Andrews (Kirkwood and Andrews, 1989), at the personal suggestion of Donald Michie, reported the application to FES of an artificial intelligence technique Michie called "behavioral cloning" (Michie et. al, 1990). A volunteer subject, who had sustained an incomplete cervical lesion of the spinal cord, performed a number of walks using a handswitch controlled FES system, whilst signals from a set of insole pressure sensors and crutch force sensors were simultaneously recorded. The rule induction algorithm ID3 was used to produce a real time, rule based clone that automatically mimicked the patient's press and release actions of the control handswitch with an accuracy of 97%. The reasoning used by the clone, when articulated as a set of If ... Then... type rules may also be understood by humans. The rule induction algorithm

assumed no a priori relationship between the classes and attributes. This allowed the designer to chose sensors that would somehow reflect the patient's intention without having to be able to articulate the exact relationship. Kirkwood, Andrews & Mowforth (Kirkwood et. al, 1989), using the fact that ID3 ranks, in information theoretic terms, the contribution of each sensor signal derived attribute, demonstrated that inductive learning could better perform sensor selection for determination and gait phases compared with a panel of human gait experts. The behavioral cloning technique has since been further developed using different rule induction algorithms and sensors together with procedures for selecting sensors based on their contributed information.

Advances to walking in paraplegia can be made through adding additional states for control. Bajd et al. (Bajd et. al, 1994) have demonstrated that FES plantar flexion, applied using a three state handswitch, during the push off phase can increase the walking speed of some paraplegics with complete lesions. Kobetic and Marsolais (Kobetic and Marsolais, 1994) used a triggered sequence of eight phases, demonstrating walking speeds up to 0.5 m/s in laboratory conditions. A timing algorithm was constructed for each individual to determine the eight phases within the gait cycle. Adjustment of the timing of the gait phases is proposed through fuzzy logic detection of gait events discussed by Chizeck (Ng and Chizeck, 1997). Kobetic and Marsolais noted that errors in the range of 20 ms could have a detrimental effect on the performance of the walking pattern.

Through the application of machine learned rule-based controllers, gait phases or gait events, such as those indicated by Kobetic and Andrews, could be derived to control FES. Kostov (Kostov et. al, 1995) has also applied this technique using Adaptive Logic Networks for stance swing detection. Presented here are the results of a feasibility study, conducted with able-bodied volunteers, to determine if supervised machine learning and a set of three accelerometers attached to a single site on the shank can reliably predict stance-swing intentions and detect gait events. The gait events we chose to detect were defined by Perry (Perry, 1992) and are widely accepted and associated with well defined motor control actions from which finite state control strategies may be formulated.

Accelerometers were chosen because they are physically small, commercially available, robust and represent a new generation of micro-machined sensors that are

potentially implantable in future neuralprostheses. The performance of a stance-swing version of the detector is compared with a clinically used hand crafted detector based on a pendulum type inclinometer (Dai et. al, 1996). Preliminary aspects of this study have previously been reported (Williamson et. al, 1996).

2.2 Methods and Materials

2.2.1 Subjects and Walkpaths

One figure of eight and one oval walkpath were marked out using masking tape on a level floor. The oval path was 20 m along the straight edges with an 8 m diameter curve at either end. The figure of eight had 16 m straight sections with 6 m diameter curves on either end. Five able-bodied subjects took part in this study, indicated in Table 2.1. Subject E walked only along the oval path. A power failure to the sensors occurred during Subject D's oval run. The subjects walked around each path twice in approximately 45 seconds.

2.2.2 Accelerometers

At the time of conducting this study, only the uniaxial accelerometers ADXL05 and ADXL50 were available. We chose to use the ADXL05 as it had a thirteen fold improvement in signal to noise ratio in comparison to the ADXL50, as calculated by comparing their noise and sensitivity specifications. Accelerations above 5 g were not expected nor observed in our test, hence the increased range of the ADXL50 was not advantageous.

The accelerometers were mounted on the ADXL50 evaluation boards, supplied by Analog Devices, as described by the application notes (Analog devices trade literature). The onboard amplifier was set with a gain of 2 giving a range of +/- 4g and an offset of 2.8 volts with the sensitive axis of the ADLX05 horizontal. The signals were recorded with 12 bit resolution using an analog to digital converter (NI-DAQ AT-MIO 16L board, National Instruments Inc.) with a sampling rate set at 200 Hz.

Three accelerometers were used in these trials. We were interested in confining the sensor system to a single location. Hence, the three appropriately arranged

accelerometers could provide complete measurement of the accelerations of the point on the brace to which they were attached.

The evaluation boards were mounted on a semi-rigid plastic plate with an adjustable elasticized Velcro strap around the shank as shown in Figure 2.1. The plastic platform was 2" by 8" and molded to the tibial crest region. The platform and strap were positioned on the tibial crest situated above the heads of gastrocnemius and soleus posteriorly as shown in Figure 2.1A. The accelerometer, labeled a in Figure 2.1B was oriented approximately along the tibial axis. The other two, labeled b and c as shown, were mounted orthogonal to the tibial axis and a, with approximately 70° between their sensitive axes.

2.2.3 Determination of reference gait phases

Force sensing resistors (FSRs) were attached to polypropylene shoe insoles of thickness 3 mm beneath the heel, medial metatarsal, and lateral metatarsal, similar to the method of obtaining foot floor contact patterns as described by Perry. The FSRs were sampled along with the accelerometers by the data acquisition system. These provided the reference signals of gait phase by using foot-floor contact patterns. The analogue FSR signals were described as either ON or OFF by a threshold level set at approximately 5% of maximum signal amplitude. Four phases of stance, loading response, mid-stance, terminal stance, pre-swing, were determined in addition to swing phase. Figure 2.2 provides a schematic describing the determination of stance and swing phases from foot floor contact patterns. These phases can also be constructed by a logic table, as seen in Table 2.2.

Swing is defined as when all ipsilateral FSRs were OFF. Loading response is initiated when the heel FSR goes ON, and terminated when either the medial or lateral FSR came ON. The latter event initiated mid stance. Mid stance terminated when the contralateral swing phase terminated, and terminal stance was initiated. Pre-swing began with the ipsilateral heel OFF and terminated when both ipsilateral lateral and medial FSRs were OFF.

2.2.4 Rough Sets

Rough Sets is an inductive supervised machine learning method (Reduct Systems trade literature) that was used to construct a rule based gait phase detector. The program divides each input variable, R, into *n* equally spaced or user selected divisions, creating an input space of R^n divisions. The distribution of outputs in each input subspace is determined. Decisions are made regarding each input subspace based on the quality of output prediction, and the precision that one output class is determined from one input subspace, and number of occurrences. If an individual rule was made for each subspace, R^n rules would be constructed. Therefore it is necessary to combine subspaces to limit the number of rules that the classifier needs to evaluate. This process must also proceed without sacrificing the accuracy of classification. Roughness and precision are two parameters that control the combination of input subspaces. These parameters determine the quantity and quality of the rules produced.

Precision is the allowable error within a rule subspace. If the precision value is set at 90%, then at least 90% of the occurrences within an input subspace would have one output variable. By increasing the precision, the quality of rules will increase, but the noise tolerance of the classifier will decrease. If the precision rate is too high, a desirable subspace could be disregarded due to noise related errors. If the rate is too low, the rules could make false output predictions.

Roughness governs the minimum size of rule subspace. By increasing the roughness, the minimum size of subspace and a minimum population of the subspace required to qualify as a rule increases. Fewer rules are generated with higher roughness levels.

DataLogic 1.3R performs two functions, rule induction (training) and rule inference (testing). After training, a table of the rules with their accuracy, their population, and the training examples used to construct the rules are provided to the program user. If desired, the user can use this information to prune the rule set by hand. Rules for which too few samples are provided could be omitted if deemed unnecessary. The testing can occur with complete or hand pruned rule sets.

2.2.5 Adaptive Logic Networks

The Adaptive Logic Networks (Armstrong and Thomas, 1995) tested were supplied in ATREE3.0. The ALNs are based on piecewise linear fitting analysis. The classification of stance/swing was done through training one network. Stance was considered a network output of zero, swing an output of one. To test the network, the output is rounded to the nearer value, indicating either stance or swing. When used as a detector of multiple gait phases, an individual ALN was trained for each decision. Five separate files needed to be generated for this approach. The output value of a training file is one during the gait phase to be determined by this ALN, and zero for all others. To discriminate phases using this method, the network with the greatest output was chosen as the predicted gait phase. This method produced a more accurate classification than the training of only one ALN to discriminate all of the gait phases.

The depth of the decision tree generated controls the size of the evaluation network. The decision tree is a reflection of the adaptive logic network generated from the training of a piecewise linear network. A maximum of twelve linear pieces is generated for evaluation of the decision tree. The twelve linear pieces are of the form:

$$o(i) = \frac{o_o + \sum_n a_n (x_n - b_n)}{o_s}$$

where:

x_n is the input

$o(i)$ is the output line

o_o is the output offset

o_s is the output scale

a_n is input scale

b_n is the input offset

The linear pieces are combined into a surface via maximum and minimum functions similar to:

A = MAX{ MIN[MAX{o(1),o(2)} ,o(3),o(4)], o(5)}

2.2.6 Training the machine learning algorithms

The machine learning algorithms constructed rule based detectors (RBD) that determined a desired output variable from attributes constructed from the input variables. The attributes we used were created from the accelerometer recordings. The desired output variable was gait phase class.

The simplest attribute to use in a system is the signal amplitude. Other attributes could include previous samples, to provide memory, various mathematical transformations of the signal amplitude such as hyperbolic tangent or exponential functions, or temporal combinations, such as a simple difference of a signal recording and its previous recording examples.

For a file to be used by the supervised machine learning program, it must contain only input attributes and output classes. Therefore, the raw accelerometer and FSR recordings required processing before implementing them into the supervised machine learning programs. Two files were recorded for each individual, one for the oval path and one for the figure of eight. For each file, the gait phase (output class) at each sampling interval was computed, as indicated in Figure 2.2. The accelerometer signals were either filtered using a low pass digital implementation of an analog filter, or left unfiltered. An example of the raw accelerometer data, filtered accelerometer data, and reference gait phase calculation is seen in Figure 2.3. The input attributes, as described previously in this section, provided to the RBD were generated from the filtered or unfiltered accelerometer signals. These attributes (inputs) were realigned with the determined gait phases (outputs) to create the processed file of input attributes and corresponding output classes. The initial samples, typically thrice the group delay of the digital filter, were then discarded. This procedure was then applied to the other file of the individual so that a file of the same input attributes was generated for the individual on both walkpaths.

The training and testing files were created from these two preprocessed files. The training file was generated by taking the first 2000 samples from each of the preprocessed files, creating a training file of 4000 points from the two walkpaths. The testing file was created from the remaining data from the two preprocessed files, consisting of

approximately 14000 samples. This size of training file, at the level of 6 input attributes, was too large for the RS program to handle efficiently. For 6 input attributes, a training file of 4000 points required over one hour to converge upon a rule base. For the same number of attributes and 2000 points, RS required 25 minutes to converge. Using only 1000 points and 6 attributes, RS could converge within 5 minutes. Therefore, only every 4^{th} sample was taken from the training file, creating a training file of 1000 points. This did not lead to a decrease in RBD accuracy.

The rule-based detector was constructed iteratively. The preprocessing of the file allowed for two degrees of freedom: digital filter implementation and attribute construction. Once implemented in the RS program, two additional degrees of freedom were added: the roughness and precision settings. Provided here is an example of the manner in which these degrees of freedom were handled. The three accelerometers were preprocessed first with a 2^{nd} order digital Butterworth filter with 5 Hz cutoff frequency. The attributes selected would first be only the signal amplitude. With this training file, the RS parameters of roughness and precision were varied to maximize the overall classification accuracy. Once this maximum classification percentage was determined, a second training file containing the signal amplitude and a simple difference of the signal amplitude and previous value was constructed. Again, various RS roughness and precision parameters were tested to maximize the overall classification accuracy. A third training file would be produced, consisting of two attributes, such as the signal amplitude and the first past point. Again, the maximum classification accuracy was determined. This process continued until the classification accuracy did not increase by increasing the number of signal attributes. The most accurate rule based detector was selected from this process, and applied to the testing file. A similar method was used to determine the most accurate ALN for classification. Many training files were generated, and the programs learning parameters and depths of decision tree were altered to achieve the best overall classification accuracy.

The preferred method of preprocessing was the use of a 2^{nd} order digital Butterworth filter and the two attributes for each accelerometer, signal amplitude and a simple difference of the amplitude of each accelerometer with its previous recording. Six

input attributes were created by this method. These attributes are computationally simple for the processors.

2.2.7 Calculation of Detection Accuracy

Accuracy was computed on a sample by sample basis, i.e. the percentage of samples for which the detector correctly selects the reference gait phase. An accuracy of 90% represents a rule base that determined the reference gait phase for 90 out of 100 samples. A pictorial example of the SML gait phase classification is provided in Figure 2.5. As can be observed by the error pattern on the lower section of the graph, the errors that are present using SML are not phases or steps that are misclassified in entirety, but are errors corresponding to a misclassified phase for a couple of samples. These single and multiple sample errors give rise to an imperfect classification rate, without corresponding to an entirely misclassified gait phase.

Two types of errors occur due to this sample by sample classification: errors when the RBD changes from one phase to another prior or later than the reference signal, and errors when the RBD changes out of one phase and back while the reference signal stays in one phase. The first type of error, typically seen with other finite state controllers, is when the classifier makes an error at a transition, i.e. mistakenly changes from state 1 to state 2 too early or too late. If the duration of this error is very short, the consequences could pass undetected. If the duration is long, then the controller would fail for this time period, and the consequences would be more severe. The second type of error occurs when the SML predicts a transition from one state to another and back again within a short period of time. This type of error has been called an instate error. This should not be seen in a refined finite state controller, and can be eliminated by using intuitive rules. For these tests, the data was sampled at 100 Hz. By using groups of three sequential points, we reduced the effective sampling rate to 33 Hz, which is in the range of stimulation frequencies used in FES. The on-line filter manipulated this group of three successive points and applied the following rule to determine the accepted gait phase.

IF (two or more of the predictions are for a phase other than the present one)

AND (this is normally the next gait phase or the next phase after that)

THEN → change to that phase

ELSE → do not change phase

This rule was applied to the output of the RS SML detector for the five gait phases and the stance-swing detector. Since only two phases of gait were detected by the latter, the AND condition in the rule was omitted.

2.2.8 Comparison of hand-crafted and machine-learned stance-swing detectors

A dual-threshold stance swing discriminator, as described by Dai et al., was compared with RS and ALN based detectors. The bandwidth of Dai's pendulum type inclinometer method was reported. A fourth order 2 Hz Butterworth filter was applied to the accelerometer oriented along the tibial axis so that the same frequency characteristics were achieved in this test as were previously reported. This was confirmed by visually comparing a voltage trace in this test to that displayed in the Dai's report, as seen in Figure 2.4. From this trace, the dual-threshold stance swing discriminator was constructed. The reference stance swing classification was determined from the FSRs of the shoe insoles, as described in section 2.2.3.

The sample points used to construct the training file for SML were used to determine the thresholds of the dual-threshold stance swing detector. Individual thresholds were set for each subject to provide a direct comparison with the machine learned rule base, as an individual training file was generated for each subject. Two threshold voltages were set: one to determine the transition from stance to swing and one to determine the transition from swing to stance. For each swing stance and stance swing transitions of the training file, the filtered accelerometer voltage was recorded. These voltages were averaged to create one threshold voltage for stance-swing transitions, and one for swing-stance transitions. These thresholds were applied to the remaining data so that the sample by sample accuracy of this method could be compared to SML.

2.2.9 Multiple Gait Phase Detection

We expanded the description of gait to four stance phases and one swing phase determined from foot-floor contact patterns. Both supervised machine learning techniques

were investigated during this study. Training files were generated from 500 sequential samples from each walk path representing approximately 10 strides sampled at 50 Hz. The testing files were evaluated at 100 Hz. This intuitive rule was applied to the output five gait phase determination. The error patterns of this technique were analyzed for subject A.

It variance in the rule-based detector accuracy was noted between the gait phases. It was known that the length of the gait phases differed, however this did not correlate directly to the disparity in detection accuracy. The variance of the reference and SML gait phase length was calculated as an indication of the repeatability of the reference and SML signal. Within a single gait phase, a higher variance of phase duration could indicate a lower repeatability and reliability of the teacher signal, and could be reflected in higher error rates for the SML detector of those phases. This investigation was conducted in an offline procedure on one individual's, subject A's, oval and figure of eight walking patterns.

The teacher signal and machine learned signals were constructed as mentioned above. This sampling frequency of this test was 100 Hz. The in-phase errors of the rule-based classifier were removed from this controller by using the intuitive rules. After the elimination of these errors, each step had only one occurrence of each phase. The length of each phase for each step for both the machine learned and the teacher signals was then calculated. A distribution of the phase timings was generated by this approach.

2.3 Results

2.3.1 Comparison of hand-crafted and machine learned stance-swing detectors

ALN 3.0 and Rough Sets 1.3R each calculated a rule base to discriminate stance and swing from the accelerometer readings for each individual. Once a sufficient accuracy on the training file was achieved, the rule-based classifier was applied to the testing file.

These training and testing files were used to generate the two-threshold stance and swing detector. Different thresholds were determined for each subject, just as different rule based classifiers were used for each subject. Figure 2.4 displays an example of the two-threshold detection of stance and swing. For all individuals, the training accuracy was

greater than 99% for both SML and the handcrafted technique. The accuracy of the testing files is displayed in table 2.3. A statistical difference was not noted by comparing the three methods ($p<0.01$)

For all subjects, the SML attributes were signal amplitude and simple difference. For subject A, the preprocessing was achieved by using a 5 Hz 2nd order Butterworth filter. The roughness and precision parameters were 0.2 and 0.9 respectively. 8950 testing points were evaluated to achieve this accuracy measurement. For subject B, the preprocessing was achieved through a 2 Hz 2nd order Butterworth filter, and 5900 test samples at 100 Hz effective rate were evaluated. For subject C, the preprocessing was achieved by using a 5 Hz 2nd order Butterworth filter, and 7200 test samples at 100 Hz effective sampling rate were evaluated.

2.3.2 Multiple Gait Phase Detection

Figure 2.3 displays the accelerometer recordings during two strides. Figure 2.3b shows the filtered accelerometer signals that were used by the machine learning algorithms. Unlike Figure 2.4, we were unable to observe a visually apparent pattern between the accelerometer traces to the gait phases seen in 2.3c. Hence, machine learned rule bases were used to extract the gait phases in 2.3c from the signals in 2.3b.

Both machine learning techniques performed multiple gait phase classification. The training files were constructed as above with the difference being that the number of output classes jumped from two, stance and swing, to five. The results from the training file are including in table 2.4.

Roughness and precision were set at 0.3 and 0.8 respectively for each individual. Signal attributes of amplitude and simple difference were found to be the best for each individual. For subject A, a 2nd order digital Butterworth filter of 2 Hz was applied to the accelerometer signals. For subject B, a 2nd order digital Butterworth filter cutoff frequency 2 Hz was applied to the accelerometer signals. For subject C, a 2nd order digital Butterworth filter cutoff frequency 5 Hz was applied to the accelerometer signal. The classification results are summarized in table 2.4. An example of the classification is

provided in Figure 2.5. As can be seen, sporadic errors occur from the classifier. Using an intuitive rule reduced this complex error pattern.

The intuitive post SML filter eliminated the instate errors. By using this rule, all of the errors would be restricted to errors at the transition between phases. These errors were then classified as either early or late detection of the next gait phase. The duration of each of these errors was recorded for each step cycle for both the stance swing classification and five gait phases classification. There are four possible errors that could be made by a stance-swing detector during a gait step cycle, namely, a transition from stance to swing made too early or too late, or a transition from swing to stance made too early or too late. These two sets of errors are mutually exclusive, as during one step the transition from stance to swing cannot be made both too early and too late. In the evaluation of the duration of these errors, an error of zero duration was recorded when a particular type of error did not occur. This produced a statistic in which the average duration of an error was less than one sample interval in some cases, which would otherwise seem incorrect.

This filter was tested on subject A for both the stance swing determination and five gait phase determination. A comparison of this result was made with Dai's stance swing determination. The results are presented schematically in Figure 2.6, and in tables 2.5 and 2.6.

For stance swing determination, the post-filtered SML did not miss a phase entirely. All of the errors were isolated to the transition periods. The overall classification percentage on a 33 Hz sample basis was 98%.

The post SML filter was also applied to subject A's five phase classification, as described in multiple gait phase classification. These results are presented in Figure 2.6 and table 2.6.

Once again, the post SML filter did not miss a gait phase. The errors were isolated to the transitions between gait phases. However, the overall accuracy remained constant at 89%. This corresponds to an average duration of the error at transition of 20 ms.

2.3.4 Variability of detection accuracy based on variance of the teacher signal

The variability of the phase length was tested on Subject A's five phase testing file which consisted of 24 strides around the oval pattern and 26 strides around the Figure 8 pattern with a sampling rate of 100 Hz. Although the same rule based detector was used for both walkpaths, the length of each phase during the two patterns was analyzed separately as a significant ($p<0.01$) difference in the length of phase was noticed between the oval and Figure 8 pattern. Figure 2.7 displays the mean and deviation of the mean for both the reference and RBD. Although the standard deviation of each of the signals is greater for the machine learned cases, the difference in deviations is significant ($p<0.05$) for only 3 of the 10 cases.

2.3.5 Real Time Operation

Real time processing speed for RBD was tested on the MC68332 to demonstrate the potential for implementation of our proposed system. By using the MC68332 as an example, conclusions about other processors can be made.

To implement the machine learned rule base controller, processor limitations of program space and implementation speed must be met. The implementation speed is reported in clock cycles as evaluated for the MC68332 and includes only the processing needed for the RBD. This was calculated by running the MC68332 with two separate codes, one containing the gait phase detection algorithms, and one without. The difference in time between the two routines was taken as the time to run the gait phase detection algorithm. Table 2.7 displays the results.

The RS program required 35% of the memory and used 10% of the computing power required by the adaptive logic networks.

2.4 Discussion

The five gait phases, loading response, mid-stance, terminal stance, pre-swing and swing, illustrated in Figure 2.2 were discriminated using hand crafted rules applied to the outputs of a three element FSR insole. Variability of these phases was observed and is summarized in Figure 2.7. Unfortunately, Perry does not describe variability in the

duration of gait phases for normal walking that can be detected from footfall patterns, or a general variance of phase length.

Examination of Figure 2.4 reveals that there are only slight discrepancies around the phase transitions and each gait phase is detected. To help interpret the detection accuracy results, consider the hypothetical case of an individual walking at one stride per second for which five gait phases are determined using data sampled at 33 Hz. If the gait phase detector were to miss the phase transition by one early or late sample every stride, then the detection accuracy would be 84.8%. However, each gait phase was detected, and the transitions were missed by only a single sample during each stride. Thus a detection accuracy of 85% and does not imply that fifteen out of every 100 steps will fail. The post SML filter localized the errors to the phase transitions, as was the case for Dai's stance-swing detector. Then the percentage of mismatched samples between the detector output and the insole signal derived reference determined the detection error.

Kostov (Kostov, 1996) classifies the two types of errors produced by machine learned rule base controllers as 'critical' and 'non-critical' errors for his stance swing phase detector. He describes critical errors as errors that occur during the middle of a gait phase. For example, a 'critical' error would be the controller predicting a momentary transition from stance to swing during the middle of stance phase. This type of error is obviously detrimental; the leg that is in stance phase during single limb support would be stimulated as appropriate at the start of a swing phase, possibly leading to a fall of the individual. This sort of obvious detriment is not seen in the 'non-critical' errors that occur by an extended or shortened gait phase. However, the effect of these sorts of errors should depend both on the type of controller that is used and the number of gait phases detected. The effect that these types of error would have has not been explored. In this trial, the effects of these errors were likened to a integral count of stimulus pulses that are missed or inserted at a gait phase transition.

Table 2.3 indicates that the hand crafted technique provide detection accuracies between 87% and 95.9% for stance swing detection. The RS detector did not produce a significantly improved performance ($p<0.10$) over either the ALN or the hand-crafted technique. However, the classification accuracy of RS was improved upon by the use of

an intuitive filter that eliminated errors occurring within a gait phase. The stance swing detection accuracy increased to 98% when using this method. In practice, this would be equivalent to one inappropriate stimulating pulse every three steps. This represents an improvement that accuracy of the hand crafted rule based, calculated in this report as 95%. Calculating detection errors in this manner allows our SML approach to be compared directly with the previously reported hand crafted method.

Reliable detection of multiple gait phases is difficult, if not impossible, with detectors based on hand crafted rules. As indicated in Table 2.4, all five of the Perry gait phases were detected using a single cluster of three accelerometers using machine learning detectors. The ALN based detector produced a better overall classification accuracy ($p<0.05$) than RS. From table 2.4 it can be seen that the swing phase (SW) was detected with more than 90% accuracy, but the mid-stance, terminal stance, and pre-swing phases were less that 90%.

The detection errors appeared uniformly distributed across the entire gait cycle, which can be seen in Figure 2.5. Using the three sample intuitive rule-based filter, given by Rule A, the errors were confined to the gait phase transitions as illustrated in Figure 2.6. This post filter did not improve the overall detection accuracy. It can be seen in Figure 2.6 that the errors are typically one or two sample periods long, as indicated by the standard deviation bars on the plot of Figure 2.6. In practice this would correspond to an error of one or two stimulus pulses at 33 Hz and may not be noticeable in a FES system.

Figure 2.6 presents the nature of the prediction errors for the RS detector. The post filter corrected any error occurring within a gait phase. However, this did not improve the overall detection accuracy. The post filter had a span of three samples and if the detector made two consecutive errors, the filter output would prematurely jump to the next gait phase i.e. the filter could add an error. In our data, the filter produced more errors than it corrected and thus lowered the overall prediction accuracy.

A correlation can be discerned between the detection accuracy, as shown in table 2.4, and the variations in the duration of the reference gait phases as shown in Figure 2.7. From Figure 2.7, the standard deviation for the reference gait phases was of the order of one sample interval for the swing (SW), loading response (LR), and pre-swing (PS), and

of the order of four sample intervals for the mid-stance (MS) and terminal stance (TS) phases. Hence, it is implied that the classification accuracy for the mid-stance and terminal stance phases was limited by the variability in the reference gait phases. This variation was also present in the data used to train the machine learning algorithms. Gait phases that had a lower variability of reference phase length had a greater training and testing accuracy. An improved method for determining the reference gait phases should improve detection accuracy.

The average periods of erroneous detection are approximately one sample interval for the swing → loading response, loading response → mid-stance, and pre-swing → swing transitions, and approximately two sample intervals for the other transitions. The difficulty in detecting mid-stance and terminal stance was due to the variability in the reference gait phase data. This is responsible for the increase in the average error duration for the terminal stance → pre-swing and mid-stance → terminal stance transitions.

The data of table 2.7 indicates that both machine learning algorithms can be implemented in real time using a microcontroller. For example, for the five phase detector, only 0.03% or 0.3% of computer time was consumed for the RS and ALN based algorithms respectively. In our tests we used a credit card sized single board MC68332 computer, the Tattletale Model 8 (supplied by Onset Computers Inc. USA) operating at 16 MHz. This computer had 2MB of RAM and a current consumption proportional to clock speed. At 16.7 MHz the current consumption was 90 mA, which could be reduced by a factor of 10 for this application. The MC68332 offers a Time Processing Unit (TPU) and integrates a Maxim MAX186 A/D converter. The TPU is a sub-processor that can be used to generate stimulus pulses without computational load applied to the main processor.

Kirkwood et al. (Kirkwood et. al, 1989) implemented a stance-swing detector for FES control of paraplegic gait using ID3 a combination of insole pressure array, goniometers and crutch force sensors. Kostov et. al. (Kostov et. al, 1995) used ALN to implement a stance swing detector for FES control of hemiplegic gait using insoles pressure sensors. Ng and Chizeck (Ng and Chizeck, 1997) described a five gait phase detector using fuzzy logic and goniometers and reported similar detection accuracy as the

present results. An advantage of this method is that the three accelerometers were positioned at a single external site that was less encumbering than those previously reported, particularly if integrated into an orthosis. Furthermore, accelerometers are generally more durable, cost less and consume less battery power than pressure sensing insole arrays and strain gauge based goniometers.

2.5 Conclusions

Low pass filtered accelerometers having zero frequency response, such as the ADLX05, can substitute for pendulum type inclinometers previously used for stance-swing detectors in FES. Accelerometers can be used in conjunction with SML to reliably detect the stance and swing phases of gait. They could also be used to clone an individual patient's skill in operating handswitch controlled FES systems. Such a detector can be synthesized using either of the supervised machine learning algorithms examined. Of the three stance-swing detectors examined, the machine learning algorithms were more accurate than the previously reported hand crafted techniques, and the detector based on Rough Sets was computationally the most efficient.

Either RS or ALN based stance-swing detectors or control clones can be readily implemented for real time operation using MC68332 microcontroller. The three ADLX05 accelerometers were located at a single site or cluster on the shank. Additional phases or events, such as those defined by Perry, can also be extracted in real time from the same cluster with a similar accuracy. This system could be used in a number of FES systems, for example, as a trigger for a drop-foot stimulator or as a behavioral clone to mimic skilled hand-switch control of FES walking systems. If the motion sensed by the accelerometers is rich in volitional movement, then intention detectors, similar to handswitch clones, could provide command and coordination input to the FES control systems. The SML algorithms enable the contributions of the sensor signals to be ranked in information theoretical terms and therefore allows changes in position or alignment to be quantitatively assessed.

Micromachined electromechanical sensors (MEMS), such as the accelerometer used in these studies, are suitable for FES control applications due to their small size, high

signal to noise ratio, reliability, low power consumption, and low cost. Although sensors were worn externally, the devices are available in small packaging formats or even as silicon dies of millimeter dimensions making them suitable candidates for implantation. Supervised machine learning may, in the future, enable the fusion of artificial sensors with natural bio-potentials sensed by electrodes.

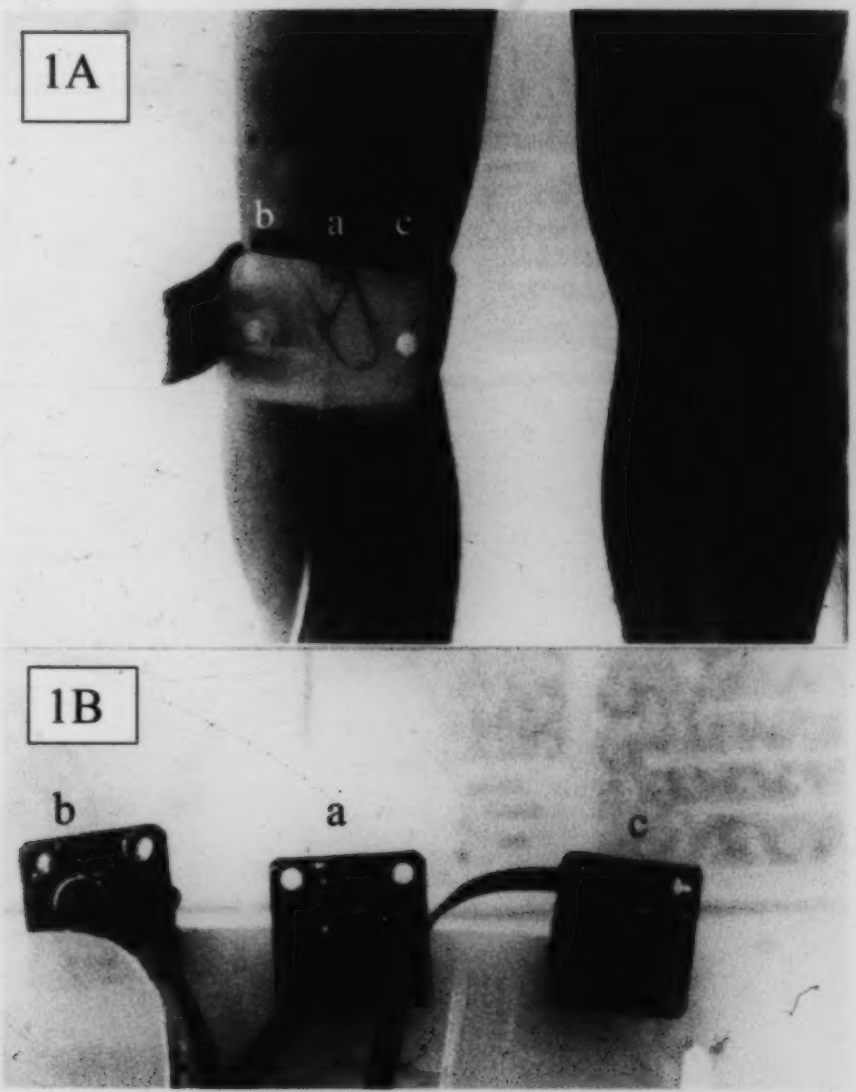

Figure 2.1

(A) - Subject wearing calf strap with three accelerometers. The strap is worn between the patella and the head of the gastrocnemius soleus muscle group.

(B) – The three accelerometers attached to the calf strap are shown. a is oriented in the vertical direction. b and c are oriented in a horizontal direction with approximately 70° between their axis of detection.

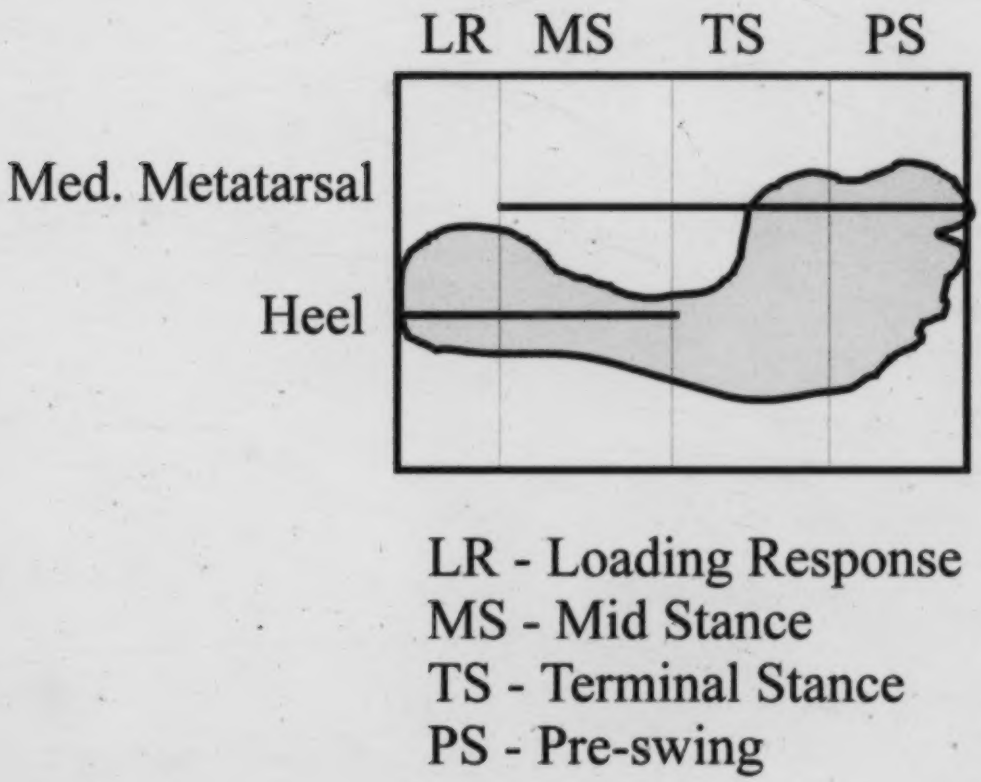

Figure 2.2: Gait Phases Determined from FSR Foot Pressures.
Four stance phases and swing were determined from bilateral insoles (force sensing resistors placed at the heel, and medial and lateral metatarsals). The following gait phases, after J. Perry, were Loading response (LR), mid-stance (MS), terminal stance (TS), pre-swing (PS). The distinction between terminal stance and pre-swing is based on contralateral foot contact.

Figure 2.3: Accelerometer Recordings and Coincident Gait Phase: The three graphs are an example of: A-Unfiltered accelerometers, B-Filtered accelerometers. In both of these graphs, the dotted line is the recording of accelerometer a in Figure 2.1B, oriented vertically. The solid and dashed lines are accelerometers b and c in Figure 2.1B, oriented in horizontal directions. C-Gait phase. Five gait phases are calculated, loading response (LR), mid-stance(MS), terminal stance(TS), pre-swing(PS), and Swing(SW). The time scale is coincident on the ordinate axis of each graph.

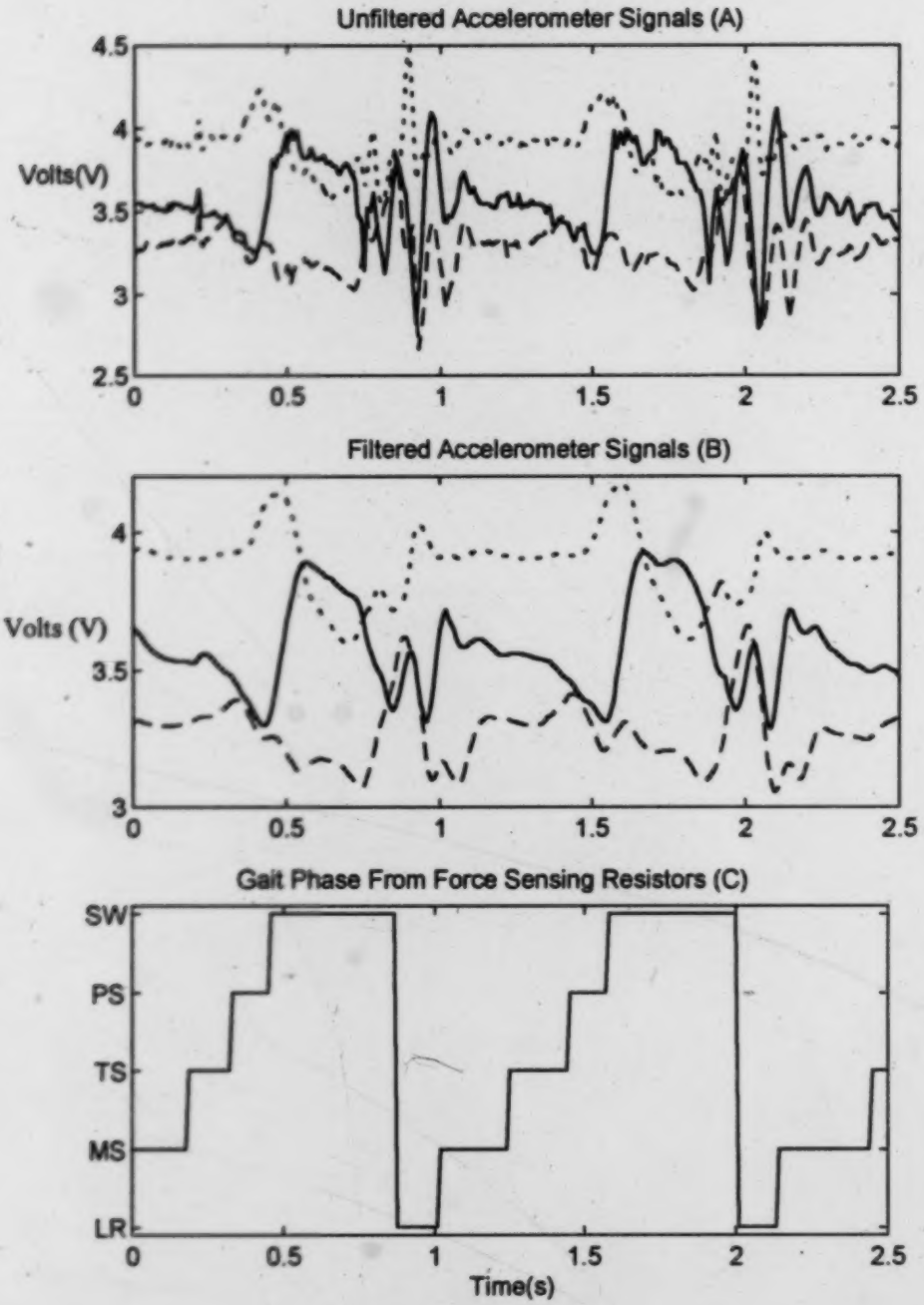
Unfiltered Accelerometer Signals (A)
Volts(V)
4.5
4
3.5
3
2.5
0
0.5
1
1.5
2
2.5
Filtered Accelerometer Signals (B)
Volts (V)
4
3.5
3
0
0.5
1
1.5
2
2.5
Gait Phase From Force Sensing Resistors (C)
SW
PS
TS
MS
LR
0
0.5
1
1.5
2
2.5
Time(s)

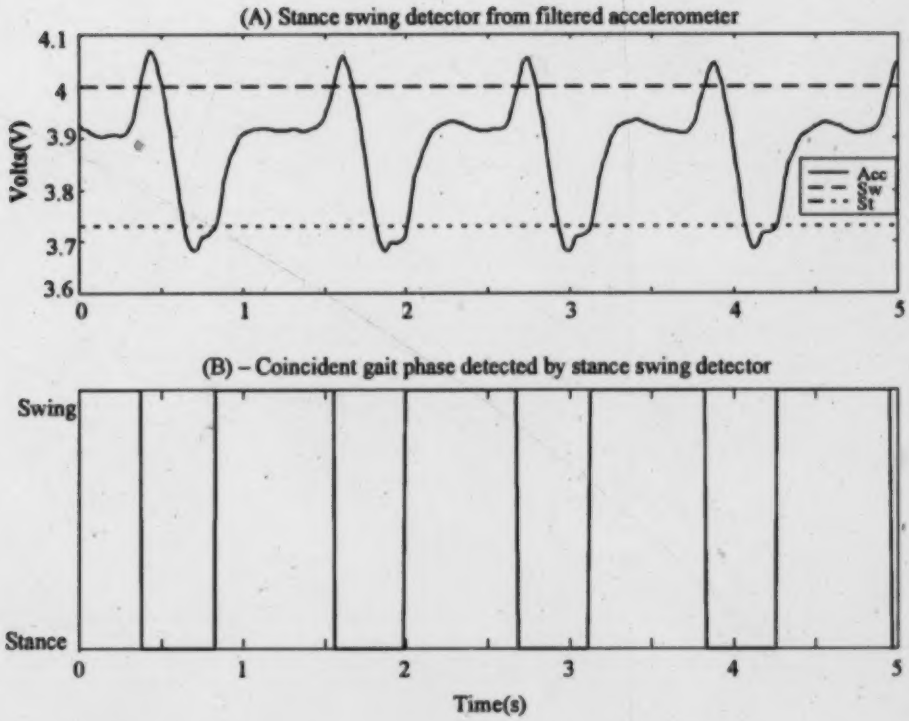

Figure 2.4: Filtered accelerometers as tilt meters.

(A) Stance and swing were detected by a filtered accelerometer using a two threshold method.

Legend: Acc-Filtered Accelerometer (Inertial tilt meter)
Sw-Swing Threshold
St-Stance threshold

(B) Coincident gait phase. Displayed is the gait phase predicted by the two threshold stance swing detector

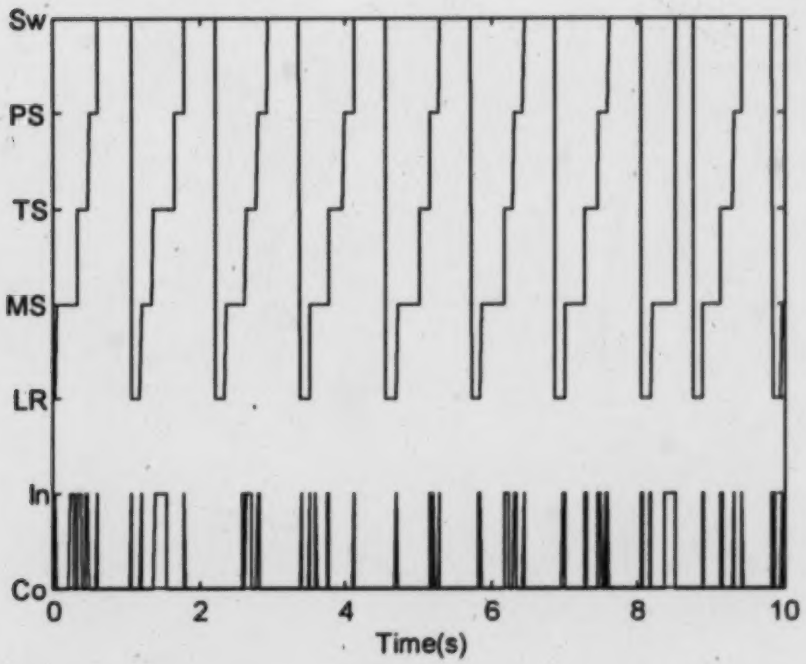

Figure 2.5: Five gait phases determined from accelerometers and a RBC.

The predictive ability of this technique is displayed on the bottom of the figure. Incorrect predictions are indicated in the (In) measurement. The errors are typically one or two sample intervals in duration.

Legend
SW-Swing
PS- Pre-Swing
TS- Terminal Stance
MS – Mid-Stance
LR- Loading Response
In - Incorrect Prediction
Co - Correct prediction

Figure 2.6: Distribution of errors using the post-filtered Rough Sets (pfRS) gait phase detector.
(Top) The error distribution for stance and swing detection using the RS classifier and the hand-crafted method. The RS detector is displayed to the left. The crosshatched bars represent the average number of correct predictions in sample intervals. The bars on the immediate left and right of the correct predictions represent the average period of the incorrectly predicted gait phase in sample intervals and whether they were early or late respectively. The standard deviations are also shown.
(Bottom) The error distributions for the five phase detector (loading response {LR}, mid-stance {MS}, terminal stance {TS}, pre-swing {PS}, and swing {Sw} as defined by Perry) by the rule based classifier evaluated at 33 Hz. The crosshatched bars represent the average number of correct sample predictions. The darkened bars immediately to the left and right of each crosshatched bar are the average number of incorrect predictions, in samples, either early or late respectively.

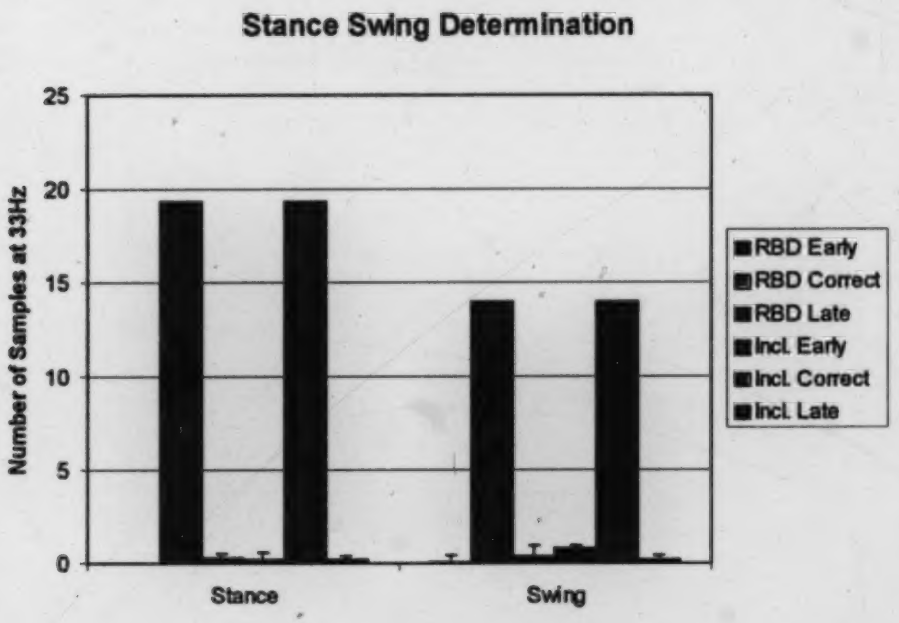
Stance Swing Determination
Number of Samples at 33Hz
25
20
15
10
5
0
Stance
Swing
RBD Early
RBD Correct
RBD Late
Incl. Early
Incl. Correct
Incl. Late

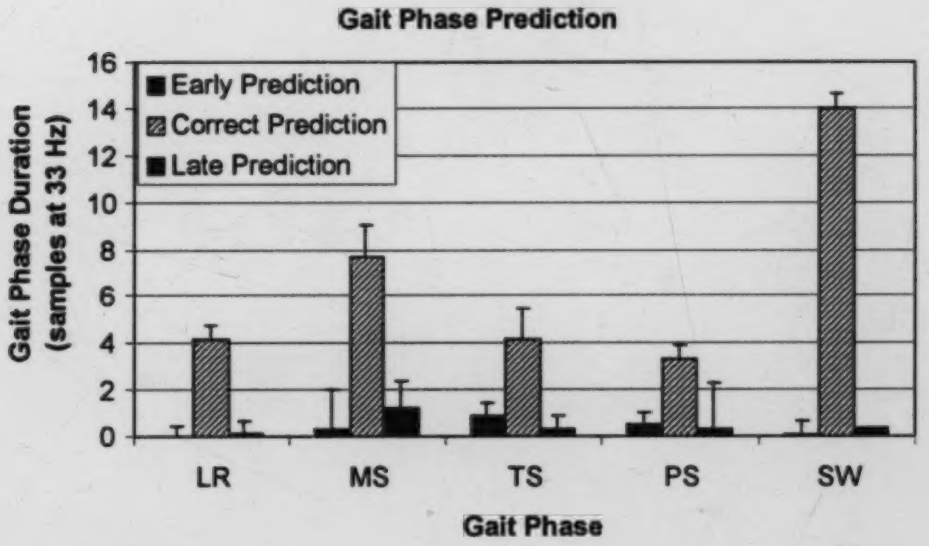
Gait Phase Prediction
Gait Phase Duration (samples at 33 Hz)
16
14
12
10
8
6
4
2
0
Early Prediction
Correct Prediction
Late Prediction
LR
MS
TS
PS
SW
Gait Phase

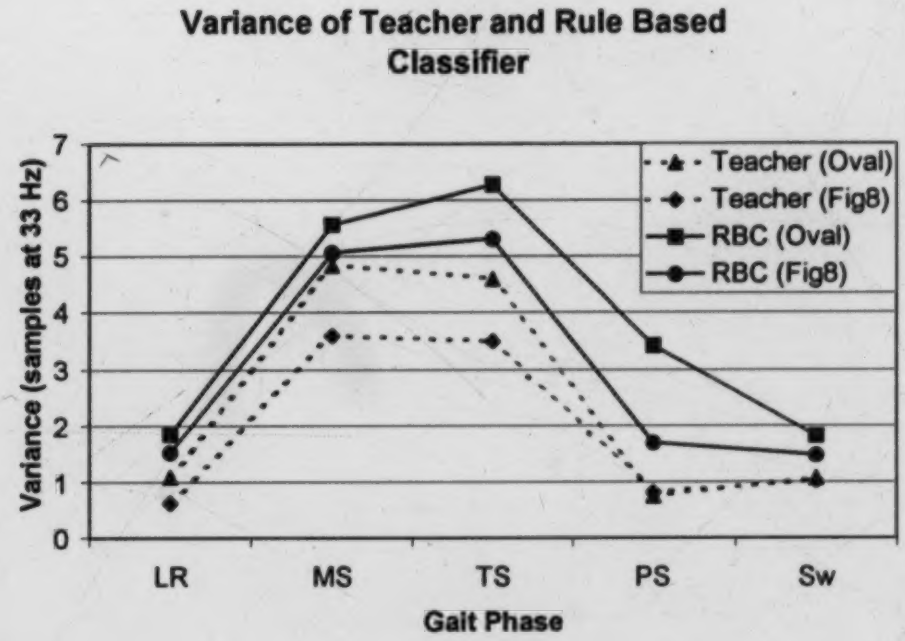

Figure 2.7 : Variance of gait phase duration.
The gait phases are loading response (LR), mid-stance (MS), terminal stance (TS), pre-swing (PS), and Swing (Sw). The teacher signals are the dashed lines. The solid lines are for the rule based classifier (RBC). The variance was evaluated at a sampling rate of 33 Hz.

Subject	Age	Weight (kg)	Height (m)	Oval Walking Speed(m/s)	Figure 8 Walking Speed (m/s)
A	20	86	1.78	1.2	1.4
B	24	66	1.66	1.3	1.4
C	22	75	1.76	1.1	1.2
D	19	59	1.70	1.3	1.1
E	20	66	1.66	1.1	No record

Table 2.1: Physical Characteristics and Average Walking Speed of Each Subject

	FSR Location					
Right Leg Gait Phases	R. Heel	R. Medial Metatarsal	R. Lateral Metatarsal	L. Heel	L. Medial Metatarsal	L. Lateral Metatarsal
Swing	OFF	OFF	OFF	-	-	-
Loading Response	ON	OFF	OFF	-	-	-
Mid-Stance	ON	(ON)	(ON)	-	-	-
Terminal Stance	ON	ON	ON	ON	OFF	OFF
Pre-Swing	OFF	ON	ON	-	-	-

Table 2.2 Gait phases from FSR recordings.
For the FSR placements, R. refers to right, L. refers to left. This table is constructed for right leg phase detection. An equivalent table can be constructed for left leg detection. ON and OFF correspond to the FSR was determined to be ON or OFF by a 5% threshold. The bracketed ON indicates that OR, i.e. if either the R. Medial Metatarsal or R. Lateral Metatarsal goes ON, then Mid-Stance is started.

Subject	Rough Sets (RS)	ALN	Hand-Crafted
A	97.06	94.17	95.90
B	94.60	87.75	93.30
C	95.60	94.39	87.10

Table 2.3: Comparison of the test set accuracy for stance and swing detection using the ALN3.0, Rough Sets and Hand Crafted detectors during level ground walking. Data was sampled at 100 Hz.

Training	Rough Sets						ALN3.0					
A	99	90	86	86	97	94	98	93	84	95	99	95
B	95	80	88	88	97	92	93	90	72	97	99	94
C	96	85	75	80	95	90	90	85	80	95	96	93
Testing												
	LR	MS	TS	PS	SW	OV	LR	MS	TS	PS	SW	OV
A	95	82	76	78	98	89	96	91	78	95	99	93
B	88	75	84	70	93	85	91	84	69	92	98	87
C	91	82	52	71	92	82	87	80	70	87	93	86

Table 2.4: Results of multiple gait phase determination by RBDs.
Loading response(LR), mid-stance(MS), terminal stance(TS), pre-swing(PS), swing(SW), and overall(OV) prediction accuracy were calculated by both Rough Sets and ALN3.0. All values are percentage correct.

	Early prediction	Correct prediction	Late prediction
RBC Swing	0 (0)	13.98	.32 (0.57)
Inclinometer Swing	.21 (0.15)	13.98	.19 (0.2)
RBC stance	0.04 (0.38)	19.34	.38 (0.2)
Inclinometer Stance	.82 (0.4)	19.34	.23 (0.15)

Table 2.5: Results of postfiltered RBC determination of stance swing.
The values in the tables are numbers of samples at 33 Hz. The table was compiled from subject A's testing walking pattern, evaluated after the intuitive rule, evaluated over 49 strides. The normal values are the number of samples of the occurrence, the bracketed values are the standard deviation of the number of samples.

	Loading Response	Mid-Stance	Terminal Stance	Pre Swing	Swing	Overall
Early	0 (0)	0.32 (1.7)	0.86 (0.54)	0.52 (0.47)	0.04 (0.57)	1.74
Correct	4.16 (0.58)	7.68 (1.34)	4.18 (1.27)	3.32 (0.58)	13.98 (.66)	33.32
Late	0.16 (0.47)	1.22 (1.18)	0.28 (0.61)	0.32 (1.98)	0.38 (0.42)	2.36
Overall Accuracy	96	83	78	80	97	89

Table 2.6 Results of postfiltered RBC determination of multiple gait phases.
Early, correct and late refer to the average number of samples at 33 Hz each gait phase was predicted to be early, correct or late. The average duration of an error is given, with the standard deviation of the error given in parenthesis. The table was compiled from subject A's testing walking pattern, evaluated after the intuitive rule, evaluated over 49 strides. Overall accuracy is given as a percentage.

	Program Size (kB)	Clock Cycles	Speed of Execution(ms)
Rough Sets	40.7	1440	0.01
ALN	120	17000	0.1

Table 2.7:Real time implementation of Rough Sets and ALN. Program size is reported in kilobytes, clock cycles as number clock cycles to implement one decision, and speed of execution is the realized implementation speed on a MC68332 running at 16.7 MHz in milliseconds.

2.6 Bibliography

Analog Devices, ADXL05JH Product specifications

Andrews B.J., Barnett R.W., Phillips G.F., Kirkwood C.A., Donaldson N., Rushton D.N., and Perkins T.A. (1989) "Rule-based control of a hybrid FES orthosis for assisting locomotion", Automedica, 11:175-200

Armstrong, W.W., Thomas, M.M., (1995) "ATREE release 3.0 software", Dendronics Decisions Ltd.

Bajd, T., Kralj, A., Karcnik, T, Savrin, R., and Obreza, P., (1994) "Significance of FES-assisted platarflexion during walking of incomplete SCI subjects", Gait & Posture, 2:5-10

Chandler, S.A.G., (1973) The control of limb movements by functional electrical stimulation, Ph.D. Thesis, University of Southampton

Craggs, M.D., The Cortical Control of Limb Prostheses, PhD thesis, University of London, 1974

Dai, R., Stein, R.B., Andrews, B.J., James, K.B., and Wieler, M., (1996) "Application of tilt sensors in functional electrical stimulation", IEEE Trans Rehab. Eng., 4(2):63-72

Heller, B.W., Granat, M.H., and Andrews, B.J., (1996) "Swing-through gait with free-knees produced by surface functional electrical stimulation." Paraplegia. 34(1):8-15

Granat, M.H., Heller, B.W., Nicol, D.J., Baxendale, R.H., and Andrews, B.J., (1993) "Improving limb flexion in FES gait using the flexion withdrawal response for the spinal cord injured person" J. BME 15(1):51-6

Graupe, D. (1989), "EMG Pattern Analysis for Patient response control of FES in Paraplegics for Walker Supported Walking, IEEE Trans. BME 36(7):711-719

Kirkwood, C.A., and Andrews, B.J., (1989) "Finite State Control of FES Systems: Application of AI Inductive Learning Techniques," Proc. IEEE EMBS pp 1020-1021

Kirkwood, C.A., Andrews, B.J., and Mowforth, P., (1989) "Automatic detection of gait events: a case study using inductive learning techniques", J. BME 11:511-516

Kobetic, R., and Marsolais, E.B., (1994) "Synthesis of paraplegic gait with multichannel functional neuromuscular stimulation", IEEE Trans. Rehab. Eng. 2(2):66-79

Kostov, A., Andrews, B.J., Popovic, D.B., Stein, R.B., Armstrong, W.W., (1995) "Machine learning in control of Functional Electrical Stimulation Systems for Locomotion", IEEE Trans. BME 42(6):541-51

Kostov, A., (1996) "Functional error assessment in gait event discrimination for FES assisted locomotion", IEEE EMBS paper 969

Kralj, A., and Bajd, T., (1989) FES: Standing and Walking after SCI, CRC Press, ISBN 0-8493-4529-4

Liberson, W.T., Holmquest, H.J., Scott, D., and Dow, M., (1961) "Functional electrical stimulation of the peroneal nerve synchronized with the swing phase of gait of hemiplegic patients," Arch. Phys. Med., 42:101-105

Michie, D., Bain, M., Hayes-Michie, J., (1990), "Cognitive models from subcognitive skills", In: Knowledge-Based Systems for Industrial Control, Eds. McGee, Grimble and Mowforth, pp 71-99, IEE Control Engineering Series 43, Peter Peregrinus Ltd. London UK

Ng, S.K., Chizeck, H.J. (1997) "Fuzzy model identification for classification of gait events in paraplegics", IEEE Trans. Fuzzy Systems, 5(4):536-544

Perry, J., (1992) Gait Analysis: Normal and Pathological Function Thorofare, N.J. : Slack Inc.

Reduct Systems trade literature, Rough Sets

Upshaw B.J., Sinkjaer T., (1997) "Natural versus artificial sensors applied in peroneal nerve stimulation" Artif. Organs 21(3):227-31

Willemsen, A.T., Bloemhof, F., Boom, H.B., (1990) "Automatic stance-swing phase detection from accelerometer data for peroneal nerve stimulation", IEEE Trans. BME 37(12): 1201-8

Williamson, R., Andrews, B.J., Au, R., (1996) "Control of Neuralprostheses II: Event Detection Using Machine Learning" Proc. RESNA'96, pp 291-293

3 Detection of Absolute Knee flexion angle and angular velocity

3.1 Introduction

The motivation for the present study is to develop sensor systems for use in feedback control of functional electrical stimulation (FES) used to restore functional movement after spinal injury or stroke. A number of closed loop control systems that have been proposed to improve standing and walking are based on sensing knee joint angle and angular velocity (Andrews et. al, 1989, Crago et. al, 1986, Crago et. al, 1996, Davoodi and Andrews, 1998, Dolan et. al, 1998, Kirkwood et. al, 1989, Mulder et. al, 1992, Petrofsky et. al. 1984, Popovic and Tepavac, 1982). For safety reasons, control may be required to limit the terminal velocity of the extending knee joint when standing-up or the seat impact velocity when sitting down (Davoodi and Andrews, 1998).

Many sensors and measurement systems exist for studying human motion, however only a few are candidates for routine FES use outside the laboratory (Crago et al 1986). A sensor frequently used for FES in laboratory demonstrations is the Biometrics (formally Penny and Giles) flexible goniometer (Biometrics Ltd., 1999). Experience with this device suggests that this device would be too fragile and expensive for practical daily use. The sensing element is a fixed length metal strain gauge, and can be easily damaged through excessive or repetitive strain and/or stress. Contact with clothing worn over the device can produce signal artifacts. The sensing element requires approximately 50-100 mA, hence power supply multiplexing circuits may be necessary for battery powered applications. Crago and colleagues (Crago et. al., 1986) noted that during sit-to-stand trials, this type of goniometer required calibration prior to each trial due to slipping of the two mounts.

Angular velocity can be derived from the goniometer by differentiation. These differentiation techniques appear to amplify the high frequency noise components of the angular velocity, as the signal and corresponding signal to noise ratio of the high frequency range is typically lower than that for a low frequency range. Selecting the appropriate cutoff frequency and the type and order of the low pass differentiating digital filter becomes critical to optimize the signal to noise ratio of the derivative. Finite impulse

response filters are often used since they do not introduce non-linear phase distortions. However, they do introduce a time delay in proportion to the half span of the filter used (Hamming, 1962, Andrews et. al, 1981) which deter from the causal estimate of angular velocity.

Accelerometers have been used in movement analysis to derive knee flexion angle and angular velocity through numerical integration (Morris, 1973, Smidt, 1977), the movement of the center of mass (Smidt, 1971, Molen, 1972), and to reconstruct forces around a joint in combination with force plate recordings (van den Bogert et. al, 1996). The algorithms used to compensate for drift of the signals and integrals require non-causal processing and are suited only to off-line applications.

In the field of FES control, Willemsen et al. (Willemsen et. al., 1991) proposed real time method to estimate knee joint angle and angular velocity using a set of accelerometers mounted on rigid metallic plates attached laterally to the thigh and shank. These plates were aligned with the long axis of these limb segments. An approximation was made that movement only occurred in the sagittal plane. A novel formula was used that circumvented the drift errors usually associated with numerical integration. Heyn et. al. (Heyn et. al, 1996) added rate gyroscopes to Willemsen's system to directly measure the segmental angular velocities, but computed the angular velocities and tilts in an offline procedure. Unfortunately, the mounting plates and straps that are required to comply with the assumptions of the formula may be too encumbering for daily use.

Dai et al. (Dai et. al, 1996) proposed the use of a miniature, pendulum type inclinometer attached to the shank to switch on and off electrical stimulation to the common peroneal nerve to prevent drop foot during hemiplegic gait. The inclinometer signal was low pass filtered using a 2^{nd} order Butterworth low pass filter with cut off at 1.5 Hz. Winter, (Winter, 1990) suggests that frequency components below 6 Hz should not be attenuated due to low pass filtering, hence low pass filtering at 1.5 Hz is expected to be unsuitable for precise determination of angular kinematics.

Rate gyroscopes have been reported for monitoring human motion. Rate gyroscopes have a zero frequency (DC) output offset when stationary (muRata trade literature, 1999). This DC offset can drift, commonly due to temperature. Compensation

for this drift is made in the estimation of angles through integration. Miyazaki (Miyazaki, 1997) integrated the output of a piezoelectric rate gyroscope attached to the leg to determine hip flexion extension angle which was then used to estimate walking speed. A 0.5 Hz high pass filtered rate gyroscope signal was generated and numerically integrated to produce thigh tilt. Kataria and Abbas (Kataria and Abbas, 1998) reported an accuracy of 4.7° for Miyazaki's method when evaluated for cyclical planar motion of a two dimensional model and implementing a high pass cutoff frequency of 0.0047 Hz. In both of these reports, the motions examined were cyclical with periods of the order of a second, hence a zero DC component of angular velocity is expected. For noncyclical motions, such as standing-up, the application of this technique might be inappropriate.

This literature review indicates that mechanical pendulum inclinometers or accelerometers, when low pass filtered, can provide useful signals for FES but are unsuitable in bandwidth for angular kinematics. Rate gyroscopes can be used to provide wider bandwidth estimates of angle for cyclical movements, although are limited due to DC drift of the device. In combination with heuristic signal processing, the rate gyroscope could be used to determine the wide band kinematics, whereas the low pass filtered accelerometer could be used to provide stable measurements of tilt and angle that are not subject to drift.

In this paper we describe a prototype system, we refer to as a Gyrogoniometer, comprising two small modules containing rate gyroscope and accelerometer devices attached to the thigh and shank that were used to determine limb segment inclinations and knee joint angulation. We compared the accuracy of the estimate of knee flexion angle and angular velocity to a two module, low pass filtered accelerometer based system.. The performance of these new sensor systems was compared to a Biometrics M180 flexible goniometer which was used as the reference. A preliminary report of the Gyrogoniometer has been reported (Andrews and Williamson, 1997).

3.2 Theory of Operation

3.2.1 Determination of Angle and Angular Velocity

Figure 3.1 illustrates a planar calculation of angles from a set of rate gyroscopes and accelerometers signals. The sampled accelerometer signals are indicated by α_x and α_y, and the rate gyroscope signal by ω. The DC offset of the rate gyroscope is ω_0. For the practical implementation of the system, the sensors are arranged in clusters and positioned on an individual as shown in Figure 3.1.

At the start of each trial, equation (1) was used to estimate the mean static tilt of the thigh and shank using a number of successive data samples, m = 50, of the accelerometer signals that were sampled at 100 Hz. The arctangent was used in preference to the arcsine function since the former is defined for an infinite range of inputs whereas the latter is defined only for the input range from –1 to +1.

$$\theta_n(t_0) = \left[\sum_1^m \tan^{-1}(a_{y,n}/a_{x,n})\right]/m \qquad (1)$$

Thereafter the dynamic tilt of the segments can then be estimated from equation (2), by integrating the signal from the rate gyroscopes.

$$\theta_n(t) = \int_{t_0}^{t} (\omega_n(t) - \omega_0)\cdot dt + \theta_n(t_0) \qquad (2)$$

The knee flexion angle was calculated as

$$\phi_n = \theta_{n+1} - \theta_n \qquad (3a)$$

The rate of change of knee flexion angle, refereed hereafter as knee angular velocity, was calculated as

$$\phi' = \omega_2 - \omega_1 \qquad (3b)$$

3.2.2 Auto-Nulling the Rate Gyroscopes and Auto-Resetting the Integrators

The rate gyroscope has a non-zero DC output, ω_0, referred to as the DC offset. In the case of the ENG05GA (muRata Trade literature) device this is approximately 2.5V. The DC offset varies with temperature; this effect is called offset drift. In order to

integrate the output of the rate gyroscope the DC offset must be calculated, also referred to as nulled or zeroed, prior to starting the integration. Any error in nulling this DC offset will accumulate without bound with integration. Any changes in the DC offset during the course of integration, for example, due to very low frequency thermal drifts can also produce large accumulated errors. If the rate gyroscope were to drift 1 mV from the initial zero velocity recording, then the accumulation of error over a 10 second period would be 9° as the sensitivity of the rate gyroscope is 1.1 mV/°s.

The rate gyroscope can be nulled at times in which the sensor cluster is not moving. These times are determined by observing the segmental inclination ($\theta(t)_{accel}$), as computed using equation (1). If the segmental inclination displays a small standard deviation (σ) over the immediately previous short interval (τ), then it is assumed that the segment has not moved. This condition is determined using the following heuristic rule, hereafter referred to as auto-nulling the rate gyroscope.

If

$$\sqrt{\frac{\int_{t_1}^{t_2}\theta(t)_{accel}^2\,dt-\left(\int_{t_1}^{t_2}\theta(t)_{accel}\,dt\right)^2}{\tau}}<\sigma \qquad (4)$$

Where $\tau = t_2 - t_1$. Then

$$\omega_o = \int_{t_1}^{t_2}\omega(t)\cdot dt \qquad (5)$$

For our tests, the value of σ was set at 0.1^0, and τ = 0.45 seconds. This heuristic rule was asserted every 0.1 seconds.

Even with auto-nulling of the rate gyroscope, the angle calculated from integrating the rate gyroscope can possess errors due to a temporary incorrect zero. The accelerometers detect the accelerations characteristic of movements of the body and the gravitational components that are responsible for the tilt of the segment. Summed over a long period of time, the averaged value of an accelerometer recording is the averaged acceleration of the body and the averaged tilt of the body. The averaged acceleration of the body is net change in velocity of the body. The net change in velocity is zero for many

human movements. For example, the velocity of the body before and after a sit to stand transition is zero, and the net change in velocity is zero. Hence, the averaged accelerometer recording is generally an estimate of the averaged tilt of the body.

A rule, if tilt angle computed from the integral of the rate gyroscope signal, using equation (2), differs by a preset amount (λ) from the tilt angle computed from the accelerometers, using equation (1), then the integral of the rate gyroscope angle will be reset to the angle calculated by the accelerometers, was imposed. This is mathematically expressed by

If

$$\frac{\left|\int_{t_1}^{t_2}\theta_{r,gyro}dt-\int_{t_1}^{t_2}\theta_{accel}dt\right|}{t_2-t_1}>\lambda \qquad (6)$$

Then

$$\theta_{r,gyro}(t_2)_{subsequent}=\theta_{r,gyro}(t_2)_{prior\ to\ reset}-\frac{\int_{t_1}^{t_2}\theta_{r,gyro}dt-\int_{t_1}^{t_2}\theta_{accel}dt}{t_2-t_1} \qquad (7)$$

This rule was asserted every 0.1 s, with the threshold λ set at 1^0. The difference between t_2 and t_1 was set at 0.45 seconds. An error in the tilt of a segment and the subsequent reset rate gyroscope integral can be introduced due to the non-gravitational accelerations measured by the accelerometers. Calculated in a previous unpublished experiment, the maximum instantaneous error by this technique due to non-gravitational accelerations is 12^0 for a person running at 18 km/h with accelerometers placed on the foot and less than 2^0 for a person rising from a seated position.

3.3 Methods and Results

3.3.1 The Sensors

Three sensor and associated signal processing systems were used:

3.3.1.1 The flexible goniometer

The Biometrics M180 device, which directly measures the relative angle between the two endpieces, was used to calculate a reference angle. The output voltage was filtered with a 2nd order, low pass Butterworth filter and then again in the reverse time sequence, i.e. anticausally, to cancel phase distortions. The 3 dB corner frequency was set at 2.5 Hz and the filtering process implemented using MATLAB v 5.2.1. To obtain angular velocity, the low pass filtered goniometer signal was differentiated using the simple difference formula:

$$\dot{\theta}(t) = \theta(t) - \theta(t-1) \qquad (8)$$

3.3.1.2 The accelerometer based inclinometer/goniometer

The 2D ADXL202JQC accelerometers have a DC response and are suitable for use as an inclinometer by measuring components of the gravity vector as indicated in equation (1). In order to remove components due to motion of the device, the output voltage of the accelerometer was low pass filtered using a single pass 2nd order digital Butterworth filter with 3 dB corner set at 2.5 Hz.

These accelerometers were placed on the thigh and shank segments. The knee flexion angle was calculated using equation (3) and estimates of knee angular velocity were derived using equation 8.

3.3.1.3 The combined rate gyroscope and accelerometer "Gyrogoniometer"

Two clusters, comprising accelerometers and rate gyroscopes were attached to the thigh and shank. Each cluster comprised one rate gyroscope, Murata part number ENC05GA (Murata trade literature 1999) and 2D accelerometers Analog Devices part number ADXL202JQC, (Analog Devices trade literature 1999). The cluster positioned on the shank contained two ADLX202 accelerometers, and the thigh cluster contained one ADLX202. Thigh and shank inclinations were calculated using equation (2) and the knee flexion angle using equation (3). Knee angular velocity is given by the difference of the two gyroscope outputs i.e. using equation 3(b). Equations (4) through (7) were evaluated in the degree to which each could compensate for errors associated with drift. The cluster

dimensions were 5 x 3 x 1.7 cm, and weight 85 g. Figure 3.2 displays a picture of the sensors.

3.3.2 Data Acquisition and Signal Pre-processing

The Biometrics M180 goniometer was powered by a +/- 2.5 V supply and amplified (Analog devices AMP04FNZ6642) at the endpiece to increase the signal to noise ratio of the device. The output voltage was input directly to a 12 bit A/D channel of the PC (National Instruments AT-MIO-16L card). This A/D converter was controlled by NI's LabWindows/CVI 5.0.1 software. A synchronization signal from the TT8 was sampled with the goniometer to coordinate the sampling of the goniometer to that of the accelerometer and rate gyroscope clusters. For the tests on the able bodied and paraplegic subject, the goniometer signal was acquired using the Maxim186 A/D converter (Maxim part number MAX186) on the TT8 and stored on the Persistor™ microdisc.

The accelerometer signals were amplified (Analog devices AMP04FNZ6642) to provide a 3 volt range for accelerations between +/- 1 g. The rate gyroscope's sensitivity was 1.1 mV/° s. These signals were sampled using a 12 bit A/D converter (Maxim part number MAX186) of 4.096 V range. The sampling time for 8 channels was 320 μs. The serial A/D converter was controlled via a QPSI bus controlled by an Onset Computers TT8 MC68332 microcontroller with a 2 MB removable microdisc flash memory (CF8 Persistor™ , supplied by Peripheral Issues Inc.) to store the signal data samples at 100 Hz.

The +/- 1 g level for each accelerometer was determined on a day prior to the trials taking place. Each cluster was set in a position for 2.56 seconds and sampled at 100 Hz. The positions were chosen such that one accelerometer was aligned with or against gravity to record a +1g or –1 g value respectively.

The ambient temperature of the room was 21 °C. The subsequent experiments were conducted on different days. To test the robustness of the system, the accelerometers were not recalibrated before each trial. The room temperature on the days of the trial varied between 20-21 °C. The variation in DC baseline of the accelerometers for a temperature variation of 1 ^{0}C was 6 mV, or 0.4 degrees and was within the

specifications for the devices. The sensitivity of the rate gyroscope was 1.1 mV/°s and was not confirmed by calibration.

Two types of tests were conducted to compare the new sensor systems against the reference flexible goniometer. The first are bench tests that involve mounting the sensors on a plastic articulated model that can be moved in a vertical plane to simulate the motions of the thigh and shank during sit-stand and stand to sit maneuvers. In the second series of tests, the sensors were attached to the legs of able bodied and paraplegic volunteers. These individuals then performed sit to stand, and stand to sit maneuvers whilst the sensor data was recorded. FES was applied to the quadriceps of the paraplegic volunteer to assist standing.

3.3.3 Bench Tests Using an Articulated Plastic Model

3.3.3.1 Single Segment Static Inclination Test

Sensor modules A and B were attached to the upper (thigh) segment of a two dimensional articulated plastic model, as shown in Figure 3.3, that could be manually moved in a vertical plane. The Biometrics M180 goniometer was attached across the pivot joint as illustrated in Figure 3.3. The goniometer was calibrated by recording the voltage at 0 and 90° as measured by the protractor shown in Figure 3.3.

While holding the base of the model stationary, the upper segment of the model was moved through a range of 100°, in steps of 5° as indicated by the protractor. At each step, the upper segment was held stationary for approximately 3 seconds. The tilt was estimated by averaging 256 A/D samples taken at 100 Hz of the goniometer and accelerometers using equation (1) with m=256. The means and standard deviations were calculated for the difference between the upper segment tilts indicated by each cluster and the goniometer for each step. When averaged over the entire 100° range of motion, the mean difference was found to be 0.45° and 0.53° for the cluster A and B respectively. These results are shown in Figure 3.4.

3.3.3.2 Dynamic Single Segment Inclination Test

The two sensor clusters and the Biometrics goniometer were arranged exactly as in the above static inclination test. The upper segment of the model was moved through a range of motion of approximately 95° in a single sweep in approximately 2 seconds. An additional two seconds of data was recorded at the beginning and the end of each trial. The reference tilt signal was taken to be the low pass filtered goniometer signal. Tilt estimates were calculated from the low pass filtered accelerometer signals using equation (1).

Tilt was also estimated by integrating the rate gyroscope signals. Six different methods were computed representing possible combinations of three zeroing techniques and two resetting techniques. These are referred to alphabetically as methods A - F and are defined as follows.

A. The rate gyroscope DC offset was nulled 24 hours before the trial and the integrator was not reset during the trial.
B. The rate gyroscope DC offset was nulled once at the beginning of each trial and the integrator was not reset during the trial.
C. The rate gyroscope DC offset was nulled automatically in accordance with equations (4) and (5), and the integrator was not reset during the trial.
D. The rate gyroscope DC offset was nulled 24 hours prior to the trial, and the integrator was reset in accordance with equations (6) and (7)
E. The rate gyroscope DC offset was nulled at the beginning of each trial and the integrator was reset in accordance with equations (6) and (7)
F. The rate gyroscope DC offset was nulled automatically in accordance with equations (4) and (5) and reset in accordance with equations (6) and (7)

A comparison was made, using the paired-T test, between segment tilt estimated by each of these methods and that estimated by the low pass filtered accelerometer method

using equation (1). Tables 3.1 and 3.2 summarize the results of eight repeated trials for each method A – F above.

The rate of change of tilt was estimated by differentiating the low pass filtered goniometer and accelerometer signals as described above. Angular velocity was also determined directly from the rate gyroscopes using equation (3b).

The integrated rate gyroscope signals nulled on a previous day (method A above) were poor estimators of tilt ($p < 0.005$). For sensor cluster A, methods B, C, E, and F were not statistically different ($p < 0.01$), as computed by individually pairing any two of the methods and examining the difference in accuracy using a paired T test. For cluster B, methods C and F produced a more accurate estimate than methods B and D ($p < 0.10$). The rate gyroscopes also provided a more accurate estimate of the angular velocity than the accelerometer based method ($p < 0.005$).

3.3.3.3 Dynamic Knee Joint angle Test Using the Articulated Model to Simulate Sit-Stand-Sit Motion

In this bench test, the two sensor clusters A and B were positioned on the upper and lower segments of the model shown in Figure 3.5. Both segments of the model were moved manually to simulate sit to stand and stand to sit maneuvers. Each maneuver was repeated six times with a five second interval between each sit-stand or stand to sit maneuver. From the previous dynamic inclination tests, we concluded that the rate gyroscopes required to be nulled either prior to each trial (methods B and D) or automatically (methods C and F) to provide an accurate estimation of tilt. Therefore, the resetting and nulling methods A and D were not tested.

The results from the maneuvers are summarized in Table 3.3. A statistical difference was not observed between the angle calculated from the accelerometers and reset/nulling methods B, C, E, and F ($p < 0.01$) in the plastic model. A more accurate calculation of the angular velocity was made using the rate gyroscopes ($p < 0.01$) than by using the accelerometers.

The resetting of the integral of the rate gyroscope occurred at the discontinuities indicated by the arrow in Figure 3.5b with resets occurring at times 2.8, 3.6, 4.6, 5.0, and

5.2 seconds as indicated. The auto-nulling of the DC offset when using method F is also indicated in Figure 3.5a occurring at times 1.2, 4.6, 5.6, and 5.8 seconds.

In Figure 3.5b, it can be seen that auto-resetting can reduce integrator error, (see instants 3.6, 4.6, 5.0 and 5.2 seconds), or increase this error (see instant 2.8 seconds). It can also be seen in Figure 3.5b that by the end of this six second trial, the drift of the DC offset of the rate gyroscope has produced a growing integration error when using method C, and that auto-nulling by method F can reduce this error in this example. Auto-resetting the integrator can compensate for integrator drift as can be seen in Figure 3.5b in the traces for methods E and F.

In table 3.3 the errors for runs 4 and 6 for the methods B and C were much larger than the errors observed for methods E and F. This was because the integrator was not reset during these runs. Therefore we discounted methods B and C from further consideration even though the overall average error for all six runs was not statistically different to the other methods ($p < 0.01$). This left two candidates for further tests i.e. methods E and F.

3.3.4 Sit-Stand-Sit Trials with Able Bodied Subjects

Repeated sit-to-stand and stand-to-sit maneuvers were performed by one able bodied female, (age 23, height 170 cm, weight 52 kg), and one able bodied male (age 27, height 190 cm, weight 80 kg). A Biometrics M180 goniometer was attached using double sided tape across the knee to provide a reference for knee joint angle. Bilateral recordings were made for both participants. The female performed 18 and the male 8 sit-stand-sit maneuvers with a rest interval of approximately 6 seconds. The standing period was approximately 6 seconds and the total time for the tests was 12 seconds. The analog to digital data acquisition rate was set to 100 Hz.

Initially we attempted a simple calibration of the goniometer by recording its averaged output with the knee in full extension and at 90 degrees of flexion as observed with a plastic protractor. However, this was found to be inadequate. Using this technique, the average knee extension was calculated to vary between 165 and 190

degrees whilst standing and 70 and 120 degrees whilst sitting. These values were visually compared with a protractor, and regarded as incorrect.

The Biometrics goniometer was calibrated for each sit-to-stand and stand-to-sit maneuver using a simple linear, two position (sitting and standing) calibration technique. The sitting and standing calibration points were determined by using the accelerometers and equation (1) as follows. The sitting angle was determined during a 0.5 second interval when the subject was sitting quietly, prior to standing up. The standing angle was determined during a 1 second interval whilst the subject was standing quietly.

Knee angulation and angular velocity were estimated using the accelerometers and the combined accelerometer and rate gyroscope methods E and F. The differences with respect to the reference goniometer derived values are summarized in Table 3.4. Differences are reported for the complete sit-stand-sit maneuver as well as for the sit-to-stand and stand-to-sit transitions. Figure 3.6 shows the estimate of knee flexion angle during a typical sit-stand-sit trial. Arrows shown in Figure 3.6a at times 1.4, 1.6 and 7.7 seconds indicate when the rate gyroscope DC offset was auto-nulled. Discontinuities in the error graph of Figure 3.6b at times 4.6, 5.1, 6.2 s indicate the instants when the integrators were automatically reset.

The methods E and F used to auto-reset the integrator and auto-null the rate gyroscopes were able to estimate the Biometrics goniometer more accurately than the method that low pass filtered the accelerometers to determine inclination for the entire sit - stand - sit maneuver, including the transitional phases ($p < 0.01$). No statistical difference was observed between the resetting/nulling methods E and F. The rate gyroscopes than made a more accurate estimate of the angular velocity than the differentiated accelerometers ($p < 0.01$).

3.3.5 Paraplegic Sit to Stand Trial Using FES

The sensor clusters and Biometrics goniometer were attached to the left leg of a male paraplegic [28 years, 7 years post injury, 180 cm, 78 kg, T-5 ASIA(A)]. This individual was skilled in the use of a simple 2 channel surface electrode FES system operationally similar to that described by Kralj and Bajd, (Kralj and Bajd, 1989). Self-

adhesive hydrogel electrodes, of dimensions 1" x 3", were placed over the approximate motor points of the vastus lateralis and rectus femoris. Reference electrodes were placed on the front of the thigh, approximately 8 cm above the knee. The goniometer was attached laterally, as shown in Figure 3.7. The left and right shank sensor clusters were mounted onto the ankle foot orthosis. The left and right upper clusters were attached to the reference electrodes.

The subject completed a total of eight standing up trials assisted by FES in one clinical laboratory session. The knee flexion angle and angular velocities were computed as they were in the above able bodied tests. Figure 3.8 shows the estimate of knee flexion angle from a typical sit to stand trial. The arrows in Figure 3.8a indicate that auto-nulling the DC offset of the rate gyroscope occurred prior to the sit to stand transition and again after the subject attained the upright standing posture. Discontinuities can be seen in Figure 3.8b at times 3.2, 7.4, 7.8, and 8.2 seconds. These discontinuities occur at times that the integrator was auto-reset. From Table 3.6 it can be seen that both methods E and F were more accurate than the accelerometer derived estimates of knee flexion angle ($p < 0.1$). The rate gyroscopes provided a more accurate estimate of the differentiated goniometer reference for knee angular velocity than the differentiated accelerometer signals ($p < 0.005$).

FES could lower the precision of a sensor system, as muscle vibrations transmitted through the skin could be detected by the sensors, and induced electrical interference due to the 200 V high voltage pulses could be 'picked up' in the sensor interface circuitry and interconnecting cables. To examine these artifacts, quiet standing tests were conducted with and without FES. Knee flexion angle and angular velocity were estimated using three methods; the goniometer, accelerometers, and auto nulling/resetting method F with the rate gyroscopes. The sensor signals were analyzed only during periods of quiet standing whilst the FES was either switched on or off. The FES could be switched off because of the knee stabilized in extension due to the ankle foot orthosis (Andrews et. al., 1989).

The paraplegic subject stood quietly during this test with his knee joints maintained in full extension. The signal components due to body motion were assumed to be in the very low frequency range, whereas, FES induced artifacts were assumed to occupy a

higher range. In standard testing procedures, a low pass filter is used to reduce the bandwidth, hence lowering the high frequency pick up of the system while maintaining the low frequency range in which the desired signal is present.

The efficacy of low pass filtering at different cut-off frequencies for reducing the residual high frequency signal power of the system was examined. The residual high frequency signal powers of the goniometer, accelerometers, and rate gyroscopes were calculated and compared to determine the effectiveness of each cut-off frequency filter level.

The FES induced artifacts on the high frequency residual of the system were examined. First, knee flexion angle and angular velocities as calculated by the accelerometer, the rate gyroscope, and the goniometer were digitally low pass filtered with 3 dB corner frequencies 2.5, 5, and 10 Hz as would typically occur in estimating knee flexion angle and angular velocity. This estimate will be referred to as X. The high frequency components were then further reduced by causally and anticausally filtering each signal with a 2^{nd} order digital Butterworth filter of 3 dB cutoff 2.5 Hz. This attenuated the remaining 20 Hz noise due to high frequency pulses and FES induced motion artifact by an additional -78 dB. These signals were noted as Y. The residual signal was calculated by subtraction of the original low pass filtered signal, X, from reduced bandwidth signal Y. This contained the residual high frequency components that were not removed by the first filtering technique in the estimate of knee flexion angle and angular velocity. The results are displayed in table 3.6.

A statistical difference was not observed between the estimates of knee flexion angle with and without FES for the Biometrics goniometer ($p < 0.01$). However, the residual high frequency power of both the accelerometer and rate gyroscope methods was significantly increased by the use of FES. The precision of the rate gyroscope method was greater than that of goniometer. Low pass filtering reduced this FES induced noise.

The use of FES did not significantly increase the RMS noise of the estimate of knee flexion angular velocity determined by the differentiated goniometer signal ($p < 0.01$), but did increase the residual high frequency power levels in both the accelerometer and rate gyroscope. The residual high frequency power of the rate gyroscope signal was

lower than that of the goniometer method. Low pass filtering was found to reduce the RMS noise.

3.4 Discussion

In every trial, except the simulated stand sit maneuvers on the plastic model, integrating the rate gyroscopes by either method E or F produced a more accurate estimate of angle and angular velocity than did the low pass filtered accelerometers method. This is displayed in tables 3.1 through 3.5.

Accelerometers were necessary to provide an initial estimation of the tilt of each segment, and to allow the initial angle between the clusters to be calculated. Thereafter, the accelerometers are used to determine the tilt of the segment to which the integral of the rate gyroscopes might be reset. The accuracy with which the accelerometers can determine their own orientation, i.e. tilt, will contribute to the overall accuracy of the rate gyroscope method. The non-linearity of the accelerometer method when compared with the goniometer was 0.5°. Therefore, this was a significant component of the overall error in the calculation of angles by the rate gyroscope method.

Inaccuracies in the rate gyroscope resetting/nulling methods E and F were 0.7 +/- 0.2° in estimating the dynamic tilt (table 3.1) when compared against the goniometer values. Since differences of +/- 0.5° were observed between the goniometer and the accelerometer methods when determining static inclinations, this suggests that much of the error may be due to the non-linearity of the accelerometer or the goniometer reference. Further tests using a more accurate reference angle sensor, such as a high resolution optical encoder, would be required to independently determine the relative contributions to the error by these sources.

In the segmental model, the accuracy of the rate gyroscope method F was found to be 2.1 degrees, which is less than the errors of the trials reported on models by Kataria and Abbas, and the computer simulations of the method proposed by Luinge et. al. For the tests on individuals, the accuracy of the rate gyroscope methods E and F was typically less than 4 degrees, seen in tables 3.3 through 3.5. This error is less than that reported by Miyazaki. This error may be due to nonlinearities in the accelerometers (0.5 degrees x 2),

cross talk of the goniometer (3 degrees), non-linearity of the goniometer (2 degrees) (Biometrics trade literature), and the allowable static difference between accelerometer and rate gyroscope integral, indicated in equation (5) (1 degree x 2). The integral of the rate gyroscopes is bounded by the angle estimated from the accelerometer, which in turn was compared with the goniometer. The combination of these errors indicates the maximum level of accuracy of the integral of the rate gyroscope. As the results from the tests on individuals are less than this error, methods E and F are considered to be of the order of accuracy of estimates of knee flexion angle by a M180 goniometer.

FES increased the RMS noise of knee flexion angle calculated by either the rate gyroscope or the accelerometer methods. However, low pass filtering with a 3 dB cutoff at 10 Hz reduced the level to less than 0.1 degrees. This is a higher precision than that observed using the low pass filtered goniometer and that obtained by low pass filtering the accelerometers.

FES also increased the RMS noise in the estimates of angular velocities. Again, low pass filtering of the rate gyroscopes signals (3 dB at 10 Hz) reduced the RMS noise level to 3 degrees per second which was less than that obtained from the goniometer (13°/s) or the accelerometer (145°/s).

As indicated in Table 1, the rate gyroscope requires nulling before each sit-stand or stand-sit transition, otherwise the large errors seen in methods A and D would ensue. Auto-nulling was therefore a more convenient alternative to manual nulling the rate gyroscope originally suggested in Andrews and Williamson (1997). Increases in accuracy due to auto-nulling were not demonstrated in these experiments, i.e. the auto-reset integral of the rate gyroscope was not statistically different than the auto-reset integral of the rate gyroscope using auto-nulling of the DC offset ($p < 0.01$). However, the duration of the tests was less than 20 seconds and drift in the DC offset was not significant. Longer duration studies would be required to assess such effects.

The use of a Gyrogoniometer for the measurement of knee flexion angle and angular velocity could have certain advantages in comparison to the M180 goniometer. The linkage between the two clusters is not of a fixed length, and hence strain and possible movement of the mounting during repetitive movements should not exist. This is a

drawback of the goniometer, and often causes problems. The only restriction on placement of the clusters is that the rate gyroscopes must be mounted perpendicular to the plane of motion of which the angle is contained. Once an initial determination of the +/- 1 g levels from the accelerometers were made, the devices did not require calibration, as demonstrated in method F. This means that these clusters could be placed on an individual who is sitting, and an immediate calculation of knee flexion angle would be made.

It has been shown that the accuracy of method F was less than 4 degrees, and only 2 degrees when the cross-channel error of the goniometer was not present. Using a goniometer, 90 degree flexion is approximated usually through a visual comparison. This induces errors due to locating the center of the knee joint, orientation of both the goniometer and the protractor with limb segments, and parallax. It is the author's belief that this error is greater than the error apparent from using the combination of rate gyroscopes. A comparison of the accuracy of the goniometer and the combination of rate gyroscopes and accelerometers can only be constructed by using a third measurement of knee flexion angle. The accuracy of this method should be an order of magnitude less than the errors of both the goniometer and the combination of the rate gyroscope and accelerometers. Camera acquisition might be suggested for this, but is not accurate enough to derive this level.

3.5 Conclusion

Low pass filtered accelerometers can determine the static tilt of a leg segment. Based on the accuracy of the accelerometers, an auto-resetting of the integral of rate gyroscopes and auto-nulling of the DC output offset provides an accurate assessment of the angle across the knee joint during sit to stand and stand to sit maneuvers. The rate gyroscopes can provide a more accurate and precise estimation of knee flexion angle and angular velocity than can be determined from accelerometers.

The difference between the angle recorded by the goniometer and the rate gyroscope was largely systematic in nature, and attributed to a difference between the

linearity of the accelerometers and the goniometer. Auto-resetting the integral of the rate gyroscope was necessary to attain this accuracy.

When the accelerometers and rate gyroscopes were combined in small clusters, they were more convenient to use than the Biometrics M180 goniometer. The absence of a mechanical linkage between the two clusters allowed for easier positioning and alignment of the clusters in comparison to the goniometer, and avoided the tendency to pull and possibly cause slippage of the device with respect to the skin during movement. After the one time, +/- 1g bench calibration of each sensor module, kinematic estimates of joint angle, velocity and segmental inclinations are immediately available upon attaching the device to an individual, and further calibration is not required.

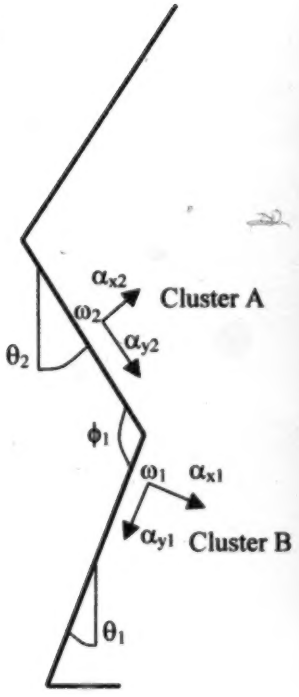

Figure 3.1 (Left) – Determination of knee angle from accelerometers and rate gyroscopes. Accelerometers α_{x1}, α_{y1} and rate gyroscope ω_1 are placed on the shank in the sagittal plane. The tilt of the shank, θ_1, is calculated from this cluster. Accelerometers α_{x2}, α_{y2} and rate gyroscope ω_2 are placed on the thigh in the sagittal plane. The tilt of the thigh, θ_2, is calculated from this cluster. The knee angle, ϕ_1, is the difference in tilts of the two segments. (Right) – Practical implementation. Cluster A is comprised of accelerometers α_{x2}, α_{y2} and rate gyroscope ω_2 and worn on the shank. Cluster B is comprised of accelerometers α_{x1}, α_{y1} and rate gyroscope ω_1 and worn on the thigh.

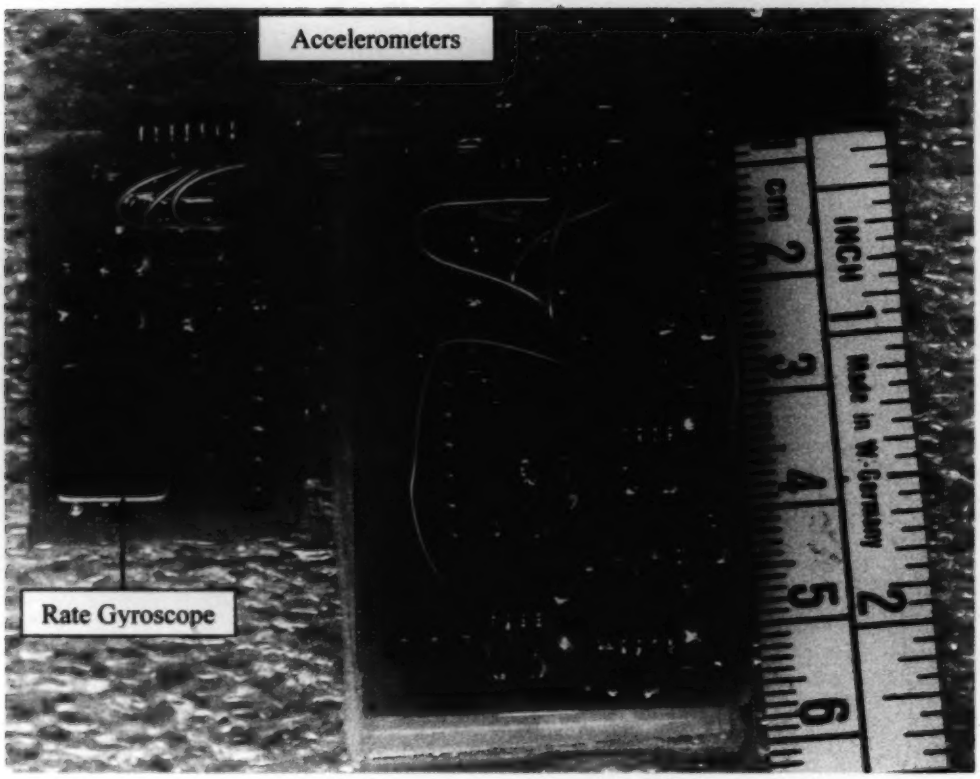

Figure 3.2 - Sensor clusters

The right cluster, cluster A of Figure 1, (5x3.3x1.7 cm) is used on the shank and includes the MAX186 chip. The left cluster, cluster B of Figure 1, (3.5x2.3x1.7 cm) is used on the thigh. The accelerometer on the right and left clusters, and the rate gyroscope on the left cluster are indicated. The rate gyroscope on the right cluster is on the side of the PCB that is not visible.

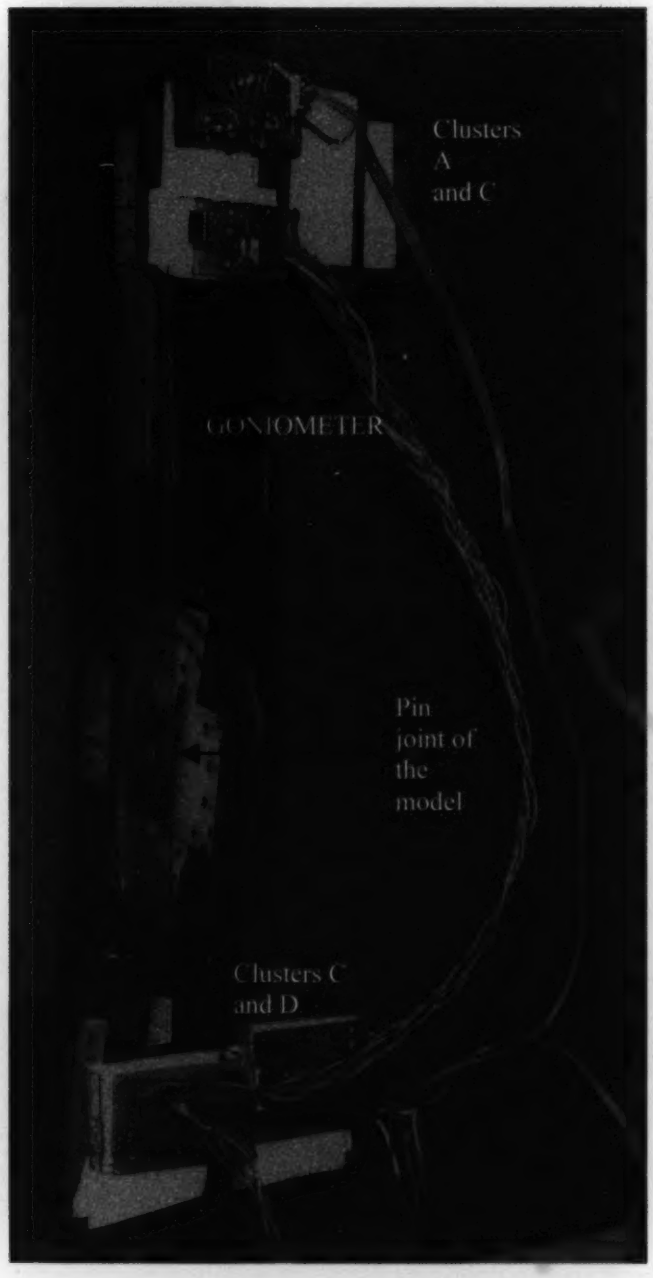

Figure 3.3: Mounting of sensor clusters and goniometer on a 2 dimensional model. The position of the goniometer and the sensor clusters are indicated. The model rotates about a single pin joint. This constrains the motion to 2 dimensions.

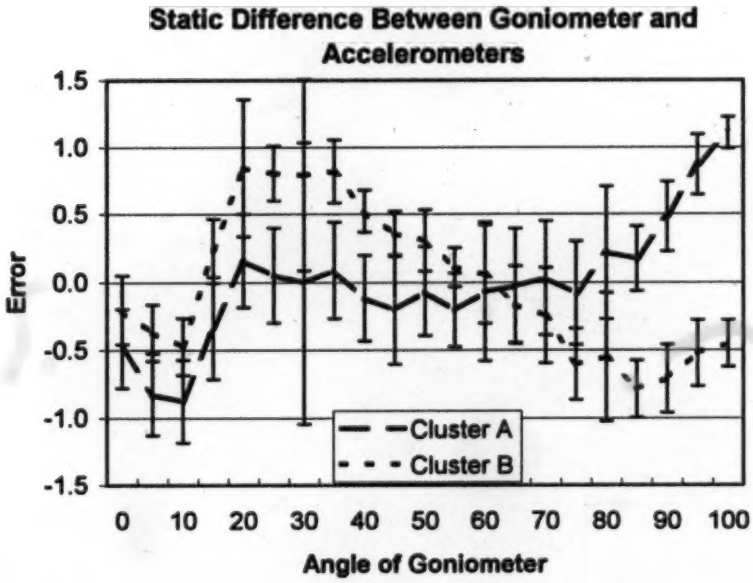

Figure 3.4: The static tilt of a single segment was calculated from the goniometer and the accelerometers for two clusters. The dotted line is the mean difference between cluster A and the goniometer; the dashed line is the mean difference between cluster B and the goniometer. The tilt of the segment as calculated by the goniometer is on the ordinate axis. The error bars indicate the first standard deviation of the tilt measurement.

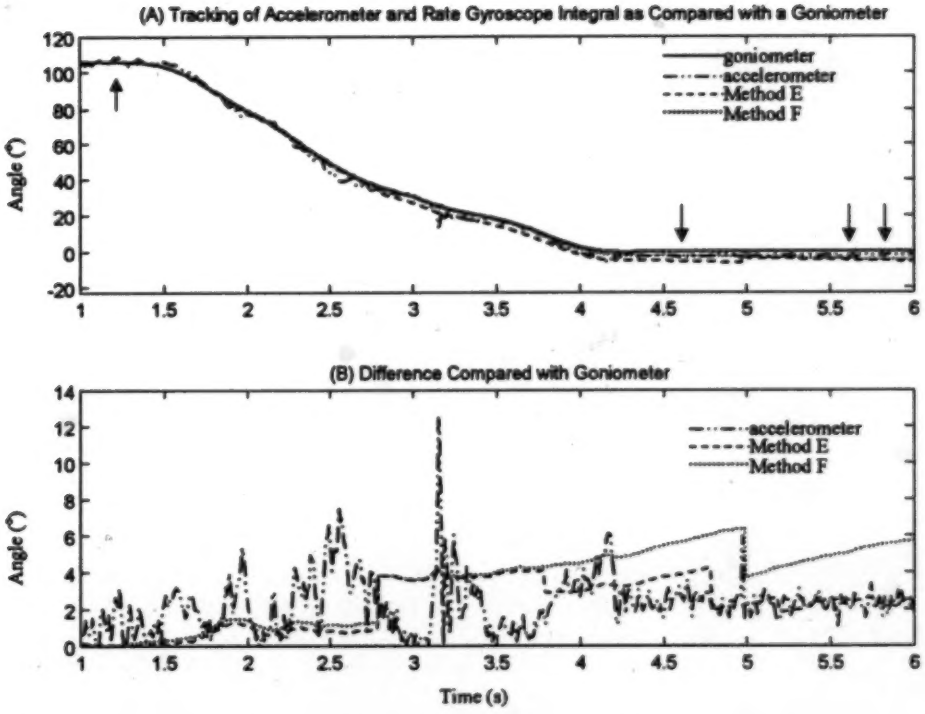

Figure 3.5: Angle calculated by goniometer, accelerometers and rate gyroscopes on the two dimensional model. The goniometer is the solid trace. The accelerometer is the long dashed and dotted line. Method E, resetting the integral of the rate gyroscope without auto-nulling the rate gyroscope, is displayed by the dotted line. Method F, resetting the integral of the rate gyroscope, and auto-nulling the rate gyroscope, is the dotted trace.

(A) displays the angle as calculated through the transition. The arrows (time = 2.8, 3.6, 4.6, 5.0, and 5.2 seconds) indicate the times at which the Method F auto-nulled the rate gyroscope.

(B) displays the difference between the goniometer and the accelerometer, method E, and method F. The breaks in this curve for Method E and Method F indicate the times at which auto-resetting of the integral occurred.

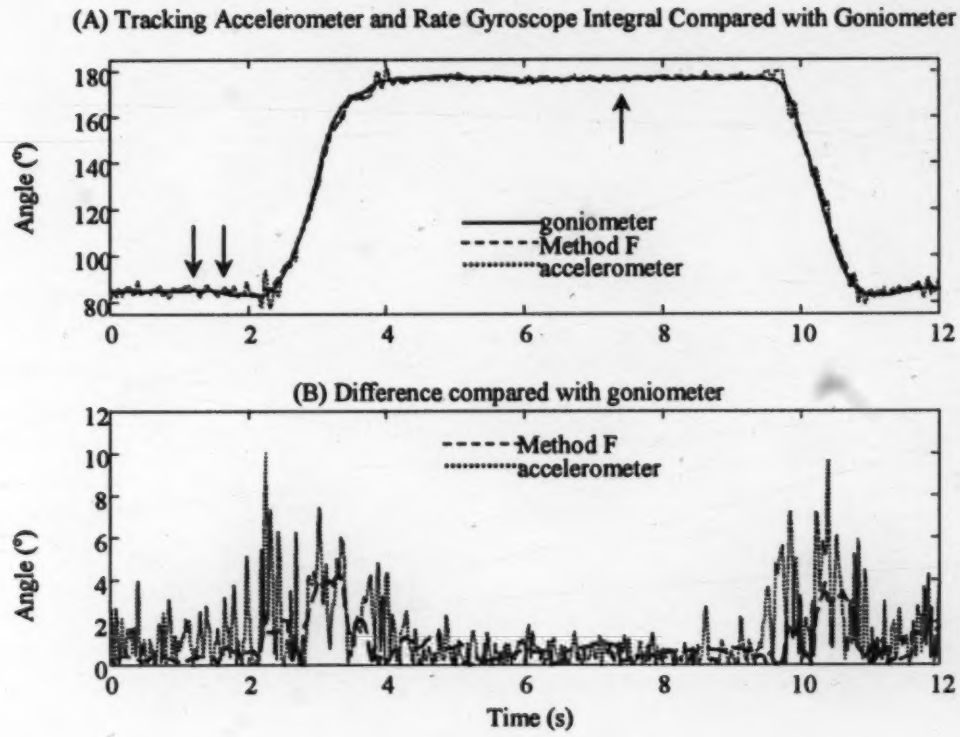

Figure 3.6 – Knee angle calculated by goniometer, accelerometers and rate gyroscope on able bodied volunteer.

(A) displays the angle as calculated through the transition.
(B) displays the difference between the goniometer and the other methods.

The goniometer is the solid line. The accelerometer is the dotted line; the auto-reset auto-nulled rate gyroscope integral is the dashed line. The arrows in (A) show when the auto-nulling of the rate gyroscopes occurs. Breaks in the error graph of the auto-reset rate gyroscope integral at times 4.8, 5, 6.2, 7.2 and 10 seconds indicate the times at which the auto-resetting occurs.

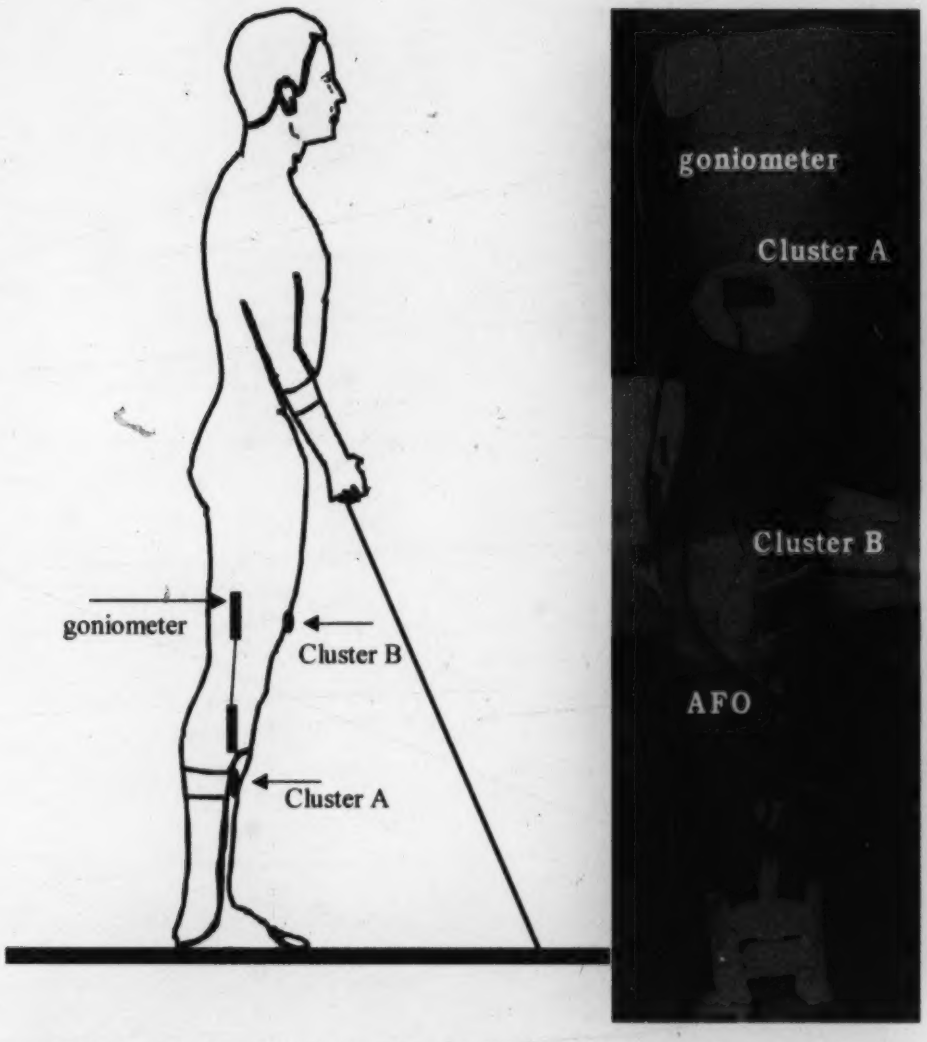

Figure 3.7: Paraplegic volunteer wearing sensor clusters, AFO, goniometer and stimulating electrodes. Sensor cluster B was mounted on the AFO as indicated in the figure. The goniometer was attached as indicated in the trade literature. The active FES electrode was placed near the motor point of the vastus lateralis. The reference electrode was placed above the knee. Sensor cluster A was mounted on the top of this electrode.

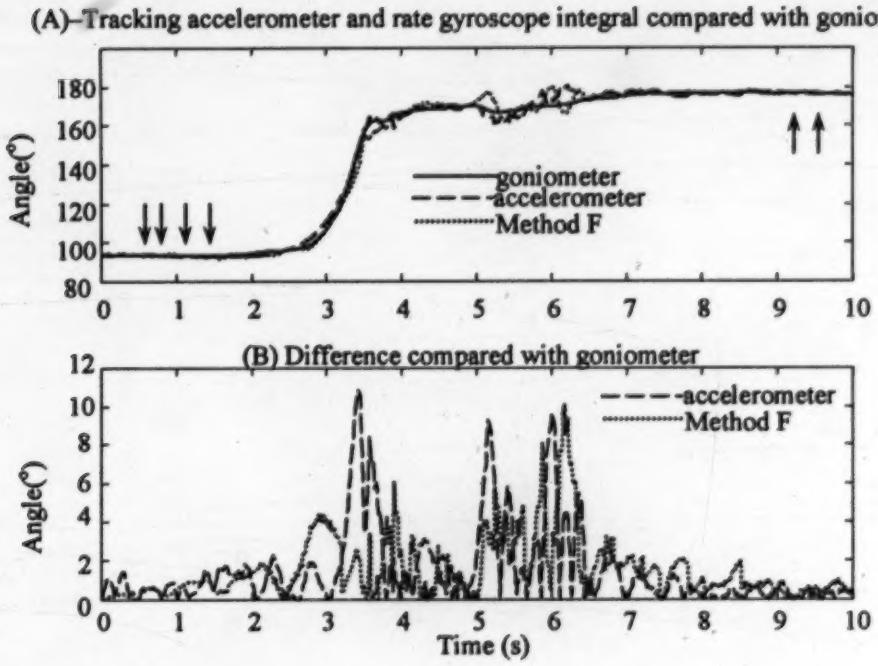

Figure 3.8 - Angle calculated by goniometer, accelerometers and rate gyroscope on a paraplegic volunteer.

(A) displays the angle as calculated through the transition.
(B) displays the difference between the goniometer and the other methods.

The goniometer is the solid line. The accelerometer is the dotted line; the auto-reset auto-nulled rate gyroscope integral is the dashed line. The arrows in (A) show when the auto-nulling of the rate gyroscopes occurs. Auto-resetting of the integrators is also displayed at times 3.2, 7.4, 7.8, and 8.2 seconds.

Integrator Reset?		No	No	No	Auto	Auto	Auto
Method for Null		Previous day	Start of trial	Auto	Previous day	Start of trial	Auto
Method	Accel.	A	B	C	D	E	F
Cluster A mean	2.33	28.67	0.71	0.73	7.51	0.72	0.77
Cluster A std	0.58	5.11	0.26	0.21	1.65	0.27	0.19
Cluster B mean	2.54	53.04	2.08	1.14	13.34	1.24	0.82
Cluster B std	0.60	9.05	0.75	0.41	4.69	0.16	0.25

Table 3.1: Tilt calculations by the accelerometer and the integral of the rate gyroscopes. Accel. corresponds to the error through calculating the tilt of the segment only through using the accelerometers. Columns A through F correspond with conditions A though F described in the text for auto-resetting and auto-nulling. The errors are reported in degrees. The results were averaged over 6 trials conducted through moving only the upper segment of the model pictured in Figure 3.3.

Angular Velocity	Accel (°/s)	Rate gyroscope (°/s)
Cluster A mean	21.57	2.86
Cluster A std	5.14	0.33
Cluster B mean	22.79	2.78
Cluster B std	5.54	0.50

Table 3.2 – Error of the rate of change of tilt as calculated by the rate gyroscopes and accelerometers as compared with the goniometer, measured in degrees per second. The results were averaged over 6 trials conducted through moving only the upper segment of the model pictured in Figure 3.3.

Trial	Accels. (Angle)	Method B (Angle)	Method C (Angle)	Method E (Angle)	Method F (Angle)	Angular Velocity from rate gyroscope (°/s)	Angular Velocity from accelerometers (°/s)
a	4.71	1.96	2.04	2.78	2.90	3.41	20.34
b	2.67	2.61	2.52	3.06	2.54	1.71	10.94
c	1.94	0.61	1.68	1.68	1.68	1.78	9.97
d	1.67	4.71	3.09	1.20	1.61	2.45	8.87
e	1.66	1.77	1.63	1.88	2.47	2.16	12.92
f	1.93	3.31	2.98	1.82	1.55	2.26	10.30
Mean	2.42	2.49	2.50	2.07	2.12	2.29	12.22
Std	1.18	1.41	1.41	0.70	0.58	0.62	4.19

Table 3.3 – Comparison of accelerometer and rate gyroscope methods for calculating angle and angular velocity on a 2 dimensional model. The error of the angle is the root mean squared difference between the angle calculated by a goniometer and the indicated accelerometer or integrated rate gyroscope method. The error of the angular velocity is the root mean squared difference between the angular velocity calculated by a goniometer and the accelerometer or rate gyroscope. The error of the angle is displayed in degrees. The error of the angular velocity is given in degrees per second. The mean and standard deviation of the six trials is displayed at the bottom of the table.

	Left					Right				
	Angle (°)			Angular Velocity (°/s)		Angle			Angular Velocity (°/s)	
Female Subject	Accel.	Rate Gyro (E)	Rate Gyro (F)	Accel.	Rate Gyro.	Accel.	Rate Gyro. (E)	Rate Gyro. (F)	Accel.	Rate Gyro.
Full routine	**3.70** (0.73)	**3.02** (1.37)	**3.17** (1.53)	**11.54** (3.41)	**5.00** (1.07)	**2.60** (1.42)	**2.24** (1.02)	**2.15** (1.00)	**9.71** (2.64)	**5.10** (1.46)
Stand up	7.74 (1.17)	3.73 (1.42)	3.71 (1.42)	19.2 (4.84)	9.01 (1.85)	6.13 (1.93)	3.12 (1.24)	3.30 (1.15)	16.5 (4.78)	8.91 (2.24)
Sit down	5.77 (1.09)	4.11 (1.38)	4.01 (1.29)	18.38 (5.06)	7.70 (2.38)	7.30 (1.89)	2.70 (1.02)	2.55 (1.08)	17.7 (4.46)	8.41 (2.40)
Male Subject										
Full routine	**3.14** (0.42)	**2.72** (0.39)	**2.80** (0.40)	**13.52** (1.67)	**6.32** (0.36)	**3.19** (0.32)	**2.89** (0.69)	**2.87** (0.40)	**47.0** (6.24)	**10.2** (2.63)
Stand up	6.13 (1.93)	3.63 (2.13)	3.81 (1.18)	16.46 (4.78)	8.91 (2.24)	5.74 (1.10)	5.57 (1.18)	5.42 (1.98)	19.2 (4.84)	14.5 (2.37)
Sit down	7.30 (1.89)	4.59 (2.49)	4.12 (1.06)	17.73 (4.46)	8.41 (2.40)	4.68 (0.40)	3.76 (0.77)	3.74 (0.76)	65.7 (21.9)	18.1 (3.14)

Table 3.4 – Comparison of accelerometer and rate gyroscope methods for calculating the angle and angular velocity on able bodied individuals. The mean and (standard deviation) of the difference in the calculation on knee angle and angular velocity as computed by goniometer and the indicated accelerometer or integrated rate gyroscope methods are shown. This average difference is displayed for the full 10 second routine as well as only during the standing and sitting maneuvers is presented. The results are averages over 18 trials for the female subject, and 8 trials for the male subject.

Trial	Accel. (°)	Method E (°)	Method F (°)	Velocity from Accelerometers (°/s)	Velocity from rate gyroscopes (°/s)
A	3.00	1.64	1.52	26.73	7.16
B	2.66	1.48	1.60	32.65	15.21
C	2.70	1.72	1.89	27.84	15.48
D	1.81	1.53	1.35	22.05	12.29
E	2.69	2.03	1.98	30.07	13.10
F	3.92	3.01	3.09	38.31	10.55
G	2.96	2.85	2.89	29.19	11.48
H	2.26	2.30	2.80	21.22	9.28
Mean	2.75	2.07	2.14	28.51	11.82
Std	0.61	0.59	0.69	5.53	2.85

Table 3.5 – Comparison of accelerometer and rate gyroscope methods for calculating the angle and angular velocity on a paraplegic individual. The average difference for the standing routine between the goniometer and the accelerometer or integrated rate gyroscope method is presented. Errors of angle are given in degrees; errors in angular velocity are given in degrees per second. The results are the average difference computed over the duration of the trial. The mean and standard deviation of the combined trails is displayed.

Angle (°)	Goniometer		Rate Gyroscopes Integral		Accelerometer	
	Without FES	With FES	Without FES	With FES	Without FES	With FES
No Filter	0.870	0.607	0.023	0.102	2.746	7.105
	0.028	0.060	0.004	0.038	0.336	1.777
10 Hz	0.293	0.222	0.003	0.019	0.981	1.292
	0.052	0.021	0.000	0.007	0.109	0.289
5 Hz	0.152	0.124	0.006	0.015	0.519	0.370
	0.040	0.013	0.001	0.003	0.036	0.057
2.5 Hz	0.067	0.057	0.009	0.026	0.213	0.118
	0.021	0.001	0.003	0.008	0.055	0.016
Angular Velocity (°/s)	Goniometer		Rate Gyroscopes		Accelerometer	
	Without FES	With FES	Without FES	With FES	Without FES	With FES
No Filter	132.649	91.141	1.482	19.527	401.304	904.581
	3.139	9.640	0.083	6.465	53.129	233.033
10 Hz	17.378	13.265	0.732	3.062	59.443	145.843
	2.330	1.226	0.101	1.100	5.622	34.864
5 Hz	6.352	4.831	0.454	1.152	21.514	35.854
	1.073	0.516	0.090	0.280	1.787	8.239
2.5 Hz	1.942	1.549	0.196	0.507	6.625	8.980
	0.404	0.146	0.058	0.133	0.180	2.020

Table 3.6 – The effect of FES on the precision of knee angle and angular velocity estimates during standing up as calculated by an electrogoniometer, rate gyroscope, and accelerometer. The open bandwidth and 2nd order butterworth filtered values are shown for each technique. The mean and standard deviation as computed in the six trials of the paraplegic subject of the residual high frequency RMS are shown.

3.6 Bibliography

Analog Devices, ADXL202 Data Sheet

Andrews, B.J., Barnett, R., Phillips, G., Kirkwood, C., Donaldson, N., Rushton, D., and Perkins, T., (1989) "Rule Base control of a hybrid FES orthosis for assisting paraplegic locomotion," Automedica, 11:175-199

Andrews, B.J., Cappozzo, A., and Gazzana, F., (1981) "A quantitative method for assessment of differentiation techniques used for locomotion analysis", In. Computing in Medicine, Eds. Paul, Jordan, Ferguson-Pell and Andrews, MacMillan Press (ISBN 0333318862), pp 146 – 154.

Andrews, B.J., Jones, D.J., (1976) "A note on the differentiation of human kinematic data", Dig. 11th Int. Conf. On Med. & Biol. Eng., pp 88-89

Andrews, B.J., Williamson, R.P., (1997) "The gyrogoniometer", Proc. RESNA '97, pp 262-4

Biometrics trade literature: The model M180 flexible goniometer, UK.

Crago, P.E., Chizeck, H.J., Neuman, M.R, and Hambrecht, F.T., (1986) "Sensors for use with functional neuromuscular stimulation," IEEE Trans. BME 33(2):256-268

Crago, P.E., Lan, N., Veltink, P.H., Abbas, J.J., and Kantor, C., (1996) "New control strategies for neuroprosthetic systems", J. Rehab. Res. Devel. 33(2):158-172

Dai, R., Stein, R.B., Andrews, B.J., James, K.B., Wieler, M., (1996) "Application of tilt sensors in functional electrical stimulation", IEEE Trans. Rehab. Eng. 4(2):63-72

Davoodi, R., and Andrews, B.J., (1998) "Computer simulation of FES standing up in paraplegia: A self adaptive fuzzy controller with reinforcement learning", IEEE Trans. Rehab. Eng. 6(2):151-161

Dolan, M.J., Andrews, B.J., and Veltink, P.H., (1998) "Switching curve controller for FES assisted standing up and sitting down," IEEE Trans. Rehab. Eng 6(2):167-171

Kirkwood, C.A., Andrews, B.J., and Mowforth, P., (1989) "Automatic detection of gait events: a case study using inductive learning techniques", J. BME, 11(6):511-6

Hamming R.W, (1962) Numerical Methods for Scientists and Engineers, McGraw-Hill,

Heyn, R.E., Mayagoitia, A., Nene, V., Veltink, P.H., (1996) "The kinematics of the swing phase obtained from accelerometer and gyroscope measurements", Proc. IEEE EMBS, pg. 857-8

Kataria, P., and Abbas, J.J., (1998) "Estimating body segment orientation using a lightweight, inexpensive gyroscope" Proc. BMES Conf. P S-133

Kennedy, J.B., and Neville, A.M., (1976) Basic Statistical methods for engineers and Scientists, Harper and Row, ISBN 0-7002-2480-7

Kralj, A., Bajd, T., (1989) Functional electrical stimulation: Standing and walking after spinal cord injury, CRC Press, CA

Miyazaki, S., (1997) "Long term unconstrained measurement of stride length and walking velocity utilizing a piezoelectric gyroscope", IEEE Trans. BME 44(8): 753-9

Molen, N.H., and Boon, W., (1972) "Measurement of momentary velocity in a study of human gait" J Biomech. 5(3):273-6

Morris, J.R., (1973) "Accelerometry--a technique for the measurement of human body movements" J Biomech. 6(6):729-36

Mulder, A.J., Veltink, P.H., Boom H.B.K., and Zilvold, G., (1992) "Low level finite state control of knee joint in paraplegic standing", J. BME 14(1):3-8

muRata data sheet, ENC-05EA rate gyroscope

Petofsky, J.S., Phillips, C.A., and Heaton, H.H., (1984) "Feedback control system for walking", Comp. Biol. Med. 14(2):135-149

Popovic, M., and Tepavac, D., (1982) "A portable 8 channel gait kinematics recording unit", Proc. IEEE EMBS, 1646-1647

Smidt, G.L., Arora, J.S., Johnston, R.C., (1971) "Accelerographic analysis of several types of walking" Am. J. Phys. Med. 50(6):285-300.

Smidt, G.L., Deusinger, R.H., Arora, J., and Albright, J.P., (1977). An automated accelerometry system for gait analysis" J. Biomech. 10(5-6):367-75

van den Bogert A, Read L, Nigg BM (1996) "A method for inverse dynamic analysis using accelerometry" J Biomech. 29(7):949-54.

Wang, F., Thrasher, A., Ouellette, N., Williamson, R., Andrews, B.J., (1997) "Machine learning control of FES: Real time implementation", Proc. IFESS'97, pg. 75-6

Willemsen, A.T., Frigo, C., and Boom, H.B., (1991) "Lower extremity angle measurement with accelerometers--error and sensitivity analysis" IEEE BME 38(12):1186-9

4 A Sensor System for Lower Limb FES Control

4.1 Introduction

Two common uses for sensors in lower limb FES control have been reported. The first is the detection of gait phases or events, for example, stance and swing detection (Liberson et. al., 1961, Dai et. al., 1996, Kirkwood et. al., 1989, Ng and Chizeck, 1997, Symmons et. al, 1986, Graupe, 1989, Kostov et. al, 1995, Upshaw and Sinkjaer, 1997, Willemsen et. al., 1990) and the detection of knee buckling during standing (Andrews et. al, 1989, Mulder et. al, 1992, Veltink and Franken, 1996). The second is the continuous or instantaneous monitoring of a joint angle, most commonly the knee flexion angle (Dolan et. al, 1998, Davoodi and Andrews, 1998, Franken et. al, 1995, Crago et. al, 1996, Thrasher et. al, 1996, Kirkwood et. al., 1989, Ng and Chizeck, 1997, Wood et. al., 1998, Veltink et. al., 1992, Fugita, 1995).

The lack of appropriate artificial sensors has been implicated as a limiting factor to the clinical application of more advanced feedback control techniques (Marsolais and Kobetic, 1988, Brandell, 1982, Hambrecht, 1972, Johnson et. al, 1995), reflected in the reviews of sensors for FES (Crago et. al., 1986, Webster et. al., 1992). The sensors typically used for FES lower limb control include electrogoniometers, pressure insoles, footswitches and inclinometers. The Penny and Giles electrogoniometer has been widely used for sensing joint angles in laboratory demonstrations. However, this device is too fragile and difficult to don and doff for everyday use. Additional concerns of alignment, mounting, and calibration of the goniometer, and migration whilst in use have been reported. Implantable Hall effect goniometers (Troyk et. al, 1984, Johnson and Peckham, 1990) are presently being developed for implanted FES neural prosthesis, although are not widely available. Switch controlled FES gait has been used previously (Kralj and Bajd, 1989), however, this imposes a conscious burden of pressing a switch to initiate a step on the user of the system (Hambrecht 1972, Lajoie et. al., 1999). This is a concern for most FES systems, reflected by attempts to automate the switch pressing (Dai et. al., 1996, Kirkwood et. al., 1989, Ng and Chizeck, 1997, Graupe, 1989, Kostov et. al, 1995, Upshaw and Sinkjaer, 1997, Willemsen et. al., 1990).

Natural sensors have been proposed for control of FES (Haugland and Hoffer, 1994, Upshaw and Sinkjaer, 1997). The detection of stance and swing has been determined to greater than 90% by analysis of epineural potentials. Yoshida and Horch (Yoshida and Horch, 1996) demonstrated closed loop control of ankle motion in an acute animal study using intrafascicular electrodes. It was noted that migration of the intrafascicular electrodes could prove problematic for further application of this approach (Sinkjaer et. al., 1997). Until epineural potentials are able to demonstrate repeatable and reliable measurement of continuous variables such as joint angles and more arbitrary gait events necessary for control of FES, other methods for feedback control of FES can be pursued.

Recently, micro-machined electromechanical sensors, such as accelerometers and rate gyroscopes, have become widely available. These sensors are small in size, and low power, making them candidates as artificial sensors for FES.

Multiple accelerometer combinations have derived angular acceleration, velocity, and tilt of a leg through integration (Morris 1973, Smidt 1977). Willemsen et. al. (Willemsen et. al., 1991, Willemsen et. al, 1990 a,b) extracted the knee joint angle and angular velocities for use in an FES system. Rigid rods were aligned with the shank and the thigh, and used to mount the accelerometers. An assumption was made that these rods would rotate within the sagittal plane. Using this constraint, a formula was derived to determine knee flexion angle that avoided numerical integration. Heyn et. al. (Heyn et. al. 1996) furthered this study by using rate gyroscopes to directly measure the angular velocity of the leg segment. Unfortunately, the arrangement of the rigid rods required for application of the formula may be too encumbering for daily application.

Accelerometers have been used to determine knee lock or unlock in able bodied individuals (Veltink and Franken, 1996). Buckling is not strictly a case of knee lock or unlock however, and expansion of this technique to paraplegic trials was not conducted.

Rate gyroscopes can be used to predict joint angle through integration of their signal. However, the DC component of the signal is subject to drift, and can change even when an object is not moving. This would be measured as a movement of the object at a constant velocity, and the error of integration due to this drift would grow without bound.

Compensation for this drift has been attempted. Miyazaki (Miyazaki, 1997) and Kataria and Abbas (Kataria and Abbas, 1998) low pass filtered the rate gyroscope output to determine the DC component, and integrated the high frequency component to determine angle. This method was tested in repetitive movements returning to an initial fixed position, hence the DC component due to the movement is zero. Expansion of this technique to cases in which the body does not return to the initial position was not attempted, and could be problematic. Hentry and Ewins (Hentry and Ewins, 1998) compensated for the drift of the DC component of the rate gyroscopes at the end of each step in a walking trial. As the angle is not calculated in real time this technique could not be used for control purposes.

In proposing a sensor system for FES control, size, encumbrance, and convenience of use must be considered (Stallard et. al, 1989, Crago et. al, 1986). The sensors should not require additional bracing to be placed on the individual, and should be worked as appropriately as possible into the presently used architecture of the FES system. This would restrict the locations of the sensors to a couple of sites for external use, such as a floor reaction orthotic (FRO), and attachments to the electrodes used for surface stimulation. This would allow the patient to don the sensor system in conjunction with the FES system. Attachments that are made across the joint should not be restricted in length; this caused problems for the use of the electrogoniometer. If the FES system is implanted, the sensors should be capable of being implanted with the stimulator. This would lead to restrictions of size, weight and power consumption.

Here we propose a modularized sensor and signal processing system that can provide real time data, such as gait phases and events, and joint kinematics, for FES control. In some configurations the requirement to align sensors with anatomical structures is relaxed by the use of supervised machine learning techniques. These techniques can be used when analytical relationships between the sensor signals and the desired FES control variables exist but are either unknown, highly complex, or impractical to apply or calibrate. We have previously described this technique as "Virtual Sensors" (Andrews, 1995).

Our use of the term "Virtual Sensors" significantly differs from the "Virtual Sensors" term used by Tong and Granat (Tong and Granat, 1998) and Heller (Heller, 1992). In these examples, the authors place "virtual sensors", such as accelerometers and inclinometers, on video recorded models of walking, and correlate their outputs to the real outputs of those sensors worn during the actual trial. This demonstrates that an artificial sensor recording from a model can be used to predict a real sensor recording on an individual. In our application, real sensors, such as accelerometers and magnetic field sensors, are placed on individuals and a map between their outputs to the variables described as inputs to feedback controllers, such as knee flexion angle and hip angle is constructed. This demonstrates that a neural network can construct useful control variables from a non-intuitive sensor system.

Preliminary reports of this work are given (Andrews and Williamson, 1997, Andrews et. al, 1995, 1996, Williamson et. al, 1996, Williamson and Andrews, 1997).

4.2 Methods

4.2.1 The Sensors

Analog devices accelerometers (Analog devices trade literature) were chosen for this application, based on their widespread availability. These accelerometers measure both the gravitational component of acceleration as well as the dynamic component of acceleration inherent in the motion of an object. Due to this aspect, these sensors are considered to be "rich" in information and have been used extensively in measuring motion.

Rate gyroscopes were chosen as a sensor. These devices measure the angular velocity of a segment. These components typically produce a DC component at zero angular velocity, as mentioned previously (muRata Devices trade literature). These sensors measure motion without a reference to gravity.

A piezoelectric strain gauge was mounted on the FRO (AMP trade literature). This device detects changes in force and not a static force. Previous experience with strain gauges mounted on the FRO indicated that the static force in the FRO varied widely. However, a change in force is always predicted due to a knee buckle.

Two types of electromagnetic systems were composed. An active RF magnetic system, similar to the one reported by Kalmus (Kalmus, 1962, Lou, et. al., 1997) was constructed. A single transmitter coil was powered at 120 kHz. The signal was received by the 2 dimensional receiver coil, and was rectified to produce a level DC signal that would vary with distance and orientation of the transmitter to the receiver.

Magnetoresistors (Phillips Trade literature), used to detect the earth's magnetic field, were also used. These sensors detect changes in the magnetic field. These sensors provided a second non-inertial sensor that complemented the inertial accelerometer sensors.

4.2.2 The Clusters, Configurations, and Data Acquisition

The sensors were combined into clusters. Each cluster was attached to a 3 wire QSPI serial bus. The master controller for the serial bus was a MC68332 microcomputer. Each sensor on the each cluster could be individually addressed by a MAX186 12 bit A/D converter. A more detailed description of the MC68332 controller is provided elsewhere (Wang et. al, 1997).

The location of the sensors was the primary consideration in the design of the system. For this experiment, three sensor configurations were used. In each experiment, three accelerometers were worn on the shank of the leg. Placing a second sensor cluster above the knee determined knee flexion angle and rate of change of knee flexion angle, referred to as knee angular velocity. If only knee flexion angle was of interest, a second cluster was placed on the thigh. If both knee and hip angles were of interest, a second cluster was worn on the belt. On this basis, three sensor configurations were constructed.

In the first configuration, three accelerometers (ADXL05JH) were mounted on a calf strap. The plastic platform was 2" by 8" and molded to the tibial crest region. The accelerometer, labeled A in Figure 4.1 was oriented approximately along the tibial axis. The other two, labeled B and C as shown, were mounted orthogonal to the tibial axis and A with approximately 70° between their axes. The platform and strap was positioned on the tibial crest situated above the heads of gastrocnemius and soleus posteriorly as shown

in the figure. This configuration was used with a machine learned rule based controller to detect multiple gait phases.

In the second configuration, three accelerometers, three magnetoresistors, and the magnetic receiver were mounted on a FRO. The sets of the three accelerometers, (ADXL05JH) and the three magnetoresistors were arranged orthogonally. A second cluster was worn on the belt. This cluster consisted of the RF transmitter, four accelerometers and four magnetoresistors. The RF transmitter was worn near the midline of the body in the frontal plane. Two accelerometers and two magnetoresistors were placed laterally on the each side of the belt and worn in the sagittal plane. In this description, hip and knee flexion angle and angular velocity were determined from a neural network. Figure 4.2 displays this sensor configuration.

In the third configuration, one cluster was attached to the FRO with a second connection to a cluster on the thigh. The cluster on the FRO had two, two-dimensional accelerometers (ADXL202JQC), one rate gyroscope (ENG05GA), and a dynamic strain gauge. The size of the cluster attached to the brace is 5 x 3.3 x 1.7 cm, with a lead running to the strain gauge. The strain gauge was bonded with epoxy resin to the FRO. The FRO was made from ¼" polypropylene. The cluster on the thigh used one, two dimensional accelerometer and one rate gyroscope. The size of this cluster was 3.5 x 2.3 x 1.7 cm. Figure 4.3 displays this configuration. This configuration was also used in conjunction without the FRO and strain gauge on able-bodied individuals. For this case, one cluster was attached directly to the shank of the leg, and one cluster was attached to the thigh. The positions for these are indicated in a schematic in Figure 4.3.

4.2.3 Gait phase detection

The gait phases are detected using rule induction and sensor configuration 1. Rough Sets™ (Rough Sets Trade literature) was used to construct the rule based controller. Attributes consisting of the three accelerometers' amplitudes and their first derivatives were calculated and used to construct the rule based controller.

Three able bodied volunteers (ages 20-24, height 1.66-1.76 cm, weight 66 – 75 kg) were asked to walk around one oval path and one figure of eight path. The recordings

from the three accelerometers attached to the leg were used to calculate the ipsilateral phase of gait. Each volunteer wore an instrumented shoe insole that determined the force beneath the heel, lateral and medial metatarsal of each foot. Both the accelerometers and the insole forces were sampled at 100 Hz. Five gait phases, loading response, mid stance, terminal stance, pre-swing, and swing, were determined from these forces beneath the foot as described by Perry (Perry, 1992).

The accelerometer recordings were low pass filtered at 5 Hz and used with their derivatives to estimate the gait phase. A rule based controller was derived from Rough Sets™ inductive rule based learning program for 10 of the 40 strides around each walkpath. The rule based controller constructed a mapping from the input attributes of accelerometer amplitude and first derivative to the output gait phases. This mapping was then applied to the remaining 30 strides to test the generalization. The rules were tested in comparison to the reference phases determined by the insole.

A hypothetical FES stimulus rate of 33 Hz was applied, so that every three 100 Hz samples could be grouped for analysis. A heuristic rule, which stated if two of the three samples predicted a change of state, then the change of state occurred, was applied to the output gait phases as determined by the rule based controller. A second heuristic rule was applied that did not allow the detector to change from the present state to an immediately prior state, i.e. a change of state from loading response to swing was not allowed. These heuristic rules had the effect of localizing the errors of the gait phase detector to the gait phase transitions. These errors are either early or late predictions of a transition to a different phase. A physical significance to these errors is hypothesized, based on previously published methods for gait event detection (Kostov, 1996, Ng and Chizeck, 1997, Dai et. al, 1996).

4.2.4 Determination of angle and angular velocity: Analytical approach

Figure 4.4 describes a planar calculation of angles from a combination of rate gyroscopes and accelerometers. The accelerometer measurements are indicated by α_x and α_y, and the rate gyroscope signal is recorded by ω. The DC offset of the rate gyroscope is $\overline{\omega_0}$.

At the start of a trial, a computer program calculates the tilt of a segment using the accelerometer measurements. This provides an initial estimation of the angle. An arctangent function is used to calculate the angle, as this function is real for an infinite range of inputs. This is an advantage over the arcsine function, which is defined only from –1 to +1.

$$\theta_n(t_0) = \tan^{-1}(a_{y,n} / a_{z,n}) \quad (1)$$

The tilt of the segment can then be calculated by integrating the signal from the rate gyroscopes

$$\theta_n(t) = \int_{t_0}^{t} (\omega_n(t) - \omega_0) \cdot dt + \theta_n(t_0) \quad (2)$$

The angle across the joint can then be calculated as

$$\phi_n = \theta_{n+1} - \theta_n \quad (3)$$

The manufacturers of the rate gyroscope specify that a drift of the DC offset exists. We derived a method for online compensation of this DC drift using heuristic rules.

The DC offset, or null, of the rate gyroscope must be calculated when the rate gyroscope is stationary. The accelerometers could be used to detect when the rate gyroscope is stationary. If the accelerometers are stationary, as determined by a low variance of the accelerometer signal, an auto-null or auto-zero can occur. This is expressed in the following mathematical equations

If

$$\sqrt{\frac{\int_{t_1}^{t_2} \theta(t)_{accel}^2 dt - \left(\int_{t_1}^{t_2} \theta(t)_{accel} dt \right)^2}{t_2 - t_1}} < \sigma \quad (4)$$

Then

$$\omega_o = \int_{t_1}^{t_2} \omega(t) \cdot dt \quad (5)$$

The value of σ was set at 0.1^0. This was computed every 0.1 s with the difference between t_2 and t_1 as 0.45 s.

Additionally, error of the integral of the rate gyroscope can exist due to an incorrect DC offset or null. The low pass filtered accelerometers should provide an accurate estimate of the tilt of a segment. Therefore, the integral of the rate gyroscope can be checked against the accelerometers' calculation of tilt to ensure that errors due to drift of the DC offset do not accumulate. This is expressed in the following mathematical equation.

If

$$\frac{\left|\int_{t_1}^{t_2}\theta_{r_gyro}dt-\int_{t_1}^{t_2}\theta_{accel}dt\right|}{t_2-t_1}>\lambda \quad (6)$$

Then

$$\theta_{r_gyro}(t_2)=\theta_{r_gyro}(t_2)-\frac{\int_{t_1}^{t_2}\theta_{r_gyro}dt-\int_{t_1}^{t_2}\theta_{accel}dt}{t_2-t_1} \quad (7)$$

This rule was evaluated every 0.1 s, with the threshold λ set at 1^0. The difference between t_2 and t_1 was taken as 0.45 seconds. These two rules produce an auto-reset integral of an auto-nulled rate gyroscope.

The sensor configuration was tested on a two degree of freedom planar model simulating a knee joint, two able bodied individuals (one male, age 27, height 185 cm, weight 80 kg, one female, age 23, height 170 cm weight 55 kg), and one paraplegic subject [32 years, 7 years post injury, 190 cm, 80 kg, T-10 ASIA(A)]. The angle across the joint was calculated for an auto-reset integral of the auto-nulled rate gyroscope, and two dimensional accelerometers filtered with a 2nd order Butterworth filter, corner frequency 2.5 Hz. This angle was referenced to a goniometer filtered causally and anti-causally with a digital 2nd order Butterworth filter at 2.5 Hz. The root mean square difference between the goniometer and the auto-reset integral of the auto-nulled rate gyroscope over the transitions.

Both segments of the two dimensional model were moved, simulating a sit to stand and stand to sit trial. This was repeated six times. In the able bodied trial, the subject was asked to stand up from a seated position, remain standing for a period of 6 seconds, and then sit down. This was repeated 24 times over the two individuals. In the paraplegic trial, the subject was asked to stand from a seated position, assisted by surface FES applied to the quadriceps. This was repeated 8 times over a period of two days.

For the able bodied and paraplegic trials, the angles across the knee joint during sitting down and standing up were calculated by equating the average angle from the filtered accelerometers and the goniometer for a 0.5 second duration while sitting and a 1 second duration while standing. This was necessary to overcome any slipping of the goniometer with respect to the skin.

4.2.5 Knee and hip kinematics: "Virtual Sensor" approach

Neural networks were used to determine knee and hip angle from the second sensor configuration. This was tested on one able bodied individual (age 23, height 173 cm, weight 75 kg). Recordings of the sensor clusters were taken in conjunction with a Penny & Giles goniometer placed across the knee and hip joints of the individual. The individual performed 30 sit to stand to sit transitions. Seat heights ranged from 45 to 55 cm and foot separation ranged from 5 cm to 30 cm. Ten of the sit to stand to sit transitions were used for training a back propagation neural network, constructed in NeuralWorks Professional II (NeuralWorks trade literature), using a gradient descent learning rule. The learning rule minimized the error between the predicted and actual hip and knee flexion angle and angular velocities in epochs of 50 sample points. A C compatible computer code was constructed from the neural network, and the remaining sit to stand to sit trials were used to evaluate the accuracy of the neural network.

4.2.6 Detecting and predicting knee buckling

Knee buckle detection and prediction was determined from the strain gauge on the FRO. Previously the strain gauge was placed on the strap of the brace (Andrews et. al, 1989).

Mounting a dynamic strain gauge directly on the brace can determine if a change in amplitude and direction of the force within the brace occurs. A knee buckle would be reflected by either an increase or a decrease of force observed at the ankle joint. A decrease in force would reflect the ground reaction vector moving posteriorly, from in front of the knee joint to behind the knee joint, and is represented by a decrease in the moment of the ground reaction force about the ankle joint. An increase in force would reflect the cumulative head arms trunk force moving posteriorly. This force is projected through the thigh to the knee and would be observed as an increased dorsiflexion moment about the ankle joint. A schematic of these two situations is shown in Figure 4.5.

For both cases, a change in force in the brace is noticed when the equilibrium of the subject standing is disturbed. Both of the changes in force observed in the ankle foot orthosis should precede a knee buckle. Knee buckling has been determined in a previous experiment by a threshold detector set at 175 degrees of knee extension.

The detection and prediction for the knee buckling was tested on one paraplegic individual [32 years, 7 years post injury, 190 cm, 80 kg, T-10 ASIA(A)]. The subject was able to stand quietly without quadriceps stimulation for excesses of 5 minutes using the FRO.

The individual used the sensor configuration 3, including the strain gauge attached to the brace. An electrogoniometer monitored the knee extension angle. A knee buckling trial would occur as follows: the quadriceps stimulation would be turned off, the subject would maintain quiet standing for approximately 5 seconds, and then the subject would induce a buckle by slowly drifting posteriorly. This is a typical cause of knee buckle. In each of the trials, it was noted that both knees would buckle, i.e. reach 175 degrees of extension, within 100 ms of each other. In other words, the patient did not balance on one leg whilst the other knee became unstable.

The goniometer and sensor clusters were recorded at 100 Hz for these trials. A threshold was set by monitoring the strain gauge outputs prior to and during the first two buckles of the individual. The thresholds were chosen at a level of strain gauge output that exceeded the variation due to movement during quiet standing, but were surpassed during a knee buckle. The thresholds were typically 20% greater than the maximum signal

level observed during quiet standing. These thresholds were then set, and used to predict the remaining buckles. Previously reported knee buckle controllers use a threshold based on knee extension angle, and return quadriceps stimulation if the knee extension angle drops below the threshold of 175 degrees. The threshold was tested for 12 trials recorded over two days of testing.

4.3 Results

4.3.1 Gait Phase detection

A rule based controller was constructed for each individual by Rough Sets™ to determine the five gait phases. Table 4.1 displays the accuracy for detection of each phase for the testing of the rule based controller after the two heuristic rules were applied. The errors were localized to the transition between the phases. Figure 4.6 displays schematically the average duration of an error at the transition from one phase to the next for one of the subjects.

The results for the gait events of swing, pre-swing, and loading response were determined to the highest degree of accuracy. Larger errors are seen between the transitions from mid-stance to terminal stance and terminal stance to pre-swing. An increased variability in the duration of these gait phases was also noted.

4.3.2 Knee Kinematics: Analytical Approach

Table 4.2 displays the results from the model, able bodied trials and paraplegic trials. Figure 4.7 displays the knee flexion angle during the standing up of a paraplegic individual.

The auto-reset integral of the auto-nulled rate gyroscopes provided a more accurate estimate of knee flexion angle, as calculated by a goniometer, than the low pass filtered accelerometers in each instance ($p < 0.01$). The RMS difference between the reset rate gyroscopes and the goniometer for the entire movements of the individuals was from 2.39 to 3.17 degrees. For both the able bodied and the paraplegic individual, the rate gyroscopes provided a more accurate estimate of the angular velocity than the differentiated accelerometers ($p < 0.005$).

4.3.3 Knee and Hip Kinematics: "Virtual Sensor" Approach

Figures 4.8 and 4.9 display graphics of the neural network computation of knee flexion angle and angular velocity and hip angle and angular velocity for the sit to stand to sit transitions. The accuracy of the method is displayed in table 4.4. Separate networks were trained for the angle and angular velocity, as the amplification of the high frequency components caused by numerical differentiation of the angle produced greater high frequency components of angular velocity than the high frequency components of angular velocity estimated by the goniometer. The delay due to causally low pass filtering, used to compensate for the difference in bandwidth, was found to lead to a greater RMS error than using a separate network.

The training results were more accurate than the testing results for each network. For the testing section of data, the neural network outputs estimated the hip angle to an accuracy of 2.1 and 2.9 degrees respectively. The knee and hip angular velocities were estimated to an accuracy of 17.6 and 16.0 degrees/s respectively.

4.3.4 Detecting and Predicting Knee Buckling

A threshold of 300 mV was set to determine if a knee buckle is incipient. This threshold was selected as a level that was higher than the maximum resting value observed during the five seconds of quiet standing before the buckle by approximately 20%. For every trial, a decrease in force was seen prior to buckling in one brace, preceding an increase in force seen in both braces. Figure 4.10 displays a graphic of the strain gauge signals and angle of the knee. Table 4.4 displays the angle of the knee when a buckle is predicted, and the time between the prediction of an incipient knee buckle and when the knee extension angle reached 175 degrees. Both knees buckled within 100 ms of each other during each of the trials.

For each trial, one of the strain gauges detected a knee buckle prior to the knee reaching 175 degrees of extension. The minimum time duration, prior to the knee reaching 175 degrees and the strain gauge threshold being was met, was 340 ms. If the two knees were to be considered in isolation of each other, there were five instances in which the knee buckle would not be detected until after the knee reached 175 degrees.

4.4 Discussion

Gait phase detection was displayed to an accuracy of greater than 80%. This is comparable to the five phase detection algorithm of Ng and Chizeck, which reported at an accuracy of 75%. By using a heuristic rule based controller, the errors of the gait phase were limited to an early or late detection of a transition to the next phase. Kostov has previously described these errors as "non-critical" (Kostov, 1996). The accuracy of the method is compared to an individual walking at one stride per second analyzed at a 33 Hz. If five gait phases are detected, and an error of a single sample is made at the each transition, the accuracy of the method evaluated on a sample by sample basis is 84.8%. The accuracy does not correlate to a missed gait phase, but only to an early or late detection of a phase. If used to initiate states controllers in a finite state FES walking system operating at 33 Hz, the error rate would correspond to initiating or delaying the state controller by a single sample interval. For this reason, the accuracy of the detector, although not ideal, should be considered sufficient to be tested in a FES system.

The phases of mid-stance and terminal stance were noted to have a larger variability of the reference signals' gait phase length. The variability of the reference gait phase length could reflect an imprecise detection of gait phase by the reference gait phase detector. The rule based controller attempts to learn this imprecise estimate of gait phase, and the decrease in accuracy of the reference signal is reflected in an imprecise rule based controller and greater inaccuracy in gait phase estimation. Ng and Chizeck have previously described this as a source of error in their experiments.

The joint angles were calculated to within 3.2 degrees of the goniometer. The rate gyroscope provided a more accurate description of knee flexion angle and angular velocity than a filtered set of accelerometers. Additionally, the rate gyroscopes directly measure the angular velocity without differentiation. Causal numerical differentiation of the knee flexion angle as calculated by the accelerometer lead to either delay in the system due to low frequency filtering, or amplification of noise. The rate gyroscope could be considered in combination to accelerometers to provide a more accurate estimate of knee flexion angle and angular velocity than low pass filtered accelerometers.

Cross talk between the channels of the goniometer is specified to add 3° of error to the measurement of angle. Cross talk is not a source of error for the calculation of angle on the model, hence the results of the model provide a more accurate estimate of the angle calculated by the goniometer than the trials on the subjects. The linearity of the goniometer is 2% of the full scale reading or about 1.8° (Penny and Giles trade literature). A combination of cross talk and the non-linearity would lead to potential inaccuracy of 4.8°. This exceeds the 3.2° difference between the integrated rate gyroscope and the goniometer. Additionally, invariant static error was noticed between the accelerometers and the goniometer on the two dimensional model. This error corresponded to the nonlinearity of the accelerometers and goniometers without inclusion of the cross talk, as expected or the allowable 1 degree threshold in comparing the integrated rate gyroscope integral to the tilt calculated by the accelerometer.

The sensor system could detect the angle across the joint immediately when placed on the individual. This is an advantage in comparison to the goniometer, which requires calibration on an individual by individual basis. Static errors could be present due to misalignment of the goniometer with the limb segments.

Knee buckling was predicted prior to the knee extension falling below 175 degrees. Typical latency of muscle is 200 ms. The time between the knee buckle detector detecting an incipient buckle and the knee reaching 175 degrees was greater than this latency for at least one knee in each of the knee buckles. This implies that a corrective and restorative force about the joint could be applied by electrical stimulation to the quadriceps prior to knee extension reaching 175 degrees.

Through early detection or prediction of the knee buckle, less force would be required to regain stability of the knee joint. As the knee buckles to a greater extent, the displacement of the center of mass behind the knee, causing a flexing moment of the knee, increases. Prediction of knee buckling would allow for a decrease in the response necessary to restore the knee to a stable position.

The vision of the knee buckle controller is to minimize the disturbing effect of a knee buckle on an individual. Ideally, this would involve restoration of knee stability prior to any movement of the knee joint. This can be detected using forces, the simplest

configuration entailing detection of force within the brace. The prior experiment has demonstrated that the forces within the brace undergo a change prior to the knee buckling. Potentially, developers of knee buckle controllers could use this information to design a controller that would allow for minimal instability while maintaining long quiet standing times.

A heuristic rule could be included in the practical implementation of the knee buckle predictor. This rule would state that if the knee extension angle were to be less than 175 degrees of extension, a knee buckle has occurred and the controller should respond. This would ensure that minimally the system would respond at least as well as a threshold detection technique based upon knee extension angle.

This sensor set is applicable to both an implanted system and a surface system. For an implanted system, precise alignment of the sensor clusters is not guaranteed. It has been shown that a neural network can estimate the knee and hip flexion angles based upon repeatable sensor inputs. Through a combination of accelerometers, rate gyroscopes, and attributes derived from these signals, such as the calculation of segmental tilt, a deterministic input space is available for a neural network. The network can then provide a mapping of the sensor signals to the desired outputs of the system.

In each of the sensor configurations, a maximum of three sensor sites was used. Sensor configuration 2 was constrained to sensor belt and the FRO. Sensor configuration 3 was constrained to the FRO and a second site above the knee worn in conjunction with a reference electrode. Additionally, this sensor configuration could be incorporated into a neoprene knee brace, described in previous experiments (Wood et. al, 1998). These two configurations should display a minimum number of clusters, and should meet an ease of use design criteria required by a sensor system.

In both sensor configurations 2 and 3, the three accelerometers, necessary for detection of gait phases, were placed on the shank. Additionally, a strain gauge signal was used in configuration 2 although not tested for knee buckling. Therefore, it is suggested that either of these sensor configurations could provide gait phase detection, knee flexion angle, knee buckle control, and either hip angle or shank and thigh sagittal inclination. These are typical variables used for control of the neural prosthesis.

These tests suggest that a small, clustered, sensor system worn in conjunction with other components of a FES system can be designed and provide the variables typically used for feedback.

4.5 Conclusion

The sensors system met or surpassed previous descriptions of similar sensor systems that addressed only one aspect of lower limb control for FES. The multiple gait phase detector exceeded the classification rate of the system proposed by Chizeck. The detection of knee flexion angle was demonstrated to be within 3.2 degrees of a goniometer by both an analytical and machine learning method. The knee buckling detection determined that a change in force could be seen within the brace prior to the knee buckling. Further testing of the device would allow for a controller to be based upon this signal.

The sensor system is localized to 3 sites, and should be convenient for use with FES. When used with the paraplegic volunteer, the cluster placed on the thigh was attached to a reference electrode placed approximately two inches above the knee in the frontal plane, implying that the sensors could be incorporated into a surface stimulation system. The lower cluster was attached directly to the brace. Calibration for knee flexion angle detection was not required on a day to day basis.

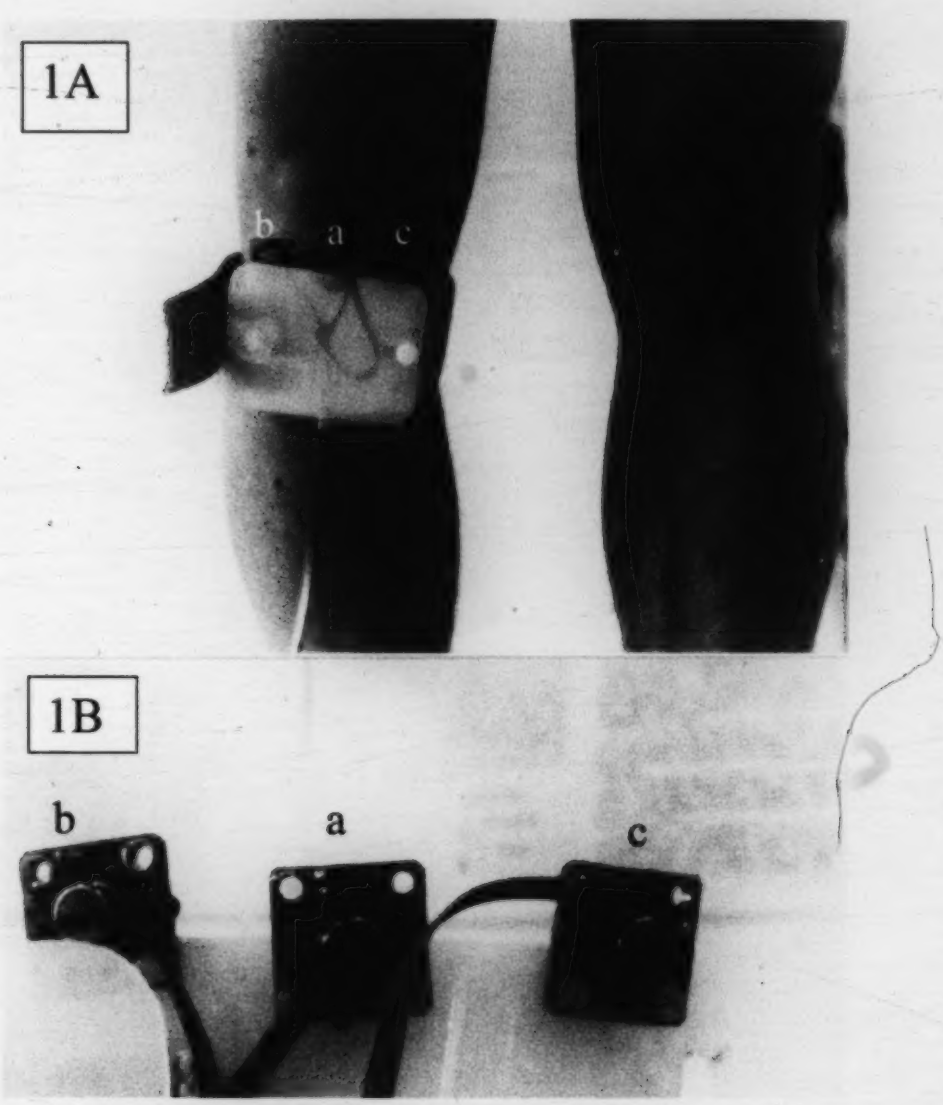

Figure 4.1:

(A) - Subject wearing calf strap with three accelerometers. The strap is worn between the patella and the head of the gastrocnemius soleus muscle group.

(B) – The three accelerometers attached to the calf strap are shown. a is oriented in the vertical direction. b and c are oriented in a horizontal direction with approximately 70° between their axis of detection.

Figure 4.2 An individual wearing sensor cluster 2. The three sites used in sensors cluster 2 are on the AFOs, indicated A1 and A2, and the belt, indicated B. The midline cluster of the belt contains the electromagnetic transmitter. Magnetoresistors and accelerometers are worn laterally. On the AFO, the sensors all of the sensors are contained in the viewed cluster. The sensor clusters are connected with a digital bus, displayed by the cables connecting the sensor clusters.

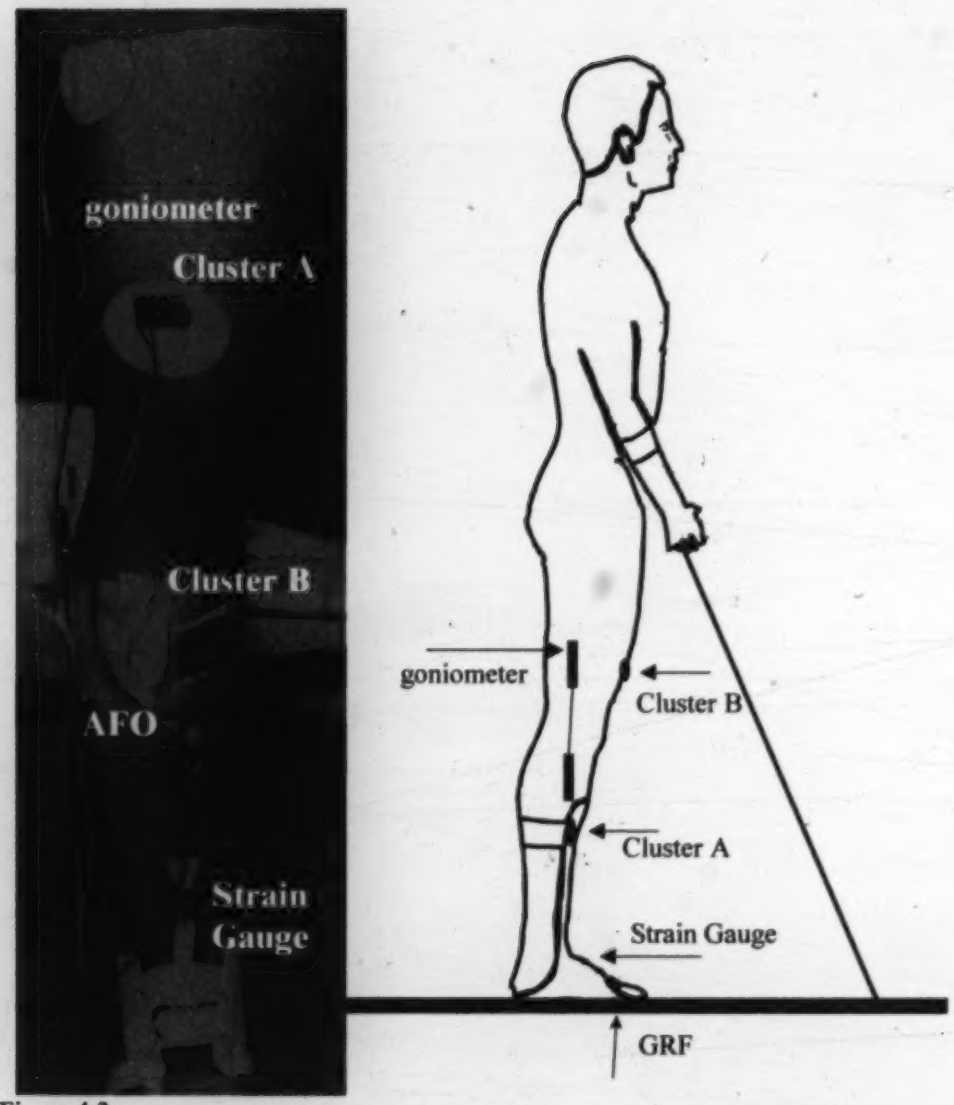

Figure 4.3:
(Left) Subject wearing sensor configuration 2. Clusters A and B are accelerometers and a rate gyroscope. Cluster A is connected to the strain gauge attached on the ankle of the AFO. A goniometer is worn on the lateral side of the knee as a comparison for knee angle.
(Right) Schematic of sensor configuration 2. Clusters A is attached to the AFO, and connected to the strain gauge mounted on the AFO and cluster B. The goniometer is worn only to during testing to check the accuracy of the sensor system.

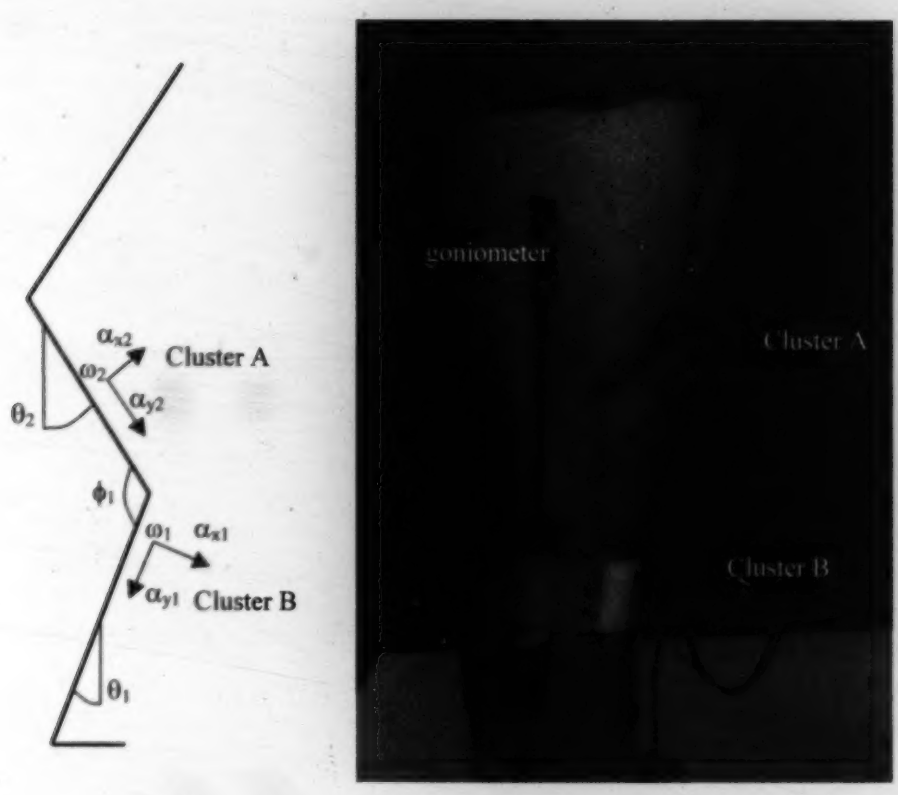

Figure 4.4:
(Left) Analytic determination on knee angle. Accelerometers α_{x1}, α_{y1} and rate gyroscope ω_1 are placed on the shank in the sagittal plane. The tilt of the shank, θ_1, is calculated from this cluster. Accelerometers α_{x2}, α_{y2} and rate gyroscope ω_2 are placed on the thigh in the sagittal plane. The tilt of the thigh, θ_2, is calculated from this cluster. The knee angle, ϕ_1, is the difference in tilts of the two segments.
(Right) Practical implementation. Cluster A is comprised of accelerometers α_{x2}, α_{y2} and rate gyroscope ω_2 and worn on the shank. Cluster B is comprised of accelerometers α_{x1}, α_{y1} and rate gyroscope ω_1 and worn on the thigh.

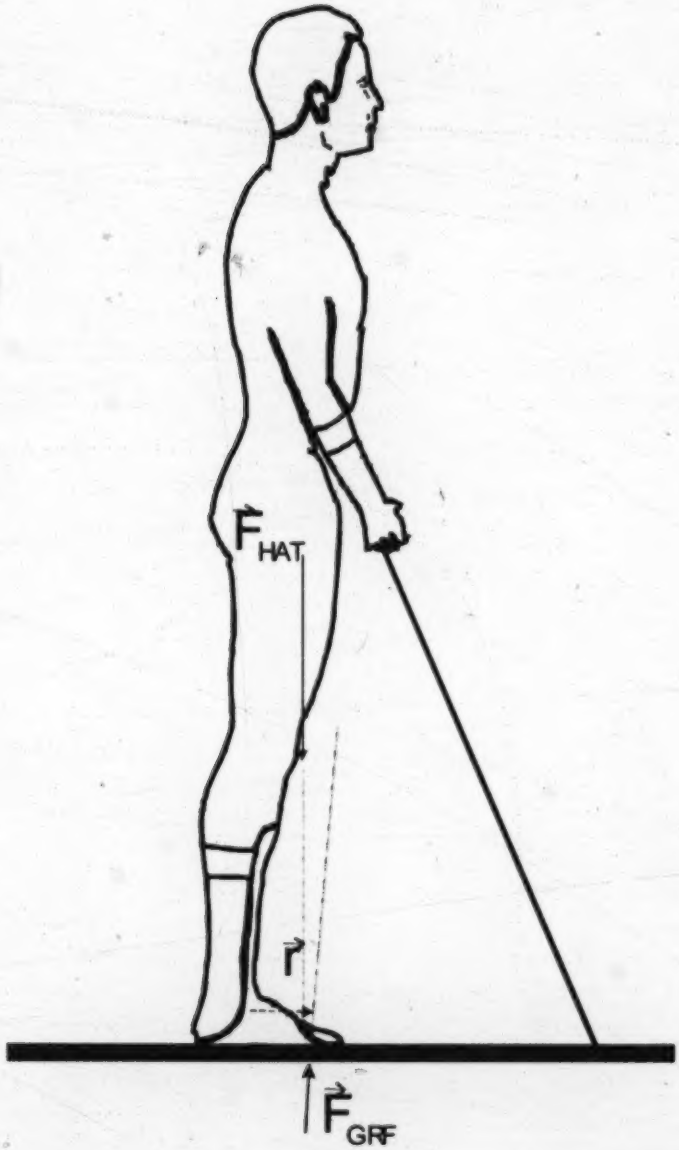

Figure 4.5: An individual is standing using assisted by a floor reaction orthosis by restricting dorsiflexion of the ankle. Both the ground reaction force (F_{grf}) and the head arms trunk force (F_{hat}) are directed in front of the knee causing extension. The moment about the ankle joint of each force is given by the cross products of r and F. Posterior movement of the F_{grf} would cause a decrease in force across the brace. Posterior movement of F_{hat} would cause an increase in force in the brace.

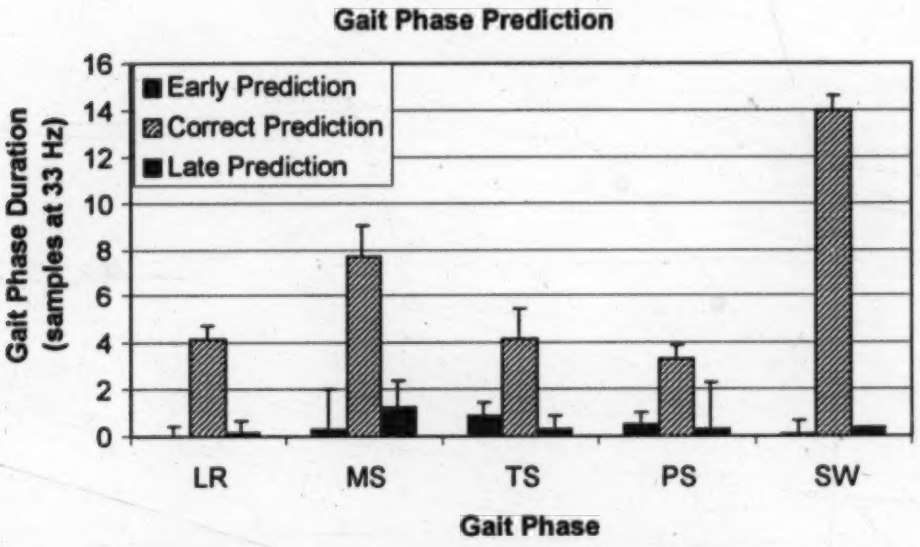

Figure 4.6: The average error at each transition is displayed with reference to the length of each gait phase detected. The gait phases used are loading response (LR), mid-stance (MS), terminal stance (TS), pre-swing (PS) and swing (SW). The average error includes zero length of transition error if an early or late prediction is not made.

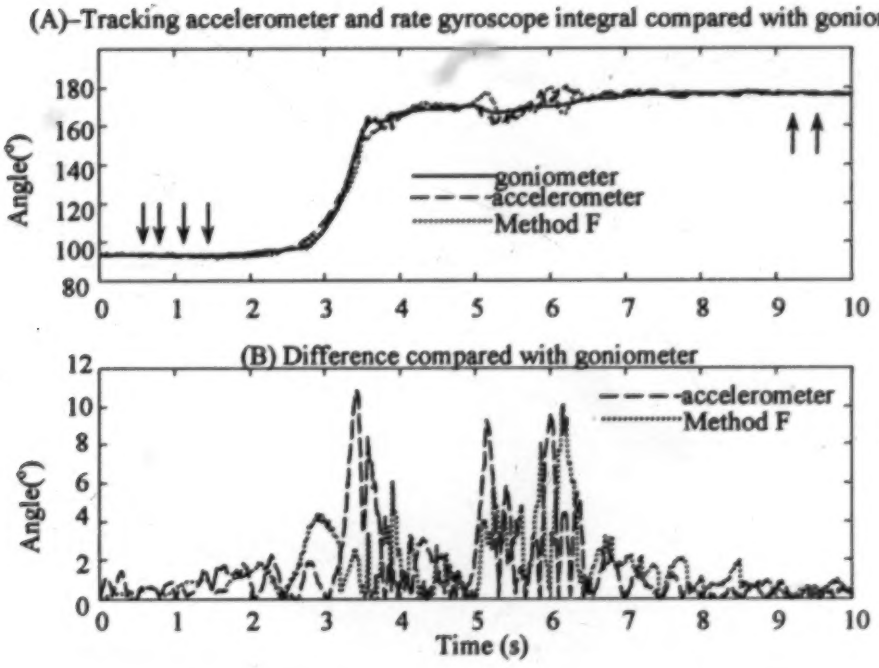

Figure 4.7: Angle calculated by goniometer, accelerometers and rate gyroscope on a paraplegic volunteer.

(A) displays the angle as calculated through the transition.
(B) displays the difference between the goniometer and the other methods.

The goniometer is the solid line. The accelerometer is the dotted line; the auto-reset auto-nulled rate gyroscope integral is the dashed line. The arrows in (A) show when the auto-nulling of the rate gyroscopes occurs. Auto-resetting of the integrators is also displayed at times 3.2, 7.4, 7.8, and 8.2 seconds.

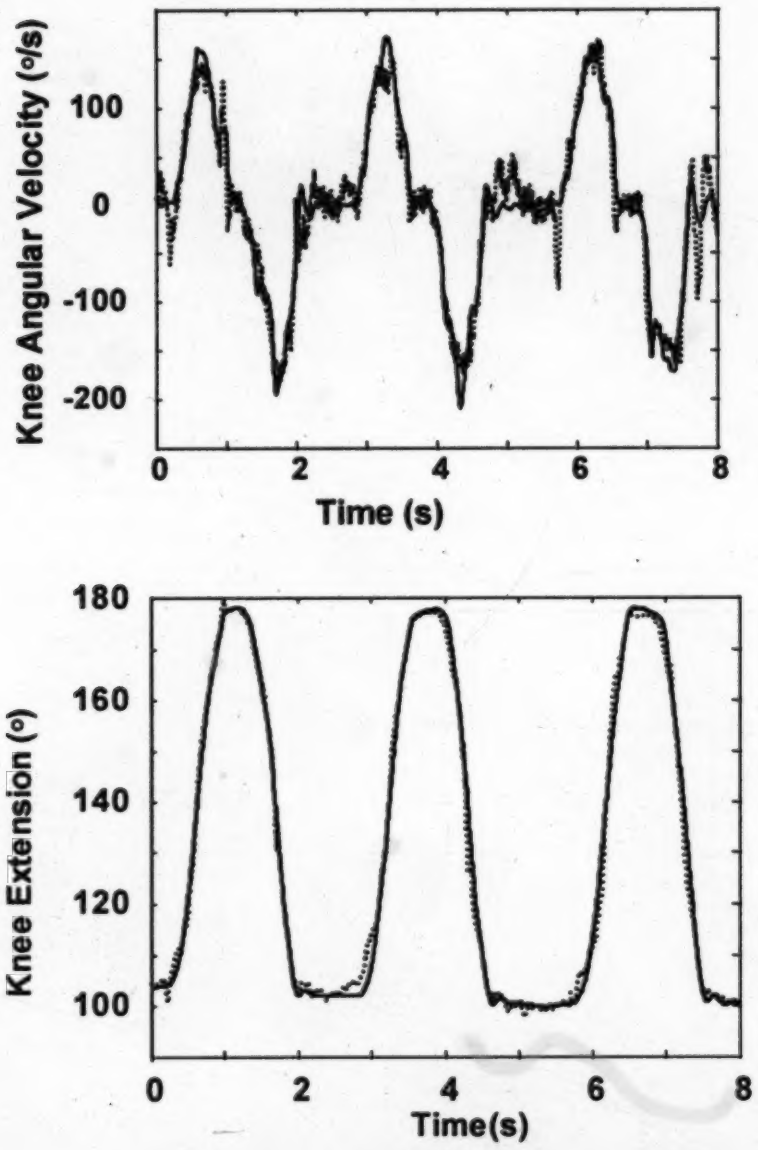

Figure 4.8: Knee extension angle and angular velocity as computed by neural networks and sensor configuration 3. The solid traces are the angles measure by the rate gyroscopes. The dotted traces are the predicted angles from the neural network outputs. The RMS error for the knee angle calculation was 2.1 degrees. The RMS error for the knee angular velocity calculation was 17.6 degrees/s.

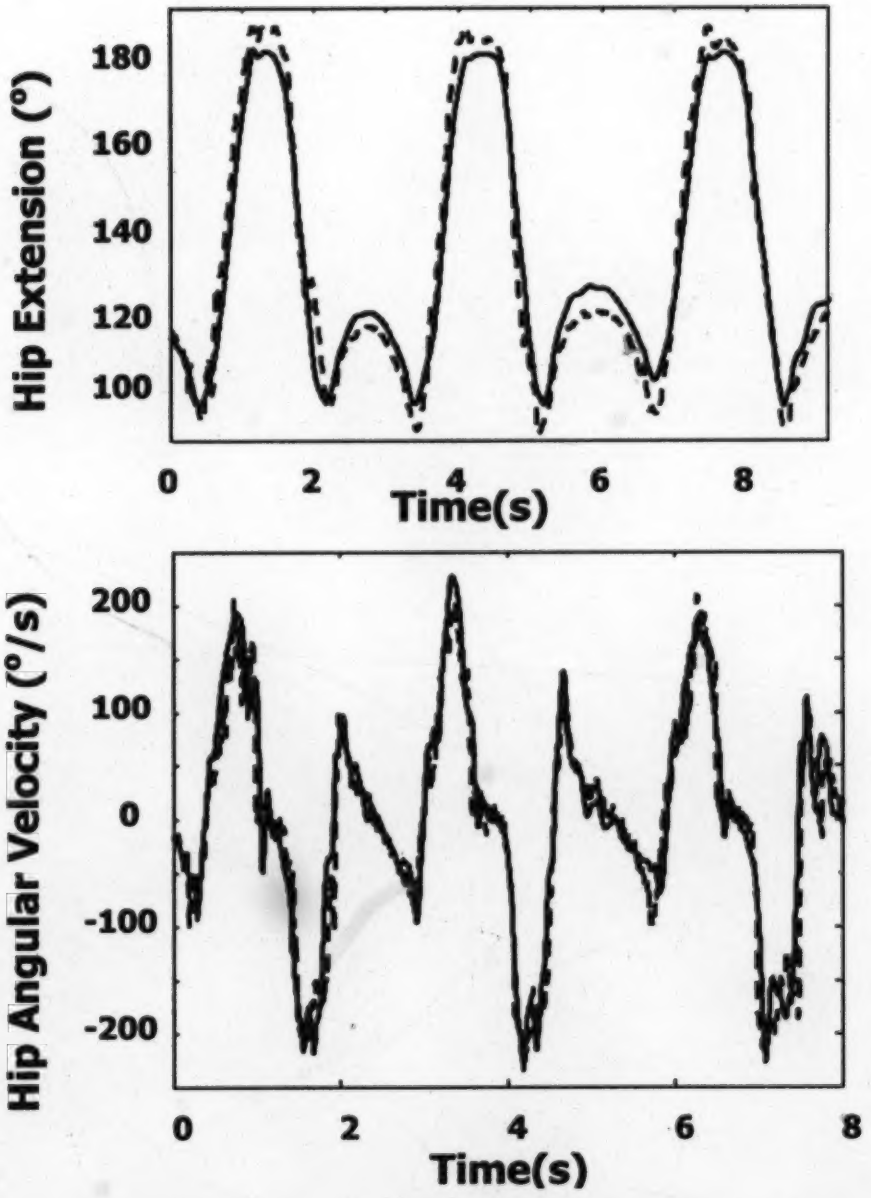

Figure 4.9: Hip angle and angular velocity as computed by neural networks and sensor configuration 3. The solid traces are the angles measure by the rate gyroscopes. The dashed lines are the predicted angles from the neural network outputs. The RMS error for the knee angle calculation was 2.9 degrees. The RMS error for the knee angular velocity calculation was 16.0 degrees/s.

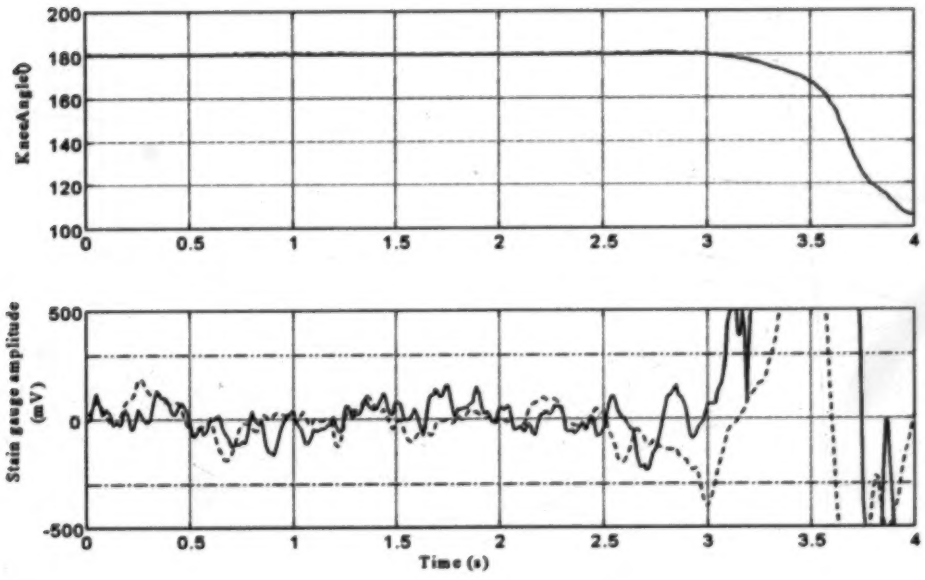

Figure 4.10:

(Top) The knee angle is recorded during a buckle with the goniometer. The knee reaches 175° at time 3.2 seconds.

(Bottom) The strain gauge signals are shown as recorded by the left (solid line) and right (dashed line) braces. The dashed line predicts a knee buckle at 2.9 seconds. The solid line predicts a buckle at 3.1 seconds.

	Gait Phases					
	LR	MS	TS	PS	SW	OV
A	96	83	78	70	97	89
B	60	71	88	66	90	81
C	72	83	55	77	91	82

Table 4.1: Five gait phases detected by post filtered Rough Sets rule based controller. Loading response (LR), mid-stance (MS), terminal stance (TS), pre-swing (PS), swing (SW), and overall (OV) prediction accuracy were calculated by applying two heuristic rules to the rule based Rough Sets detector. The results are displayed for the three able bodied volunteers in the study. All values are given as percentage of correct gait phases predictions versus the actual gait phase as determined by the foot floor contact pattern.

	Angle (°/s)		Angular Velocity (°/s)	
	Accelerometer	Rate Gyroscope	Accelerometer	Rate Gyroscope
Model –Tilt	2.33 (0.58)	0.77 (0.19)	21.57 (5.14)	2.86 (0.33)
Model – Angle	2.42 (1.18)	2.07 (0.70)	12.22 (4.19)	2.29 (0.62)
A – Left	3.70 (0.73)	3.17 (1.53)	11.54 (3.41)	5.00 (1.07)
A – Right	2.60 (1.42)	2.15 (1.00)	9.71 (2.64)	5.10 (1.46)
B – Left	3.14 (0.42)	2.80 (0.40)	13.52 (1.67)	6.32 (0.36)
B – Right	3.19 (0.32)	2.87 (0.40)	47.0 (6.24)	10.2 (2.63)
C	2.75 (0.61)	2.14 (0.69)	28.51 (6.82)	11.82 (2.71)

Table 4.2 : Columns 2 and 3 display the mean and (standard deviation) of errors in computing the angle between two segments of a model and knee angle for sit to stand to sit transitions in two able bodied individuals (A, B) and sit to stand transitions for one paraplegic individual (C). Columns 4 and 5 display the mean error and (standard deviation) for the calculation of angular velocity in the same movements. Left and right designations are given to the bilateral recordings performed with the able bodied volunteers.

	Left Strain Gauge		Right Strain Gauge	
	Knee extension angle at detect	Time prior to 5° flexion	Knee extension angle at detect	Time prior to 5° flexion
Trial 1	179.8	1.16	180	1.20
Trial 2	179.6	0.45	178.4	2.12
Trial 3	178.0	0.34	178.2	0.45
Trial 4	178.4	0.34	177.5	0.17
Trial 5	178.2	0.10	179.8	0.45
Trial 6	179.4	1.41	167.5	-0.68
Trial 7	177.9	0.70	177.3	0.17
Trial 8	179.9	3.83	178.2	-0.12
Trial 9	179.7	0.62	176.6	0.21
Trial 10	175.7	0.59	177.3	0.72
Trial 11	179.6	0.68	163.4	-0.45
Trial 12	180.0	2.17	180.0	2.17
Trial 13	179.7	0.77	179.8	1.15
Trial 14	179.8	0.59	172.2	-0.32
Trial 15	180.0	1.34	179.2	0.96
Trial 16	168.3	-0.28	177.5	0.50
Trial 17	179.0	0.50	173.3	-0.16

Table 4.3: Time prior to and angle at prediction of knee buckling. The time prior to the knee buckle detector of instability for each knee and the knee reaching 175 degrees (5 degrees of flexion) is displayed in columns 3 and 5. The angle of knee extension at detection of instability is recorded in columns 2 and 4.

	Knee Angle (°)	Knee Angular Velocity (°/s)	Hip Angle (°)	Hip Angular Velocity (°/s)
Training	1.4	16.1	1.6	13.1
Testing	2.1	17.6	2.9	16.0

Table 4.4: "Virtual sensor" calculation of knee and hip angle and angular velocity. Training occurred on six examples of sit to stand to sit transitions. The testing of the virtual sensor occurred on the remaining twelve recordings of the sit to stand to sit transitions.

4.6 Bibliography

Analog Devices trade literature, ADXL05JH and ADXL202JQC

Andrews, B.J., Barnett, R., Phillips, G., Kirkwood, C., Donaldson, N., Rushton, D., and Perkins, T., (1989) "Rule Base control of a hybrid FES orthosis for assisting paraplegic locomotion," Automedica, vol 11:175:199

Andrews, B.J., and Williamson, R.P., (1997) "Joint Motion Sensors for FES: The Gyro-goniometer", RESNA '97, 262-4

Andrews, B.J., Williamson, R., Ouellette, N., Koles, A., (1996) "Control of Neuralprostheses I: Sensor Fusion," Proc. RESNA'96, pp. 282-284

Andrews, B.J., Au, R., Williamson, R., (1995) "Event Detection for FES Control Using Rough Sets & Accelerometers," Proc. 2nd International FES Symposium in Sendai, pp. 187-193

Amp Inc. Trade Literature, Piezofilm sensors product guide

Andrews, B.J., and Williamson, R. (1997) "Joint Motion Sensors for FES: The Gyro-goniometer," Proc. RESNA '97, pp. 262-264

Brandell, B.R., (1982) " Development of a universal control unit for functional electrical stimulation (FES)," Am. J. Phys. Med. 61(6):279-301

Crago, P.E., Chizeck, H.J., Neuman, M.R., and Hambrecht, F.T., (1986) "Sensors for Use with Functional neuromuscular Stimulation," IEEE Trans. BME 33(2):256-268

Crago, P.E., Lan, N., Veltink, P.H., Abbas, J.J., and Kantor, C., (1996) "New control strategies for neuroprosthetic systems", J. Rehab. Res. Devel. 33:(2):158-172

Dai, R., Stein R.B., Andrews, B.J., James, K.B., and Wieler, M., (1996) "Application of tilt sensors in Functional Electrical Stimulation", IEEE Trans. Rehab. Eng. 4(2): 63-72

Davoodi, R., and Andrews, B.J., (1998) "Computer Simulation of FES Standing Up in paraplegia: A self adaptive fuzzy controller with reinforcement learning", IEEE Trans. Rehab. Eng. 6(2):151-161

Dolan, M.J., Andrews, B.J., and Veltink, P.H., (1998) "Switching curve controller for FES assisted standing up and sitting down, " IEEE Trans. Rehab. Eng. 6(2):167-171

Franken H.M., Veltink, P.H., Baardman, G., Redmeyer, R.A., and Boom, H.B.K., (1995) "Cycle to cycle control of swing phase of paraplegic gait induced by surface electrical stimulation", Med. Biol. Eng. & Comp. 33:440-451

Fugita, K, Shinga, K, Takahashi, H, (1996) "Analysis of FES-induced upper limb motion for machine learning control", IEEE EMBS, paper 672

Graupe, D. (1989), "EMG Pattern Analysis for Patient response control of FES in Paraplegics for Walker Supported Walking, IEEE Trans. BME 36(7):711-719

Hambrecht, (1972) "Neural control aspects of functional neuromuscular stimulation", FNS Workshop, Bethesday Maryland

Haugland, M.K., and Hoffer, J.A., (1994) "Slip information provided by nerve cuff signals: Application in closed loop control of functional electrical stimulation IEEE Trans. Rehab. Eng. 2(1):29-36

Hentry, J.R., and Ewins, D.J., (1998) "Applications of gyroscopic angular velocity sensors in FES systems", Proc. Int. Work. Vienna FES, pg 157-60

Heyn, R. E., Mayagoitia, A., Nene, V., and Veltink, P.H., (1996) "The kinematics of the swing phase obtained from accelerometer and gyroscope measurements", Proc. IEEE EMBS, pg 857-8

Heller, B.W., (1992) The production and control of functional electrical stimulation swing-through gait , Ph.D. Thesis, Strathclyde University

Johnson, K.O., Popovic, D., Riso, R.R., Koris, M., Van Doren, C., and Kantor, C., (1995) "Perspectives on the role of afferent signals in control of motor neuroprostheses" Med. Eng. & Phys. 17(7): 481-96

Johnson, M.W., and Peckham, H.P., (1990) "A two degree of freedom joint angle transducer", Proc. 12th IEEE EMBS pg. 510-511

Kalmus, H.P, (1962) "A new guiding and tracking system,", IRE Trans. Aerosp. Navig. Electron., 9:7-10

Kirkwood, C.A., Andrews, B.J., and Mowforth, P., (1989) "Automatic detection of gait events: a case study using inductive learning techniques", J. BME, 11(6):511-6

Kralj, A., and Bajd, T., (1989) Functional electrical stimulation : Standing and walking after spinal cord injury CRC Press, CA.

Kostov, A., Andrews, B.J., Popovic, D., Stein, R., and Armstrong, W., (1995) "Machine learning in control of functional electrical stimulation systems for locomotion, IEEE Trans. BME. 42(6):541-551

Kostov, A., (1996) "Functional error assessment in gait event discrimination for FES assisted locomotion", IEEE EMBS paper 969

Lajoie, Y., Barbeau, H., Hamelin, M, (1999) "Attentional requirements of walking in spinal cord injured patients compared to normal subjects", Spinal Cord 37:245-50

Liberson W.T., Holmquest H.J., Scot, D., and Dow, M., (1961) "Functional electrotherapy: Stimulation of the peroneal nerve synchronized with the swing phase of the gait of hemiplegic patients," Arch. Phys. Med. Rehab., 42:101-105

Lou, E., Durdle, N.G., Raso, V.J., and Hill, D.L., (1997) "Measurement of the magnetic field in the near-field region and self inductance in free space due to a multiturn square-loop:, IEE Sci. Meas. Tech. 144(6):252-6

Marsolais, E.B., and Kobetic, R., (1988) "Development of a practical electrical stimulation system for restoring gait in the paralyzed patient" Clin. Ortho. & Rel. Res. (233):64-74

Miyazaki, S (1997) "Long term unconstrained measurement of stride length and walking velocity utilizing a piezoelectric gyroscope", IEEE Trans. BME 44(8): 753-9

Morris, J.R., (1973) "Accelerometry-a technique for the measurement of human body movements" J. Biomech. 6(6):729-36

Mulder, A.J., Veltink, P.H., Boom, H.B.K., and Zilvold, G., (1992) "Low level finite state control of knee joint in paraplegic standing", J. BME 14(1):3-8

muRata devices trade literature, ENC05 Rate gyroscope

Neural Works trade literature, NeuralWorks Professional II

Ng, S.K, and Chizeck, H.J., (1997) "Fuzzy model identification for classification of gait events in paraplegics", IEEE Trans. Fuzzy Systems, 5(4):536-544

Perry, J., (1992) "Gait Analysis: Normal and Pathological Function", Thorofare, N.J.: SLACK Inc.

Phillips Trade literature, KMZ10A1 magnetoresistors

Penny & Giles Ltd. Trade literature on the model M180 flexible goniometer, UK 1996

Reduct Systems Trade Literature, Rough Sets 1.3

Sinkjaer, T., Riso, R., Mosallaie, F. K, Jensen, W., and Lawrence, S., (1997) , "Nerve cuff recordings of muscle afferent activity during passive joint motion in a rabbit", IFESS'97, 219-220

Smidt GL. Deusinger RH. Arora J. and Albright JP (1977). "An automated accelerometry system for gait analysis" J. Biomech. 10(5-6):367-75, 1977

Stallard, J., Major, R.E., and Patrick, J.H., (1989) "A review of the fundamental design problems of providing ambulation for paraplegic patients", Paraplegia. 27(1):70-5

Symmons, J., McNeal, D., Waters, R., and Perry, J., (1986) "Trigger switches for implantable gait stimulation", Proc. RESNA 9th Ann. Conf. 319-321

Thrahser, T.A., Wang, F, Andrews, B.J., and Williamson, R.P., (1996) "Control of neuralprotheses I : Self adaptive neuro-fuzzy control using reinforcement learning" Proc. RESNA '96, 492-4

Tong, K.Y., and Granat, M.H., (1998) "Vitrual artificial sensor technique for functional electrical stimulation" Med. Eng. & Phys., 20:458-68

Troyk, P., Poyezdala, J., and Jaeger, R., (1984) "Implantable goniometer for the human knee", Proc. IEEE EMBS pg. 224

Upshaw, B.J., and Sinkjaer, T., (1997) "Natural versus artificial sensors applied in peroneal nerve stimulation." Artif. Organs 21(3):227-31

Veltink, P.H., and Franken, H.M., (1996) "Detection of knee unlock during stance by accelerometry." IEEE Trans Rehab. Eng. 4(4):395-402

Veltink, P.H., Chizeck, H.J., Crago, P.E., el-Bialy, A., (1992) "Nonlinear joint angle control for artificially stimulated muscle." IEEE Trans. BME 39(4):368-80

Wang, F., Thrasher, T., Ouellette, N, Williamson, R., and Andrews, B.J, (1997) "Machine Learning Control of FES: Real Time Implementation," Proc. 2nd Annual Conference of the International Functional Electrical Stimulation Society, pp. 75-76,

Willemsen, A.T., Bloemhof, F., and Boom, H.B., (1990a) "Automatic Stance Swing Detection from Accelerometer Data for Peroneal Nerve Stimulation," IEEE Trans. BME, 37(12):1201-8

Willemsen, A.T., van Alste, J.A., and Boom, H.B., (1990b) "Real-time gait assessment utilizing a new way of accelerometry" J. Biomech. 23(8):859-63

Willemsen, A.T., Frigo, C., and Boom, H.B., (1991) "Lower extremity angle measurement with accelerometers--error and sensitivity analysis" IEEE Trans. BME 38(12):1186-93

Webster, J.G., (1992), "Artificial sensors suitable for closed loop control of FNS", from Neural Prostheses: Replacting motor functional after disease or disability, Stein, R.B., Peckham, P.H., and Popvic, D.P, eds. Oxford Press, ISBN 0-19-507216-2

Williamson, R., Andrews, B.J., Au, R., (1996) "Control of Neuralprostheses II: Event Detection Using Machine Learning" Proc. RESNA'96, pp291-293

Williamson, R, and Andrews, B.J., (1997) "Sensors for FES Control," Proc. 2nd Annual Conference of the International Functional Electrical Stimulation Society, pp. 213-215, 1997

Wood, D.E., Harper, V.J., Barr., F.M.D., Taylor, P.N., Phillips, G.F., Ewins, D.J., (1998) "Experience in using knee angles as a part of a closed loop algorithm to control FES assisted paraplegic standing", Proc. Int. Work. FES Vienna 137-140

Yoshida, K., and Horch K., (1996) "Closed-loop control of ankle position using muscle afferent feedback with functional neuromuscular stimulation", IEEE BME 43(2):167-76

5 Electrical Nerve Blocking : A computer simulation

5.1 Introduction

Present neural prostheses can only impose limited control over the peripheral nervous system. Neural prosthetic control could be greatly enhanced and extended if these devices could selectively activate or completely block axons in addition to electrically exciting axons, as evidenced by attempts to electrically block and selectively stimulate axons. Applications for selective electrical stimulation and blocking could include the suppression of unwanted reflex activity in the bladder (Rijkoff et. al., 1997) and bowel (Peckham and Creasey, 1992), and mobility enhancement through the suppression of spasticity in hemiplegia (Perry, 1993) and cerebral palsy (Chicoine et. al, 1997).

For the block to be applied in mobility assistance, it should activate and deactivate in the order of ten milliseconds. If the proposed technique is electrical in nature, a balanced or biphasic waveform is needed to maintain the integrity of the metal electrodes and prevent irreversible electrochemical effects that may damage tissue (Walter et. al, 1996). In addition to balanced charge delivery at the electrode, a maximum current density must abstain from irreversible, ionization processes. Therefore, the current must be limited at any electrode. When the block is applied to a mixed nerve, the generation of action potentials in sensory axons may be painful or uncomfortable for those with intact sensory pathways, or produce undesirable reflex activity.

Anodal, or DC, blocking has been previously described as a method for electrical nerve blocking and selective stimulation (Rijkoff et. al, 1997, Brindley and Craggs, 1980). However, anodal blocking requires monophasic current injection by electrodes. This can produce irreversible processes at the electrodes and lead to electrode corrosion. Long term application of the anodal blocking could exceed the charge per phase injection described for electrode longevity.

The generation of unidirectional action potentials for selective nerve stimulation has been described for application in the bladder (Sweeney and Mortimer, 1986, Fang and Mortimer 1991). In these applications, the nerve was repeatedly stimulated with

quadratrapezoidal pulses to generate unidirectional action potentials. This method might be limited to motor nerves as it can produce bidirectional action potentials in the small, pain sensing afferents. A posterior rhizotomy is typically used with collision blocking to eliminate adverse affects due to stimulation of reflexes and pain receptors (Grunewald et. al, 1997).

High frequency stimulation at 600 Hz has been described for control of muscle force (Solomonow, 1984) and the bladder (Shaker et. al., 1997, Walter et. al., 1993). The high frequency stimulation causes a block of the muscular contraction, attributed to an endplate depletion mechanism (Solomonow, 1984). Walter et. al, reported adverse side effects of leg flexion and secondary bladder contractions when applying this technique was applied to the sacral nerve of cats. This suggests that reflex activity could be problematic if high frequency stimulation for the purposes of achieving a block is applied to mixed nerves.

McCreery et. al. (McCreery, 1995) have noted that continuous 50 Hz stimulation for 8 hours or 100 Hz stimulation for 4 hours could produce early axonal death. Based on this study, blocking of the muscular contraction through repetitive activation could cause axonal death if sustained for greater than 4 hours.

Rattay (Rattay, 1990) demonstrated a local conduction block in a computer simulation of a 10 μm Hodgkin-Huxley type axon using a monopolar electrode with a 2 kHz sinusoidal stimulus. In this paper, we extend these computer simulations to myelinated axons over a range of axon diameters, frequencies, and electrode distances, to investigate the possibility of a switchable, localized electrical nerve block. The results of these simulations are considered in conjunction with reports of high frequency electrical nerve blocking in animal trials.

5.2 Background

Wedenski (Wedenski 1885) described a block of muscular force due to high frequency stimulation of the axon. Solomonow (Solomonow, 1984) described a block using rectangular monophasic pulses at frequencies below 20 kHz. The power that was needed to induce the block was minimized by a stimulation frequency of 600 Hz.

Solomonow has described this block as Wedenski block, and suggested it could be due to endplate depletion.

Tanner (Tanner, 1962) noted that a 20 kC alternating current, of an unspecified shape and amplitude, appeared to suppress components of the compound action potential in dissected sciatic frog nerve. Woo and Campbell (Woo and Campbell, 1964) confirmed Tanner's results. They demonstrated that the 20 kC blocking could produce a tetanic muscular response without a characteristic compound action potential and thought this effect was due to an asynchronous stimulation of large fibers. Using potential recordings from an isolated nerve fiber, they also displayed that a 20 kC waveform could block the transmission of action potentials without generating action potentials.

Tai and Jaing (Tai and Jaing, 1994) investigated peripheral nerve blocking via cathodal currents. As anodal currents can stimulate the nerve, cathodal currents can block the nerve. They used cathodal currents of up to 20 mA to selectively generate action potentials in smaller diameter axons of a frog sciatic nerve, and included computer simulations that reinforced their findings.

Bowman (Bowman, 1981) examined rectangular pulse blocking by investigating the electrical response and firing rates of a single nerve fiber distal to a rectangular pulse generator. He concluded that high frequency pulse trains could generate a block either through endplate depletion or through a localized conduction block. He reported the localized conduction block would occur at stimulus amplitudes of five times the current that is necessary to initiate an action potential in the same diameter axon for frequencies greater than 2 kHz.

Muller (Muller, 1969) demonstrated a localized conduction block. He stimulated an isolated sciatic nerve of a frog with a 5 kHz signal at a distance of 2 centimeters and two to six times the current necessary to produce a compound action potential. He was able to show that in isolated nerves, excitations generated by a cathode could be blocked. He restates a previous hypothesis that middle frequency currents lower the membrane potential without eliciting full depolarization of the membrane.

Tanner, Woo and Campbell, Solomonow, and Bowman all demonstrate a Wedenski block due to repetitive activation of the nerve from high frequency stimulation.

However, the experiments of Woo and Campbell, Bowman, and Muller suggest that a second, localized conduction block that does not produce repetitive stimulation of the axon also exists.

Computer modeling supports electrical nerve blocking by repetitive stimulation of the axon. Rattay demonstrates (Rattay, 1990) a train of action potentials is produced in the Hodgkin-Huxley model by 2 kHz sinusoidal stimulation. However, Rattay also notes that a 2 kHz sinusoidal signal can be used to locally block the Hodgkin-Huxley axon at higher currents.

Both localized electrical nerve blocking and high frequency blocking due to repetitive stimulation have been described in computer models and in animal trials. However, both of these blocks appear in a similar frequency range, which could lead to confusion between the two effects and a variability of results. Rattay's description of high frequency blocking by modeling is intriguing. It appears to meet the requirements for an electrical nerve block that are necessary for control of spasticity, as it is biphasic, does not cause excitation of the nerve, and activates and deactivates within milliseconds. The availability of peripheral nerve models, including a human model, has allowed for the opportunity to test this technique. These simulations could provide a non-invasive intermediate step in determining the feasibility of this technique, and allow for characterization of the effect before undertaking animal trials.

5.3 Methods

5.3.1 Spatially Extended Nodal Kinetic Models

Since Hodgkin and Huxley (Hodgkin and Huxley, 1952) developed the first empirically based model of the unmyelinated axon of a squid, various models have been proposed for other species. Frankenhauser and Huxley (Frankenhauser and Huxley, 1964) reported a model for myelinated frog nerve, Chui et. al. (Chui et. al, 1979) and Sweeney (Sweeney et. al., 1987) reported a model for the myelinated rabbit axon, Schwarz and Eikhof (Schwartz and Eikhof, 1987) for reported a model for myelinated rat nerve, and Schwarz, Reid and Bostock (Schwarz, Reid and Bostock, 1995) reported a model for

human myelinated peripheral nerve. The equations for the ionic currents of these models are listed in appendix 5.1

The voltage sensitive ionic gates are proteins represented statistically, implying that a quantum mechanical process is involved in the conformational change between opening and closing of the gates. This implies transitional times for the gates to open or closed would be in the order of picoseconds or less, which is six orders of magnitude smaller than the time step size used in modeling the axons. It is therefore assumed that the transition time of the ionic gates is not a source of error for the models. The other equations in the models of the axon are based on a simple electrical circuit, and should introduce errors only due to simplification of the system.

To examine nerve blocking, the axon model should include the propagation of the action potential from node to node. McNeal (McNeal, 1975) proposed a model of conduction that assumed the myelin sheath to be a perfect insulator, i.e. have infinite resistance. A diagram of this model is seen in Figure 5.1. Using this model, Rattay (Rattay, 1990) has applied Kirchoff's current law at $V_{i,n}$ to obtain

$$0 = i_{ionic,n} + R_a\left(V_{i,n} - V_{i,n-1}\right) + R_a\left(V_{i,n} - V_{i,n+1}\right) + c_m \frac{d(V_{i,n} - V_{e,n})}{dt} \qquad (1)$$

Equation (1) can be simplified using reduced voltages, i.e.

$$V_n = V_{i,n} - V_{e,n} - V_{rest} \qquad (2)$$

where

V_n is the reduced membrane voltage at node n

$V_{i,n}$ and $V_{e,n}$ are the potentials inside and outside of the axon with respect to infinity, as in equation (1) and Figure 5.1

V_{rest} is the resting membrane voltage

The intraaxonal resistivity, R_a, can be reduced into its components

$$R_a = \frac{\alpha x}{4\rho_i \cdot L \cdot \Delta x} \qquad (3)$$

By combining terms 2 and 3, and making this substitution, equation (1) can then be rewritten as

$$\frac{dV_n}{dt} = \left[-i_{ionic} + \frac{ax_d \cdot \Delta x}{4\rho_i \cdot L} \left(\frac{V_{n-1} - 2V_n + V_{n+1}}{\Delta x^2} + \frac{V_{e,n-1} - 2V_{e,n} + V_{e,n+1}}{\Delta x^2} \right) \right] / c_m \quad (4)$$

where

dV_n/dt is the change in voltage across the membrane with respect to time

i_{ionic} is the ionic current flow across the membrane provided by the FH, SE, SRB, and CRRSS models listed in appendix 1

ax_d is the axon diameter

Δx is the distance between the nodes of Ranvier

ρ_i is the internal axon resistivity

L is the width of the node of Ranvier

V_n is the reduced nodal voltage at node n

$V_{e,n}$ is the voltage external to the axon at node n

c_m is the membrane capacitance

Rattay (Rattay, 1990) has previously derived equation (4), and refers to the final term as the activating function. This term dictates how an external electric field can influence an axon. The electric field is due to an external system of electrodes, which can be modeled separately.

If the myelin sheath is not assumed to be a perfect insulator, the model must include an electrical node placed in between the nodes of Ranvier. The myelin sheath can be modeled by a single electrical node, as subdivision of the myelin sheath does not significantly alter the model's behavior (Rubenstein, 1991). The ionic currents at these nodes will be nonspecific leakage currents, and the capacitance would be the capacitance of the myelin sheath across the membrane. The change in voltage at the electrical nodes of the myelin sheath is therefore

$$\frac{dV_n}{dt} = \left[\frac{V_{n,myelin}}{R_{myelin}} + \frac{ax_d \cdot \Delta x}{4\rho_i \cdot L} \left(\frac{V_{n-1} - 2V_n + V_{n+1}}{\Delta x^2} + \frac{V_{e,n-1} - 2V_{e,n} + V_{e,n+1}}{\Delta x^2} \right) \right] / c_{myelin} \quad (5)$$

Models for nerve cuff electrodes that have been described (Altman and Plonsey, 1986, Veltink, 1988, and Struijk et. al., 1991) require finite difference equations to be solved. Initially examined here is a simpler electrode, the monopole i.e. a point source with a large reference return plate placed at a very large distance.

For the monopole, the electric potential field of a monopolar source with a return electrode at a large distance in cylindrical polar coordinates is

$$V_e(r,z) = \rho_e \cdot I_{el} / 4\pi\sqrt{r^2 + z^2} \quad (5)$$

where:

$V_e(r,z)$ is the voltage at a position in space

r, z are the radial and longitudinal separation of the electrode and a point in space. For the simulations, z corresponds to the distance along the axon, Δx in equations (1) and (3), and r corresponds to the perpendicular distance from electrode to the axon.

ρ_e is the external resistivity

I_{el} is the current of the electrode

The simulations were performed using fourth order Runge-Kutta integration implemented in MATLAB v5.1 on a Pentium II PC, 233 MHz. A typical simulation, for a real time interval of 20 ms, with 30 nodes required about 3 minutes of computer time.

The effects of high frequency stimulation were observed when applied to the four peripheral nerve models, (SRB, SE, CRRSS, FH) using an axon with an imperfectly insulated myelin sheath, comprising 30 active nodes. Models were also generated that contained a perfect myelin sheath. The results from the models with a perfect myelin sheath are not presented here, as they do not display different characteristics than the imperfect myelinated models.

The temperature was set at 37 °C for the SRB, SE, and CRRSS models, and 20 °C for the FH model.

Three sets of experiments were performed. In the first test, the qualitative effects of high frequency electric currents were determined. An axon of 30 active nodes of Ranvier and 31 passive myelin sheaths was constructed for each model. Current was progressively increased over node 15 until an effect was observed. This continued until it was determined that an increase in current would not further alter the reaction of the axon. At this point, a test for a local transmission block was performed. For this test, an axon comprising 40 active nodes was simulated for each model. Action potentials were generated using a cathodal stimulus at node 3. High frequency blocking currents were applied at node 20. This provided a minimum of 8.5 mm of separation between the cathodal stimulus and the blocking waveform. The action potential generated due to the cathodal current was observed to propagate undisturbed along the axon in the absence of any high frequency currents. The blocking current was progressively increased in 5 μA increments until the membrane voltage at node 38 was not changed due to the stimulation at node 3. This type of test was conducted for the SE, SRB, CRRSS and the FH models for axon diameters ranging from 5 to 15 μm, and sinusoidal frequencies ranging from 1 to 20 kHz. For the SRB model, changes in location of the blocking electrode with respect to the axon were also tested. The blocking electrode was varied in placement from between two nodes of Ranvier to directly above one node of Ranvier, and moved perpendicularly from 0.25 mm to 2 mm from the axon.

In the second test, an approximation to the validity of the predicted nodal voltages was examined during the application of the blocking current. For each of the models, the high frequency stimulation caused oscillation of the voltage across the membrane. For the SRB and SE models, a voltage range in which the model was determined is published, and a direct comparison can be made between the voltages across the membrane produced by high frequency currents and the published results. The FH and CRRSS models do not publish the range of voltages in which the models were constructed. Therefore a first order comparison is made between the voltages across the membrane produced by the high frequency oscillation and the height of the action potential.

In the third test, a potential mechanism for the localized block was predicted. The membrane voltage and gating potentials during the range of the continuous action potential generation and the localized blocking of the axon were examined. The high frequency currents caused an oscillatory response of the membrane voltage and gating potentials at the frequency of the stimulation. Slower changes in the membrane voltage and gating potentials underlying this oscillation were also observed.

5.4 Results

5.4.1 Excitation and Blocking Using High Frequency Currents

The results of various current levels of a 10 kHz sinusoidal current on a 10 μm fiber of the SRB model are shown in Figure 5.2. The blocking electrode was placed between nodes 15 and 16 at a perpendicular distance of 1 cm. The first effect, in order of increasing current, is the generation of a single action potential that propagates in both directions. This occurs at a current level of 847 μA for this diameter, and displayed in Figure 2a. It can be seen in the figure that the action potential propagates away from nodes 15 and 16 to nodes 14 and 17 as time increases along the ordinate axis. The second effect is the generation of a continuous train of action potentials. These action potentials propagate in both directions along the axon. This is seen in Figure 5.2b of the model, and is produced at a current of 909 μA. The action potentials are seen as propagating away from nodes 15 and 16 as time increases along the ordinate axis. The frequency of the action potential generation is not synchronized with the frequency of stimulation. As this current level is increased, the frequency at which the action potentials are generated increases. In Figure 5.2b, the frequency of action potential generation is 125 Hz. The third effect is the cessation of the continuous generation of action potentials, as seen in Figure 5.2c, and is produced at a current of 1.241 mA. Only a single action potential that propagates away from nodes 15 and 16 occurs at this level of current. Figure 5.2d shows the localized transmission block of a node. Action potentials are generated by a cathodal stimulation at node 3. These action potentials can be seen as propagating away from node 3 as time increases. A blocking current is applied to node 15. It is seen that only a single action potential is generated at the onset of the blocking current, which propagates away

from node 15. Propagation of the action potentials generated at node 3 can be seen proximally to node 15 but not distally from node 15. This occurs at a current level of 1.741 mA. A localized block of the transmission of the action potentials occurs.

The 4 models were tested over a range of axon diameters from 5 μm to 15 μm. A 10 kHz stimulating frequency was chosen and the stimulating electrode was placed directly between two nodes of Ranvier at a distance of 1 mm. The results from these trials appear in Figure 5.3.

The 4 models were tested over a range of frequencies from 1 to 20 kHz. A 10 μm diameter axon was chosen and the stimulating electrode was placed directly between two nodes of Ranvier at a distance of 1 mm. The results from these trials are seen in Figure 5.4.

For the CRRSS model and the FH model, an initial action potential is produced, and a continuous train of action potentials is produced. This is observed over a range of frequencies, as seen in Figure 5.3a and b, and over a range of fiber diameters, as seen in Figure 5.4a and b. In the SE and SRB models, an initial action potential, continuous action potential generation, a cessation of the continuous action potential generation, and a block are observed. The levels at which these effects are generated are displayed in Figures 5.3c and d, and 5.4c and d for a range of frequencies and diameters.

The current level required to produce a single action potential, continuous action potential generation, cessation of continuous action potential generation, and a block as related to the placement of the blocking electrode are displayed in Figure 5.5. Movement of the electrode along the axon altered the current required to produce stimulation and blocking of the axon. An increase in current was required for the initial action potential, continuous action potential generation and cessation of continuous action potential generation, as the electrode moved away from the node of Ranvier. A decrease in current was required for the generation of a block.

The perpendicular distance from the electrode to the axon was varied between 0.25 and 2 mm in steps of 0.25 mm. The results of these trials are shown in Figure 5.6. An increase in the level of current was necessary for each of the effects as stimulated by a

monopolar electrode at an increasing distance from the axon. The current increase is exponentially related to the distance, as is expected from the equations.

5.4.2 Integrity of Models During High Frequency Excitation and Blocking

Table 5.1 compares the voltage excursions seen by the SRB, SE, FH and CRRSS model at 10 kHz. The voltage excursion was measured during times that the high frequency currents did not produce an action potential.

Voltage ranges of the SRB and SE models were published, but were not published for the CRRSS model and the FH model. A direct comparison of the effects cannot be done on the FH and CRRSS models, but a first order approximation of these models' integrity can still be made by noting the excursion in these models due to the high frequency current.

The voltage excursions due to the high frequency stimulation in the CRRSS and the FH models are smaller than those seen in the generation of an action potential in each model, -80 - 30 mV for CRRSS, and -78- 46 mV for FH. The voltage ranges predicted for the effects of high frequency stimulation for the SRB are within the range explored by the publishers of the model. The voltage ranges predicted for the effects of high frequency stimulation in the SE model are outside the published range of the model by 1.5 %. Further increases in the blocking current will raise increase the voltage range across the membrane, causing the model to exceed these boundaries. For this increase in blocking current, the models continue to predict a block.

5.4.3 A Potential Mechanism for Blocking

An action potential in the SRB model lasts approximately 2.4 ms, which is 24 times the period of the 10 kHz currents. On this basis, it is presumed that the changes in the membrane voltage can be observed without the high frequency oscillations. Therefore, the high frequency oscillations were averaged over each cycle of the current so that the slower changes in the membrane voltage could be observed.

The high frequency stimulation caused both a continuous train of action potentials and a localized block of the axons. Figures 5.7a and b display the membrane voltage and the Na^+ inactivation gate (h) for the node directly under the stimulating electrode.

Continuous action potential generation occurs at stimulating currents of 1.0 to 1.2 mA for electrodes placed directly over and directly between node of Ranvier respectively. In both graphs, as the current increases, the frequency at which the axon excites also increases. This reduces the amount of time that the Na^+ inactivation gate (*h*) has to recover before generating the next action potential. This in turn reduces the amount of Na^+ that can cross the membrane and lead to a depolarization. At 1.3 mA for the Figure 5.7b an action potential is no longer generated.

The block of the axon occurs because the propagating action potential is unable to pass to the next node of Ranvier. Figure 5.8a displays the graphs of the membrane voltage of the node of Ranvier nearest to blocking electrode for a simulation in which an action potential is generated distally and blocked by high frequency current. Figure 5.8b displays the graphs of the membrane voltage for next the nodes of Ranvier.

The action potential approaching the blocked node causes a depolarization in the membrane voltage, seen near time 8.7 ms. As the blocking current increases, the size of this depolarization decreases. In Figure 5.8b, the depolarization at the next node is increased in amplitude and duration over the resting membrane voltage for 1.7 and 1.75 mA for the graph. The depolarization induced by the preceding node is reinforced in both amplitude and duration. For these current levels, the action potential is able to pass through the node of Ranvier. For the other current levels, the depolarizations in Figure 8b are not sufficiently large to cause a reinforcement of the depolarization. Hence, the level of the depolarization decreases as it is passed to the subsequent node, until a depolarization due to the action potential is not observed. This is noted as a localized block of the action potential.

5.5 Discussion

High frequency electrical currents are thought to cause a block at the neuromuscular junction first described by Wedenski, which is supported by the FH and CRRSS models of the axon. However, the SE and SRB models suggest that a localized block of action potentials is possible.

The current – diameter relationship shown in Figure 5.3 is expected. Larger diameter axons are more sensitive to electrical stimulation. This is displayed for each model. This graph also suggests that the block is selective, based on the diameter of the axon.

Figure 5.4 displays the effects of different frequencies of stimulation on a single diameter of axon. An increase in current is needed to achieve the same effect at a higher frequency in each of the SE, CRRSS, SRB, and FH models. The axon itself can be oversimplified to a capacitor – resistor network, similar to a low pass filter. Figure 5.7 indicates that an increase in average voltage across the membrane is required to produce the effects of continuous action potential generation and blocking if the frequency increases. Hence, it would take more current for this voltage to be achieved at higher frequencies in which the charging of the capacitor has less time per cycle to charge. On this basis, it is expected that an increased frequency would require additional current to produce the effects.

There are two deviations from this generalization displayed. A discontinuity of the frequency-current graph is seen between 6 and 7 kHz in the Figure 5.4c. At the 2.7 mA required to produce a block at 5 kHz, a voltage excursion across the membrane of –188→ 102 mV is produced. This is compared to a voltage excursion across the membrane 7 kHz and 1.7 mA of –124 → 8 mV. At 7 kHz, the current needed to block the axon produced a voltage across the membrane in the range of the model of the axon. At 5 kHz, the current needed to produce the block causes voltage excursions greater than the range of the model. In the SRB model a cusp is observed in Figure 5.4d at 4 kHz, although the significant change in current and voltage observed as in the SE model is not repeated for this cusp in the SRB model. Examination of the current flowing across the axon, the average voltage across the axon, and the ionic gates at frequencies on either side of the cusp did not lead to an explanation for this cusp.

The direction of this study is to propose a method for nerve blocking that could be tested in an animal trial. As the models display a discontinuous result that is unstable with respect to frequency in this range of frequencies, an increased chance for variability of

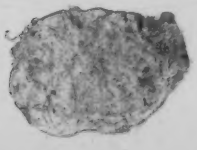

results could occur in the animal trials near these frequencies in comparison to frequency ranges that do not display discontinuities.

The level of stimulation current necessary to cause the block increases with an increase in distance from the blocking electrode, displayed in Figure 5.6, as is expected. The current also varied due to the positioning of the electrode with respect to the nodes of Ranvier, as shown in Figure 5.5, although to a smaller degree. Stimulation of the nerve from a cuff electrode should reduce the dependence of current level on the location of the axon (Goodall et. al., 1996). This could be demonstrated by using a cuff model of an electrode.

In normal axon conduction, the relative refractory period of the axon is determined by the rate at which the *h* gate can reopen after an action potential passes through the node. In cathodal blocking, the *h* gate remains closed, hence action potentials cannot propagate through the nodes. The high frequency stimulation displayed is similar. In Figure 5.7, the state of the *h* gate during high frequency stimulation is displayed. A positive trigger by the high frequency source, i.e. the rising edge of the sinusoid in this study, is repetitively applied to the axon and causes the stimulation. However, even in the presence of the positive trigger, a closed *h* gate will not allow an action potential to be generated.

Although the model does not produce action potentials at this level of stimulation, a propagating action potential can pass through the area of the sinusoidal current. Smith and Koles (Smith and Koles, 1970) displayed that an action potential propagating in models of myelinated axons could be blocked if the myelin sheath was removed or damaged. However, an action potential could propagate with a decrease in the action potential height at a node of Ranvier if the subsequent node of Ranvier could reinforce the action potential height due to the subsequent node of Ranvier's ionic currents. A slowed conduction velocity of the axon was observed in these models due to the demyelination.

This is similar to the mechanism proposed to cause conduction block due to high frequency stimulation. The sinusoidal waveform prevents conduction of the action potential by lowering the change in voltage seen at the node of Ranvier due to the propagating action potential. The transmission of this small change in voltage at the node

of Ranvier to the subsequent node is not reinforced sufficiently by ionic currents to maintain propagation of the action potential. Hence, the depolarization decays as it is passed from one node to the next instead of being reinforced. This is observed as a localized block of the transmission of the action potential.

Previous studies (Muller, 1969) on the effect of middle frequency currents at 5 kHz on the nerve have suggested a localized nerve block. These studies noted a sustained depolarization of the axon. These studies might have observed an averaged voltage across the membrane. From Figure 5.7, the average voltage predicted across the membrane due to the 10 kHz stimulation is increased, i.e. a sustained depolarization of the axon without the generation of an action potential is produced. These previous studies support the result of the computer modeling.

Woo and Campbell conducted experiments on the lumbar dorsal roots of a cat. Below is an excerpt of one of their reports. "The proximal of two electrode pairs on the tibial nerve conducted 20 Kc of varying voltage. The distal of the two electrode pairs delivered a supramaximal single shock which was sweep synchronized. Recording was from a fine filament of the last lumbar dorsal root. It was seen that the fiber responded with a single conducted impulse to each supramaximal shock. As the AC voltage was increased, rhythmic firing began which increase in frequency, then became irregular and of lower frequency and finally ceased. The fiber was not blocked, however, for the response to the single shock continued. As the voltage increased more, this response was blocked." (Woo and Campbell, 1964)

This description in 1964 by Woo and Campbell is directly reflected in Figures 5.7 and 5.8. These graphs predict that the AC voltage will first cause a continuous train of action potentials, noted above as a rhythmic firing of the axon. As the voltage increases, the frequency will increase until a threshold is reached. Beyond this threshold, increases in voltage will a decrease in the rhythmic firing of the axon, until the axon does not fire due to the AC currents. However, a localized block of the nerve is not exhibited at this point. A further increase in the voltage is required to produce a block.

More recently, Bowman noted a localized conduction block of cat and human axons. He primarily used 4 kHz pulses, a frequency in which the frequency current

relationship of the SE (cat) model is discontinuous, and recorded individual action potentials in a single axon and muscle force. Although his results were variable, his recordings of a localized conduction block add credence to the results of the computer models.

In light of these previous reports of a localized block, a new set of animal trials is suggested. The results of the animal trials could then be directly compared with the results of the computer models to provide a better description of the effect of high frequency currents on axons.

The localized block displayed by the computer models exhibits the characteristics desired in a block for peripheral nerve. It activates and deactivates rapidly. The block is biphasic in nature, hence the electrode deterioration caused by monophasic pulses is not a concern. The block can also exist without continuously generating action potentials. Early axonal death, reported by Agnew and McCreery, should not be a concern for the block.

5.6 Conclusions

The computer simulations demonstrate both the motor endplate depletion associated with high frequency stimulation of axons, and the localized electrical nerve blocking as modeled by Rattay and reported by Muller, Bowman, Tanner, and Woo and Campbell. The simulations predict an initial action potential and are generated at the onset of the block, followed by an immediate localized conduction block. The block can be turned off within 4 ms of the removal of the sinusoidal blocking current. The block is selective based on fiber diameter, and requires greater currents at higher frequencies. The local block prevents conduction through the area of the block through lowering the response of the node of Ranvier to a propagating action potential. At 10 kHz in the SRB model, a decrease change in membrane voltage due to a propagating action potential corresponds to a localized conduction block of the axon.

For the SRB model, the high frequency currents caused oscillations in the membrane voltage within the range of voltages used to generate the model.

Each model does not exhibit the same type of results and the extrapolation of the results from one species to another could not be supported. Animal trials are suggested to test the validity of the computer models.

The SRB Model

$$\dot{V} = [-I_{Na} + I_{Kf} + I_{Ks} + I_{leakage}]/c_m$$

$$I_{Na} = m^3 h P_{Na} \frac{EF^2}{RT} \frac{[Na]_o - [Na]_i \exp(EF/RT)}{1 - \exp(EF/RT)}$$

$$I_{Kf} = n^4 g_{Kf}(E - E_K)$$

$$I_{Ks} = s g_{Ks}(E - E_K)$$

$$I_{leakage} = g_{leakage}(E - E_{leakage})$$

The Schwarz-Eikhof Model

$$\dot{V} = [-I_{Na} - I_K - I_{leakage}]/c_m$$

$$I_{Na} = m^3 h P_{Na} \frac{EF^2}{RT} \frac{[Na]_o - [Na]_i \exp(EF/RT)}{1 - \exp(EF/RT)}$$

$$I_K = n^4 P_K \frac{EF^2}{RT} \frac{[K]_o - [K]_i \exp(EF/RT)}{1 - \exp(EF/RT)}$$

$$I_{leakage} = g_{leakage}(E - E_{leakage})$$

The Frankenhauser-Huxley Model

$$\dot{V} = [-I_{Na} - I_K - I_p - I_{leakage}]/c_m$$

$$I_{Na} = m^3 h P_{Na} \frac{EF^2}{RT} \frac{[Na]_o - [Na]_i \exp(EF/RT)}{1 - \exp(EF/RT)}$$

$$I_K = n^2 P_K \frac{EF^2}{RT} \frac{[K]_o - [K]_i \exp(EF/RT)}{1 - \exp(EF/RT)}$$

$$I_p = p^2 P_K \frac{EF^2}{RT} \frac{[Na]_o - [Na]_i \exp(EF/RT)}{1 - \exp(EF/RT)}$$

$$I_{leakage} = g_{leakage}(E - E_{leakage})$$

The CRRSS Model

$$\dot{V} = [-I_{Na} - I_{leakage}]/c_m$$

$$I_{Na} = g_{Na} m^2 h (E - E_{Na})$$

$$I_{leakage} = g_{leakage}(E - E_{leakage})$$

Rate Constants

$$\dot{m}, \dot{n}, \dot{h}, \dot{s}, \dot{p} = -(\alpha_{m,n,h,s,p} + \beta_{m,n,h,s,p}) m, n, h, s, p + \alpha_{m,n,h,s,p}$$

$$\alpha_m, \alpha_n, \alpha_s, \alpha_p = \frac{A(E - B)}{1 - \exp\left(\frac{B - E}{C}\right)}$$

$$\alpha_h, \beta_m, \beta_n, \beta_s, \beta_p = \frac{A(B - E)}{1 - \exp\left(\frac{B - E}{C}\right)}$$

$$\beta_h = \frac{A}{1 + \exp\left(\frac{B - E}{C}\right)}$$

SRB	CONSTANTS		
	A (ms^{-1})	B (mV)	C (mV)
α_m	1.8555	66.5609	10.2729
β_m	0.086037	62.3462	9.1631
α_n	0.033582	-26.3109	11.0453
β_n	2.2994	56.1701	13.3591
α_h	0.007976	-8.2406	1.1000
β_h	0.014198	9.0365	10.5025
α_s	0.00122	72.4608	23.5511
β_s	0.0007389	4.9226	21.7869

SE	CONSTANTS		
	A (ms^{-1})	B (mV)	C (mV)
α_m	1.87	25.41	6.06
β_m	3.97	21	9.41
α_n	0.13	35	10
β_n	0.32	10	10
α_h	-0.55	-27.74	9.06
β_h	22.6	56	12.5

FH	CONSTANTS		
	A (ms^{-1})	B (mV)	C (mV)
α_m	0.36	22	3
β_m	0.4	13	20
α_n	0.02	35	10
β_n	0.05	10	10
α_h	-0.1	-10	6
β_h	4.5	45	10
α_p	0.006	40	10
β_p	0.09	-25	20

	FH Model	SE Model	SRB Model	CRRSS Model
P_{Na}	0.008 cm/s	1.64×10^{-9} cm^3/s	3.52×10^{-5} cm^3/s	
P_K	0.0012 cm/s	0.067×10^{-9} cm^3/s		
P_S	0.00054 cm/s			
g_{Na}				1445
gks			30 nS	
gkf			15 nS	
g_l	30.3 kΩ/cm^2	43 nS	14 nS	128
V_l	0.026 mV	0 mV	0 mV	-0.01 mV
V_{Na}				115 mV
V_K			-84 mV	
$[Na]_o$	114.5 mM	154 mM	154 mM	
$[Na]_i$	13.7 mM	8.71 mM	35 mM	
$[K]_o$	2.5 mM	2.9 mM	5.6 mM	
$[K]_i$	120 mM	155 mM	155 mM	
$Q_{10}\,\alpha_m$	1.8	2.2	2.2	3
$Q_{10}\,\beta_m$	1.7	2.2	2.2	3
$Q_{10}\,\alpha_h$	2.8	2.9	2.9	3
$Q_{10}\,\beta_h$	2.9	2.9	2.9	3
$Q_{10}\,\alpha_n$	3.2	3.0	3.0	3
$Q_{10}\,\beta_n$	2.8	3.0	3.0	
$Q_{10}\,\alpha_s$			3.0	
$Q_{10}\,\beta_s$			3.0	
T	20 °C	37 °C	37 °C	37 °C
rhoi	0.1	0.045	0.07	
L	1.5 μm	2	1.5	
c_m	2 μF/cm^2	1.4 pF	1.4	2.5 μF/cm^2

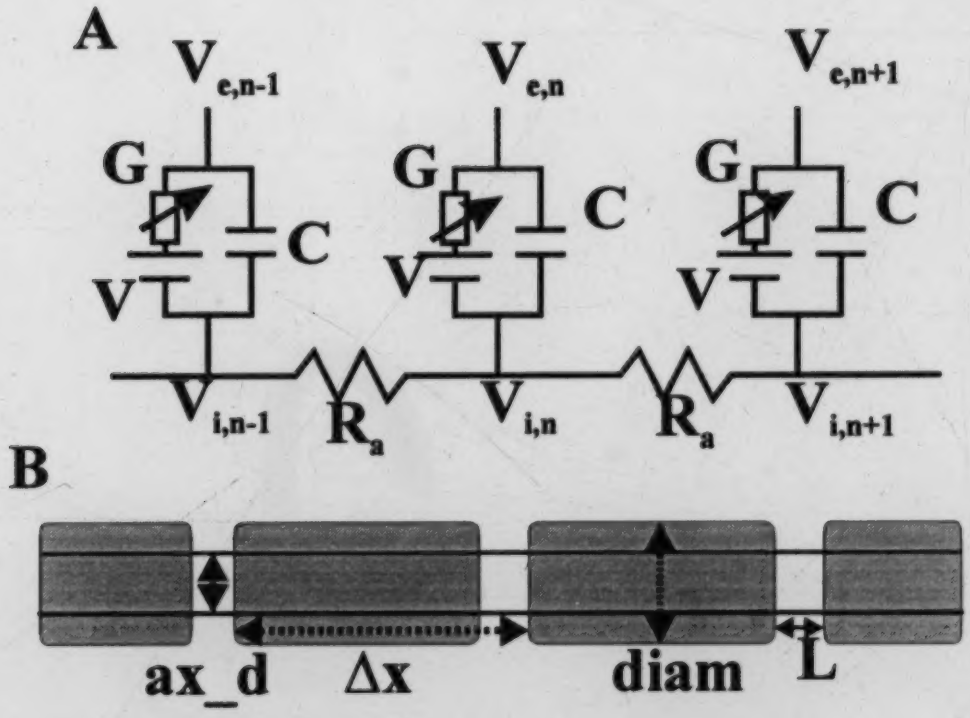

Figure 5.1 Schematic for spatially extending nonlinear nodal kinetic models.

(A) is a circuit diagram for the conduction in an axon (McNeal, 1976) and currents at the node of Ranvier. From this model, equation (1) is derived. Voltage sensitive gates, (G) display a variable conductance based on the voltage across the membrane. The voltage across the membrane is seen due to the external voltage (V_e), the internal voltage (V_i), and a voltage due to the difference in ion concentration across the membrane (V). R_a is the intraaxonal resistance, and C is the capacitance of the membrane at a node of Ranvier. Only a single ionic gate and potential is shown to simplify the diagram. In the SE model, 3 voltage sensitive gates and ionic batteries, (Na^+, K^+, and leakage) are used.

(B) is a diagram displaying the dimensions for the axon used in equation (1)

diam is the diameter of the axon
ax_d is the diameter of the node of Ranvier
L is the longitudinal length of the node of Ranvier
dx is the distance between node of Ranvier

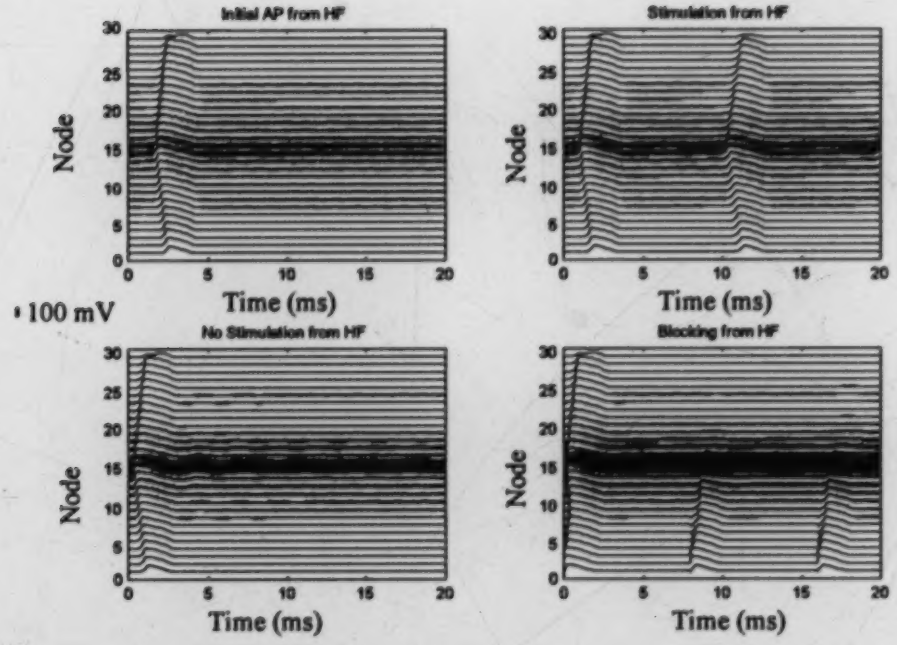

Figure 5.2: The effects of high frequency currents on the spatially extended myelinated Schwartz-Reid-Bostock model. The voltage graphs for 30 nodes of Ranvier are displayed in each plot. The voltage trace for each node is separated by 100 mV, as indicated by the legend in the middle left side of the figure.
(Upper Left) – An single action potential is generated by stimulating node with a sinusoidal current, I_{peak} = 0.85 mA, from a monopolar electrode, directly above node 15.
(Upper Right) – Repetitive action potentials are generated by stimulating node with a sinusoidal current, I_{peak} = 0.91 mA, from a monopolar electrode, directly above node 15. The frequency of the action potentials generated in 120 Hz.
(Lower Left) – A single action potential is generated by stimulating node with a sinusoidal current, I_{peak} = 1.25 mA, from a monopolar electrode, directly above node 15.
(Lower Right) – A series of action potentials are produced at node 5. An initial action potential is generated by stimulating node with a sinusoidal current, I_{peak} = 1.75 mA, from a monopolar electrode, directly above node 15. The action potentials generated at node 5 do not propagate through node 15.

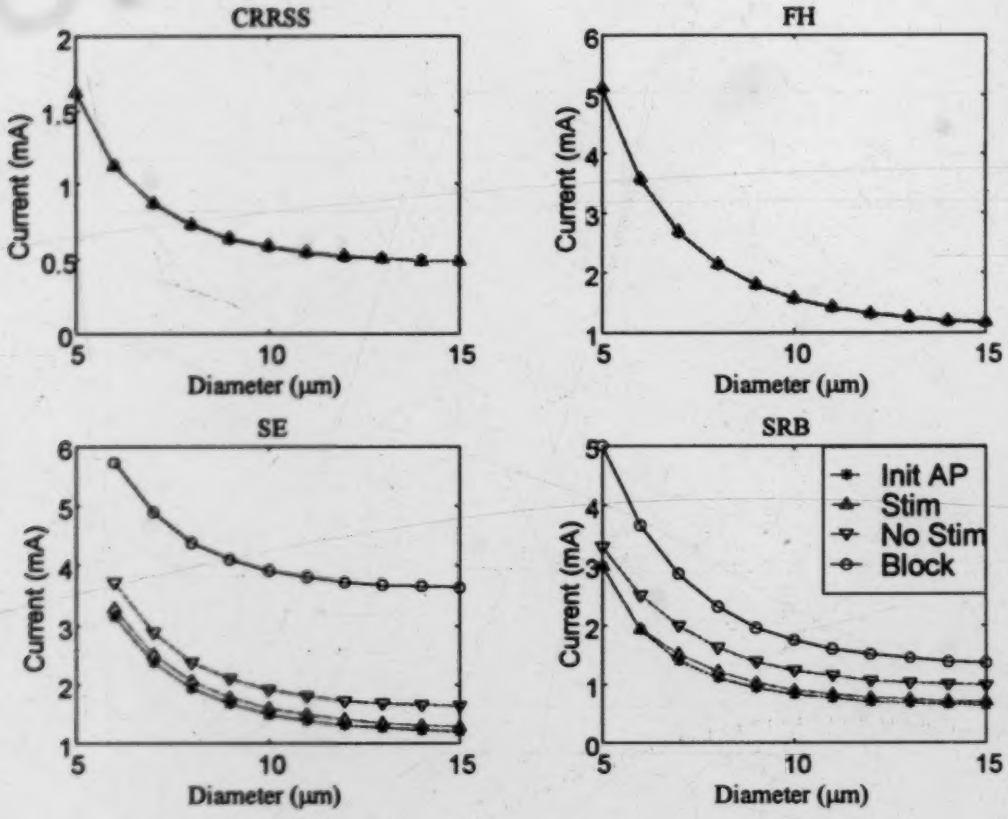

Figure 5.3 – Diameter – current relationship for the CRRSS, FH, SE, and SRB models. A legend for each of the graphs is seen in the lower right. The lowest current value to produce and initial action potential, repetitive stimulation, cessation of repetitive stimulation, and block is shown dashed. 10 kHz frequency was used in each simulation.
(Upper left) – CRRSS model – The model produces an initial action potential and repetitive stimulation. Cessation of stimulation and blocking are not produced.
(Upper right) – FH model – The model produces an initial action potential and repetitive stimulation. Cessation of stimulation and blocking are not produced.
(Lower left) – SE model – An initial action potential, repetitive stimulation, cessation of stimulation, and blocking are predicted by the model.
(Lower right) – SRB model – An initial action potential, repetitive stimulation, cessation of stimulation, and blocking are predicted by the model.

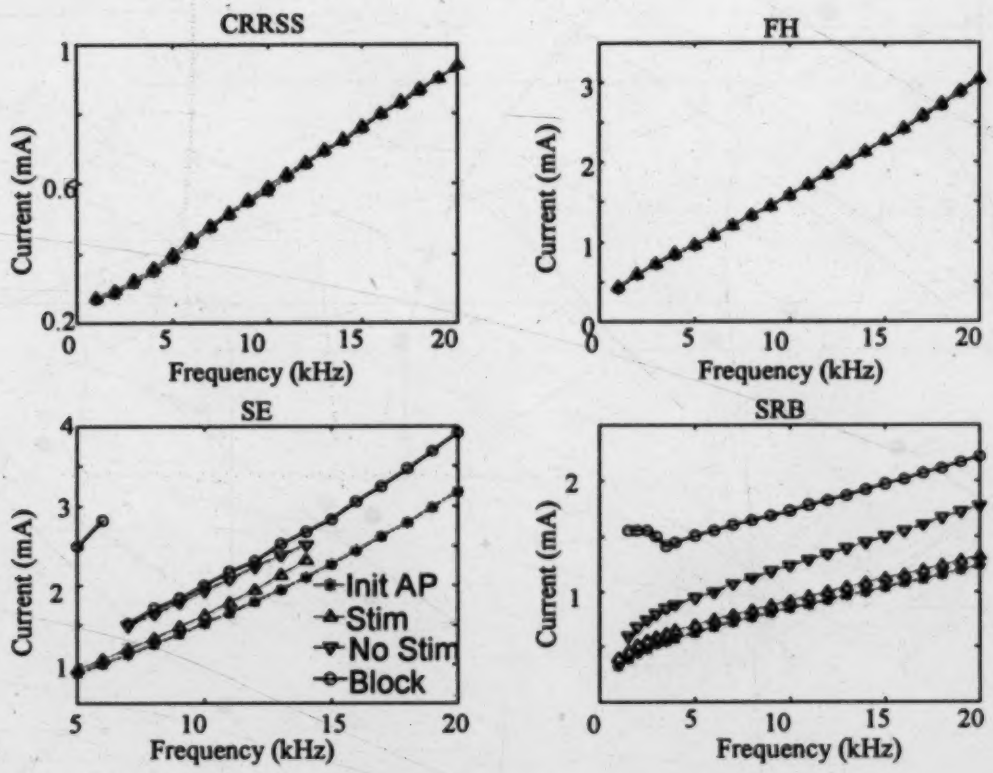

Figure 5.4: Frequency – current relationship for the CRRSS, FH, SE, and SRB models. A legend for each of the graphs is seen in the lower left. The lowest current value to produce and initial action potential, repetitive stimulation, cessation of repetitive stimulation, and block is shown dashed. 10 μm diameter fiber was used in each simulation.
(Upper left) – CRRSS model – The model produces an initial action potential and repetitive stimulation. Cessation of stimulation and blocking are not produced.
(Upper right) – FH model – The model produces an initial action potential and repetitive stimulation. Cessation of stimulation and blocking are not produced.
(Lower left) – SE model – An initial action potential, repetitive stimulation, cessation of stimulation, and blocking are predicted by the model. A break occurs in the blocking graph between 6 and 7 kHz. Above 14 kHz, sinusoidal currents do not cause repetitive stimulation.
(Lower right) – SRB model – An initial action potential, repetitive stimulation, cessation of stimulation, and blocking are predicted by the model. A cusp is seen in the blocking curve at 4 kHz.

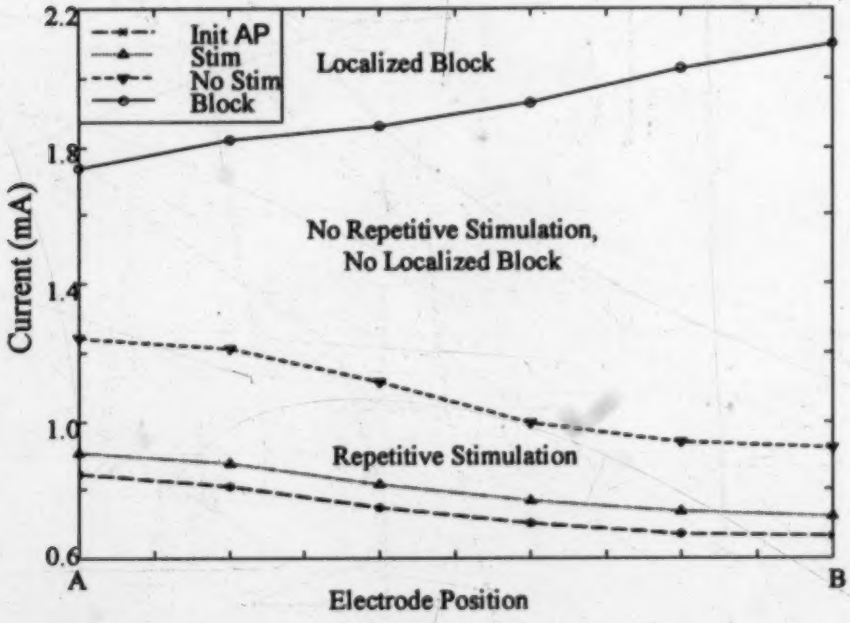

Figure 5.5: The influence of electrode position one effects of high frequency current. Electrode position. (A) has the electrode positioned directly between two nodes of Ranvier. (B) has the electrode positioned directly over one node of Ranvier. The threshold current levels needed to produce an initial action potential (dashed line with starred points), repetitive firing (dotted line with triangle points), cessation of action potential firings (dashed line with inverted triangle points), and localized blocking (solid line with circle points) are shown. As the electrode moves further from being directly over a node of Ranvier, the current to block the axon decreases whereas the current needed for repetitive firing and an initial action potential increases.

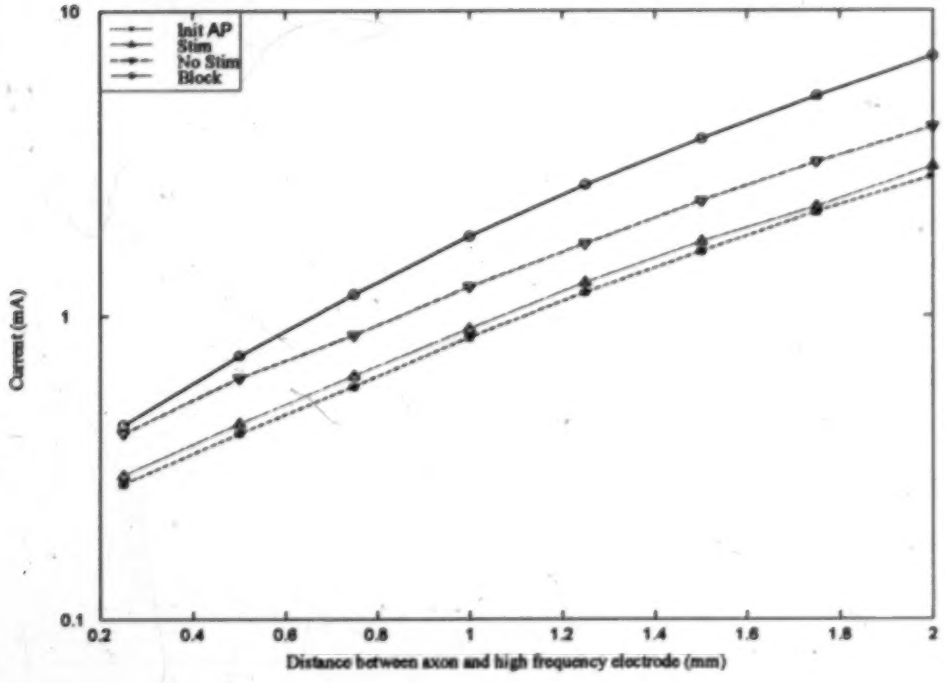

Figure 5.6 – Relationship of current to distance between electrode and axon. The threshold current levels needed to produce an initial action potential (dashed line with asterisk points), repetitive firing (dotted line with triangle points), cessation of action potential firings (dashed line with inverted triangle points), and localized blocking (solid line with circle points) are shown. The level of current needed to produce each effect increases exponentially with increasing distance between the axon and the electrode.

Figure 5.7 –

(Top) Mean per cycle voltage of the node beneath the high frequency (10 kHz) electrode. A current level of 0.85 mA causes only a single action potential. Peak current levels of 1.0, 1.1, 1.2 mA cause repetitive action potentials to firing. The rate that the action potentials fire increases with an increase in current. At a current level of 1.3 mA, the repetitive firing of action potentials ceases.

(Bottom) – h gate (Na^+ inactivation gate) of the node beneath the high frequency electrode. The h gate recovers to a probability of 0.6 after the action potential when stimulated by 0.85 mA. As the peak current increases, indicated by levels of 1.0, 1.1., and 1.2 mA, the h gate recovers to a diminishing levels. At 1.3 mA, the h gate does not open sufficiently for an action potential to start. The h gate remains closed, and static indicating action potentials will no longer fire.

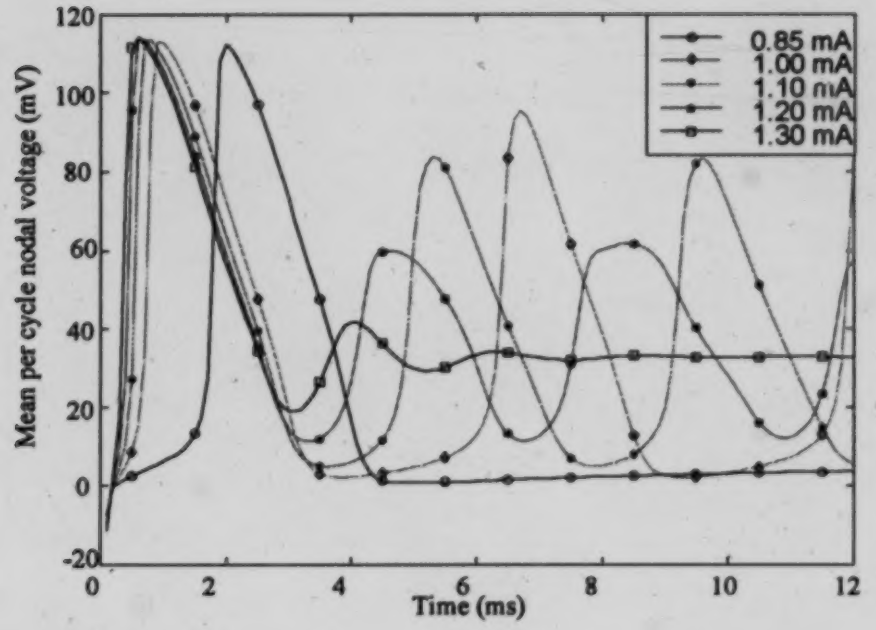
Mean per cycle nodal voltage (mV)
Time (ms)
0.85 mA
1.00 mA
1.10 mA
1.20 mA
1.30 mA

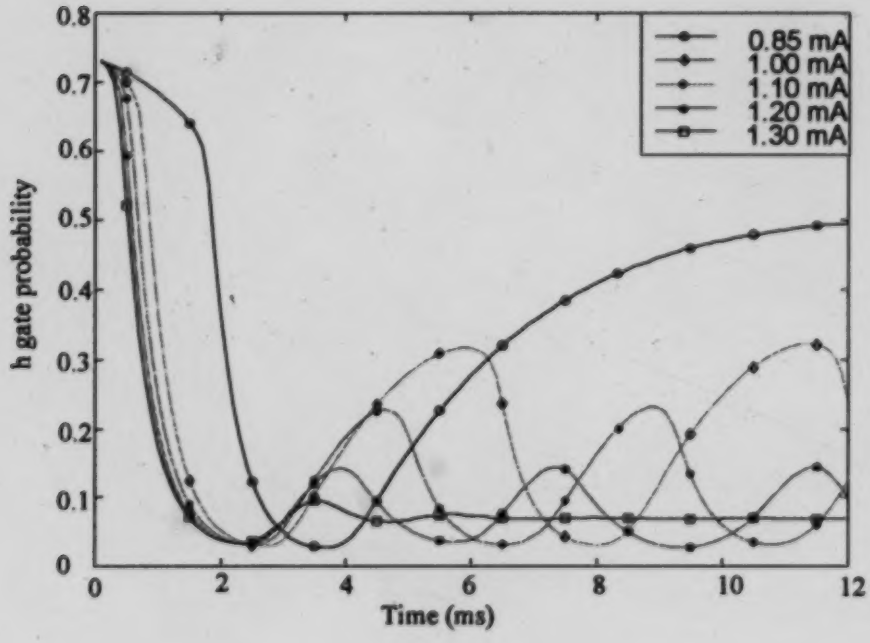
h gate probability
Time (ms)
0.85 mA
1.00 mA
1.10 mA
1.20 mA
1.30 mA

Figure 5.8

(Top) Mean per cycle voltage of the node beneath the high frequency (10 kHz) electrode. The initial action potential caused by the stimulation is shown (time 1 ms). As the high frequency current increases, the mean membrane voltage increases, as shown for high frequency current levels 1.7, 1.75, 1.8, 1.9, and 2.0 mA. Due to this fact, the change in membrane voltage due to a propagating action potential, shown at time 8.5 ms, has a decreasing effect on the membrane voltage.

(Bottom) Mean per cycle voltage of the node after the blocking electrode. The initial action potential caused by the stimulation is shown (time 1 ms). As the high frequency current increases, the mean membrane voltage increases, as shown for high frequency current levels 1.7, 1.75, 1.8, 1.9, and 2.0 mA. However, these mean membrane voltages are high as the ones in 8(a). The propagating action potential (time 8.5 ms) is causes a change in the membrane voltage. For blocking currents of 1.7 and 1.75 mA, the change in membrane voltage is greater is of greater height and duration than the ones seen at that current level in 8(top), indicating the is reinforced by axonal currents and the action potential will continue to propagate. For blocking currents of 1.8, 1.9 and 2.0 mA, the change in membrane voltage is not reinforced by axonal currents, indicating the action potential propagation is blocked.

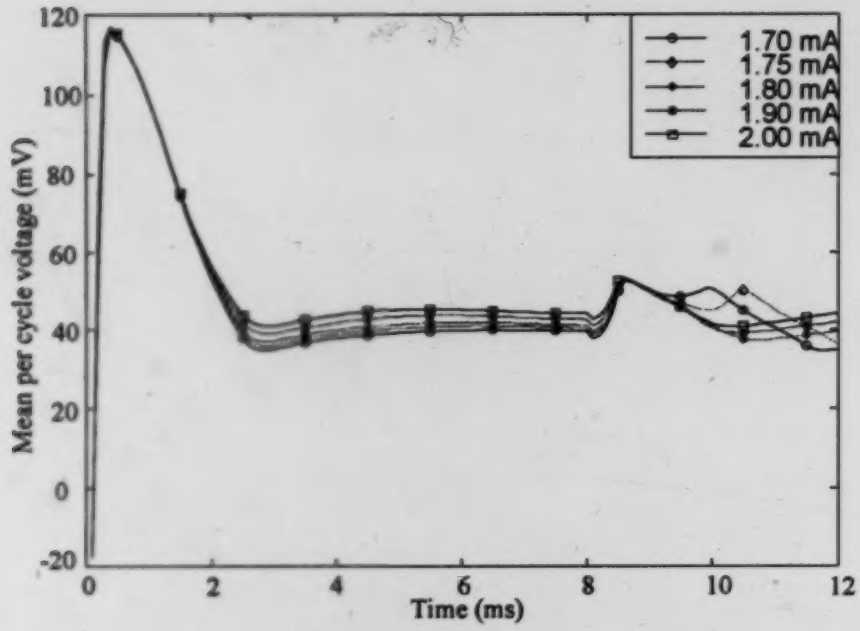
1.70 mA
1.75 mA
1.80 mA
1.90 mA
2.00 mA
Mean per cycle voltage (mV)
Time (ms)
120
100
80
60
40
20
0
-20
0
2
4
6
8
10
12

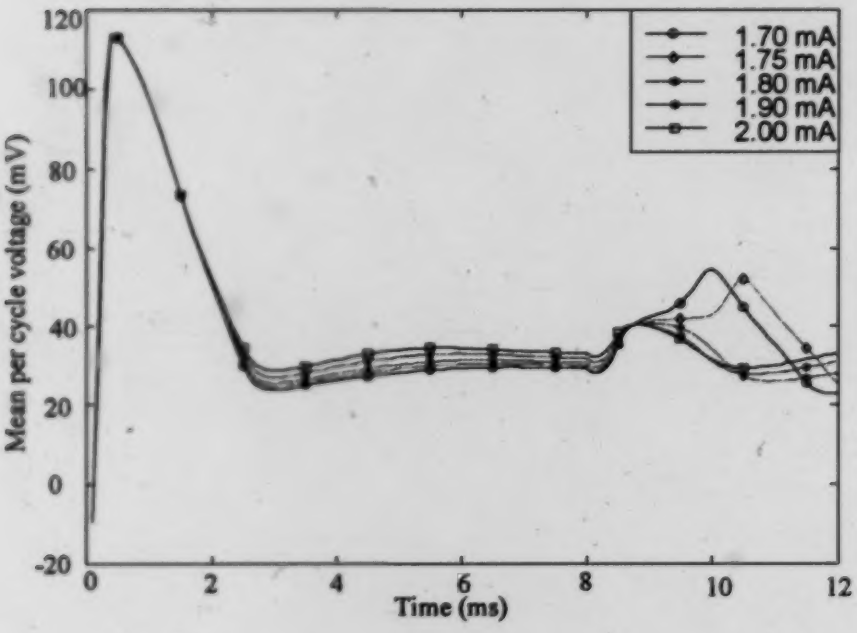
1.70 mA
1.75 mA
1.80 mA
1.90 mA
2.00 mA
Mean per cycle voltage (mV)
Time (ms)
120
100
80
60
40
20
0
-20
0
2
4
6
8
10
12

	Published limits	Initial AP	Repetitive Stimulation	Cease Rep. Stimulation	Blocking
SRB	-145→115 mV	-120 → 47 mV	-122 → 44 mV	-117 → 20 mV	-142 → 58 mV
SE	-128→ 47mV	-131→ 16 mV	-132→ 18 mV	-142 → 18 mV	-131 → 42 mV
CRRSS	Not publ.	-56 → 5 mV	-56 → 5 mV	Not Present	Not Present
FH	Not publ.	-45→ 34 mV	-45 → 35 mV	Not Present	Not Present

Table 5.1 : Integrity of models during excitation and blocking due to high frequency currents. These voltage excursions are for the SRB, SE, CRRSS, and FH models at a fiber diameter of 10 μm. The electrode was positioned 1 mm from the nerve directly between two nodes of Ranvier. These excursions are compared to the published limits of the model, seen in column 2.

5.7 Bibliography

Altman, K.W., Plonsey R., (1986) "A two-part model for determining the electromagnetic and physiologic behavior of cuff electrode nerve stimulators", IEEE Trans. BME, 33: 285-293

Chicoine, M.R., Park, T.S., and Kaufman, B.A., (1997) "Selective dorsal rhizotomy and rates of orthopedic surgery in children with spastic cerebral palsy", J. Neurosurgery, 86: 34-39

Bowman, B.R. (1981), "Electrical Block of Peripheral Motor Activity", Ph.D. Thesis, Edvard Kardelh University of Ljubljana

Chiu, S.Y., Ritchie, J.M., Rogart, R.B., and Stagg, D., (1979) "A quantitative description of the membrane currents in rabbit myelinated nerve", J. Physiol., 292: 146-166

Fang, Z.P., and Mortimer, T., (1991) "Selective Activation of Small Motor Axons by Quasitrapezoidal Current Pulses," IEEE Trans. BME, 38: 168-174

Frankenhaeuser, B., and Huxley, A.F., (1964) "The action potential in the myelinated nerve fiber of Xenopus Laevis as computed on the basis of voltage clamp data," J. Physiol., 109: 302-315, 1964

Goodall, E.V., deBreij, J.F., Holsheimer, J., (1996) "Position-selective activation of peripheral nerve fibers with a cuff electrode", IEEE Trans. BME 43(8):851-6

Hodgkin, A.L., Huxley, A.F., (1952) "A quantitative description of membrane current and its application to conduction and excitation in nerve," J. Physiol., 117: 500-544

McAllister, R.E., Noble., D., and Tsien, R.W., (1975) "Reconstruction of the electrical activity of cardiac Purkinje fibers", J. Physiol. vol. 251: 1-59

McCreery, D.B., Agnew, W.F., Yuen, T.G.H., and Bullara, L.A., (1995) "Relationship between stimulus amplitude, stimulus frequency and neural damage during electrical stimulation of sciatic nerve of cat," Med. & Biol. Eng. & Comput., vol. 33, pp. 426-429, May, 1995

McNeal, D.R., (1976) "Analysis of a model for the excitation of myelinated nerve", IEEE Trans. BME, vol. 23: 329-337

Muller, A., (1969) "Studies on electroanesthesia with middle frequency current", Proc. 2nd International Symoposuim on Electrotherapeutic Sleep and Electroanethesia, Grax, Aust., pp. 291-295,

Peckham, P.H., and Creasey, G.H., (1992) "Neural prostheses: clinical applications of functional electrical stimulation in spinal cord injury", Paraplegia, 30: 96-101

Perry, J., (1993) "Determinants of muscle function in the spastic lower extremity," Clinical Orthopaedics and Related Research, 288: 10-26

Rattay, F., (1990) Electrical Nerve Stimulation. Wein, Austria, Springer-Verlag, Ch. 5-7 pp. 73-139

Rijkhoff, N.M.J., Wijkstra, H., van Kerrebroeck, P.E.V., and Dubruyne, F.M.J., (1997) "Urinary Bladder Control by Electrical Stimulation: Review of Electrical Stimulation Techniques in Spinal Cord Injury," Neurology and Urodynamics, 16: 39-53

Rubinstein, J.T., (1991) "Analytical theory for extracellular electrical stimulation of nerve with focalelectrodes. II Passive myelinated axon", Biophysics Journal, 60:538-555

Schwarz, J.R., and Eikhof, G., (1987) "Na^+ currents and action potentials in rat myelinated nerve fibers at 20 and 37°C," Pflugers Arch., vol. 409: 569-577

Schwarz, J.R., Reid, G., Bostock, H., (1995) "Action potentials and membrane currents in the human node of Ranvier", Pfulgers Arch., vol. 430: 283-292

Sheriff, M.K., Shah, P.J., Fowler, C., Mundy, A.R., and Craggs, M.D., (1996) "Neuromodulation of detrusor hyper-reflexia by functional magnetic stimulation of the sacral roots", Brit. J. Urology., 78: 39-46

Smith R.S., and Koles Z.J., (1970) "Myelinated nerve fibers: computed effect of myelin thickness on conduction velocity" American Journal of Physiology. 219(5):1256-8

Solomonow, M., (1984) "External control of the neuromuscular system", IEEE Trans. BME, 31: 572-763

Struijk, J.J., Holsheimer, J., van Veen, B.K., and Boom, H.B.K., (1991) "Epidural spinal cord stimulation: Calculation of field potentials with special reference to dorsal column nerve fibers", IEEE Trans. BME, 38(1):104-110

Sweeney, J.D., Mortimer, J.T., and Durand, D., (1987) "Modeling of mammalian myelinated nerve for functional neuromuscular electrostimulation", Proc. 9th IEEE EMBS, Boston, MA, pp. 1577-1578

Sweeney, J.D., and Mortimer, T., (1986) "An Asymmetric two-electrode cuff for generation of unidirectionally propagated action potentials," IEEE Trans. BME, 33: 541-549

Tai, C., and Jaing, D., (1994) "Selective stimulation of smaller fibers in a nerve trunk and single cathode by rectangular current pulses", IEEE Trans. BME, 41: 286-291

Tanner, J., (1962) "Reversible blocking of nerve conduction by alternating current excitation," Nature, 195: 712-713

Veltink, P.H., Van Alste, J.A., and Boom, H.B.K., (1988) "Simulation of intrafascicular and extraneural nerve stimulation", IEEE Trans. BME, 35: 69-75

Walter, J.S., Wheeler, J.S., Robinson, C.J., and Wurster, R.D, (1993) "Inhibiting the Hyper-reflexic Bladder With Electrical Stimulation in a Spinal Animal Model," Neurology and Urodynamics, 12: 241-253

Walter, J.S., Riedy, L., Zaszczurynski, P., Cogan, S.F., and LiuY.-P., (1996) "Coating of Stainless Steel Electrodes with Iridium for Applications in Functional Electrical Stimulation," pg. 273-275 RESNA '96

Wedenski, N., (1885) "Wie rasch ermude der nerc", Zbl. Med Wis 22:65-8

Woo, N., and Campbell, B., (1964) "Asynchronous firing and block of peripheral nerve conduction by 20 kc alternating current", Bull. L.A. Neurol. Soc., 29: 87-94

6 Electrical Nerve Blocking : Practical Considerations

6.1 Introduction

Neural prostheses are presently limited in their application, as selective activation of the axons and blocking of axon conduction to arrest spasticity are not possible. Most 'blocking' techniques actually elicit repetitive volleys of action potentials (Brindley and Craggs, 1978, Sweeney and Mortimer, 1986, Solomonow, 1984, Bowman and McNeal, 1986, Tai and Jaing, 1994, Woo and Campbell, 1964). McCreery et. al. (McCreery et. al, 1995) have shown that repetitive firing of the nerves at frequencies as low as 50 Hz can cause early axon death.

Williamson and Andrews (Williamson and Andrews, 1999) proposed a method of localized electrical nerve blocking which was demonstrated in computer models. Its advantage over the previous methods is that it is local to an area of the nerve. Hence this technique should not cause nerve damage as described by McCreery. The currents used in the model do not have a zero frequency component. Hence, the integrity of the electrodes is not a concern in the same manner as in anodal blocking (Rijkoff et. al., 1997, 1998, Brindley and Craggs, 1980, Robblee and Rose, 1990). The models also suggested that the block could be turned on and off rapidly.

High frequency currents used by Williamson and Andrews had been thought to cause continuous generation of action potentials and a block of muscular contraction first described by Wedenski (Wedenski, 1885). This is supported by the work of Solomonow, Woo and Campbell, Bowman, and Tai and Jaing. Each of these groups used monophasic pulses to generate a block of muscular contraction. Bowman (Bowman, 1981) also described trials that suggested a localized block of axon transmission.

Muller (Muller, 1969) reported a block using a 5 kHz signal. He thought the block was due to a decrease in membrane potential that could be produced by the high frequency current without producing full depolarization. The models of Williamson and Andrews suggested that the high frequency currents could cause this effect. Woo and Campbell (Woo and Campbell, 1964) reported that in single axon recordings high frequency currents would cause repetitive action potentials at a frequency of 300 Hz. As the level of current

increased, the frequency of stimulation would decrease until action potentials were no longer produced by the high frequency current. This result was exhibited in the models of Williamson and Andrews.

The variation of results from trial to trial and experimenter to experimenter can suggest that the block is unstable and would be difficult to repeat. On this basis, questions can arise about the possible implementation of the high frequency block described by computer models.

The models of the nodal kinetics of axons are produced by averaging multiple recordings of a parameter over a number of axons. Chui et. al. (Chiu et. al, 1979) displayed varied measurements made on multiple axons of the rabbit. Schwarz et. al. (Schwarz et. al, 1995) constructed their model by using four nerve samples, but did not include or mention a variation in parameters between axons. It is reasonable to suspect variances in the parameters. Frijn et. al. (Frijn et. al, 1994) demonstrated that the adjustment of the nodal kinetics can be used to provide better descriptions of repetitive firing of the axons. McIntyre and Grill (McIntyre and Grill, 1998) altered the parameters of the CRRSS model to enable anodal break. Rattay has adapted the Hodgkin-Huxley and Frankenhaeuser-Huxley models for cochlear conduction (Rattay, 1997, Motz and Rattay, 1986). The Hodgkin and Huxley model has also been altered to represent bursting (Lee et. al, 1983), to include ionic pumps (Scriven, 1981), and for the Purkinje fibers of the heart (McAllister et. al, 1975). This implies that the models are not the only representations of neuron conduction; different types of axons have the same structure with a slight difference in parameters. The model for an electrical nerve blocking method would have greater credence if the block could be achieved over a range of parameters of the model. A test that alters the parameters of the model and maintains a demonstration of the nerve block would support the possibility of a physically realizable nerve block.

The localized block by high frequency oscillating currents, as demonstrated in the models, uses a pure sinusoidal current. During a physical trial of the block, it is expected that a pure sinusoidal current would not be possible to generate. A level of systematic and random noise would contaminate the blocking waveform. Computer simulations can be used to check if the block is resistant to this type of noise.

Additionally, a localized block has not been explicitly demonstrated in a whole nerve preparation that notes that the block is local. Both Bowman and Woo and Campbell, when using the block, record action potentials from a single axon. Bowman's experimental results varied from trial to trial, and he could not propose a technique for generating a localized block that could be consistently repeated. A preliminary test could confirm the presence of this type of block and suggest its feasibility in a whole nerve.

6.2 Methods

6.2.1 Modeling

The modeling technique has been described in the companion paper. The SRB (Schwarz et. al, 1995) model of nodal kinetics is used. A modified McNeal (McNeal, 1976) model of saltatory conduction was used that included the resistance and capacitance of the myelin sheath. All models were simulated in MATLAB v5.2.1 on a P400 computer. The standard nerve modeled in each exercise was a spatially extended SRB model using a 10 μm axon of 25 nodes of Ranvier and 26 passive myelin sheaths stimulated by an oscillating current delivered by a monopolar source at a distance of 1 mm directly over node of Ranvier 15. A block was noted when an action potential starting at node of Ranvier 3 of the axon would not elicit a depolarization of node of Ranvier 23 of the axon of greater than 50 mV. The temperature of the simulations was 37 °C.

6.2.2 Parameter Changes

Thirty six of the thirty eight parameters of the SRB model were varied. The two parameters that were not varied were leakage voltage, V_L and the K^+ equilibrium potential V_k. Each parameter was varied independently by +/- 25, 10, 5, and 1% of its published value. The height of the action potential was recorded. This served as a reference to which the change in current required to produce a block was correlated.

The threshold for the blocking current was calculated for each variation in the parameter. First, it was determined if an action potential block occurred due to a stimulating current of 1.74 mA, the current required to produce a block in the axon without a parameter change. If a block was achieved, the current threshold was dropped

in steps of 25 μA until the block no longer existed or the adjustment reached 500 μA. If a block was not achieved, the current threshold was increased by steps of 25 μA until a block was achieved or the adjustment reached 500 μA. Once an adjustment in blocking current exceeded 500 μA, further adjustment of the current level did not occur. If the model did not predict a localized conduction block within 500 μA, it was recorded that a localized conduction block did not occur. A confusion matrix was constructed relating the percent change in the action potential height to the percent change in the current needed to generate a nerve block, and is displayed in Table 6.1.

6.2.3 Noise on the Input of the System

The threshold for stimulation was calculated for the SRB model using stimulation levels contaminated with both an offset bias and random noise. The offset bias ranged in +/- 0.20 mA. The random noise ranged in standard distribution from 0 mA to 0.20 mA. The blocking threshold for each of these simulations was calculated, and is displayed in Table 6.2.

6.2.4 Animal Model

A 250 g female rat was anesthetized with an intraperitoneal injection of 45 mg/kg pentobarbital sodium (Somnotol). Pentobarbital sodium (45 mg/kg ip) was administered for general anesthesia in a 1:5 dilution. The trachea was cannulated for mechanical ventilation when necessary.

The sciatic nerve was exposed. One bipolar cuff electrode, constructed of Silastic tubing (inside diameter 1.98 mm outside diameter 3.18 mm, length 6 mm, contacts of 15 strand Cooner wire) was placed around the sciatic nerve. A symmetrical tripolar cuff electrode, length 6 mm with electrode spacing of 2 mm, was placed around the common peroneal nerve. Both cuff electrodes were split, prior to placing around the nerve, and then sutured closed using 2-0 silk suture. A third, intramuscular electrode, made by bared ends of Teflon coated fine silver wires (75 μm), was inserted near the motor point of the tibialis anterior. The ipsilateral knee was held in place using a stereotaxic frame. All ipsilateral muscle groups, other than the tibialis anterior, were denervated. The tendon

from the tibialis anterior was cut and attached to a strain gauge. Force was amplified and viewed on a Tektronix dual time base storage oscilloscope (model 5441), and monitored continuously on a Gould 1200S pen recorder. The force of selected muscle twitches was also digitized and stored on disk by and LSI-11 computer (Digital Equipment). The force from the muscle was recorded under different stimulus conditions. The body of the rat was warmed using radiant heat above the animal and a heating pad beneath the animal.

Action potentials and muscle firings were produced using 50 μs synchronized pulses from the bipolar and intramuscular electrodes at a frequency of 0.25 Hz. The muscle twitch produced by the intramuscular electrode preceded the muscle twitch from the cuff electrode by 1 second.

The two outer contacts of the tripolar cuff electrode were connected to the ground of a sinusoidal stimulator. The center contact of the cuff was connected to a variable frequency, variable amplitude sinusoidal waveform generator. The height of the first harmonic of the waveform, the largest frequency domain component of noise, was attenuated by 38 dB, measured on a Hewlett Packard digital storage oscilloscope, Model 54600A.

The synchronized action potentials were initiated. After two or three recordings of these action potentials, the blocking waveform was turned on to a predetermined voltage and frequency. The initiation of the sinusoidal waveform would typically cause a muscular twitch of variable duration, and a partial block of the muscle twitch induced by the bipolar cuff electrode. After the force recordings regained a regular pattern, the sinusoidal waveform was turned off. The force generated by the twitch after the block was turned off was also recorded.

6.3 Results

6.3.1 Parameter Changes

Thirty six parameters were varied in the SRB model in the range of –25 to 25%. Current steps of 25 μA, 1.14 % of the blocking threshold, were taken to determine if a block would still exist. Table 6.1 displays the results in a confusion matrix format.

For the 288 possible simulations, 154 had a less than 1% change in the action potential height. Thirty eight of the simulations did not allow for an action potential.

For the 249 simulations that allowed for an action potential to propagate, 22 of the simulations did not allow for the blocking to exist within a range of 500 μA. A majority (85%, 212/249) allowed for blocking to occur within 5% of the level required under the usual parameter conditions.

6.3.2 Noise on the Input of the System

Figure 6.1 displays the results of the tests of adding noise to the input of the stimulation. This graph presents a single result for each level of random and systematic current calculation. Multiple realizations for blocking current on the level of random noise, but different seed for the random number generator, were not conducted. Figure 6.2 displays the trends of the minimum blocking current with respect to only systematic or random noise. In the top graphic, the blocking current is noted for different levels of bias current. This was computed by averaging the 6 trials of random noise levels shown in Figure 6.1. In the bottom graphic, the blocking current required for a single level of random noise is displayed. This was computed by averaging the 11 trials of bias current levels shown in Figure 6.1.

A decrease in the level of current was required to produce a block for an anodally biased current. Similarly, a cathodally biased current caused an increase in the blocking current required. Using a paired T-test, a significant difference was not observed between the different levels for random noise levels up to 0.2 mA ($p < 0.01$).

6.3.3 Experimental Results

Figure 6.3 displays the two typical recordings of force seen in a trial. In Figure 6.3a, six muscle twitches, three from each of the bipolar and intramuscular electrodes, were recorded. A single muscle twitch was produced at the initiation of the sinusoidal waveform of 3.2 mA (rms) at 13 kHz applied to the tripolar cuff electrode. Subsequently, four twitches produced by the intramuscular electrode are produced. The sinusoidal waveform was turned off in the one second between the pulse applied to the intramuscular electrode and the bipolar cuff electrode. A single muscle twitch was produced when this

sinusoidal waveform was turned off. The muscle twitch caused by the bipolar cuff electrode was observed. Three paired twitches of the bipolar cuff electrode and the intramuscular electrode were recorded.

The blocking waveform completely blocked the action potentials produced by the bipolar cuff electrode. After the blocking waveform ceased, the muscle twitch produced by the bipolar cuff electrode was equivalent to muscle twitch force produced by the bipolar cuff prior to the blocking waveform. The force produced by the intramuscular electrode did not vary, irrespective to the application of the blocking waveform.

In Figure 6.3b, four muscle twitches, two from each of the bipolar and intramuscular electrodes, were recorded. A prolonged muscular contraction was produced at the initiation of the sinusoidal waveform of 2.0 mA (rms) at 8 kHz applied to the tripolar cuff electrode. Subsequently, nine twitches due to stimulation at the intramuscular electrode were produced. A partial block of the nine twitches produced by the bipolar cuff electrode was produced. The sinusoidal waveform was turned off, producing a single twitch. Three paired muscle twitches caused by the bipolar cuff electrode and the intramuscular electrode were observed.

The high frequency currents partially blocked the action potentials produced by the bipolar cuff electrode. After the high frequency currents ceased, the muscle twitch produced by the bipolar cuff electrode was equivalent to muscle twitch force produced by the bipolar cuff prior to the blocking waveform. The force produced by the intramuscular electrode was increased if it occurred within the duration of the initial muscular contraction produced by the onset of the high frequency currents. After this transient, the force produced by the intramuscular electrode did not vary during the rest of the application of the high frequency currents, or after the high frequency currents were removed.

These trials were repeated for the frequencies between 7 kHz and 17.5 kHz. The amplitude of the sinusoidal waveform was chosen as the minimum current required to produce the maximum blocking of the force of the muscle twitch due to the bipolar cuff electrode.

The bipolar cuff electrode was stimulated both with a single 50 μs pulse, and with 5, 50 μs pulses spaced by 15 ms. The repeated stimulation was used to produce a short tetanic contraction in the absence of the blocking current. The results of these trials are displayed in Table 6.2.

Column 1 indicates that frequencies between 7.5 and 10 kHz produce an initial contraction of the muscle at the onset of stimulation. This contraction of the muscle typically lasts longer than 3 seconds. However, it is observed from Figure 5.3b that this contraction does not elicit fatigue of the muscle. A complete block of the action potentials produced by bipolar cuff electrode is not observed for these frequencies. For frequencies above 12.5 kHz, a complete, temporary, localized block of the nerve is observed. As the frequency increases, the level of stimulation necessary to produce the block increases.

6.4 Discussion

The blocking effect was resistant to most changes in the model's parameters, seen in Table 6.1. Although the change in current level necessary to produce a block often exceeded the change in the action potential height, it was the qualitative effect of whether the block was still present within a modest change in predicted currents that was of interest to the investigation. Additionally, 98% of the changes in the model's parameters that produced less than 0.7 mV change in action potential height suggested a localized block.

Figures 6.1 and 6.2 demonstrate that the model suggests blocking in the presence of systematic and random noise. A random noise component 12% or less of the blocking current did not alter the level of current required to produce a block. An anodally biased current suggested that a lower sinusoidal current level would be required to produce a block.

The proposed mechanism for the block suggests that the block is caused by an increase in the average voltage of the node that is blocked. On this basis, it could be thought that a cathodally biased sinusoidal current would produce a block at a lower sinusoidal current level than an anodally biased one. However, the localized transmission block occurs due to a decrease in the change in membrane voltage at a node resulting from

an incoming action potential. For the simulations displayed in Figure 6.2, the blocking electrode was placed 1 mm from the axon. Excitation of the axon is based on the 2nd longitudinal spatial derivative of the voltage (Rattay, 1990). Therefore, the anodal stimulation caused an increase in the average nodal voltage of the nodes adjacent to the node that was blocked. The raise in voltage at the adjacent node caused this node to exhibit less of a change in membrane voltage due to the incoming action potential. It is this lessening of the change in membrane voltage due to a propagating action potential that causes the block. The cathodal stimulation caused a decrease in the average voltage of the nodes adjacent to the node that was blocked. This lowering of the voltage at the adjacent node caused this node to exhibit an increase in the change in membrane voltage due to the propagating action potential. This increase in the nodal voltage then transmitted to the blocked node, and requires more current at the blocking node to cause the block.

The addition of random noise to the simulation had very little effect. As seen in the simulations, the blocking is caused by an increase in the average nodal voltage. Hence, random noise is not expected to cause a change in the current required to block action potential transmission. This is reflected in Figure 6.2b.

The animal experiment correlated but did not specifically reproduce the findings of the computer models. The computer models predict that the application of the sinusoidal waveform should either produce a continuous generation of action potentials at a frequency of 150 to 300 Hz, or a block of the axon. The computer model also suggests that a sinusoidal stimulation at a frequency of 15 kHz and above should not produce a repetitive train of action potentials.

For frequencies at 12.5 kHz and above, the model predicts an initial twitch of greater height and duration than the action potential twitch, and a localized block of the nerve. The block of the nerve is demonstrated as a localized transmission block because the intramuscular electrode produces muscle twitches irrespective of the sinusoidal waveform. The twitches caused by the intramuscular electrode would not be seen if the blocking current caused a continuous train of action potentials which would fatigue the neuromuscular junction.

For frequencies below 10 kHz, the duration of the initial muscular contraction cannot be explained on the basis of the computer models. If the sinusoidal waveform produces a continuous train of action potentials of the nerve, it is expected from the computer models that these action potentials would continue to be generated. However, it is shown in Figure 6.3 and displayed in Table 6.1 that there is a limited duration of the repetitive firing of the axon. The intramuscular electrode is still able to produce muscle twitches after the force decreases due to the onset of the sinusoidal waveform. This indicates that the loss in force of the muscle is not caused by fatigue of the muscle. An explanation for the loss of temporary, declining, but not fatiguing force produced by the onset of the sinusoidal stimulation cannot be provided on the basis of the previously reported models and animal experiments.

In the experiments by Solomonow, forces due to a tetanic contraction were completely suppressed due to 600 Hz stimulation. The 600 Hz stimulation was thought to cause endplate depletion. Application of a twitching force between the blocking point of the nerve and the muscle should not produce muscular twitches. It is suggested that the mechanism that is causing the block seen in the trials of this paper is not the same as those caused by repeated 600 Hz stimulation. Further trials using both 600 Hz stimulation and the higher frequencies used in this experiment are required to confirm this supposition.

6.5 Conclusion

The current required to produce a localized transmission block in computer simulations varies due to changes in the parameters of the SRB model, although continues to display a block in the majority of models that conduct an action potential. An anodal biased stimulation will require a lower oscillating current level to produce a block than a cathodal biased stimulation. Qualitatively, the localized block is resistant to noise on the blocking signal.

A localized transmission block of a rat axon can be produced using a sinusoidal current in the frequency range of 7.5 kHz – 17.5 kHz delivered through a cuff electrode. If the frequency chosen is less than 10 kHz, an initial muscular contraction that does not

fatigue in the order of seconds is produced. The localized block will then continue for the duration of the sinusoidal stimulation. If the frequency chosen is above 12.5 kHz, a single twitch of the muscle is observed at the onset of the block. The localized block lasts for the duration of the sinusoidal stimulation.

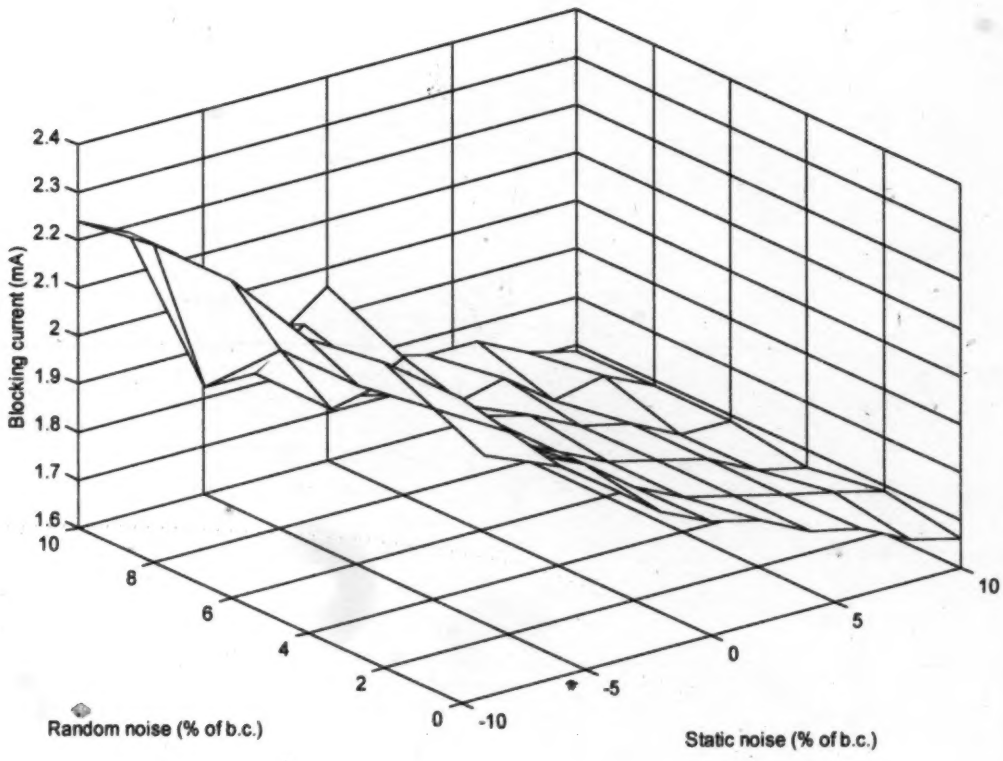

Figure 6.1 – Mesh diagram relating minimum blocking current for various levels of systematic and random noise. The level of current for each axis is given in mA. The level of current required to produce the block is lowered with in an increasing positively (anodally) biased current. The level of current required to produce a block is does not vary greatly with an increasing level of RMS noise added to the blocking waveform. The scale for the random and static noise levels is a percentage of the blocking current required without if the static and random noise.

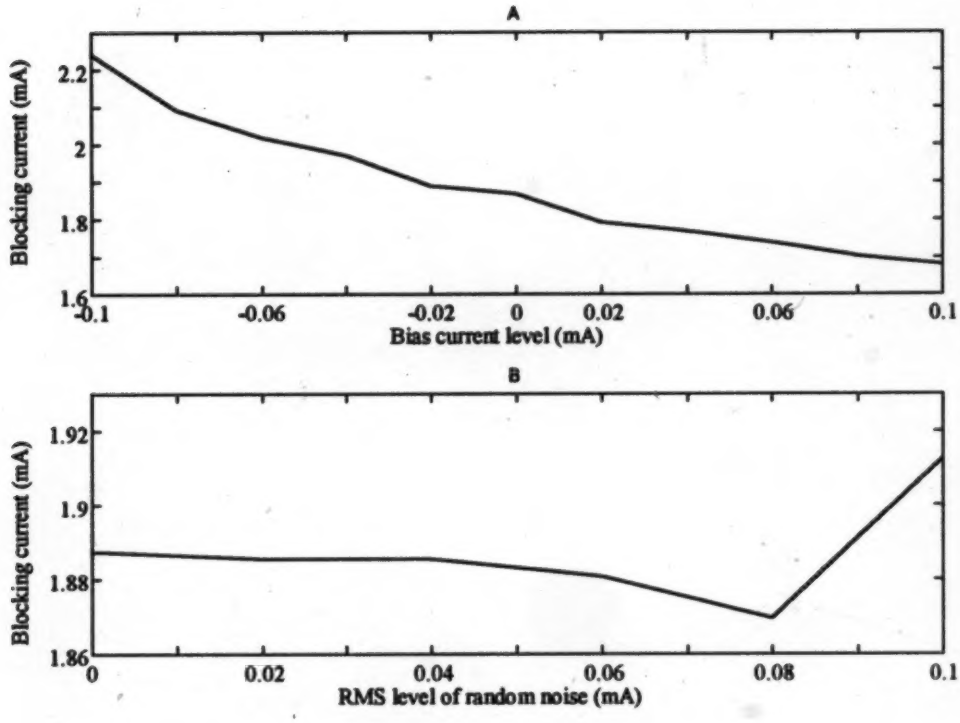

Figure 6.2

(A) Relationship of biased sinusoidal waveform to required peak amplitude of sinusoidal waveform. The blocking current required is the average of the blocking currents for the various RMS noise levels shown in Figure 6.1. As the bias current becomes more anodal, the level of current needed to block the node increases.

(B) Relationship of RMS noise added to the sinusoidal waveform and peak amplitude of the blocking waveform. The blocking current required is the average of the blocking currents for the various bias current levels shown in Figure 6.1. There is no statistical difference in the level of blocking current due to an increase in the noise.

Figure 6.3

(Top) Blocking of muscle twitches using a 17.5 kHz sinusoidal stimulus. The bipolar electrode is more distal from the muscle than the blocking electrode. Prior to the block, twitches from the intramuscular electrode and bipolar electrode occur every 4 seconds, and are spaced by one second. At the onset of the block, a single twitch of the muscle occurs. After this point, muscular twitches due to the intramuscular electrode continue, although the twitches due to the bipolar electrode do not. When the block is turned off, a single twitch is observed. The twitch due to the bipolar electrode is returns.

(Bottom) Blocking of muscle twitches using a 8 kHz sinusoidal stimulus. Prior to the block, twitches from the intramuscular electrode and bipolar electrode occur every 4 seconds, and are spaced by one second. At the onset of the block, a prolonged contraction of the muscle occurs. A muscle twitch elicited by the intramuscular electrode and the bipolar electrode is seen during this contraction. After 6 seconds, this muscular contraction ceases. Twitches due to the intramuscular electrode are still present. However, the twitches due to the bipolar electrode are partially blocked. When the block is turned off, a single twitch of the muscle occurs. The twitches due to the bipolar electrode return to the force recorded prior to the application of the block.

Blocking at 17.5 kHz

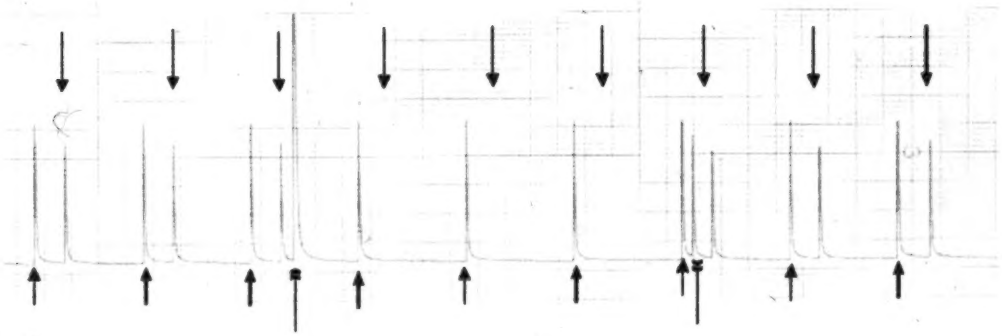

Blocking at 8 kHz

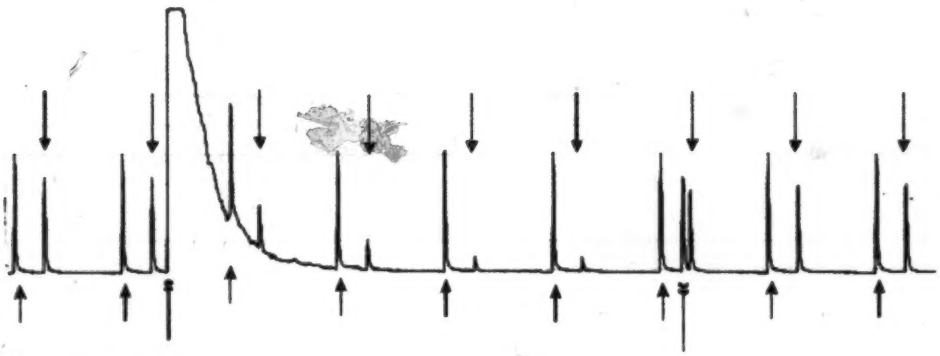

Legend

↑ Twitch due to intramuscular electrode

↓ Twitch due to bipolar electrode

| Onset of blocking current

| Turning off of blocking current

% change AP. Height	Number of Occurrences	Change in Blocking Current (%)							
		0-1	1-2	2-3	3-4	4-5	5-10	10-20	20+
0-.1	154	140	7	3	1	2	0	0	1
.1-.5	47	17	5	5	3	4	6	3	4
.5-1	8	0	0	1	1	0	0	1	5
1-2	8	0	0	0	0	1	3	0	4
2-5	12	0	1	0	0	1	6	2	2
5-10	17	2	1	0	0	1	8	0	5
10-100	4	1	2	0	0	0	0	0	1
No AP	38	0	0	0	0	0	0	0	38

Table 6.1: Percent change in the blocking current with respect to percent change in action potential height. A single parameter of the SRB model was varied between +/- 25% of its original value. The change in the action potential height was noted. This change in action potential height is recorded in conjunction with the change in the current required to produce a block of the axon.

Frequency	Current	Block of single twitch force	Block of tetanic force	Prolonged muscle activation at start of block
7.5 kHz	2.0 mA	No	No	Yes (5 s)
8 kHz	2.0 mA	Yes	No	Yes (3 s)
9 kHz	1.9 mA	Yes	No	Yes (4 s)
10 kHz	2.0 mA	Yes	No	No
12.5 kHz	2.37 mA	Yes	Yes	No
15 kHz	2.5 mA	Yes	Yes	No
17 kHz	2.7 mA	Yes	Yes	No

Table 6.2 : Results of nerve blocking in an animal trial. For all cases, the force produced by the intramuscular electrode was maintained during the block. The frequency and rms current of the sinusoidal current are displayed in columns 1 and 2. Column 3 indicates if the specified current and frequency could block (reduce the force produced by the bipolar cuff was reduced below 0.01 N) the muscle twitch of a single stimulation. Column 4 indicates if the specified current and frequency could block (reduce the force produced by the bipolar cuff below 0.01 N) the muscle twitch due to 5 50 μs pulses spaced by 15 ms. Column 5 indicates if the prolonged muscular force seen in Figure 6.3b at the start of the blocking waveform is observed.

6.6 Bibliography

Brindley, G.S., and Craggs, M.D., (1980) "A technique for anodally blocking large nerve fibres through chronically implanted electrodes" Journal of Neurology, Neurosurgery & Psychiatry. 43(12):1083-90

Brindley, G.S., and Craggs, M.D., (1978) "One-way stimulation of the large fibres of spinal roots through chronically implanted electrodes" J. Physiol. 281:12P

Bowman, B.R., (1981) "Electrical Block of Peripheral Motor Activity", Ph.D. Thesis, Edvard Kardelj University of Ljubljana, Ljubljana, Yugoslavia

Bowman, B.R., and McNeal, D.R., (1986) "Response of single alpha motoneurons to high frequency pulse trains: Firing behavior and conduction block phenomenon", Appl. Neurophysiol., 49:121-38

Chiu, S.Y., Ritchie, J.M., Rogart, R.B., and Stagg,D., (1979) "A quantitative description of the membrane currents in rabbit myelinated nerve", J. Physiol., 292:146-166

Frijns, J.H.M., Mooij, J., and ten Kate, J.H., (1994) "A quantitative approach to modeling mammalian myelinated nerve fibers for electrical prosthesis design", IEEE Trans. BME, 41:556-566

Lee, Y.S., Chay, T.R., and Ree, T., (1983) "On the mechanism of spiking and bursting in excitable cells", Biophys. Chem. 18:25-34

McAllister, R.E. Noble, D., and Tsien, R.W., (1975) "Reconstruction of the electrical activity of cardiac Purkinje fibres", J. Physiol. 251(1):1-59

McIntyre, C.C.., and Grill, W.M., (1998) "Sensitivity analysis of a model of mammalian neural membrane", Biol. Cybern. 79(1):29-37

McNeal, D.R., (1976) "Analysis of a model for the excitation of myelinated nerve", IEEE Trans. BME, 23:329-337

McCreery, D.B., Agnew, W.F., Yuen, T.G.H., and Bullara, L.A., (1995) "Relationship between stimulus amplitude, stimulus frequency and neural damage during electrical stimulation of sciatic nerve of cat," Med. & Biol. Eng. & Comput., 33:426-429

Motz, H., and Rattay, F., (1986) "A study of the Hodgkin-Huxley and the Frankenhaeuser-Huxley model for electrostimulation of the acoustic nerve", Neuroscience, 18(3):699-712

Muller, A., (1969) "Studies on electroanesthesia with middle frequency current", Proc. 2nd International Symposium on Electrotherapeutic Sleep and Electroanethesia, Grax, Aust., pp. 291-295

Rattay, F., (1990) Electrical Nerve Stimulation, Wein, Austria, Springer-Verlag, Ch. 5-7 pp. 73-139

Rattay, F., (1997) "Simulation of the electrically stimulated auditory nerve," Artif. Org. 21(3):213-5

Robblee, L.S., and Rose, T.L (1990), "Electrochemical guidelines for selection of protocols and electrode materials for neural stimulation," 25-66 from Neural prostheses: Fundamental studies, WF Agnew, DB McCreery, eds. Prentice Hall, 1990 , New Jersey, 07632

Schwarz, J.R., Reid, G., and Bostock, H., (1995) "Action potentials and membrane currents in the human node of Ranvier", Pfulgers Arch., 430:283-292

Scriven, D.R.L., (1981) "Modeling repetitive firing and bursting in a small unmyelinated nerve fiber", Biophys. J. 35:715-30

Sweeney, J.D., and Mortimer, T., (1986) "An Asymmetric two-electrode cuff for generation of unidirectionally propagated action potentials," IEEE Trans. BME, 33:541-549

Solomonow, M., (1984) "External control of the neuromuscular system", IEEE Trans. BME, 31:572-763

Tai, C., and Jaing, D., (1994) "Selective stimulation of smaller fibers in a nerve trunk and single cathode by rectangular current pulses", IEEE Trans. BME, 41:286-291

Williamson, R., and Andrews, B.J., "High frequency electrical currents for blocking peripheral nerves: Results of computer modelling I", submitted in conjunction

Woo, N., and Campbell, B., (1964) "Asynchronous firing and block of peripheral nerve conduction by 20 kc alternating current", Bull. L.A. Neurol. Soc., 29:87-94

Wedenski, N., (1885) "Wie rasch ermude der nerc", Zbl. Med Wis 22:65-8

7 Discussion

7.1 Introduction

The main focus of this thesis is to investigate the feasibility of a new neural prosthesis that would use electrical currents to stimulate muscles weakened by paralysis and dynamically block neural transmissions leading to unwanted muscular contractions. To be effective, this approach requires a sensor system that can determine control variables with sufficient accuracy and precision. Furthermore, the sensor system must be able to determine important gait events and phases of locomotion.

Electrical stimulation is known to produce muscular contractions with sufficient force and rapid response to be practical. The response time of muscles is based upon the rate of stimulation used by the controller. There is no known dynamic nerve blocking technique. To be effective, the blocking technique would need to have a response time comparable to the time resolution of the sensor system.

The results for each study are described first with reference to the objectives and hypotheses. Then, these results are compared to other investigations in their area and combined into the proposed neural prosthesis.

7.2 The Sensor System

7.2.1 Knee Flexion Angle and Angular Velocity

Knee flexion angle and angular velocity are used in control of standing (Dolan et. al., 1998, Davoodi and Andrews, 1998) and walking (Ng and Chizeck, 1997, Kirkwood et. al., 1989, Petrofsky et. al., 1984). The sensor system was compared to the Penny and Giles goniometer, the standard device used to measure knee flexion angle. The accuracy of the Penny and Giles goniometer was specified as 4 degrees. The precision of the auto-reset integral of the auto-nulled rate gyroscope, as indicated in Table 3.6 is 0.8 degrees. During sit to stand to sit transitions of an able bodied individual, the accuracy of the sensor system was better than 3.2 degrees, indicated in Table 3.4. This is within the specified accuracy of the reference device used to determine the knee flexion angle. This met objective 1b and supported hypothesis 1. The accuracy of this method was also

subsequently demonstrated for FES assisted standing of a paraplegic individual. This met objective 1b and supported hypothesis 1. For recordings with or without FES, the precision of the measurement of knee flexion angle was 0.1 degrees, indicated in Table 3.6. The stimulus artifact and electrical and mechanical vibrations did degrade the accuracy of the measurement of knee flexion angle, noticed by comparing the results of Table 3.4 and 3.5. The precision of knee angular velocity did decrease due to electrical stimulation, as indicated in Table 3.6. However, the rate gyroscope displayed a more precise measurement of the angle than the Penny and Giles goniometer.

Other groups have discussed limits in detecting knee flexion angle. Kataria and Abbas (Kataria and Abbas, 1998) state that their method of calculating slowly moving angles on a 2 dimensional model produced errors of 4.2 degrees. Crago (Crago et. al, 1986) stated that knee flexion angle detection accuracy of 0.05 rad (2.9 degrees) statically, or 0.15 rad (8.7 degrees) dynamically, is sufficient for controllers. Popovic and Tepavac (Popovic and Tepavac, 1982) indicate that a static error of 8 degrees due to using Penny and Giles goniometers type M180 is present, and cannot be easily removed. Heyn et. al. (Heyn et. al., 1996) proposed a method for detecting knee flexion angle, although do not report accuracy of the method with discernable units of measurement. They also note that this method requires computer intensive offline calculations to determine knee flexion angle and is therefore restrictive for online control applications. The accuracy reported for the auto-reset integral of the auto-nulled rate gyroscope exceeded the reported accuracy of these other methods, and is within the accuracy specified for control of a neural prosthesis.

The application of the sensor system is not limited to the detection of knee flexion angle. The knee flexion angle is calculated by first calculating the tilt of the thigh and the shank. Figure 3.4 indicates that the accuracy of the accelerometers for determining tilt of a segment is 0.5 degrees. The precision of the knee flexion angle calculation was determined in Table 3.7 to be 0.1 degrees for the rate gyroscope in the presence of FES. Potentially, a neural prosthetic controller could use the angle of these two segments. Franken (Franken and Veltink, 1995) has described a cycle to cycle controller of gait based on hip angle while the patient was standing on a treadmill in a harnessed upright

position, based upon the one step ahead controller of Granat et. al., (Granat et. al, 1991). From the description of the apparatus, the pelvis is nearly immobile; changes in hip angle would result from rotation of the femur towards the pelvis and not rotation of the pelvis towards the femur. Hence, the angle of the thigh with respect to gravity is the direct variable of interest, and sufficient feedback for their system and could be calculated from the tilt of the thigh.

7.2.2 Knee Buckle Prediction

Changes in force in a FRO should precede knee buckling, as seen in Figure 4.10. The predictive force sensor and signal processing system was tested in quiet standing of a paraplegic individual. An indication of an incipient knee buckle, as determined by the force sensor and signal processing, preceded the buckle of the knee by a minimum of 340 ms, indicated in Table 4.4. This met objective 1c, and supports hypothesis 1. Such prediction would allow time for the stimulation to the quadriceps to respond and establish a contraction prior to the knee buckling. Predictive or anticipatory FES control of knee buckling may also lead to a less disturbing knee buckle as less stimulation and muscular force is required. The user will be closer to a stable position once the stimulation is applied to the quadriceps, and the knee buckle should be less disruptive to any activities the user is participating in.

The detection and control of knee buckling is pursued by Shimada et. al. (Shimada et. al, 1995). A faster detection of knee buckling was made using a stretch sensor attached to the back of the knee when compared to a goniometer. However, prediction of a knee buckle, prior to its occurrence, is not being presently investigated.

7.2.3 Gait Phase Prediction

In this study, able bodied walking was analyzed. A rule base detector was constructed. Intuitive rules were applied to the output of the rule based detector. These rules had the effect of localizing the sporadic errors typical of a rule based detector to the transitions between the gait phases. An average error during the transition for these individuals was 40 ms. A maximum error of transition of any one gait phase to the next was 90 ms. The average error at the transition from one phase to the next was less than

one sample period greater than the variance of the reference method. The precision of this method is within one sampling period of the precision of the reference signal. It was demonstrated that this error was better than a similar method for five phase gait event detection (Ng and Chizeck, 1997), and equivalent to the detection accuracy of a stance swing detector (Dai et. al, 1996). This met objective 1a and supports hypothesis 1.

The proposed system uses a feedback controlled finite state controller. Errors at the transition would either prematurely initiate or postpone the stimulation pattern delivered to a particular muscle group. Feedback control is proposed to ensure that the stimulation pattern to the muscle groups is producing an appropriate trajectory. It is hypothesized that in a FES system, the presence or absence of one or two stimulation pulses, as is predicted by the timing resolution of the gait phase event detector, could be compensated by the feedback controller.

Kostov (Kostov, 1996) has investigated stance swing detection using restriction rules. He described two types of errors, classing the errors in timing at the transition from one gait phase to the next as 'non-critical' errors, and the errors that occur during a gait phase as 'critical'. For example, a 'critical' error would be the controller predicting a momentary transition from stance to swing during the middle of a stance phase. This type of error is obviously detrimental; the leg that is in stance phase during single limb support would be stimulated as would be typical at the start of a swing phase, possibly leading to a fall of the individual. This sort of obvious detriment is not seen in the 'non-critical' errors that occur by an extended or shortened gait phase. 'Non-critical' errors are the only type of errors present in the method for gait phases detection described in chapter 2. The disruption to a gait pattern caused by these errors has not been investigated. However, Kostov has demonstrated that his system will still function in the presence of these errors, i.e. the patient can still walk. Additionally, it was shown in chapter 2 that Dai's system, and probably the commercial system on which it is based, has these errors and is still useful and functional. This suggests that these 'non-critical' errors occurring at the transition from one phase to the next do not cause a catastrophic detriment to walking assisted by FES, but more likely minor subtler detractions. Testing in a multiple gait phase system would be required to strengthen this observation.

7.3 Electrical Nerve Blocking

The computer models predict a localized block of axon transmission for myelinated rat and human nerves. The high frequency stimulation is predicted to produce an action potential within 2 ms of the onset of the stimulation, and continue to block afterwards. Action potential propagation is predicted to resume within 4 ms upon the cessation of the blocking waveform. For a range of high frequency stimulation levels below the threshold for blocking, excitation of the axon is predicted in a frequency range of 150 to 300 Hz. The blocking waveform obeys the reverse recruitment order typical of electrical stimulation of peripheral nerves. A change in the level of current required to produce a block was necessary to accommodate for changes in the nodal kinetics of the SRB model, but a localized conduction block of the axon was still predicted. Similarly, the addition of static or random noise to the blocking waveform changed the level of current required to produce a block, but a localized conduction block of the axon was still predicted. Thus objectives 2a, 2b and 2c are met, and hypothesis 2 is supported.

An animal trial verified some key results of the computer simulations. At the onset of the stimulation, a twitch would occur. The magnitude of the twitch force was greater than that due to due to a single supra-maximal pulse but less than that of a tetanic contraction. A localized block of the action potentials was determined for the rat tibial nerve for blocking frequencies above 12.5 kHz. The computer models suggest that a block of the rat nerve should be present above 7 kHz. The nerve was able to recover in less than one second after the removal of a block applied for 20 s. A greater time resolution for the cessation of a block was not conducted. Hence, a localized nerve block was demonstrated in the animal trial, meeting objective 2d. Hypothesis 2 is supported.

Most other descriptions of electrical nerve blocking require the continuous stimulation of the axons. It is unproven, but suggested by Agnew and McCreery (Agnew and McCreery, 1990), that this could cause early axonal death for prolonged application of the stimulation. The computer models predict a method for nerve blocking that does not excite the axons is possible. This is supported by an animal trial. Bowman (Bowman, 1981), Muller (Muller, 1969), and Woo and Campbell (Woo and Campbell, 1964) have

previously suggested the possibility of an electrically induced localized nerve conduction block. This is supported by the both the computer simulations and the animal trial.

7.4 A New Neural Prosthesis

The results of each of these individual tests would need to be combined into a neural prosthetic system, using inputs from a sensor system to trigger and regulate blocking and stimulation of peripheral axons. The requirements of the sensor system, stimulation, and blocking are examined in a clinically reported case of a potential user. Selected is the case of a child with crouched gait due to cerebral palsy. The motor impairment seen in this patient is typical, and unable to be addressed by a single present therapy. The development of a new neural prosthesis that incorporates both stimulation and blocking of axons is necessary. The EMG patterns and gait deviations are displayed in Figure 7.1 (Perry, 1992).

The EMG patterns from this patient display spastic actions of the gracilis, semimembranosis, and biceps femoris long head, inadequate rectus femoris, persistent vastus intermedius, and out of phase adductor longus. The desired controller would block the spastic actions of the sciatic nerve branches innervating the gracilis, semimembranosis, and biceps femoris from loading response to pre-swing, block the femoral nerve branches innervating the vastus intermedius from terminal stance until terminal swing, stimulate the femoral nerve branches innervating the rectus femoris during pre-swing, block the obturator nerve branches innervating adductor longus during terminal swing until mid-stance, and stimulate during terminal stance until mid-swing.

The block, as described by the animal tests, exhibited an initial twitch of twice the duration of the twitch of the muscle, at the onset of the block. Taking the initial twitch timing into consideration, the block should be applied to the nerve at a time in which the twitch force would not be detrimental to the gait pattern, i.e. during a phase of gait that the muscle would normally be active. For the gracilis, semimembranosis, and biceps femoris long head, the block could be applied to the sciatic nerve branches at the transition from mid to terminal swing. At this time, the twitch would help to flex the knee to achieve foot clearance directly before the blocking effect would occur, and enable knee

extension after the onset of the block. The block would continue through the stages of terminal swing, loading response, mid-stance and terminal stance. The block should then immediately be turned off. The immediate cessation of the block is a second characteristic demonstrated in the computer simulations.

The block of the branch of the femoral nerve innervating of the vastus intermedius requires discrimination of mid-stance and terminal stance, and mid-swing and terminal swing. The initial twitch at the onset of the block during mid-stance would be inconsequential, as the knee should be extended during this phase, a moment that is reinforced by the twitch of the muscle. The stimulation of the nerve innervating the rectus femoris requires discrimination of the pre-swing phase. The block of the adductor longus requires discrimination of mid-stance and terminal stance, and mid-swing and terminal swing. The initial twitch at the onset of the block suggests that the block should be applied earlier than the transition to terminal swing, as the muscle is still contracting at this time. Figure 7.1 displays the duration for stimulation and blocking for the nerves innervating each of the muscles.

The event detector exhibited a precision of 40 ms, based upon the repeatability of the reference signal. The transitions at which the block are applied occur as the spastic muscle would change from a phase of gait that a contraction is desired to a phase of gait that a contraction is undesired. Hence, the timing of the initial twitch could be situated at a time where it would not interfere with the gait pattern. A block that is applied 40 ms too early would therefore block the last 40 ms of a muscles' contraction before it would naturally cease. This loss of moment should be compensated from the twitch due to the onset of the block. A block that is applied 40 ms too late would cause a twitch of the muscle approximately 55 ms after the muscle would normally cease to function. The extra moment produced by this muscular contraction could be detrimental in some cases. Realizing these limitations of the system, the controller should be programmed to err on the side of an early block.

For the patient listed above, it is suggested that the block be applied to the nerve branches innervating the gracilis, semimembranosis, and biceps femoris long head at the transition from mid to late swing. The knee flexion moment caused by this twitch could

add to an inappropriate knee flexion at heel strike. However, this might be compensated naturally for through the Ia reflex arc, as the antagonist muscle would undergo a smaller decrease in length than expected causing an increase in recruitment of that muscle group. If this natural response of the system is not seen, a short stimulation pulse to the antagonist muscle could be used to offset the moment produced about the joint at the initiation of the block. A third compensatory mechanism exists due to the feedback controller. As knee flexion angle will also be measured by the system, if the knee flexion angle was not sufficient during terminal swing stimulation of the rectus femoris could assist knee extension.

For the gracilis, semimembranosis, and biceps femoris long head, the block of the branches of the sciatic nerve innervating these muscles is suggested to cease at the transition from terminal stance to pre-swing. From the Figure 7.1, it is noted that the muscle is not required to be active nor is spastically firing for a period of approximately 150 ms around this time. The resolution of the gait event detector, demonstrated in the able bodied test to have a maximum error of 90 ms, does not impede the cessation of the block of this muscle.

The block that is applied to the femoral nerve branches innervating the vastus intermedius should terminate at the start of terminal swing. If the block was terminated prematurely, it would lead to an increase in moment of the knee extension. Considering that one of three vasti is contracting at a normal level for 40 ms early in a phase of 120 ms, the error corresponds to approximately 11% of the time integrated moment. This should not cause a problem in the gait cycle. Additionally, the transition from mid-swing to terminal swing is also used as the onset of the block of the nerves innervating the gracilis, semimembranosis, and biceps femoris long head. If the block would be applied to the nerves innervating these muscles is too early, an increase in knee flexion moment would be caused at the same time the increase in knee extension moment. These two moments could offset one and other.

The onset of the block to the adductor longus at the transition from mid-stance to terminal stance would be coincidental with the cessation of the stimulation of this muscle. A deviation of the hip flexion pattern was not noted even when this muscle was firing out

of phase. Therefore, it is thought that a resolution of 40 ms to reinstate normal activation of this muscle would not be detrimental to the gait pattern. The timing for the cessation of the blocking for the adductor longus should not have a detrimental effect for the reason listed above. Considering the timing resolution of the sensor system and the timing mechanics of the blocking waveform, a potential for this neural prosthesis is suggested.

There are other factors that are necessary to consider in the design of the prosthesis. The blocking waveform can not be distributed on the surface, implying that the system must be implanted. The current that produces the block should be contained, as it has been shown to excite electrically active cells, implying that cuff electrodes should be used. Slot et. al. (Slot et. al, 1997) demonstrated that cuff electrodes could damage the nerve, although conduction velocity of the nerve is preserved. This suggests that the damaged individual axons are lost, but the properties of the preserved axons are not deterred. This is supported by the work of Larsen et. al. (Larsen et. al, 1998), who has shown that an initial decrease in the number of myelinated axons can be observed due to implantation of a cuff electrode. However, 16 months after the implantation of the cuff, the number of axons has returned to the previous level. Further studies should be conducted to confirm that cuff electrodes are not permanently damaging to peripheral nerve. Many of the present studies in this area are acute studies that have reported a loss of axons due to cuff electrodes, and have not investigated the possibility of recovery.

The power consumption of the device must also be considered. Present implanted neural prostheses are powered either transcutaneously or by battery. The inclusion of sensors and blocking to this new version neural prostheses is severe in consideration of power consumption. Present accelerometers require 0.5 mA, and the rate gyroscopes require 10 mA. A microcontroller is required to record this data and run the control algorithms. Microcontrollers minimally require 10 mA of current. The total current consumption of the sensor system and controller is 56 mA. As a comparison with present technology, the Neopraxis stimulator, powered transcutaneously, would typically require 0.625 mA (10 channels at currents of 5 mA, frequency 25 Hz, and pulse width 500 μs).

Nerve blocking, as suggested in this description, requires continuous current levels of 3-4 times stimulation levels, or 20 mA per channel of blocking.

The sensors and computer could be worn externally, and gains could be expected in power consumption of the rate gyroscopes and microcontrollers. However, a limit is placed by the present current requirement for the block. Implantable batteries are not sufficient for this power consumption. Externally transduced power can be inefficient, as low as 20%, (Ko, et. al, 1977). Using this calculation, the external current necessary for blocking of four channels would be 320 mA. Rechargeable batteries typically can supply 400 mAh. Hence, the amount of time per day a person could use the device is limited by the current requirements of the block and the life of the battery. Significant gains in battery size or power transduction are required to execute these blocks.

Current through a single electrode must also be considered. It was noted in the above description of the system that a current of 20 mA might be necessary for the blocking waveform. For FES, safe current limits have been based on integrated pulse width duration (Walter et. al, 1996). At 10 kHz, a 20 mA peak RMS current would have a charge per phase of 170 μC. Using a safe limit of 300 $\mu C/cm^2$, a 6 mm wide, 3 mm diameter cuff electrode would be within the charge per phase limits. On this basis, corrosion of the metal electrodes should not be a limiting factor.

The proposed neural prosthesis, incorporating selective stimulation and blocking with a single sensor system, is presently limited in application due to practical considerations of long term safety of the cuff electrode design, power delivery, and consumption of the system. Although the studies were able to propose directions for the development of a sensor system and localized nerve blocking, further research is required to develop the system into a single unit.

7.5 Implications of This Study to FES

Although unable to resolve itself into a single neural prosthetic device, elements of the system can be implemented in and outside other areas of FES. The sensor system resolved knee flexion angle through calculating the tilt of the thigh and shank segments, and has been shown to provide the variables used by lower limb FES control routines. It

is proposed as a potential replacement to the goniometer, based on a greater accuracy, durability, and ease of use. Future tests by other investigators will determine if these findings are supported. Applications of this technique are not limited to the rehabilitation industry. The algorithms provide a method for a wide band three dimensional tilt meter. Presently, Microstrain™ has marketed a device that uses only accelerometers to perform this function, and is limited in either bandwidth or precision as demonstrated in this study.

The integral of the rate gyroscope used to determine angle was not calibrated individually for each user. The sensors were placed on each individual for testing, and the angles were then determined. This is an advantage in comparison to the angle detection by the goniometer, and lends itself to more widespread use. Although temperature was noted to affect the offset of the accelerometer measurements, this can be compensated.

Although not discussed within the present literature, closed loop control within the state on instantaneous variables, such as knee flexion angle and hip flexion angle, could allow for better regulation of the FES outputs. This has been explored for the sit to stand controllers. For walking, the step has certain qualitative objectives, foot clearance, knee extension at terminal swing, and stride length. It is known from kinesiological studies, that within a goal oriented system, such as walking, certain motions are more efficient and require less muscular excitation and energy than other movements. A preprogrammed feed-forward stimulation technique modified by a closed loop controller could provide a trajectory that is more efficient for walking. The application of the cycle to cycle controller would modify the feed-forward controller based upon the response of the muscles. The continuous monitoring of variables such as knee flexion angle would allow for compensation of the feed-forward control routines. With the availability of appropriate sensors, this hypothesis could be tested. Crago (Crago et. al., 1996) has discussed a concept along this line of thinking, using models to predict the outcome of the stimulation, comparing this to variables such as knee flexion angle, and adjusting both the feed-forward stimulation and the models to compensate for the errors.

If floor reaction orthotic is worn to enable prolonged standing, a detection device has been demonstrated that can control quiet standing. Control routines can be derived

using this sensor as an input, and comparing it to the previous methods for control of quiet standing.

This detection of gait phases is an example of a technique, and not the end product. Five gait phases that were not intuitively related to the sensors were chosen, and a mapping was constructed between the sensor signals and the desired output variable. This provides an example of the detection of events for control of gait, and not necessarily the events that need to be detected to control gait. Similarly, detection of temporally localized, repetitive spastic action could be detected and subsequently suppressed via a localized nerve blocking method. It is these types of events that are useful for a control routine that would be learned by the sensor system.

The resolution of the timing of the gait phases was limited by the variance of the parameters that it was attempting to map. For the subjects listed in Figures 7.1 and 1.1, a high repeatability of the spastic actions is predicted. Hence the events that the rule based controller is mapping should exhibit a lower variance and be detected more reliably. This would cause a decrease in the errors at the transitions.

The blocking waveform that is suggested could also be used for control of micturition. The present methods for this are post stimulus voiding (Brindley and Rushton, 1990), Mortimer's collision blocking method (Grunewald et. al., 1998), Solomonow's high frequency stimulation, expressed by Shaker et. al, (Shaker et. al, 1998), and Rijkoff's method of anodal blocking (Rijkoff et. al., 1998). The localized electrical nerve block proposed in this thesis would still present the advantage over some of the previous systems in that it does not cause mass action of the neurons that the potential axonal death associated with it, and has a balanced current. This opens the possibility of further study. However, the level of electrical current needed for the block could be a pose a problem for chronic use.

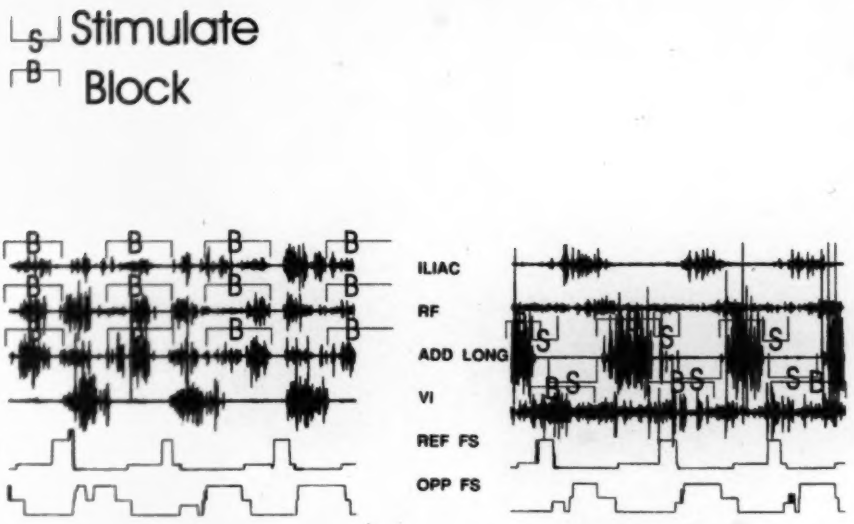

Figure 15.21I Dynamic electromyography, spastic diplegia. GRAC = gracilis; SMEMB = semimembranosis; BFLH = biceps femoris long head; BFSH = biceps femoris short head; REF FS = reference foot switch; OPP FS = opposite foot.

Figure 15.21J Dynamic electromyography, spastic diplegia. ILIAC = iliacus; ADD LONG = adductor longus; RF = rectus femoris; VI = vastus intermedius; REF FS = reference foot switch; OPP FS = opposite foot.

Figure 7.1 EMG and recordings for individual with crouched gait spasticity. The EMG patterns display deviations of spastic actions of the gracilis, semimembranosis, and biceps femoris long head, inadequate rectus femoris, persistent vastus intermedius, and out of phase adductor longus. The desired controller would block the spastic actions of gracilis, semimembranosis, and biceps femoris from loading response to pre-swing, block vastus intermedius from terminal stance until terminal swing, stimulate rectus femoris during pre-swing, block adductor longus from terminal swing until mid-stance, and stimulate from terminal stance until mid-swing.

7.6 Bibliography

Brindley, G.S., Rushton, D.N., (1990) "Long-term follow-up of patients with sacral anterior root stimulator implants" Paraplegia. 28(8):469-75

Crago, P.E., Chizeck, H.J., Neuman, M.R., and Hambrecht, F.T., (1986) "Sensors for Use with Functional neuromuscular Stimulation", IEEE Trans. BME 33:(2):256-268 Feb. 1986

Crago, P.E., Lan, N., Veltink, P.H., Abbas, J.J., and Kantor, C., (1996) "New control strategies for neuroprosthetic systems", J. Rehabilitation Research and Development 33:(2)158-172

Dai, R., Stein, R.B., Andrews, B.J., James, K.B., and Wieler, M., (1996) "Application of tilt sensors in functional electrical stimulation", IEEE Trans. Rehab Eng. 4:(2)63-72

Franken, H.M., Veltink, P.H., Baardman, G., Redmeyer, R.A., and Boom, H.B.K., (1995) "Cycle to cycle control of swing phase of paraplegic gait induced by surface electrical stimulation", Med. Biol. Eng. & Comp. 33:440-451

Granat, M.H., Nicol, D.J., Baxendale, R.H., Andrews, B.J., (1991) "Dishabituation of the flexion reflex in spinal cord-injured man and its application in the restoration of gait" Brain Research. 559(2):344-6

Grunewald, V., Bhadra, N., Creasey, G.H., and Mortimer, J.T., (1998)"Functional conditions of micturition induced by selective sacral anterior root stimulation: experimental results in a canine animal model." World J Urol. 16(5):329-36

Heyn, R. E., Mayagoitia, A., Nene, V., and Veltink, P.H., (1996) "The kinematics of the swing phase obtained from accelerometer and gyroscope measurements", Proc. IEEE EMBS, pg 857-8

Kataria, P., and Abbas, J.J., (1998) "Estimating body segment orientation using a lightweight, inexpensive gyroscope" Proc. BMES Conf. P S-133

Kirkwood, C.A., Andrews, B.J., and Mowforth, P., (1989) "Automatic detection of gait events: a case study using inductive learning techniques", J. Biom. Eng, 11(6):511-6

Ko, W.H., Liang, S.P., Fung, C.D., (1977) "Design of radio frequency powered coils for implant instruments", Med. Biol. Eng. Comput. 15:634:640

Kostov, A., (1996) "Functional error assessment in gait event discrimination for FES assisted locomotion", Proc. IEEE EMBS, pg 969-71

Larsen, J.O., Thomsen, M., Haugland, M., Sinkjaer, T., (1998) "Degeneration and regeneration in rabbit peripheral nerve with long-term nerve cuff electrode implant: a stereological study of myelinated and unmyelinated axons" Acta. Neuropathologica, 96 (4) : 365-378

Ng, S.K., and Chizeck, H.J., (1997) "Fuzzy model identification for classification of gait events in paraplegics", IEEE Trans. Fuzzy Systems, 5(4):536-544

Pedotti, A., Ferrarin, M., Quintern, J., Riener, R., (1996) Neuroprosthetics, Springer-Verlag, ISBM 3-540-61084-7

Petrofsky, J.S., Phillips, C.A., and Heaton, H.H.,(1984) "Feedback control system for walking in man", Comp. Biol. Med. 14(2):135-49

Phillips, C. (1991), Functional electrical rehabilitation: technological restoration for restoring after spinal cord injury, Springer-Verlag, New York

Phillips, C.A., (1988) "Sensory feedback control of upper and lower extremity motor prosthesis", CRC Crit. Reviews 16(2)-105-40

Popovic, M., and Tepavac, D., (1982) "A portable 8 channel gait kinematics recording unit", Proc. IEEE EMBS

Shimada, Y., Sato, K, Kagaya, H., Ebata, K., Kodama, H., Konishi, N., Muyamoto, S., Matsunaga, T., Sato, M., (1995) "Closed loop control for functional electrical stimulation with percutaneous electrode in paraplegics", 5th Int. Work. FES Vienna

Slot, P.J., Selmar, P., Rasmussen, A., Sinkjaer, T., (1997) "Effect of long-term implanted nerve cuff electrodes on the electrophysiological properties of human sensory nerves" Artificial Org. 21 (3): 207-209

Stein, R.B., Peckham, P.H., Popovic, D. B., (1992) Neural Prostheses, Oxford University Press, ISBN 0-19-507216-2

Shaker, H.S., Tu, L.M., Robin, S., Arabi, K., Hassouna, M., Sawan, M., and Elhilali, M.M., (1998) "Reduction of bladder outlet resistance by selective sacral root stimulation using high-frequency blockade in dogs: An acute study," J. Urology, 160, 901-907

Walter, J.S., Reidy, L, Zaszczurynski, P., Cogan, S.F., Liu, Y-P., (1996) "Coating stainless steel electrodes with iridium for applications in functional electrical stimulation", RESNA '96, 273-275

8 Conclusions

The general objectives of this thesis were to demonstrate, through pilot studies, directions for the development of a new generation of neural prosthesis that would apply both blocking and stimulating electrical pulses to peripheral nerves. Two niches were identified in the literature, namely the lack of a suitable sensor system and a means of dynamically blocking peripheral nerve. From the results of the study, the following conclusions are made.

1. Signal processing techniques, including the use of heuristic rules and machine learning, can be used with available and suitably positioned sensors to estimate control variables and detect events for control of lower limb FES. Knee flexion angle can be determined to the same accuracy as the Penny and Giles M180 goniometer for sit to stand transitions. Major gait events can be determined using supervised machine learning and heuristic rules. A predictor of knee buckling can be generated using a strain gauge applied to the ankle foot brace.

2. The proposed sensor system can provide feedback for control of standing up in a paraplegic individual. Specifically, knee flexion angle and angular velocity can be determined as with sufficient accuracy and precision for FES assisted standing.

3. High frequency electrical currents can be applied to axons to produce three observable effects in mammalian nerve models: single action potential generation, repetitive stimulation, and localized axon blocking.

4. High frequency electrical currents above 12.5 kHz applied to the common peroneal nerve of an adult rat produced a localized and dynamic block.

8.1 Recommendations for Future Research

As this was a preliminary study into directions absent in the development of a neural prosthesis, many areas of further development beckon.

1. Continued application of the sensor system and techniques. The sensor system that is proposed could be expanded to include detection of hip and ankle angle. A third dimension to the system, so that the sensor could determine tilt or orientation in three dimensions instead of one.

2. The determination of gait phases could be incorporated into a controller similar to that of Kobetic and Marsolais. The gait phase detector could provide triggers for the stimulation of many different muscle groups. This could then be compared with a system based strictly on a time series of stimulation, similar to what is used presently by Marsolais.

3. The sensor system, as designed presently, could be transferred to different users to compare the ease of use of the system with the goniometer. It is my belief that this sensor is easier to use than the goniometer, however, this can only be shown through application of other individuals.

4. A signal predictive of incipient knee buckling was determined from a strain gauge mounted on a FRO. This signal could be incorporated into a controller for quiet standing, and compared to the present methods for control.

5. Further animal and computer modeling for the determination of the high frequency blocking. Resolution for the turn off time of the block needs to be addressed. The effects on the small diameter fibers are not determined, and would be necessary for future application. Alteration of the blocking cuff geometry and waveform shape, as suggested by computer models, might be able to produce a waveform that does not produce an initial twitch and uses less current than the present method. The long term effects of the nerve block should also be explored. Finally, a test of the block in human subjects could be conducted to determine the feasibility of the block.

6. Control for the turning on and off of the nerve block could be enhanced if spastic actions could be detected from epineural recordings. This would involve an epineural electrode placed proximal to the blocking cuff, with a separation between the epineural and blocking cuff determined by the amount of time required to detect a spastic versus a desired muscular activation.